Université de Montréal

Quantitative functional MRI of the Cerebrovascular Reactivity to CO_2

par
Felipe B. Tancredi

Département de physiologie
Faculté de médicine

Thèse présentée à la Faculté des études supérieures
en vue de l'obtention du grade de Philosophiæ Doctor (Ph.D.)
en génie biomédical

Février, 2015

© Felipe B. Tancredi, 2015.

Université de Montréal
Faculté des études supérieures

Cette thèse intitulée:

Quantitative functional MRI of the Cerebrovascular Reactivity to CO_2

présentée par:

Felipe B. Tancredi

a été évaluée par un jury composé des personnes suivantes:

Guy Cloutier,	président-rapporteur
Richard D. Hoge,	directeur de recherche
Oury Monchi,	membre du jury
Kevin Whittingstall,	examinateur externe
Jean da Silva,	représentant du doyen de la FES

Thèse acceptée le: . . . . . .

RÉSUMÉ

Le dioxyde de carbone (CO_2) est un résidu naturel du métabolisme cellulaire, la troisième substance la plus abondante du sang, et un important agent vasoactif. À la moindre variation de la teneur en CO_2 du sang, la résistance du système vasculaire cérébral et la perfusion tissulaire cérébrale subissent des changements globaux. Bien que les mécanismes exacts qui sous-tendent cet effet restent à être élucidés, le phénomène a été largement exploité dans les études de réactivité vasculaire cérébrale (RVC). Une voie prometteuse pour l'évaluation de la fonction vasculaire cérébrale est la cartographie de la RVC de manière non-invasive grâce à l'utilisation de l'Imagerie par Résonance Magnétique fonctionnelle (IRMf). Des mesures quantitatives et non-invasives de de la RVC peuvent être obtenus avec l'utilisation de différentes techniques telles que la manipulation du contenu artériel en CO_2 ($PaCO_2$) combinée à la technique de marquage de spin artériel (*Arterial Spin Labeling*, ASL), qui permet de mesurer les changements de la perfusion cérébrale provoqués par les stimuli vasculaires. Toutefois, les préoccupations liées à la sensibilité et la fiabilité des mesures de la RVC limitent de nos jours l'adoption plus large de ces méthodes modernes de IRMf. J'ai considéré qu'une analyse approfondie ainsi que l'amélioration des méthodes disponibles pourraient apporter une contribution précieuse dans le domaine du génie biomédical, de même qu'aider à faire progresser le développement de nouveaux outils d'imagerie de diagnostique. Dans cette thèse je présente une série d'études où j'examine l'impact des méthodes alternatives de stimulation/imagerie vasculaire sur les mesures de la RVC et les moyens d'améliorer la sensibilité et la fiabilité de telles méthodes. J'ai aussi inclus dans cette thèse un manuscrit théorique où j'examine la possible contribution d'un facteur méconnu dans le phénomène de la RVC : les variations de la pression osmotique du sang induites par les produits de la dissolution du CO_2.

Outre l'introduction générale (Chapitre 1) et les conclusions (Chapitre 6), cette thèse comporte 4 autres chapitres, au long des quels cinq différentes études sont présentées sous forme d'articles scientifiques qui ont été acceptés à des fins de publication dans

différentes revues scientifiques. Chaque chapitre débute par sa propre introduction, qui consiste en une description plus détaillée du contexte motivant le(s) manuscrit(s) associé(s) et un bref résumé des résultats transmis. Un compte rendu détaillé des méthodes et des résultats peut être trouvé dans le(s) dit(s) manuscrit(s). Dans l'étude qui compose le Chapitre 2, je compare la sensibilité des deux techniques ASL de pointe et je démontre que la dernière implémentation de l'ASL continue, la pCASL, offre des mesures plus robustes de la RVC en comparaison à d'autres méthodes pulsés plus âgées. Dans le Chapitre 3, je compare les mesures de la RVC obtenues par pCASL avec l'utilisation de quatre méthodes respiratoires différentes pour manipuler le CO_2 artérielle ($PaCO_2$) et je démontre que les résultats peuvent varier de manière significative lorsque les manipulations ne sont pas conçues pour fonctionner dans l'intervalle linéaire de la courbe dose-réponse du CO_2. Le Chapitre 4 comprend deux études complémentaires visant à déterminer le niveau de reproductibilité qui peut être obtenu en utilisant des méthodes plus récentes pour la mesure de la RVC. La première étude a abouti à la mise au point technique d'un appareil qui permet des manipulations respiratoires du CO_2 de manière simple, sécuritaire et robuste. La méthode respiratoire améliorée a été utilisée dans la seconde étude – de neuro-imagerie – où la sensibilité et la reproductibilité de la RVC, mesurée par pCASL, ont été examinées. La technique d'imagerie pCASL a pu détecter des réponses de perfusion induites par la variation du CO_2 dans environ 90% du cortex cérébral humain et la reproductibilité de ces mesures était comparable à celle d'autres mesures hémodynamiques déjà adoptées dans la pratique clinique. Enfin, dans le Chapitre 5, je présente un modèle mathématique qui décrit la RVC en termes de changements du $PaCO_2$ liés à l'osmolarité du sang. Les réponses prédites par ce modèle correspondent étroitement aux changements hémodynamiques mesurés avec pCASL ; suggérant une contribution supplémentaire à la réactivité du système vasculaire cérébral en lien avec le CO_2.

Mots clés: Reactivité de la vasculature cérébrale, dyoxide de carbone, IRM fonctionnelle, Arterial Spin Labeling, perfusion cérébrale, pression osmotique du sang.

ABSTRACT

Carbon dioxide (CO_2) is a natural byproduct of cellular metabolism, the third most abundant substance of blood, and a potent vasoactive agent. The resistance of cerebral vasculature and perfusion of the brain tissue respond to the slightest change in blood CO_2 content. The physiology of such an effect remains elusive, yet the phenomenon has been widely exploited in studies of the cerebral vascular function. A promising avenue for the assessment of brain's vascular function is to measure the cerebrovascular reactivity to CO_2 (CVR) non-invasively using functional MRI. Quantitative and non-invasive mapping of CVR can be obtained using respiratory manipulations in arterial CO_2 and Arterial Spin Labeling (ASL) to measure the perfusion changes associated with the vascular stimulus. However, concerns related to the sensitivity and reliability of CVR measures by ASL still limit their broader adoption. I considered that a thorough analysis and amelioration of available methods could bring a valuable contribution in the domain of biomedical engineering, helping to advance new diagnostic imaging tools. In this thesis I present a series of studies where I exam the impact of alternative manipulation/ASL methods on CVR measures, and ways to improve the sensitivity and reliability of these measures. I have also included in this thesis a theoretical paper, where I exam the possible contribution of an unappreciated factor in the CVR phenomenon: the changes in blood osmotic pressure induced by the products of CO_2 dissolution.

Apart from a general introduction (Chapter 1) and conclusion (Chapter 6), this thesis comprises 4 other chapters, in which five different research studies are presented in the form of articles accepted for publication in scientific journals. Each of these chapters begins with its own specific introduction, which consists of a description of the background motivating the study and a brief summary of conveyed findings. A detailed account of methods and results can be found in the accompanying manuscript(s). The study composing Chapter 2 compares the sensitivity of two state-of-the-art ASL techniques and show that a recent implementation of continuous ASL, pCASL, affords more robust measures of CVR than older pulsed methods. The study described in Chapter 3

compares pCASL CVR measures obtained using 4 different respiratory methods to manipulate arterial CO_2 ($PaCO_2$) and shows that results can differ significantly when manipulations are not designed to operate at the linear range of the CO_2 dose-response curve. Chapter 4 encompasses two complementary studies seeking to determine the degree of reproducibility that can be attained measuring CVR using the most recent methods. The first study resulted in the technical development of a breathing apparatus allowing simple, safe and robust respiratory CO_2 manipulations. The improved respiratory method was used in the second – neuroimaging – study, in which I and co-authors investigate the sensitivity and reproducibility of pCASL measuring CVR. The pCASL imaging technique was able to detect CO_2-induced perfusion responses in about 90% of the human brain cortex and the reproducibility of its measures was comparable to other hemodynamic measures already adopted in the clinical practice. Finally, in Chapter 5 I present a mathematical model that describes CVR in terms of $PaCO_2$-related changes in blood osmolarity. The responses predicted by this model correspond closely to the hemodynamic changes measured with pCASL, suggesting an additional contribution to the reactivity of cerebral vasculature to CO_2.

Keywords: Cerebrovascular reactivity, carbon dioxide, functional MRI, Arterial Spin Labeling, cerebral perfusion, blood osmotic pressure.

CONTENTS

LIST OF TABLES

LIST OF FIGURES

LIST OF APPENDICES

LIST OF ABBREVIATIONS

MRI	Magnetic Resonance Imaging
fMRI	functional MRI
ASL	Arterial Spin Labeling
PASL	Pulsed ASL
CASL	Continuous ASL
pCASL	pseudo-CASL
de-pCASL	dual-echo pCASL
PICORE	Proximal Inversion with Control for Off-Resonance Effects
QUIPSS	Quantitative Imaging of Perfusion with a Single Subtraction
Q2TIPS	QUIPSS version 2 using thin slice saturation
TR	Time of Repetition
TE	Time of Echo
TI	Time of Inversion
VTI	Variable Times of Inversion
SNR	(temporal) Signal to Noise Ratio
tSNR	temporal SNR
CNR	Contrast to Noise Ratio
BOLD	Blood Oxygenation Level Dependent
DCE	Dynamic Contrast Enhanced
DSC	Dynamic Susceptibility Contrast
PCA	Phase Contrast Angiography
PET	Positron Emission Tomography

CVR	CerebroVascular Reactivity
CBF	Cerebral Blood Flow
CBV	Cerebral Blood Volume
VASO	VAScular Occupancy
EVC	ExtraVascular Compartments
NVC	NeuroVascular Coupling
GM	Grey Matter
WM	White Matter
CPP	Cerebral Perfusion Pressure
MAP	Mean Arterial Pressure
CA	Carbonic Anhydrase enzyme(s)
Lp	Hydraulic conductivity
Hb	Hemoglobin
$CMRO_2$	Cerebral Metabolic Rate of O_2 consumption
NVC	NeuroVascular Coupling
av_{diff}	arterio-venous difference
BBB	Blood-Brain Barrier
BAB	Blood-to-Air Barrier
HRF	Hemodynamic Response Function
RRF	Respiratory Response Function
ET	End-Tidal
Fi	Fraction inspired
FA	Fraction Administered
BH	Breath-Hold
FI	Fixed-Inspired
HV	HyperVentilation
PC	Prospective Control

FR	Flow Rate
HC	HyperCapnia
HO	HyperOxia
CO_2	Carbon dioxide
$FiCO_2$	Fraction of inspired CO_2
PCO_2	Partial pressure of CO_2
$PaCO_2$	arterial PCO_2
$P_{ET}CO_2$	End-Tidal PCO_2
O_2	Oxygen
FiO_2	Fraction of inspired O_2
PO_2	Partial pressure of O_2
PaO_2	arterial PO_2
$P_{ET}O_2$	End-Tidal PO_2
N_2	Nitrogen gas
NO	Nitric Oxide
H^+	Hydrogen ion / proton
HCO_3^-	Bicarbonate
$NaHCO_3^-$	Sodium bicarbonate

GRAPPA	GeneRalized Autocalibrating Partially Parallel Acquisition
MPRAGE	Magnetization Prepared RApid Gradient Echo imaging
FWHM	Full Width at Half Maximum
GRE	GRadient Echo
EPI	Echo Planar Imaging
GLM	General Linear Model(ing)
ROI	Region Of Interest
VC	Visual Cortex

3D	Three Dimensional
MNI	Montreal Neurologic Institute
CV	Coefficient of Variance
SD	Standar Deviation
SE	Standar Error
IS	InterSurgical
TM	Teleflex Medical

CHAPTER 1

INTRODUCTION

The brain is a highly metabolic organ demanding a constant and substantial blood supply [66]. It is estimated that about 15% of the cardiac output flows to the cerebral vasculature. Approximately 80% of that supply flows within two highly pressurized pair of arteries, known as the internal carotids, which are originated nearly mid way between the brain and the heart. The remaining 20% reaches the brain through downstream branches of the vertebral arteries. The ultimate destination of arterial blood delivery is the capillary bed, which consists of a vast array of microscopic vessels, possessing a single layer of endothelial cells devoid of smooth muscle, that rest embedded within the brain [211, 232]. Given the ubiquity of their presence, capillaries are generally considered an integral constituent of the organ's tissue. They provide porosity to the brain, allowing blood to perfuse it. It is at the capillary level that intravascular blood is in its most intimate contact with the organ's surrounding tissue, and where most of the necessary exchange between blood and the brain takes place. At the distal side of the capillary bed, the venular tree passively collects the outflowing blood at a very low and steady hydrostatic pressure.

The cerebral vascular system counts on stringent auto-regulatory mechanisms that grant stability to the brain's perfusion [397]. It has been observed that, in normal conditions, global perfusion of the brain remains unchanged for a wide range of systemic arterial pressures [133]. Cerebral vasculature regulates its resistance (dilating or contracting) in order to preserve the organ's normal perfusion against variations in the body's systemic pressure. The rate of perfusion in the cerebral tissue is not regulated by the pressure exerted on the organ, but rather, on the resistance of its vessels. Another interesting feature of cerebrovascular function is that, cerebral perfusion pressure remains fairly constant for a wide range of different flow/perfusion rates [314]. The brain function is secured by intricate and multi-level mechanisms of resistance regulation (involving neuro- and myogenic reflexes) that allow cerebral perfusion to change as required while

maintaining cerebral blood pressure under strict control.

To properly function the brain depends on a fit and responsive vasculature. Characterization of cerebrovascular function, *i.e.* its ability to dilate and contract, is gaining increasing interest due to its probable role in age related cognitive decline and in a number of neurological conditions [111, 259, 297]. For instance, arterial stiffness and deficits in cerebral perfusion have been associated with the development of vascular dementia and Alzheimer's Disease (AD) [104, 395]. It has been speculated that deficiencies in the auto-regulatory mechanisms controlling cerebral resistance would impair normal cognitive processes and possibly damage the brain tissue [118, 166]. Measurements of the vasculature response to a stimulus may provide a useful index of the integrity of such mechanisms, aiding the understanding, diagnostics, prognosis and treatment evaluation of different cerebral diseases.

Carbon dioxide (CO_2) is the natural byproduct of oxidative metabolism and the most abundant of the blood's constituents after water and NaCl. It also occurs to be one of the most potent vasoactive agents [218]. Although the exact mechanisms remain to be elucidated, it has been widely observed that the cerebral vasculature promptly responds to experimental changes in the arterial CO_2 content (or $PaCO_2$) [116, 193, 215]. Whereas for increasing levels of $PaCO_2$ – known as hypercapnia – the resistance of cerebral vasculature drops, yielding a global increase in cerebral perfusion, for lower $PaCO_2$ levels – known as hypocapnia – there is an increase in vascular resistance and decrease in perfusion. Here the terms hyper- and hypocapnia are used to denote benign and transitory changes in arterial CO_2, not a clinical condition; and we consider that mild to moderate changes in blood CO_2 do not exert a significant influence on brain metabolism, only on its vasculature. The phenomenon has been exploited in the development of functional MRI (fMRI) applications for non-invasive measures of cerebrovascular function, or reactivity (CVR) [67, 104, 184, 224, 297]. In this type of fMRI, perfusion-weighted images are continuously acquired during a respiratory manipulation inducing $PaCO_2$ changes. Analysis of the fMRI signal issues a map of the cerebral perfusion response to CO_2, which is usually normalized by the amplitude of the CO_2 change and termed CVR map.

As depicted by fMRI, perfusion responses (*i.e.* control of vascular tone) can be lo-

calized to regions on the scale of millimeters [299] and possibly less [148]. While it is possible to estimate a global index of CVR measuring changes in the flow velocity of main arteries feeding the brain [1, 325], fMRI-based methods allow an in-depth spatial characterization of CVR [343]. Furthermore, certain techniques allow measuring the amount of blood that, having reached the capillary bed, exchanges with the tissue, *i.e.* tissue perfusion, the prime parameter characterizing blood supply in the organ. In addition to providing an exquisite measurement of the cerebrovascular function, combined fMRI measures of tissue perfusion and blood oxygenation during hypercapnia can be used to estimate the cerebral metabolic rate of O_2 consumption ($CMRO_2$) [156, 158], an important parameter in functional studies of the whole brain. Brain metabolism can also be assessed by Positron Emission Tomography (PET), but PET measures of $CMRO_2$ require the injection of radioactive tracers. Other than emitting ionizing radiation, such tracers have extremely short half-lives, which further limits the applicability of the PET method. A non-invasive and more readily available estimate of $CMRO_2$ based on fMRI-CVR methods, can greatly contribute to brain research and the neuroradiology practice.

Although indisputably valuable, the broader adoption of CVR measures are still hampered by limitations of current methods, which are introduced below.

fMRI methods

A primary concern in the imaging assessment of CVR is the sensitivity and specificity of the imaging method.

The MRI techniques permitting the specific and non-invasive measure of cerebral perfusion are collectively known as Arterial Spin Labeling (ASL) [75, 396, 403, 408]. The ASL method does not depend on the injection of external agents to obtain the perfusion contrast in its images: to create the perfusion contrast, ASL uses spatially-selective inversion to make blood water temporarily function as an endogenous contrast agent. The ASL – or perfusion-weighted – image is in fact the result of a subtraction between two images: a labeled and a control one. These two images are virtually the same except for the additional label signal in one of them, which accounts for the ASL perfusion contrast. The ASL labeling is accomplished by preparatory MR pulses that excite the spins

of inflowing blood prior to entering the image region. Image readout is played when the magnetically labeled blood has had time to perfuse the brain tissue and exchange water with the surrounding parenchyma, thereby generating a water-labeled image. The control image is acquired under (nearly) the same experimental conditions except that inflowing spins do not receive the label during the labeling phase. The difference signal in the subtracted control-labeled image corresponds to the amount of brain water that has been renewed during the imaging time (*i.e.* perfusion of the tissue) and is thus a relatively small fraction (<2%) of the raw image signal. At this signal level, thermal and physiological noise severely impact the statistical significance of the perfusion measure, and the low signal-to-noise ratio (SNR) of current readout methods still poses a challenge for the sensitivity of ASL.

In measurements of CVR, however, it is the control over the spin labeling that raises more important concerns [404]. Irrespective of the ASL technique, the large shifts in global perfusion elicited by $PaCO_2$ manipulations can compromise efficiency and timing control of the label, yielding ASL perfusion measures that inaccurately underestimate CVR.

In Chapter 2 of this thesis, I examine the performance of two state-of-the-art ASL methods in measuring perfusion changes induced by a carefully controlled mild hypercapnic challenge. One is a typical implementation of the pulsed type (PASL), wherein a large volume of inflowing blood is instantaneously labeled using a short radio-frequency pulse; the other is a recently introduced variant of the continuous method (CASL), named pseudo-continuous ASL (pCASL), wherein blood flowing through a labeling plane at the level of carotids and vertebral arteries is continuously inverted using phase-modulated radio-frequency energy. My findings will justify the choice of pulse sequence for the the remainder of experimental acquisition composing Chapters 3 and 4 of this thesis.

Functional stimulus

Another aspect to consider in the measurement of cerebrovascular reactivity, is the vasoactive stimulus used to induce the vascular response, namely the $PaCO_2$ manipulation.

Hypercapnia is caused whenever the rate of CO_2 production exceeds the rate of its elimination. That can be achieved, for instance, by supplying someone with air mixtures containing higher amounts of CO_2 than what is normally found in atmospheric air (which is virtually zero). A common strategy is to administer a CO_2 mixture of fixed composition for inhalation, also known as hypercapnic induction by "fixed inspired CO_2 dose" (FI) [110, 188]. The FI method is relatively simple but, because the actual degree of hypercapnia achieved depends on several biometric and physiological parameters, the cerebral blood flow response may vary between subjects. This may not be a concern since end tidal (expiratory) partial pressure of CO_2 ($P_{ET}CO_2$) – a surrogate for $PaCO_2$ [421] – can be readily monitored in subjects and be used to normalize CVR measures [245]. However, in experiments requiring a predeterminate vascular stimulus – such as those reported in Chapter 2 of this thesis – the variable $P_{ET}CO_2$ output might represent a problem. The modest changes in blood oxygen levels during the FI CO_2 manipulation may also render the method unsuitable for experiments requiring a stringent control over this variable.

Over the last ten years, interest has emerged in systems for the prospective and independent targeting of specific $P_{ET}CO_2$ and $P_{ET}O_2$ values. Perhaps the most advanced example is the Thornhill Research Inc. (TRI) RespirAct [306, 341, 348]. Others include the simple contrivance for clamping $P_{ET}CO_2$ and $P_{ET}O_2$ despite rapid changes in ventilation described by Banzett *et al.* [18] and the system for dynamic forcing of $P_{ET}CO_2$ and $P_{ET}O_2$ described by Wise *et al.* [400]. All of the latter methods involve continuous adjustments of the inspired gas composition, based either on feed-back from real-time monitoring of end-tidal values or physiological (feed-forward) modeling of gas exchange.

We will focus here on the TRI RespirAct system, since it is the closest to commercial availability and was the system employed for experiments reported in this thesis. The RespirAct uses a prospective control approach: prior to the experiment, based on a comprehensive model of gases storage-exchange in the body compartments, the system computes the composition of gas mixtures to be inspired in order to achieve a desirable end tidal output and then delivers gas mixtures with variable compositions according to a

predetermined schedule. The system is supplied with 4 gas mixtures of different O_2 and CO_2 composition enabling a variety of different respiratory challenge schemes. To ensure control over administered gases, the gas delivery is achieved using a special breathing circuit that is usually sealed to the subjects' face using adhesive tape. Also, subjects need to be instructed to empty the gas supply reservoir of the circuit at every breath. Despite the versatility and robustness of this gas method, availability of the RespirAct system has been restricted to research sites due to its cost and limited production as an investigational device.

Hypercapnia can also be induced without any gas administration, by simply performing a breath-hold (BH), *i.e.* suspending elimination of endogenously produced CO_2 [187, 269, 340]. Although the simplest of the hypercapnic manipulations, BH methods pose several concerns such as its applicability in subjects who may be unable to follow instructions, the short duration of the manipulation, the impossibility of measuring expired CO_2 levels during the breath-hold, and potential confounds associated with concurrent hypoxia (the breath-hold also interrupts reposition of O_2) .

The above-mentioned methods represent a wide variety of trade-offs between simplicity and rigor. Although the TRI RespirAct system has been compared favorably against fixed-inspiration methods, it is possible that simple enhancements to FI methods (such as paced breathing and careful monitoring of end-tidal values) may render these competitive with prospective targeting systems such as the RespirAct. There also remains a widespread interest in the BH methods due to their simplicity and availability. A thorough analysis of these alternate methods should allow researchers and clinicians to select the most appropriate technique for a given application.

In Chapter 3 of this thesis I compare CVR measures obtained using the BH, the FI and the RespirAct methods, in an experimental set of well controlled conditions.

Measurement reproducibility

The clinical adoption of CVR methods hinges on the reproducibility of related measures as well as on the availability of imaging/stimulation techniques.

Because of their simplicity and few confounds, fixed-inspired (FI) approaches con-

tinue to be the most widely adopted method to induce blood gas changes. In addition, as will be demonstrated in Chapter 3 of this thesis, the FI method can provide robust measures of CVR. These make the FI method a good candidate to integrate CVR imaging methods for clinical use. Nevertheless, the respiratory apparatus commonly utilized to deliver gas mixtures still limit the reproducibility of FI respiratory stimuli and related fMRI responses.

The study in Chapter 2 shows that the pCASL perfusion imaging technique is more sensitive and accurate than PASL in measuring CVR, thus constituting a more suitable imaging method for this type of application. Also, the scientific community seems to have converged to a consensus that pCASL is the technique with the most potential to promote the clinical adoption of ASL perfusion imaging in a broader sense [7] – the method has quickly popularized and become available in most scanner platforms. Pseudo-CASL has already been tested in different applications and a recent report shows that its measures of resting perfusion are more reliable than those obtained with PASL [61]. The degree of reproducibility of pCASL measures in applications involving modulations in blood gases, however, remained to be determined.

In the first study of Chapter 4 I propose refinements to the FI method that improve reproducibility of its respiratory manipulations. In the second study I examine the reproducibility of pCASL measures in a gas-based application exploiting the improved FI approach.

CVR signal modeling and interpretation

The magnitude of CO_2-induced perfusion responses is usually computed by linear modeling of the perfusion signal based on basis functions that can be summed to represent the anticipated time-domain MRI signal [107, 128, 347]. The basis function (also referred to as regressor) representing the CO_2 response may consist of the monitored values of $P_{ET}CO_2$ for instance. Alternatively, the design of the respiratory paradigm (representing the periods of increased/decreased $PaCO_2$) can be convolved with a hemodynamic response function (HRF) corresponding to the impulse response function in a linear system. This HRF usually consists of a gamma variate function, derived from

an empirical observation of responses to brief neuronal stimulation [34, 123, 407], but HRFs specific to respiratory responses have also been proposed [27]. Although both of the above mentioned modeling methods can afford robust estimates of the magnitude of CO_2-responses, they do not account for the physiology underling the CVR phenomenon.

In fact, the underpinnings of CO_2 reactivity remains elusive [419]. Several physiological parameters have been shown to impact on the vascular response to blood CO_2; however, the exact mechanisms and interactions between them, are still uncertain. Pioneer investigators of CVR once formulated a thorough quantitative description of the phenomenon but the responses predicted by the model were found to be slower than the responses observed experimentally, and the authors concluded that a faster mechanism should be involved [130]. In that study, as in others [373], the osmotic effects induced by CO_2 dissolution have not been contemplated. When dissolved in blood, CO_2 increases HCO_3^- concentration and blood osmotic pressure [32], to which the cerebral and other vasculature are also quite reactive [43, 112, 140, 362]. It is possible that the vascular reactivity to CO_2 includes the participation of blood HCO_3^- and osmolarity.

In Chapter 5 of this thesis I investigate the role of osmotic forces in the vascular reactivity to CO_2. I present a mathematical model relating $PaCO_2$ to blood osmolarity, linking the latter to cerebral perfusion changes, and show that the predicted responses are in close agreement with the CO_2-induced hemodynamic changes observed using ASL. The proposed model can be regarded as a physiologically meaningful CO_2-HRF. It relates vascular reactivity to gaugeable physico-chemical phenomena; and explains how physiological parameters such as resting blood volume and blood-brain-barrier (BBB) permeability may be reflected in the ASL perfusion signal.

CHAPTER 2

PULSED AND CONTINUOUS ASL IN CVR

The objective of this study was to compare the performance of pCASL and PICORE Q2TIPS PASL in measuring global perfusion responses elicited by mild hypercapnia in a clinical 3T scanner.

♯

2.1 Arterial Spin Labeling

Arterial Spin Labeling is a class of MRI techniques allowing dynamic, quantitative and non-invasive imaging of tissue perfusion [7, 77, 87, 294, 399, 403]. Unlike contrast-enhanced imaging techniques, ASL does not require an exogenous contrast agent to generate its perfusion-weighted image. In ASL, the perfusion tracer consists of arterial blood water that has been temporarily labeled by radio-frequency (RF) pulses. The RF labeling pulses invert the magnetic polarity of blood water spins right before they flow into the image region, resulting in a small flow-dependent contrast. If this image is then subtracted from a control image, acquired under the same conditions except without the labeling pre-pulses, the resultant difference image will include only the flow-dependent signal. The intensity of this image is a function of the amount of tagged blood perfusing the region of interest in the interval between labeling and image readout [48, 51, 75, 384, 404, 410].

This approach provides a specific measurement of perfusion, unlike the more widely applied blood oxygenation level-dependent (BOLD) MR contrast mechanism [198, 228]. Although more sensitive than ASL in detecting hemodynamic changes, BOLD provides an ambiguous measure that depends on different physiological parameters such as blood flow, blood volume and rate of oxygen extraction/consumption [49, 157]. Other than a vascular component, the BOLD signal has a contribution from cellular respiration. ASL may be employed in place of BOLD when it is desirable to focus on purely vascular re-

sponses, such as studies of a pathology which may have separate vascular and metabolic components. Recent applications of ASL include characterization of cerebral vasculature function by a measure of the hemodynamic response to changes in the arterial content of CO_2 ($PaCO_2$) [9, 188, 274]. In this modality of functional MRI, the functional stimulus consists of experimental hypercapnia (increased levels of $PaCO_2$), a vascular stimulus inducing global increases in cerebral perfusion. The resulting functional maps depict the spatial distribution of the cerebral vasculature reactivity (CVR) to CO_2, an index that may be used to estimate the brain's vascular health. These CVR measures can also serve to 'calibrate' the BOLD signal, *i.e.* to factor out the contribution of flow and volume from the latter signal, allowing estimates of cerebral metabolic rate of oxygen consumption ($CMRO_2$) [44, 106, 158]. While $CMRO_2$ estimates can be obtained with other nuclear medicine imaging techniques, fMRI methods provide a measure that is absolutely non-invasive. Functional MRI of the cerebral reactivity to CO_2 may become an important tool in the clinical assessment of both vascular and metabolic functions in the brain; however, limitations in the ASL methods still pose a challenge to their broad adoption.

ASL methods can be classified into pulsed and continuous types, or PASL and CASL respectively. While in PASL the magnetic labeling, or inversion, of spins is achieved instantly (<30 ms) using a magnetic pulse, in CASL spins are gradually inverted by a continuous (typically 1-2 s) MR stimulation.

2.2 Continuous ASL

In CASL, a slice selective gradient defines a labeling plane intersecting the major arteries of the neck while a low amplitude RF irradiation is continually (1-2 s) applied to invert the spins that flow through that plane (Figure 2.1 right) [298, 308, 396]. From entering to leaving the labeling plane the inflowing spins undergo what is denominated a flow-driven adiabatic inversion [246]. Efficiency of this adiabatic inversion is a function of sequence parameters (*viz.* gradient strength and energy of the RF radiation) and velocity of flowing spins [277]. During the labeling period, tagged spins travel from the

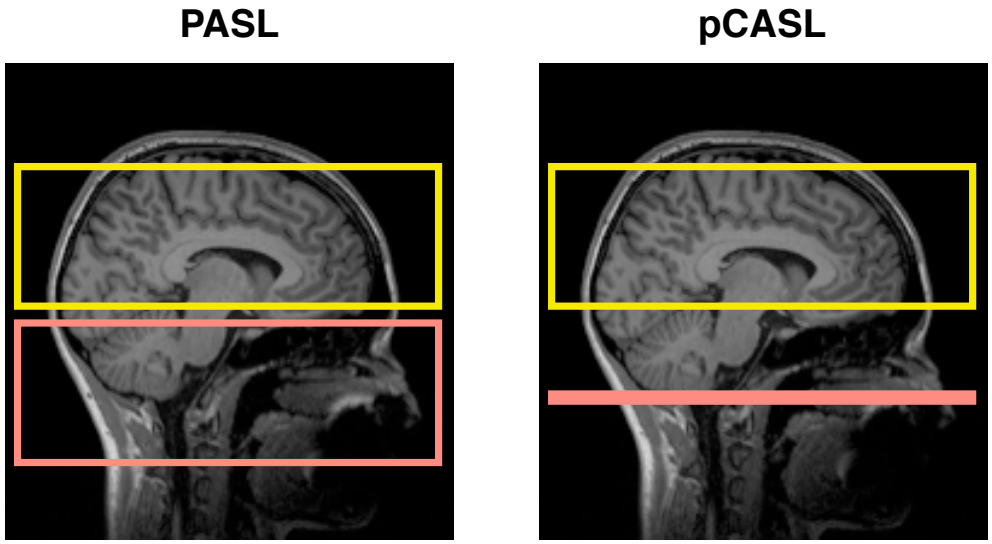

Figure 2.1: PASL and pCASL labeling schemes. In PICORE PASL an inversion pulse (red) is applied at the level of the neck to label a fixed volume of blood. After the inversion, at TI_1, saturation pulses are applied to the label slab to impose a fixed duration to the bolus tag. Image (yellow) is acquired at TI_2 when the entire bolus should have been delivered to the tissue. In pCASL a long train of low-energy RF pulses (red) is applied below the imaging region, also at the level of the neck. The blood spins passing through the labeling plane during the labeling period undergo an adiabatic inversion, continually accumulating in the tissue. Image readout (yellow) is played after a delay to allow complete delivery of tagged blood.

labeling to the imaging plane, gradually accumulating in the parenchymal tissue there. The image is acquired after a delay, which is intended to minimize contribution of large arteries to the perfusion signal and ensure that the perfusion quantification is accurate [4, 265]. At the moment of acquisition, accumulation of spins in the parenchymal tissue should have peaked and label signal be exhibiting a decay [1].

As mentioned above, efficiency of continuous labeling depends on the flow velocity of spins crossing the labeling plane [404], which vary along the labeling period due to the pulsatile nature of arterial flow [409]. Although sensitive to physiological variations in arterial flow, CASL labeling efficiency is in fact estimated as the average efficiency along the whole period of labeling, which will vary little from acquisition to acquisition; at least under normal conditions. On the other hand, during hypercapnia, when flow

1. Labeled spins start to decay immediately after the label, however, as they accumulate in the parenchyma, the labeled image signal increases despite the T_1 decay. The label signal begins to decay when blood delivery is complete.

velocity in the main arteries can be significantly increased, drops in the mean label efficiency of CASL might yield underestimated measures of perfusion – a concern for the assessment of CVR.

A major concern that is common to virtually all ASL methods is the control over off-resonance effects: the spurious effects of the labeling irradiation on the spins pertaining to the image region [406]. The control is usually achieved by duplicating the off-resonance effects of labeling on the control image so that the effect is cancelled in the subtracted image. In CASL however, such control becomes impracticable in multi-slice acquisitions due to the geometry of the labeling [74]. Off-resonance effects can be minimized by performing the labeling with a dedicated coil of narrow radiation aperture, placed directly over the region of the neck where flowing spins are to be labeled [361, 424]. Nonetheless, the dual coil approach requires special hardware, has a strong dependency on the labeling geometry and adds to the distance between the label and imaging plane (which reduces the labeled image signal). An alternate method for the control of CASL off-resonance effects in multi-slice imaging includes the amplitude modulation (AM) of the labeling RF [5, 387]; however, the latter approach is exceptionally energy demanding and its labeling efficiency is usually limited due to safety constraints for RF power deposition (particularly at high magnetic fields). Another obstacle for the implementation of CASL methods is the limited support for the continuous mode of RF irradiation offered by standard MRI hardware. Clinical scanners are optimized for pulsed RF operation, often precluding the use of heavy duty cycles implicated in CASL.

A recently introduced variant of CASL, named pseudo-continuous ASL (pCASL) [72, 408], emulates the continuous labeling method by replacing the continuous RF irradiation with a train of short pulses of approximately 500 μs duration; and creates the control image based on the re-inversion of spins instead of mimicking the label pulse in a distal plane. While more compatible with standard clinical MR hardware, this strategy offers control over off-resonance effects in multi-slice imaging and also higher labeling efficiency than the original continuous method.

2.3 Pulsed ASL

In PASL, the labeling is achieved using a short and strong RF pulse (10-30 ms) that instantaneously inverts a large volume of blood spins [403]. As opposed to CASL, PASL labeling is insensitive to the velocity of spins, reaching a nearly optimum ($\sim$95%) inversion efficiency that is not affected by flow velocity [404]. Among the several different PASL geometries, PICORE (Proximal Inversion of magnetization with a Control for Off-Resonance Effects) is probably the most widely adopted scheme and the one which most resembles the CASL approaches (Figure 2.1 left) [403]. As the name implies, in PICORE PASL the labeling is applied proximal to the imaging plane, *i.e.* at the level of the carotids and vertebral arteries. Slice selective gradients define a labeling band of 10-20 cm thickness, placed parallel to and nearly 1 cm below the imaging band. The gap between the labeling and imaging bands is intended to preserve the spins in the imaging band from spurious excitation due to imperfections in the spatial profile of labeling pulses. Labeling is then followed by a delay to give time for the whole volume of tagged blood to leave the labeling plane, cross the gap and arrive at the imaging region before the readout (the interval is known as Time of Inversion, TI). For the acquisition of the control image, the labeling pulse is repeated with a shift in its center frequency and in the absence of the accompanying band selective gradient, which allows duplicating (controlling for) the off-resonance effect of the labeled image without the effective labeling of spins [2].

The signal of a PASL subtracted image – similarly to CASL – is proportional to the amount of tagged blood that has accumulated in the tissue during the period between the labeling and imaging readout. Put differently, the volume of tagged blood contributing to the PASL signal is proportional to the blood flow (volume by unit time) multiplied by a duration (time). However, the bolus of labeled blood created by the PASL labeling pulse has a fixed volume, making it impossible to determine flow differences. Accurate flow quantification is possible by acquiring a series of subtracted perfusion images at variable inversion time delays from the inversion pulse and fitting the tag inflow curve with a

2. The spurious excitation of off-resonance spins in the imaging band (off-resonance effect) is further mitigated by complementary fat saturation applied to the imaging band just prior to the labeling pulses.

kinetic model of the bolus time dependence. Nonetheless, such variable TI techniques are time consuming [248] and may not be an option, particularly in cases involving vascular stimulation by hypercapnia. One approach to control for the label duration – hence avoiding inaccuracies associated with changes in the latter parameter when estimating flow with a single TI subtracted image – is to impose a fixed duration to the bolus by saturating the MR signal in the tag region at a fixed time after the labeling pulse. This is the essence of techniques such as Quantitative Imaging of Perfusion with a Single Subtraction (QUIPSS) version II [405] and its variant Q2TIPS [241]. In Q2TIPS the saturation consists of a series of saturation pulses applied to a thin slice at the distal end of the tag band (proximal to the image band). These methods will ensure a fixed label duration as long as the trailing edge of the tagged blood bolus does not exit the initial tagging region before the saturating pulses are applied.

The initial, and most widely adopted, implementation of the QUIPSS II method used an interval TI_1 between the inversion and the onset of saturation pulses of 700 ms, with a label band thickness of 100 mm [176, 389, 405]. The interval TI_2 between the inversion pulse and the excitation pulse for the first slice was 1400 ms. This study showed that, at global CBF rates observed during rest or during moderate focal activation such as that produced by finger tapping, the trailing edge of a 100 mm label bolus would take longer than 700 ms to exit the initial tagging region (meaning that the QUIPSS II saturation would control the tag duration). However, during global flow increases, which are known to have a large impact on the flow velocity in the major arteries feeding the brain [20, 303], it is quite possible that the trailing edge of the label bolus will clear the tag region prior to TI_1, rendering any QUIPSS II saturation pulses ineffective and creating a situation that may underestimate flow. This concern can be mitigated to some extent by using a thicker label slab (*i.e.* 150-200 mm), but in general there may always be some level of global flow above which the control of label duration by spatially selective saturation becomes ineffective. A comparison of results obtained with different tag widths is shown in the Appendix I. It should be noted that wide tag bands accentuate the spurious effect caused by imperfections in the label band profile; longer pulses or larger gaps may be necessary to compensate for that, both of which tend to reduce SNR.

2.4 Pulsed *vs.* Continuous ASL in measuring CO_2-induced CVR

PASL has long been the predominant form of ASL, possibly due to simpler implementation and broader compatibility with available MRI hardware. CASL, which has been actually the earliest ASL method proposed, offers several theoretical advantages but its adoption has been limited due to the complexity of controlling for off-resonance effects in multi-slice scans and the high transmitted RF power demanded. The recent introduction of pCASL methods, which emulates the continuous irradiation with a pulsed-like strategy, has allowed the more widespread adoption of the CASL approach [7].

A possible advantage of CASL, and variants such as pCASL, for quantification of flow changes during hypercapnia (*i.e.* CVR) is that it provides an implicit control over the label duration (the time-width of the label equals the labeling time). Such techniques also offer an increase in the SNR of individual flow subtraction images, albeit at the expense of a slightly lower imaging rate (which reduces statistical power). A potential confound in CASL methods (including pCASL) is that the labeling efficiency may suffer from B_0 inhomogeneities [175]; and vary if there are large changes in arterial flow such as in CVR measures [13]. However, because of the use of a short gap between RF pulses in the pCASL implementation, the label efficiency is relatively insensitive to potential field inhomogeneity effects at the typical labeling location for a range of flow velocities. Dai *et al.* showed that pCASL label efficiency is at least 80% as long as field inhomogeneity is within 3 ppm at 3T [72]. This value was estimated based on theoretical calculations by Wu *et al.* [408] in which the flow velocity was varied from 20 to 80 cm/s, and further verified experimentally in a recent study using phase-contrast MRI as the reference [13]. Dependency of labeling efficiency on flow velocity still poses a challenge to CVR measures using CASL and variants.

A number of groups have published ASL measures of the increase in perfusion produced by hypercapnia. At the time of the present study, most other studies had used pulsed ASL, whereas only two had used CASL or variants. Table 2.I summarizes studies (from 2000 to 2010) reporting measures of CVR using ASL and respective differences in in terms of instrumentation and vascular stimulus used (based on references

[8, 13, 47, 60, 139, 188, 225, 256, 274, 293, 353]). CVR measures had been usually reported using a massive average over grey-matter (GM) although some groups have also been interested in measuring CVR in the visual cortex (VC) for other purposes (often to investigate the relationship between CVR and visually-evoked fMRI responses). "Present data" refers to results obtained in this Chapter's study. The type and sub-type of labeling approach adopted, *i.e.* whether the labeling was pulsed or continuous, what was the specific type of geometry and whether the sequence included any control for label duration, are indicated in the second and third column: "ASL type" and "Variant." As it can be seen, in that period, only two studies had reported CVR using the continuous approach. The vast majority of studies used PASL PICORE with QUIPSS II control for label duration. Next columns show, differences regarding sequence parameters such as "slab" thickness and inversion times ("TI_1" and "TI_2") in PASL; and label duration in CASL ("duration"). Methods also differed with respect to the stimulus, *i.e.* the hypercapnic "Manipulation". Gas manipulations had been carried out mostly using fixed-inspired method, and lately the RespirAct apparatus. The doses administered for inhalation ("CO_2 dose") and elicited changes in end-tidal CO_2 levels ($\Delta P_{ET}CO_2$) are also reported. And finally, the population studied (all healthy subjects), ASL CBF measures ("%ΔCBF") and computed "CVR" are given in the 3 right most columns. CVR values shown in italics were not reported in the actual study; they have been computed from reported changes in CBF and $P_{ET}CO_2$.

Paper	ASL Type	ASL variant	slab (cm)	PASL TI1 (ms)	TI2 (ms)	CASL duration (s)	Manipulation	CO_2 dose (%)	$\Delta P_{ET}CO_2$ (mmHg)	Field (T)	Population	ΔCBF (%Δ)	CVR (Δ%CBF/mmHg)
	Measured in GM												
Stefanovic 2006	PASL	PICORE / QUIPSS II	15	500	1100	–	Fixed-inspired	5.0	8.0	1.5	adult	20	*3*
Stefanovic 2006	PASL	PICORE / QUIPSS II	15	500	1100	–	Fixed-inspired	10.0	21.0	1.5	adult	70	*3*
Nöth 2006	PASL	PICORE / QUIPSS II	10	600	1300	–	Rebreathing	–	6.0	1.5	adult	24	*4*
Stefanovic 2006	PASL	PICORE / QUIPSS II	15	500	1100	–	Fixed-inspired	7.5	13.0	1.5	adult	50	*4*
Kastrup 2001	PASL	FAIR	–	–	1200	–	Fixed-inspired	5.0	13.0	1.5	adult	87	*7*
Kastrup 2001	PASL	FAIR	–	–	1200	–	Breath-Hold	–	–	1.5	adult	62	*7*
Mark 2010	PASL	PICORE / QUIPSS II	10	700	1300	–	Fixed-inspired	10.0	11.3	3.0	adult	18	*2*
Mark 2010	PASL	PICORE / QUIPSS II	10	700	1300	–	Fixed-inspired	5.0	3.3	3.0	adult	11	*3*
Mark 2010	PASL	PICORE / QUIPSS II	10	700	1300	–	RespirAct	–	4.7	3.0	adult	16	*3*
Present data	**PASL**	PICORE / QUIPSS II	**16**	**700**	**1400**	**–**	**RespirAct**	**–**	**4.8**	**3.0**	**adult**	**14**	***3***
Mark 2010	PASL	PICORE / QUIPSS II	10	700	1300	–	Fixed-inspired	7.5	5.2	3.0	adult	13	*3*
Mark 2010	PASL	PICORE / QUIPSS II	10	700	1300	–	RespirAct	–	7.0	3.0	adult	20	*3*
Mark 2010	PASL	PICORE / QUIPSS II	10	700	1300	–	RespirAct	–	10.0	3.0	adult	29	*3*
Chen 2010	PASL	PICORE / QUIPSS II	15	700	1300	–	RespirAct	–	-3.0	3.0	adult	–	*4*
Chen 2010	PASL	PICORE / QUIPSS II	15	700	1300	–	RespirAct	–	-6.0	3.0	adult	–	*4*
Chen 2010	PASL	PICORE / QUIPSS II	15	700	1300	–	RespirAct	–	4.5	3.0	adult	–	*5*
Nöth 2006	PASL	PICORE / QUIPSS II	10	600	1300	–	Rebreathing	–	6.3	3.0	adult	29	*5*
Bulte 2009	PASL	PICORE / QUIPSS II	10	700	1400	–	Fixed-inspired	4.0	6.5	3.0	adult	30	*5*
Nöth 2008	PASL	PICORE / QUIPSS II	10	600	1300	–	Rebreathing	–	5.7	3.0	adult	32	*6*
Chen 2010	PASL	PICORE / QUIPSS II	15	700	1300	–	RespirAct	–	9.0	3.0	adult	–	*7*
Hajjar 2010	CASL	–	–	–	–	–	Fixed-inspired	5.0		3.0	elderly	–	*1*
Present data	**CASL**	**pCASL**	**–**	**–**	**–**	**1.5**	**RespirAct**	**–**	**4.6**	**3.0**	**adult**	**20**	***4***
	Measured in VC												
Present data	**PASL**	PICORE / QUIPSS II	**16**	**700**	**1400**	**–**	**RespirAct**	**–**	**4.8**	**3.0**	**adult**	**25**	***5***
Perthen 2008	PASL	PICORE / QUIPSS II	10	600	1500	–	Fixed-inspired	5.0	8.4	3.0	adult	47	*6*
Ances 2008	PASL	PICORE / QUIPSS II	20	700	1500	–	Fixed-inspired	5.0	6.5	3.0	adult	47	*7*
Leontiev 2007	PASL	PICORE / QUIPSS II	20	700	1400	–	Fixed-inspired	5.0	9.3	3.0	adult	81	*9*
Ances 2008	PASL	PICORE / QUIPSS II	20	700	1500	–	Fixed-inspired	5.0	8.1	3.0	elderly	79	*10*
Aslan 2010	CASL	pCASL	–	–	–	1.7	Fixed-inspired	5.0	8.9	3.0	adult	40	*5*
Present data	**CASL**	**pCASL**	**–**	**–**	**–**	**1.5**	**RespirAct**	**–**	**4.6**	**3.0**	**adult**	**35**	***8***

Table 2.I: ASL measures of CVR in the literature (2000-2010).

Although the reported CASL measures lay within the range determined with PASL, the wide variation in gas manipulations used and small number of CASL publications made it difficult to establish whether there was any systematic difference in apparent reactivity. Considerably more data was available on resting blood flow measured using both PASL and CASL methods, and the average baseline perfusion values indicated that under resting conditions the two methods were comparable (Table 2.II, based on references [23, 52, 57, 121, 154, 274, 275, 285, 298, 361, 384, 387, 412, 416]). While a number of recent studies had compared the sensitivity and quantitative results provided by pulsed and continuous ASL sequences for both baseline flow and in neuronal activation paradigms, there had been no systematic comparison of the performance of these two types of ASL during hypercapnic manipulations. The objective of the following study was therefore to provide such a comparison using a controlled hypercapnic manipulation to ensure a high degree of reproducibility in the end-tidal CO_2 values attained.

For the experiments in this study 10 healthy subjects, aged 18-35 were scanned in a 3T MRI clinical system using a 32 channel head coil. We compared pCASL and PICORE Q2TIPS (a type of PASL) using the commonly adopted TI_1/TI_2 of 700/1400 ms, and a considerably thicker labeling slab of 16 cm. Hypercapnic manipulation was conducted utilizing the TRI RespirAct system, which was set to produce controlled 5 mmHg increases in the subjects' end tidal CO_2, two times along a 10 minute scan. Results of this study have been published in the Journal of Magnetic Resonance Imaging. I and co-authors have concluded that pCASL performs better than PASL in measuring global perfusion changes associated with a mild hypercapnic challenge.

Paper	ASL Variant	Field (T)	Population	CBF in GM (ml/100g/min)
	PASL			
Nöth 2006	PICORE / QUIPSS II	1.5	adult	48
Campbell 2006	QUASAR / QUIPSS II	1.5	elderly	57
Campbell 2006	QUASAR / QUIPSS II	1.5	adult	67
Wang 2002	FAIR	1.5	adult	74
Cavucola 2009	PICORE / QUIPSS II	3.0	-	52
Nöth 2006	PICORE / QUIPSS II	3.0	adult	55
Nöth 2008	PICORE / QUIPSS II	3.0	adult	56
Present data	**PICORE / QUIPSS II**	**3.0**	**adult**	**56**
Ho 2010	QUASAR / QUIPSS II	3.0	adult	57
Cavucola 2009	FAIR	3.0	-	58
Glodzik 2010	FAIR	3.0	elderly	60
Cavucola 2009	QUASAR / QUIPSS II	3.0	-	61
Wang 2002	FAIR	4.0	adult	59
	CASL			
Biagi 2007	-	1.5	adult	58
Parkes 2004	-	1.5	adult	58
Ye 2000	-	1.5	adult	68
Parkes 2004	-	1.5	adult	68
Wang 2002	-	1.5	adult	70
Biagi 2007	-	1.5	teen	79
Biagi 2007	-	1.5	children	97
Pohmann 2010	pCASL	3.0	adult	37
Xu 2009	pCASL	3.0	elderly	43
Xu 2009	pCASL	3.0	adult	48
Wang 2005	-	3.0	adult	50
Talagala 2004	separate coil	3.0	adult	56
Present data	**pCASL**	**3.0**	**adult**	**57**

Table 2.II: ASL measures of resting perfusion (2000-2010). This table brings a summary of the studies reporting ASL measures of CBF during resting conditions. ASL measures differed basically with respect to instrumentation: PASL and CASL variants ("ASL Variants") and magnetic field strength ("Field"). CBF measures in GM are shown in the right most column.

2.5 Stuty manuscript

Comparison of Pulsed and Pseudocontinuous Arterial Spin-Labeling for Measuring CO_2-Induced Cerebrovascular Reactivity

Authors: Felipe B. Tancredi, Claudine J. Gauthier, Cécile Madjar, Divya S. Bolar, Joseph A. Fisher, Danny J. J. Wang and Richard D. Hoge

Status: Published in the *Journal of Magnetic Resonance Imaging* vol. 36, p. 312-321, 2012. DOI 10.1002/jmri.23658

Purpose: To compare the performance of pulsed and pseudocontinuous arterial spin-labeling (PASL and pCASL) methods in measuring CO_2-induced cerebrovascular reactivity (CVR). **Materials and Methods:** Subjects were scanned using both ASL sequences during a controlled hypercapnia procedure and visual stimulation. CVR was computed as the percent CO_2-induced increase in cerebral blood flow (Δ%CBF) per mmHg increase in end-tidal PCO_2. Visually evoked responses were expressed as Δ%CBF. Resting CBF and temporal signal-to-noise ratio were also computed. Regionally averaged values for the different quantities were compared in grey matter (GM) and visual cortex (VC) using t-tests. **Results:** Both PASL and pCASL yielded comparable respective values for resting CBF (56$\pm$3 and 56$\pm$4 mL/min/100g) and visually evoked responses (75$\pm$5% and 81$\pm$4%). Values of CVR determined using pCASL (GM 4.4$\pm$0.2, VC 8$\pm$1 Δ%CBF/mmHg), however, were significantly higher than those measured using PASL (GM 3.0$\pm$0.6, VC 5$\pm$1 Δ%CBF/mmHg) in both GM and VC. The percentage of GM voxels in which statistically significant hypercapnia responses were detected was also higher for pCASL (27$\pm$5% *vs.* 16$\pm$3% for PASL). **Conclusion:** pCASL may be less prone to underestimation of CO_2-induced flow changes due to improved label timing control.

Key Words: ASL, Hypercapnia, Cerebrovascular Reactivity

INTRODUCTION

Hypercapnia is known to elicit a global increase in cerebral blood flow (CBF) [85, 190], a phenomenon that has been exploited in various magnetic resonance imaging (MRI) applications including measures of cerebrovascular reactivity (CVR) [186, 256] and calibrated MRI for estimation of task-induced cerebral metabolic rate of oxygen ($CMRO_2$) changes [9, 158]. These techniques rely on arterial spin-labeling (ASL), which provides dynamic and noninvasive images of CBF.

Pulsed ASL (PASL) has long been the predominant form of ASL, due possibly to simpler implementation and broader compatibility with available MRI hardware. The continuous approach (CASL), which was the earliest ASL method proposed [75], offers several theoretical advantages but its adoption has been limited due to the complexity of controlling for off-resonance effects in multislice scans and the high transmitted radiofrequency (RF) power demanded. The recent introduction of pseudocontinuous ASL (pCASL) methods, which emulate the continuous irradiation with concatenated series of short RF pulses [408], has allowed the more widespread adoption of the CASL approach.

A major factor affecting the amplitude of the ASL subtraction signal is the dynamics of label timing [4, 265, 414]. In PASL, techniques such as QUIPSS I and II [405], and variants such as Q2TIPS [241], have been adopted to impose a fixed duration to the label passage and hence avoid inaccuracies associated with changes in the latter parameter. Label duration is controlled as long as the trailing edge of the tagged blood bolus does not exit the initial tagging region before the saturating pulses are applied. During global flow increases, which are known to have a large impact on the flow velocity in the major arteries feeding the brain [258], it is possible that the trailing edge of the label bolus will clear the tag region earlier, rendering QUIPSS saturation pulses ineffective and creating a situation that underestimates flow.

A potential advantage of CASL (and variants such as pCASL) for quantification of flow changes during hypercapnia is that it provides an implicit control over the label duration. CASL also offers an inherently higher flow contrast, resulting in increased temporal signal-to-noise ratio (SNR) of individual flow subtraction images, albeit at the

expense of a slightly lower imaging rate (reducing statistical power). The longer minimum TR value typically associated with CASL techniques is less of a limitation for hypercapnic manipulations, which tend to use relatively long block designs. A potential confound is that CASL's labeling efficiency may be altered by changes in the arterial flow velocity [13, 298, 404].

A number of recent studies have compared the sensitivity and quantitative results provided by PASL and CASL for both baseline flow and the local responses observed in neuronal activation paradigms [61, 384, 404, 408], but there has been no systematic comparison of the performance of these two types of ASL during hypercapnic manipulations, and in fact very few hypercapnia studies to date have used CASL.

The aim of this study was to compare the performance of two ASL sequences in measuring global CBF responses elicited by mild hypercapnia: one using the widely adopted PICORE Q2TIPS pulsed labeling approach, and one using pseudocontinuous labeling. The local flow responses stimulated by a visual paradigm were also examined.

MATERIAL AND METHODS

Ten healthy subjects were recruited for the study (two females, eight males, ages 24-33). All subjects gave informed consent and the protocol was approved by the Research Ethics Committee of our institution.

Functional MRI Protocol

Each functional imaging run consisted of three blocks of baseline alternated with two blocks of stimulation, each lasting 120 seconds. In two runs the manipulation consisted of a step increase in end-tidal PCO_2 ($P_{ET}CO_2$), while in the other two runs a visual stimulus was used. The order of the conditions was randomly varied between subjects.

Visual Stimulation

The visual stimulus was a black-and-white radial checkerboard, contrast reversing at 16 Hz. The stimulus was presented using an LCD projector (EMP-8300, Epson, Toronto, ON, Canada) onto a translucent screen viewed by subjects through a mirror

integrated into the Siemens head coil. The visual baseline was a uniform grey screen with the same spatial mean luminance as the checkerboard pattern. Subjects breathed atmospheric composition medical air throughout visual stimulation runs.

Hypercapnic Manipulation

$P_{ET}CO_2$ and end-tidal PO_2 ($P_{ET}O_2$) were independently targeted via the administration of gases containing mixtures of O_2, CO_2, and N_2 to a sequential gas-delivery breathing circuit [341] by a computer-controlled gas blender [306] (RespirAct, Thornhill Research, Toronto, ON, Canada). The RespirAct was programmed to maintain a constant $P_{ET}CO_2$ of 40 mmHg and $P_{ET}O_2$ at 100 mmHg at baseline, and iso-oxic ($P_{ET}O_2$ maintained at 100 mmHg) increase in $P_{ET}CO_2$ by 5 mmHg for the hypercapnic stimulus. $P_{ET}CO_2$ and $P_{ET}O_2$ were monitored continuously by the RespirAct and as a safety measure pulse rate and arterial O_2 saturation were also monitored using a pulse-oximeter (InVivo Instruments, Orlando, FL).

The same grey screen and fixation marker used as the baseline condition in the visual stimulation protocol was maintained throughout the hypercapnia runs.

MRI Acquisition

Imaging was performed on a 3 T scanner (TIM Trio, Siemens Medical Solutions, Erlangen, Germany) using a 32-channel receive-only head coil. A T1-weighted anatomical acquisition (MPRAGE with TR/TE/α = 2300/3ms/90° 64x64 matrix and 1 mm^3 resolution) was followed by four functional scanning runs.

Each of the stimulation paradigms (hypercapnia and visual) were carried out with both types of ASL scan (PASL and pCASL). Pulsed ASL was performed using the PICORE labeling geometry [403] with a tag width of 160 mm and a 10 mm gap. The Q2TIPS method [241] was used with TI1/TI2 = 700/1400 ms and stop time 1350 ms. Other sequence parameters were TR/TE/α = 2000/10ms/90°

In the pCASL acquisitions, labeling was performed over a 1.5-second period using a series of 25° Hanning window-shaped RF pulses of 500 μs duration and separated by 360 μs gaps. These were applied along with a 6 mT/m gradient and the labeling plane was placed 100 mm below the center of the imaged volume. A postlabeling delay of

900 ms was used, while other sequence parameters were TR/TE/α = 3000/10ms/90°.

For both types of ASL the same gradient-echo EPI with fat saturation was used (slices 6 mm thick, 1 mm gap, 4 mm in-plane resolution, 64x64 matrix and bandwidth of 3 kHz/pixel), using a partial k-space acquisition factor of 7/8 and GRAPPA parallel imaging (acceleration factor of two [131]). In the PASL scans six slices were acquired, while 16 slices were imaged in the pCASL acquisitions. The different numbers of slices were due to implementation details of the respective ASL sequences; care was taken in subsequent analyses to control for this. The stack of oblique axial slices were positioned to maximize coverage of the occipital lobe and oriented along a plane passing through the trunk and splenium of the corpus callosum.

Image Analysis

All MRI data were analyzed using the Neurolens software package (www.neurolens.org). Image series were first motion-corrected [69], spatially smoothed (6 mm full-width at half-maximum [FWHM] 3D Gaussian kernel), and intensity normalized. The flow-weighted signal was then isolated using linear surround subtraction. Voxel-wise CBF response amplitudes for each condition (visual stimulation or hypercapnia, henceforth referred to as "visual" or "CO_2" conditions) were then estimated by fitting the time-course data with a general linear model (GLM) consisting of a block response term (convolved with a single-gamma hemodynamic response function: HRF time-to-peak = 5.4 sec, FWHM = 5.2 sec) [123] plus a third-order polynomial to model resting flow and drift. Global CBF responses to hypercapnia were estimated by defining a grey matter (GM) region of interest (ROI) mask for each subject. These ROIs were generated through segmentation of the MPRAGE acquisition and resampled to the spatial resolution of the ASL scans [3].

To estimate CBF responses in visual cortex (VC) evoked by the visual and hypercapnic stimuli, ROIs were defined based on activation maps for the visual stimulation data (circular bias was avoided through steps described below). For both ASL types a VC ROI was first derived from the visual activation map by thresholding the T-maps at $P < 0.001$

3. A more detailed description of this procedure is given in next Chapter's manuscript.

and manually removing activated regions outside the occipital lobe. Visual stimulation responses achieved very high significance in most subjects with both techniques, permitting a more stringent threshold P value (0.001) than was later used to assess the detection power for hypercapnic responses ($P < 0.05$). The large visual response meant that the statistical detection of visual responses was substantially "overpowered," making the visual ROI largely insensitive to the exact threshold used (mitigating concerns about potential circularity in this approach).

The threshold T-values were determined as described in [407], which takes into account the brain volume imaged and effective spatial resolution to correct for multiple comparisons. This resulted in slightly different threshold values for different subjects and scan techniques, but these were all very close to an average threshold value of 5.6. To remove the impact of total volume coverage on thresholding, this average threshold value was used in all 18 functional scans.

Since VC masks based on activation masks from a specific technique (referred to as "technique-specific VC") are likely to emphasize voxels with large responses in the respective method, we also generated VC masks that were the "union," or "intersection", of the technique-specific VCs (referred to as union and intersection VC ROIs, respectively). Technique-specific VC ROIs were utilized to compare the results that would be obtained in studies based entirely on one of the two ASL types. To rule out possible bias from ROI differences, we also performed comparisons using common VC ROIs, *i.e.* the union or intersection VC ROIs.

To determine response amplitudes during visual stimulation and hypercapnia, the average GLM "effect-size" (based on the fit parameters, or β's) within the ROI was used as the response amplitude, which was then divided by the ROI-averaged baseline (constant) term from the same model fit (β_0) and multiplied by 100 to convert to percent change. ROI-averaged time series were similarly expressed in percent change by normalizing the signal to the constant fit term after removing drift terms from the GLM fit.

We computed the mean $P_{ET}CO_2$ values for the different conditions (normocapnia and hypercapnia) and the true $P_{ET}CO_2$ increase as the difference between them (transition phases were excluded). The ROI-average CVR was computed by dividing the

average percent change in CBF within the ROI by the $P_{ET}CO_2$ increase in mmHg.

We also computed the ROI-averaged temporal SNR (tSNR) for baseline flow and T-values for both baseline flow and functional responses from the model fit. The number of voxels for which the T-value exceeded a threshold corresponding to $P < 0.05$ was also determined for the different conditions. The tSNR was defined as the baseline CBF signal amplitude (from the constant term of the GLM model fit), divided by the root-mean-square value of the residual error between the measured signal at each voxel and the modeled signal. The use of GLM residuals, as opposed to simple mean and standard deviation values, provides stability measures, which we feel are more closely linked to statistical detection power.

A T-value for the estimate of baseline CBF was also computed (*i.e.* testing the hypothesis that resting CBF was different from zero) as the constant term of the GLM model fit divided by the residual standard error (equivalent to the residual standard deviation adjusted for the number of images, and hence degrees of freedom, in the series). Similarly, T-values were computed for the response amplitudes during visual stimulation and hypercapnia. As a metric of the sensitivity of the two ASL methods for detection of resting flow and visual or hypercapnic responses, we first determined the number of voxels for which the T-value for the condition in question exceeded a threshold corresponding to $P < 0.05$ (corrected). The number of detected voxels was then divided by the total number of voxels in a given ROI (either GM or VC).

Maps of absolute flow – baseline and response to hypercapnia – were also generated using Eq. 1 in Ref. [385] for PASL and Eq. 1 in Ref. [386] for pCASL. For PASL, the following parameter values were used: blood-brain partition coefficient = 0.9, labeling efficiency = 0.95, blood T1 = 1.49 seconds, GM T1 = 1.4 seconds. The same parameters were used for pCASL, except that a labeling efficiency of 0.80 [408] was assumed. Baseline values were subsequently averaged within GM.

As the final analysis step, group averages were computed for percent effect-sizes, the ASL time series, CVR, tSNR, T-value, absolute baseline flow, and detection rate. Results are always shown as the group mean $\pm$ standard error (SE).

Based on the above averages, we tested the hypothesis that PASL estimates of CVR

are systematically lower than those obtained using pCASL by comparing measures from the respective techniques in a one-tailed Student's t-test. tSNR, T-values, and voxel counting were also compared using a one-tailed t-test. The resting flow values from the two methods were compared using a two-tailed t-test.

For qualitative comparisons, unthresholded maps of absolute CBF, tSNR, and various response measures such as effect-size, T-value, and ΔCBF were overlaid on high-resolution anatomic T1 scans. Unthresholded maps were used because this provided the truest depiction of sensitivity and specificity in the data (thresholding can introduce an "iceberg effect," in which slightly subthreshold peaks or regions are obscured).

RESULTS

Data from one subject could not be used due to excessive artifacts in one of the PASL series.

Functional Response Signals

Figure 2.2 shows ROI average time courses recorded using the two ASL methods during visual stimulation and hypercapnia. For hypercapnia, signals are shown for both GM and VC ROIs. It is qualitatively evident that the pCASL signals exhibit consistently better stability. Both techniques yield clearly discernible visual responses.

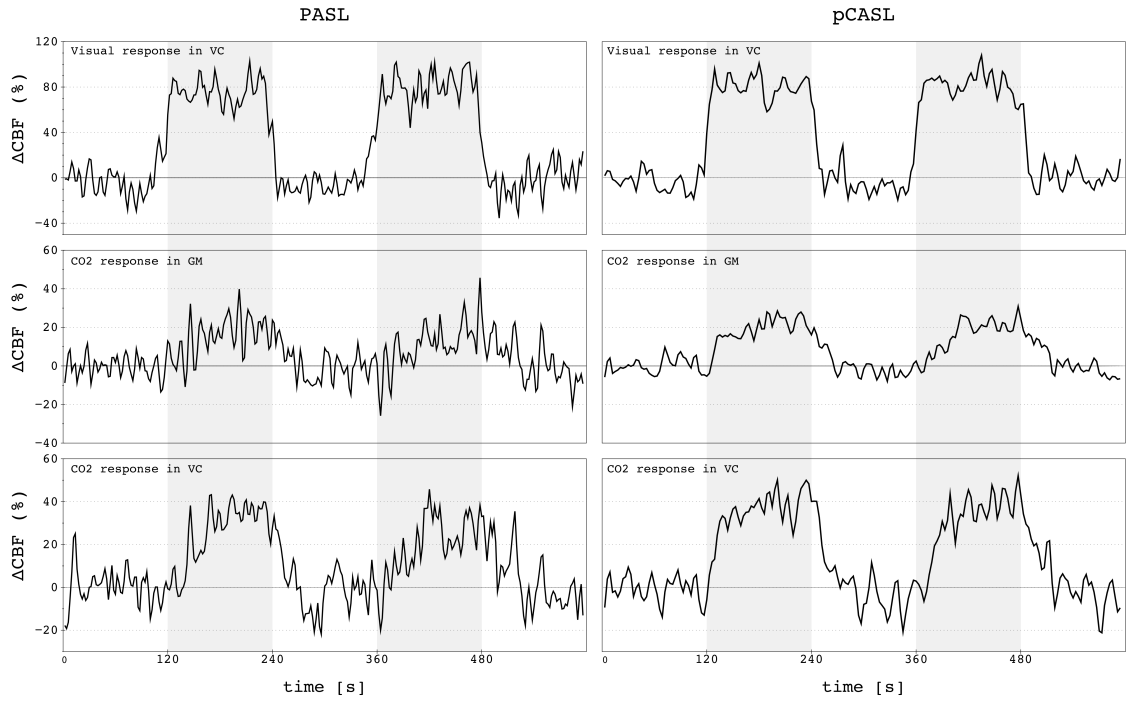

Figure 2.2: ASL signal time courses. ASL signal time courses. Evoked CBF response signals for PASL (left) and pCASL (right) during visual stimulation and hypercapnia. ROI average signals are shown for hypercapnia in ROIs throughout all GM and also restricted to VC. Shaded regions in the plots indicate the 2-minute blocks of stimulation.

Baseline and CO_2 Response Maps

Both PASL and pCASL maps of baseline blood flow, shown in rows 2 and 3 of Fig. 2.3, provided a clear delineation of cortical anatomy – comparable to segmented GM masks shown in top row of the same figure – revealing the expected perfusion contrast between grey and white matter. Baseline CBF values measured in GM were 56±3 and 56±4 mL/min/100g for PASL and pCASL, respectively. Maps of the baseline tSNR (4^{th} and 5^{th} rows) were computed by dividing the baseline blood flow signal (*i.e.* the effect size from the contrast selecting for the constant term in the linear model) by the residual standard deviation. The tSNR of PASL in GM was generally lower and more heterogeneous than that of pCASL. The bottom two rows of Fig. 2.3 show maps of the T-value for the resting flow signal, in which the baseline effect was divided by the residual standard error (taking into account the different imaging rates) instead of the standard deviation. This indicates that the improved per-image tSNR of pCASL and higher imaging

rate of PASL balance each other [13], resulting in roughly equivalent overall statistical power for detection of baseline flow in both cases.

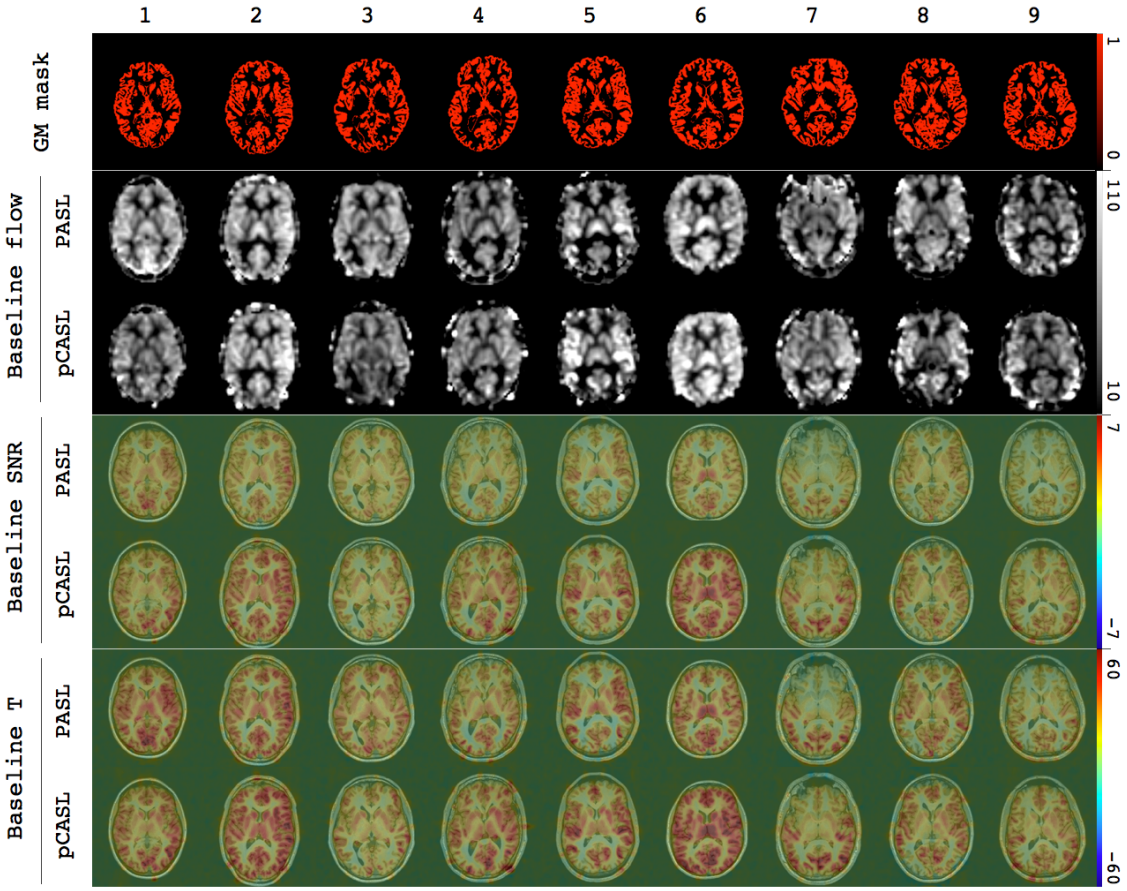

Figure 2.3: GM masks and baseline flow maps. The top row shows automatically segmented GM masks (red color scale) for all subjects. Subsequent rows show baseline flow maps, at the corresponding locations, acquired using PASL and pCASL (in alternating rows). Rows two and three show maps of absolute flow in units of mL/min/100g. Rows four and five show the SNR (β_0 divided by the GLM residual SD) for resting blood flow during the hypercapnia runs. Rows six and seven show corresponding maps of T-statistic (β_0 divided by GLM residual SE).

T-maps computed for the response to hypercapnia (Fig. 2.4, rows 1 and 2) generally exhibited large variations in sensitivity over cortical GM for both techniques. However, this is likely due to spatial variations in the tSNR. Inspection of the raw effect-size maps for this response reveals more homogeneous apparent flow responses throughout cortical GM (rows 3 and 4), particularly for the pCASL sequence (statistical inference is not pos-

sible with these maps, but they are a more direct reflection of the response amplitude). Maps of absolute DCBF (bottom two rows) exhibited similar patterns to the effect-size maps.

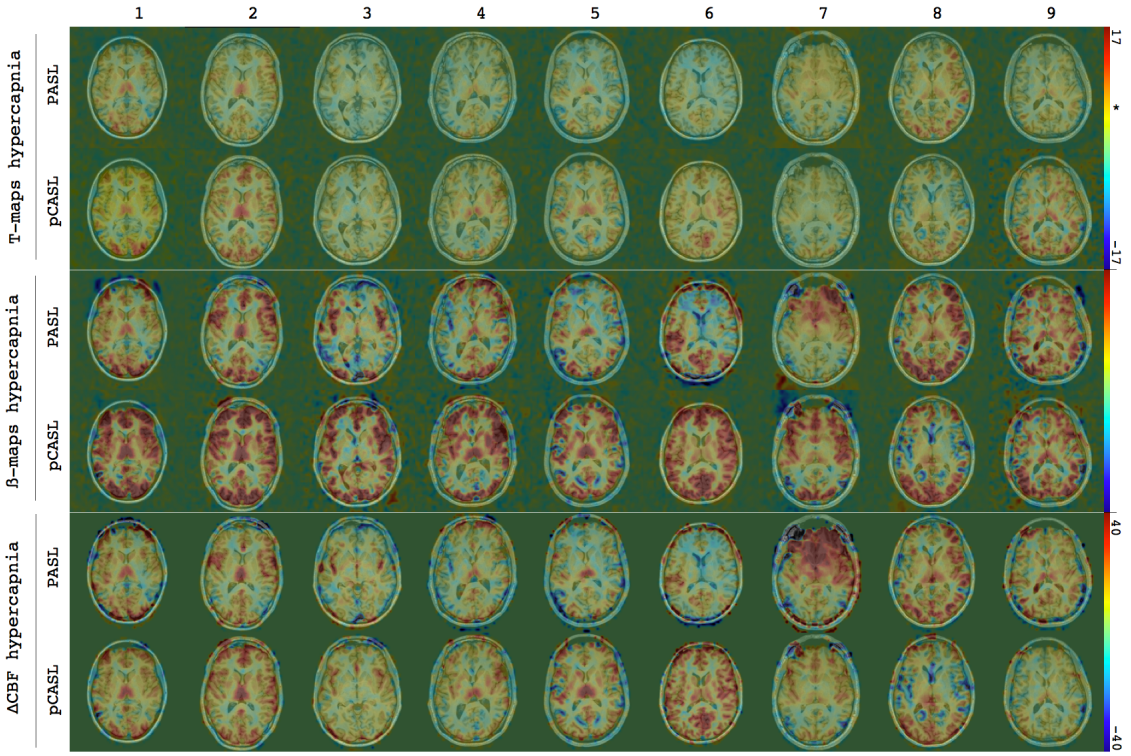

Figure 2.4: Hypercapnia response maps. Rows one and two show maps of T statistic for the CBF response to hypercapnia as measured using PASL and pCASL, respectively. The color mapping for T statistic values has been adjusted so that the transition from yellow to orange, indicated by the star, corresponds to $P < 0.001$ (corrected). Rows three and four show maps of the GLM effect sizes of the CBF response. Rows five and six show the size of the flow change, given in mL/min/100g.

Visual Response Maps and ROIs

In spite of the differences observed between subjects and pulse sequences for CO_2 responses, both PASL and pCASL resulted in similar maps of visual activation, demonstrating good sensitivity and specificity as indicated in the statistical maps shown in the top two rows of Fig. 2.5. These maps allowed calculation of visual ROIs for use in the other quantitative analyses shown below. The ROIs thus computed were of generally

comparable extent and position for both methods.

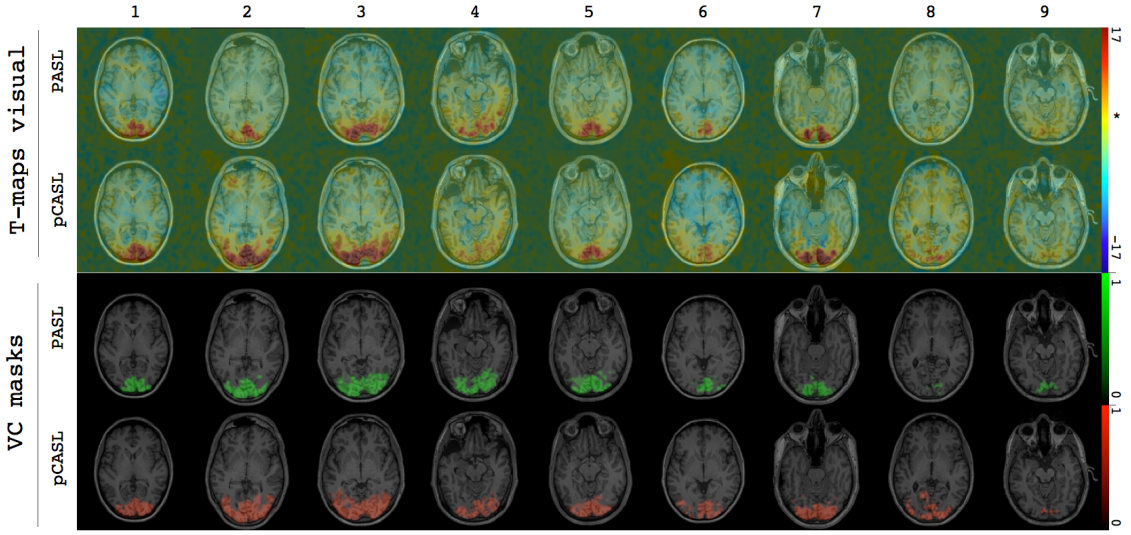

Figure 2.5: Visual response maps and VC masks. Rows one and two show maps of T statistic for the CBF response to visual stimulation for PASL and pCASL data, respectively. The color mapping for T statistic values has been adjusted so that the transition from yellow to orange, indicated by the star, corresponds to $P < 0.001$ (corrected). Rows three and four show ROIs encompassing VC in the different subjects, based on the visual activation data from the respective ASL sequences (green for PASL, red for pCASL).

Temporal SNR of Baseline CBF

Group average tSNR for GM and VC is shown as bar graphs in Fig. 2.6A. The tSNR values computed for pCASL were generally higher than those found for PASL, a difference that achieved statistical significance ($P < 0.01$) in the GM ROI. Respective tSNR values for PASL and pCASL in GM were 1.9 ± 0.1 and 2.4 ± 0.2; those in VC were 2.4 ± 0.1 and 2.7 ± 0.2.

In spite of the higher tSNR of pCASL (Fig. 2.6A), the increased imaging rate of PASL resulted in equivalent statistical power in the two types of image series, leading to similar detection rates for resting blood flow in GM voxels, as shown in Fig. 2.6B. The respective percent detection rates for resting CBF in GM voxels with PASL and pCASL were 93 ± 2 and 95 ± 1. Resting CBF detection rates within the VC mask (*i.e.* the fraction of voxels within the VC that exhibited baseline flow signal significantly different from

0) were 98.1±0.8 (PASL) and 97.5±0.9 (pCASL). Average T-values for resting CBF in GM were 23±2 (PASL) and 25±2 (pCASL); T-values in VC were 29±2 (PASL) and 26±3 (pCASL).

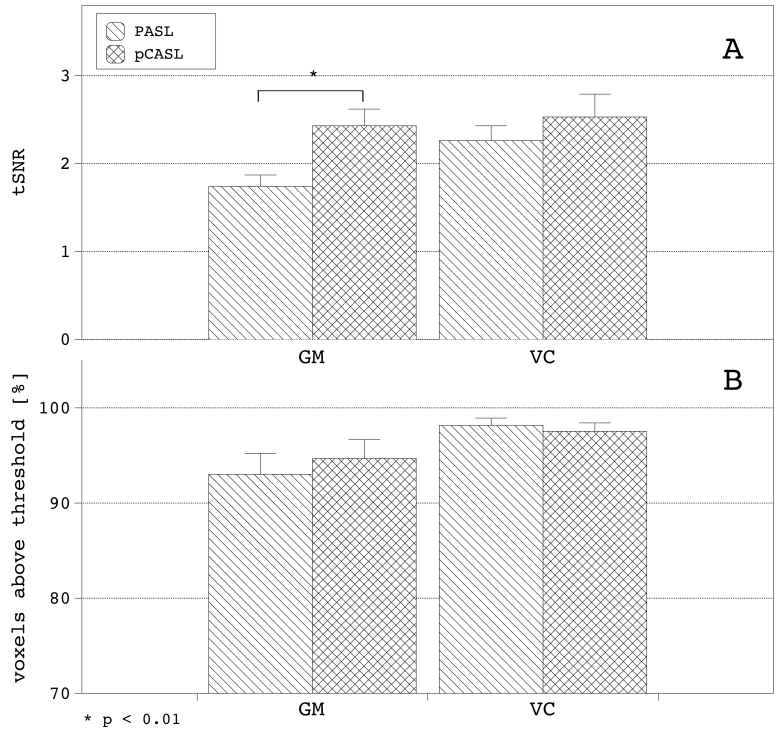

Figure 2.6: Temporal SNR and sensitivity for baseline flow. a: tSNR for baseline CBF (mea±SE) computed in GM and VC. **b:** Percent of GM and VC voxels with statistically significant baseline flow signal.

Functional Flow Changes

The ability to impose targeted changes in $P_{ET}CO_2$ allowed us a high degree of reproducibility of the stimulus. Nonetheless, while individual results demonstrated control within a tolerance of ±2 mmHg in different individuals and scans, the range of CVR measures in GM was much larger in PASL than in pCASL ([0.7-6.1] *vs.* [3.0-5.2] Δ%/mmHg, respectively).

Figure 2.7 shows percent flow increases in response to hypercapnia and visual stimulation obtained using the two ASL sequences in different ROIs (converted, in the case of hypercapnia, to a CVR index by dividing by the increase in $P_{ET}CO_2$). Both methods

show comparable values for the visually evoked flow increases, with the exception of values averaged over the union VC ROI, which were significantly different. For the hypercapnic responses, PASL resulted in apparent CVR values that were systematically and significantly ($P < 0.05$) smaller than those measured using pCASL. This was observed using ROIs covering both all GM and VC. Comparisons were repeated using different criteria for the VC ROIs (*i.e.* technique-specific, intersection, and union VC ROIs) and these were found to provide consistent results in all cases.

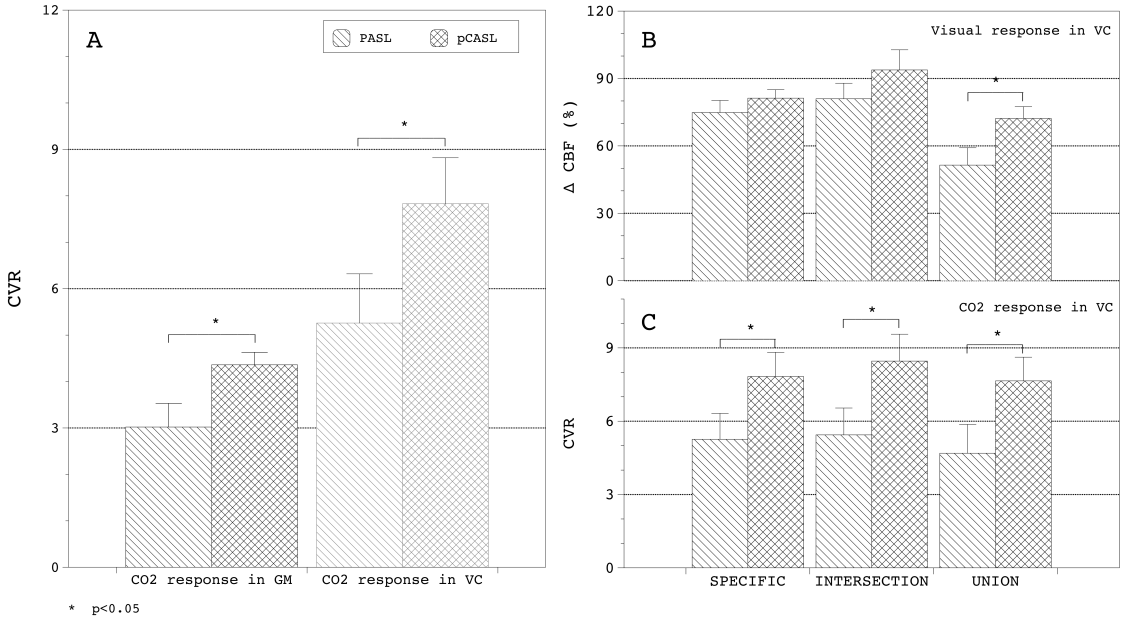

Figure 2.7: CBF responses to hypercapnia and visual stimulation. **a:** CVR to hypercapnia measured in GM and VC ROIs. **b:** Δ%CBF values for visual stimulation in VC. **c:** CVR measured in VC as delineated using alternate ROI selection criteria: 1) technique-specific (this approach is used in A); 2) intersection; and 3) union.

Results for individual subjects and group averages are summarized in Table 2.III.

		Hypercapnia in GM			*Hypercapnia in VC*			*Visual response in VC*
	$\Delta P_{ET}CO_2$ (mmHg)	Baseline (mL/min /100g)	Response (Δ%CBF)	CVR (Δ%CBF / mmHg)	Baseline (mL/min /100g)	Response (Δ%CBF)	CVR (Δ%CBF / mmHg)	Response (Δ%CBF)
PASL								
subject 1	5.3	56.3	17.7	3.3	63.6	26.5	5.0	53.2
subject 2	5.4	64.2	15.5	2.9	59.3	21.8	4.0	70.2
subject 3	4.0	62.0	5.1	1.3	58.6	5.1	1.3	81.1
subject 4	5.7	52.6	15.7	2.8	48.2	29.6	5.2	92.2
subject 5	4.0	52.8	16.3	4.1	47.1	35.0	8.8	61.0
subject 6	4.7	73.4	5.8	1.2	93.7	10.5	2.2	77.2
subject 7	4.7	52.9	3.2	0.7	67.1	11.8	2.5	89.8
subject 8	5.2	49.6	25.8	5.0	52.7	48.3	9.3	94.9
subject 9	3.8	39.4	23.2	6.1	44.6	35.5	9.4	53.9
mean±SE	4.8 ± 0.2	56 ± 3	14 ± 3	3.0 ± 0.6	59 ± 5	25 ± 5	5 ± 1	75 ± 5
pCASL								
subject 1	5.4	50.6	27.4	5.1	49.2	46.0	8.5	74.3
subject 2	5.6	66.8	27.0	4.8	53.1	36.2	6.5	76.5
subject 3	3.9	49.9	16.7	4.3	34.1	26.7	6.8	96.6
subject 4	5.5	54.9	19.4	3.5	49.1	28.2	5.1	68.4
subject 5	4.2	56.2	21.9	5.2	39.0	49.7	11.8	74.9
subject 6	5.1	81.2	15.5	3.0	85.7	12.6	2.5	69.9
subject 7	4.2	57.0	17.4	4.1	43.5	40.4	9.6	83.6
subject 8	4.1	46.0	18.8	4.6	41.2	42.9	10.5	99.6
subject 9	3.7	43.5	18.1	4.9	32.8	35.1	9.5	88.5
mean±SE	4.6 ± 0.3	56 ± 4	20 ± 1	4.4 ± 0.2	48 ± 5	35 ± 4	8 ± 1	81 ± 4

Table 2.III: Individual Baseline Flow and Responses. $\Delta P_{ET}CO_2$ is the increase in end-tidal CO_2 during the hypercapnia scan. Columns 2 and 5 show baseline flow values measured in gray matter (GM) and in the visual cortex (VC) ROIs, respectively. ROI-averaged percent changes, *i.e.* flow responses, are shown in columns 3, 6, and 8. Columns 4 and 7 show cerebrovascular reactivity (CVR) values, computed as the flow response per mmHg of $\Delta P_{ET}CO_2$.

Figure 2.8A shows the average T-values for the hypercapnic response in GM and VC, while Fig. 2.8B shows the corresponding detection rates (the two measures convey related but not identical information about the distribution and extent of the apparent response). The average T-value provided by pCASL for CO_2 response in GM was greater ($P < 0.03$) than that measured with PASL. The PASL average T-value was 2.0 ± 0.3, while that obtained with pCASL was 2.9 ± 0.4. PASL and pCASL average T-values of CO_2 response in VC were: 3.9 ± 0.6 and 5.2 ± 0.6. The difference between the latter values was only marginally significant ($P < 0.08$) with both values higher ($P < 0.05$ and $P < 0.005$) than the correspondingT-values computed in GM. The pCASL sequence detected GM responses to hypercapnia at a significantly higher rate ($27\pm5\%$) than PASL ($16\pm3\%$ detection). In VC the corresponding detection rates for the CO_2 response were 56 ± 7 and 42 ± 9.

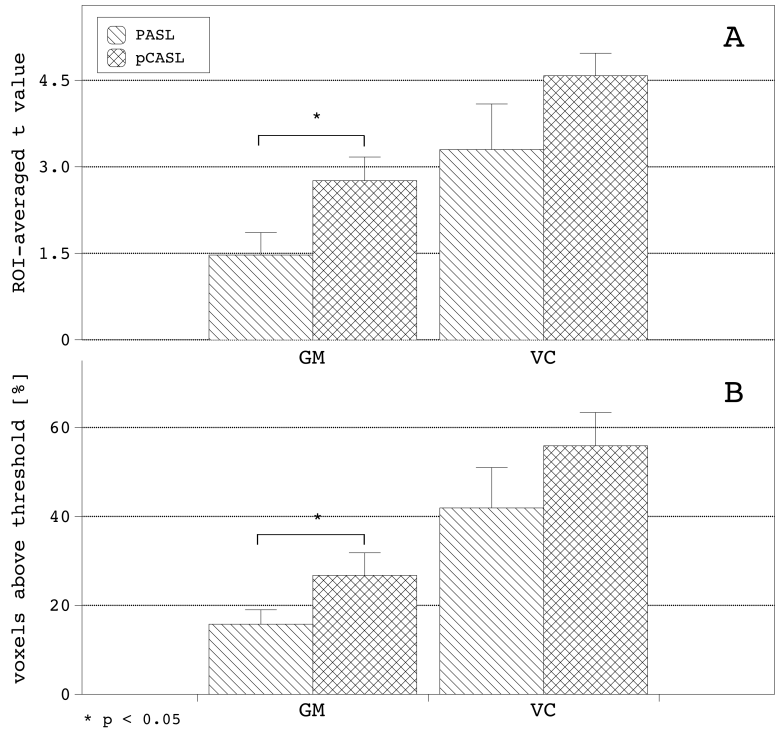

Figure 2.8: Average T-values and detection power for hypercapnic responses. a: Average T statistic values (mean±SE) for the CBF response to hypercapnia measured in GM and VC. **b:** Percent of GM and VC voxels showing statistically significant response to the stimulus.

Visual responses measured by PASL and pCASL in V1 were similar. Although the extent and amplitude of the pCASL response tended to be larger, the differences did not achieve statistical significance. The visual detection counts for PASL and pCASL, respectively, were 290±60 and 400±100 voxels (counts instead of percentage rates are used here because no independent segmentation of VC was available as in the case of GM). The visually evoked percent change in CBF measured by PASL was 75±5%, while that measured by pCASL was 81±4%. Average T-values in V1 for the visual activation were 9.6±0.8 for PASL and 9.7±0.9 for pCASL. ROI average values quoted here are for technique-specific VC ROIs.

While the visually evoked flow response may be stronger than the response to a mild hypercapnic stimulus, the response is local, limited to the VC. The VC, although extensive, is just a fraction of the total volume of the brain, and so is the brain's total flow increase with respect to the local flow increase. We found that the GM averaged flow percent change during visual stimulations were 5±2% and 7±3% for PASL and pCASL, respectively. These two figures correspond to ≈40% of the flow changes in GM as computed to the hypercapnic stimulus.

DISCUSSION

In this study we compared the performance of pulsed and pseudocontinuous ASL sequences for measuring global CBF responses elicited by mild hypercapnia. We also compared results obtained for resting cerebral blood flow and focal visual stimulation. A number of differences were noted, which may be due to the different temporal characteristics of the two labeling approaches.

Early implementations of the QUIPSS II method [403] used an interval TI_1 between the inversion and the onset of saturation pulses of 700 ms, with a label slab thickness of 100 mm (the limited thickness probably due to use of a transmit-receive head coil for inversion). This initial report showed that, at global CBF rates observed during rest or during moderate focal activation such as that produced by finger tapping, the trailing edge of a 100-mm label bolus would take longer than 700 ms to exit the initial

tagging region (meaning that the QUIPSS II saturation would control the tag duration). However, during global flow increases, which are known to have a large impact on the flow velocity in the major arteries feeding the brain, it is quite possible that the trailing edge of the label bolus will clear the tag region prior to TI_1, rendering any QUIPSS II saturation pulses ineffective and creating a situation that may underestimate flow. This concern can be mitigated to some extent by using a thicker label slab (*i.e.* 150-200 mm) as done in the present study, but in general there may always be some level of global flow above which the control of label duration by spatially selective saturation becomes ineffective.

In CASL, the control over the label duration is implicit, thus relieving the latter concern. Such techniques also offer an increase in the tSNR of individual flow subtraction images, although the imaging rate is typically somewhat lower; and a reduction in variability due to pulsatile changes in flow velocity during the cardiac cycle. A potential confound in CASL methods (including pCASL) is that the labeling efficiency may suffer from field inhomogeneities, and vary if there are large changes in arterial flow. However, because of the use of a short gap (360 ms) between RF pulses in our pCASL implementation, the label efficiency is relatively insensitive to potential field inhomogeneity effects at the labeling location. Dai *et al.* showed that efficiency is at least 80% as long as field inhomogeneity is within 3 ppm at 3T. This value was estimated based on theoretical calculations by Wu *et al.* in which the flow velocity was varied from 20 to 80 cm/s, and further verified experimentally in a recent study using phase-contrast MRI as the reference.

Our results in indicate that the intrinsic per-image tSNR of the continuous method remains higher (Fig. 2.3, 4^{th} and 5^{th} rows; Fig. 2.6A). The increased imaging rate of PASL, however, compensates for this, as shown by the maps of T-value (Fig. 2.3, last two rows) and the number of voxels after thresholding of T-maps (Fig. 2.6B). Indeed, PASL and pCASL provide maps (Fig. 2.3, 2^{nd} and 3^{rd} rows) and absolute values of baseline flow that are virtually indistinguishable (Table 2.III), indicating that both methods are good candidates for imaging and quantifying resting CBF in healthy volunteers. Nevertheless, different results might be obtained in the case of abnormally slow flow rates, as

these could exacerbate T_1 label decay, which is more prevalent in pulsed methods.

The most notable differences between the two ASL methods were found in the depiction of the hypercapnia responses. Inspection of the T-maps for the CO_2 manipulation (Fig. 2.4, first two rows) reveals that the anticipated pattern of GM response is poorly demonstrated for most subjects in both PASL and pCASL. This is surprising, since BOLD data during comparable manipulations consistently indicates a very strong hemodynamic response throughout GM. However, the effect-size maps give a more direct indication of the response amplitude (middle two rows) than the T-maps, in which there is a division by the residual standard error. It is likely that the spatial patterns seen in the T-maps are largely driven by the spatial patterns of noise, which tend to obscure the globally uniform GM flow response. When the effect-size maps are considered, it is apparent that pCASL provides a more reliable depiction of the global GM response (note lack of PASL response in large areas of cortical GM in subjects 2, 3, 4, and 7). Although the effect-size maps provide a qualitative depiction of the response pattern, they are closely related to maps of absolute change, which can be computed using the approach described above for resting CBF. Quantitative maps of ΔCBF (bottom two rows) are computed in this way and the response measured by pCASL appears to demonstrate a more uniform depiction of GM flow increases.

The meanT-value for hypercapnic response within the GM and visual ROI masks was consistently higher for pCASL, achieving statistical significance for the average over the GM mask (Fig. 2.8A). This corresponded with increased voxel detection rates by pCASL for hypercapnia, as shown in Fig. 2.8B. This latter bar graph shows the percentage of voxels within the GM and VC masks in which the ASL T-values for hypercapnic response exceeded a threshold corresponding to $P < 0.05$ (corrected). Since it can be assumed that, in reality, all GM voxels underwent increased blood flow in the healthy volunteers imaged in this study, the low detection rates indicate that thresholded T-maps of hypercapnic CBF response are likely to be unreliable for the assessment of CVR, regardless of ASL technique.

Figure 2.7 shows estimated CVR values as measured with PASL and pCASL. The estimated CVR values provided by pCASL are significantly higher than those measured

with PASL in both regions GM and VC. This difference was apparent regardless of the ROI prescription method used (technique-specific, intersection, or union). In contrast, the visually evoked responses were not significantly different, except when averaged over the union of activated areas detected by both methods. This is probably due to both the large amplitude of the visually evoked response and the fact that pulsed ASL tag dynamics are less affected by focal than by global flow changes. It should be noted that, in spite of the large peak amplitude of the visual flow response, when averaged over all GM it represents a substantially smaller increase in whole-brain blood flow ($7\pm3\%$ via pCASL) than hypercapnia (20 ± 1). The difference found for the union ROI can be explained by the fact that pCASL tended to yield visually evoked changes over a more extensive region than did PASL.

Although similar responses were observed for focal flow increases, our results show a systematic reduction in the apparent CO_2-induced flow increase measured with PASL relative to values obtained with pCASL. The demonstration that PASL and pCASL yield virtually indistinguishable values for resting CBF, as well as for visually evoked flow responses, reinforces our suspicion that global physiological manipulations like mild hypercapnia pose a special challenge for PASL methods. Our results suggest that typical implementations of PASL may fail to control tag timing at high CBF rates, thereby underestimating CBF responses.

In conclusion, the use of pCASL instead of PASL may help improve the sensitivity and accuracy of MRI measurements relying on global manipulation such as measurements of CVR and $CMRO_2$.

The lack of a "gold standard" measure of CVR prevents us from ruling out the possibility that pCASL is also affected by sources of systematic error during hypercapnia, such as reductions in labeling efficiency as postulated by Aslan *et al.* [13] (who postulated a 36% underestimation of the CBF change during a 9 mmHg increase in $P_{ET}CO_2$, which could imply an underestimation of CBF change in our 5 mmHg manipulation by up to 20%). Further study using methods such as phase-contrast flow quantification is clearly warranted. Another promising avenue of investigation is the use of pulsed or continuous ASL methods with variable delay times[155], which allow measurement of

the tag inflow curve and, by fitting with kinetic models, quantitative estimation of CBF. These may help refining and validating single-subtraction versions of ASL techniques.

CHAPTER 3

CO_2 MANIPULATIONS

The specific objective of this study was to compare CVR measures obtained using a variety of approaches to manipulate CO_2 levels, including breath-hold and two different gas administration methods.

♯

3.1 Blood and respiratory gases

One of the primary functions of the vascular system is to permit the many tissues of the body to exchange gases with the environment [138]. The blood that is pumped by the left ventricle of the heart circulates through the arterial vascular tree carrying O_2 to be consumed in oxidative metabolism in the tissues. The blood about to perfuse the tissues is rich in O_2 and called arterial blood. At the same time it delivers O_2, the perfusing blood removes byproducts of metabolism from the tissue, mostly CO_2. Following these exchanges, blood leaves the tissue low in O_2 and high in CO_2, being named venous blood. Blood re-arterialization, *i.e.* O_2 replenishment and CO_2 elimination, takes place at the lungs, two organs allowing a protected interface between blood and the external environment – the blood-air-barrier (BAB) – through which gases can passively diffuse. In the lungs, most of the incoming blood consists of the venous blood resulting from the systemic gas exchanges, that is pumped by the right ventricular chamber of the heart. The blood that leaves the lungs is arterial blood that will flow back to the heart and refill its left chambers for recirculation.

The rate of gas exchange between blood and air, *i.e.* arterialization of venous blood, depends on the pressure gradients across the BAB, and these are determined by the composition of inspired air and minute volume (the volume inspired per unit time) [242]. When breathing air with atmospheric composition at rest, a ventilatory rate between 6 to 12 breaths per minute is necessary to keep an adequate gradient across the BAB.

When such gradients are disturbed, either by changes in minute volume or in inspired concentrations, blood will leave the lungs and perfuse the body with different amounts of O_2 and CO_2 than those normally occurring: if loaded with higher amounts of CO_2 the arterial blood is denoted hypercapnic; if depleted of CO_2, it is denoted hypocapnic.

There has been increasing interest in assessing cerebrovascular function using fMRI measures of the perfusion changes induced by manipulations in arterial CO_2 content [93]. The CO_2 manipulation in these type of applications often consists of hypercapnia induced by the administration of CO_2-enriched gas mixtures [256] or breath holding [269], although some groups have also been interested in drug-induced hypercapnia [336], and others in hyperventilation maneuvers inducing hypocapnia [347].

3.2 Administration of inspired gases in fixed concentrations

The "fixed inspired CO_2" manipulation method (FI) consists of administering CO_2-enriched gas mixtures of fixed composition for inhalation [188]. The mixture is usually composed of 5% of CO_2 balanced with air, which, while keeping inspired O_2 at 95% of its normal levels, shifts partial pressure of inspired CO_2 from 0 mmHg to 38 mmHg. This causes a steep decrease in the gradient of CO_2 diffusion across the BAB, reducing the ability of the blood to clear this gas and yielding hypercapnia [1]. With the incomplete arterialization of venous blood, $PaCO_2$ raises in a continuous fashion, as revealed by end-tidal PCO_2 ($P_{ET}CO_2$) monitored samples. This process depends on several physical/physiological parameters (minute volume, baseline levels of arterial and venous PCO_2, the size of CO_2 compartments such as lungs, blood and muscular tissue, etc) but that can be modeled as an exponential growth of just two distinct phases. This approximation provides robust estimates of $PaCO_2$ increases. Because in CVR measures the changes in cerebral perfusion can be normalized to the latter quantity, the variable $PaCO_2$ outputs produced by the FI methods are less of a concern. However,

1. For highly concentrated mixtures ($\geq$7%) it is possible that the the gradient of CO_2 across BAB reverses, leading to a situation where blood will absorb CO_2 for a certain period until venous CO_2 levels surmount the inspired concentration and re-reverse the gradient. The discussion will be limited to 5%-CO_2 mixtures.

in experiments depending on a stable plateau of hypercapnia for more prolonged acquisition [149] or in those requiring specific hypercapnic challenges [30], the variable, unrestrained, $PaCO_2$ output might represent a limitation. Also, there may be an increase in minute volume and PaO_2 associated to CO_2-induced air hunger [400]. The possible increases in PaO_2 during the manipulation might influence CO_2 reactivity measures and represent an additional limitation of the method.

To summarize, in FI methods the gas input is fixed whereas the resulting $PaCO_2$/PaO_2 output is uncertain. Even though FI is the most commonly employed method of hypercapnic manipulation there are some concerns about its applicability in experimental settings requiring a stringent control over the latter variables.

3.3 Prospective targeting of CO_2 and O_2 levels

The targeting of specific end-tidal levels is possible using feed-back computer controlled gas mixing systems that can quickly adjust inspired doses according to monitored values of respiratory gases [206, 400]. However, these systems may be bulky, difficult to replicate and operate at high flow rates. Alternatively, the RespirAct marketed by Thornhill Research Inc is a compact gas administration system that produces controlled modulations in respiratory gases using a prospective, feed-forward approach, which minimizes gas consumption [306, 348].

The RespirAct system is supplied with 4 gas mixtures [2] of different composition: one with 100% O_2 ; one with 21% O_2 / 79% N_2 ; one with 10% O_2 / 90% N_2 ; and one with 20% CO_2 / 10% O_2 / 70% N_2 [3]. The gas delivery circuit accompanying the system allows controlling the volume of inspired gas (as long as the subject empties the bag with delivered mixtures at each breath). Based on demographic, physical and estimated physiological input data the system computes the sequence of gas compositions and volumes to be administered in order to achieve a desired hypercapnic output. Most likely, the system estimates the size of the lungs' different compartments (*i.e.* inspira-

2. The system needs all four connections to properly operate. A fifth gas mixture is required for calibration

3. As a safety measure, the system does not use any mixture with less than 10% O_2 .

tory and functional residual capacities), the arterio-venous CO_2 difference and the body CO_2 storages, to determine the $P_{ET}CO_2$ respiratory response function [4] and with that information generates the input that should give rise to the prescribed output. To produce a step change in $P_{ET}CO_2$, for instance, the RespirAct system delivers particularly highly concentrations of CO_2 at the beginning of hypercapnic blocks to force a rapid transition of CO_2 levels in the lungs (< 3 breaths); then, by gradually decreasing the amount of CO_2 delivered during the block it keeps $P_{ET}CO_2$ steady, maintaining a stable hypercapnic level [18]. Perhaps more importantly, the possibility of independently targeting $P_{ET}CO_2$ and $P_{ET}O_2$ allows reproducing sharply defined hypercapnic plateaus while avoiding incidental changes in $P_{ET}O_2$ [172].

The Respiract method is indisputably valuable for certain applications and for a more sophisticated characterization of the cerebral vasculature. However, the method adds complexity to the gas manipulation. Other than requiring the proprietary TRI RespirAct device, a RespirAct experiment involves 5 gas mixtures and disposable delivery circuits that are usually more expensive than the medical masks used in FI methods. The method also requires more time for preparation. Furthermore, it consists of a gas administration technique that relies on compliance by the subject. As previously mentioned, the RespirAct system delivers a volume$\times$dose for inhalation and to ensure an effective manipulation subjects need to empty the fresh gas reservoir at every breath. Lastly, the mask is fit on to the subjects' face using adhesive tape to seal the edges, which can be uncomfortable, difficult for individuals with facial hair, and makes the mask harder for a subject to remove rapidly if they so desire. It may be possible to determine CVR using simpler means.

3.4 Breathing maneuvers

A very simple an readily available means to induce hypercapnia is to perform a breath-hold (BH) [159, 187, 269]. By suspending elimination of CO_2, $PaCO_2$ will naturally rise, following an logistic growth that (probably) resembles the one observed dur-

4. *i.e.* its theoretical model would be able to estimate the bi- or multi-exponential $P_{ET}CO_2$ response issuing from a FI step change in inspired CO_2

ing the FI manipulation. Since the breath-hold imposes a general suspension of gas exchange across the BAB, it also results in a significant decrease in PaO_2, an effect that might confound estimates of CO_2 reactivity. Besides, accurate estimates of the respiratory responses are challenging. These can be obtained from the difference between two end-tidal points, one sampled immediately before and one immediately after the breath hold [269]. For that, subjects are asked to perform the breath-hold at some point during the expiratory phase and then, at the end of the breath-hold, give a small forced exhale. However, when the forced exhale is not sufficient to allow the sampling of alveoli gases, respiratory responses are underestimated. Other concerns related to the method include: 1) the short duration and small magnitude of the stimulus, which might render the detection of vascular responses difficult as the ASL signal is very noise; 2) the possible discomfort associated with apnea; and 3) difficulty complying with instructions.

As an alternative to breath hold, some groups have explored CO_2 manipulations based on hyperventilation and hypocapnia [5] [347, 382]. Hypocapnia can be sustained for prolonged periods without much discomfort and $P_{ET}CO_2$ levels are continually available during hyperventilation. More importantly, the method is widely available. Nonetheless, the comparison between CVR measures obtained with hyper- and hypocapnic methods should be done with care. The perfusion changes measured with hypocapnic methods reflect the constriction reflex of cerebral vasculature, rather than the dilation seen in hypercapnic manipulations. The CO_2 vascular response is dose dependent and it has been observed that perfusion changes are more prominent in hypercapnia than in hypocapnic regimens [60]. Such non-linear behavior – as in many other physiological processes – can be described by a logistic function [20, 314], which defines an interval of relative linearity, beyond which responses tend to attenuate and plateau. It would be quite valuable to identify the interval of $P_{ET}CO_2$ levels to which changes in perfusion are equivalent, as it would permit a more effective comparison between CVR measures based on different methodologies.

5. Hyperventilation increases minute volume and the gradients of diffusion cross the BAB, which accelerates the CO_2 washout and cause hypocapnia.

3.5 Respiratory and vascular responses

The CO_2 manipulation methods described here represent a wide variety of trade-offs between simplicity and theoretical rigor. As CVR measures are likely to gain increasing importance in multi-site studies of aging and disease-related neurophysiological effects, a thorough analysis of such respiratory manipulations was deemed fundamental.

The study in this Chapter has been devised to determine whether CVR measures obtained with BH, FI and the Respiract hypercapnic methods would be comparable and whether any difference in subjects' tolerability and/or compliance would be observed. To verify to which extent vasoconstriction reactivity measures differ from CVR measures of vasodilation, a hyperventilation maneuver has been included in the comparison. Linear modeling of respiratory traces allowed robust estimates of $P_{ET}CO_2$ responses in each of the different manipulations. Given the varied stimulation profiles, individual $P_{ET}CO_2$ models were used as response regressors in the linear modeling of fMRI signals. To help identifying the linear regions of perfusion change, CO_2-perfusion data from the different manipulations were put together and fitted with a sigmoidal dose-response model. Sample consisted of ten young healthy subjects and CVR maps for the different manipulations were obtained with the pCASL method. Results of this study have been published as a full research article in the Journal of Cerebral Blood Flow and Metabolism. Whereas hypocapnia-based CVR measures differed significantly from hypercapnia-base ones, it has been found that the three hypercapnia induction methods yield comparable CVR measures when these are expressed as the relative change in perfusion per mmHg increase in $P_{ET}CO_2$. When CVR was expressed as the absolute change in perfusion per mmHg increase in $P_{ET}CO_2$, Respiract related measures differed from FI and BH. These two operated in the linear region of the CO_2 dose-response curve, manipulating $P_{ET}CO_2$ between 30 and 45 mmHg. Regarding discomfort and difficulty ratings, differences were not statistically significant; however, the authors noted that results in older groups or those affected by disease could be different.

3.6 Stuty manuscript

Comparison of cerebral vascular reactivity measures obtained using breath-holding and CO_2 inhalation

Authors: Felipe B. Tancredi and Richard D. Hoge
Status: Published in the *Journal of Cerebral Blood Flow & Metabolism* vol. 33, p. 1066-1064, 2013. DOI: 10.1038/jcbfm.2013.48.

Stimulation of cerebral vasculature using hypercapnia has been widely used to study cerebral vascular reactivity (CVR), which can be expressed as the quantitative change in cerebral blood flow (CBF) per mmHg change in end-tidal partial pressure of CO_2 ($P_{ET}CO_2$). We investigate whether different respiratory manipulations, with arterial spin labeling used to measure CBF, lead to consistent measures of CVR. The approaches included: (1) an automated system delivering variable concentrations of inspired CO_2 for prospective targeting of $P_{ET}CO_2$), (2) administration of a fixed concentration of CO_2 leading to subject-dependent changes in $P_{ET}CO_2$), (3) a breath-hold (BH) paradigm with physiologic modeling of CO_2 accumulation, and (4) a maneuver combining breath-hold and hyperventilation. When CVR was expressed as the percent change in CBF per mmHg change in $P_{ET}CO_2$), methods 1 to 3 gave consistent results. The CVR values using method 4 were significantly lower. When CVR was expressed in terms of the absolute change in CBF (mL/100g per minute per mmHg), greater discrepancies became apparent: methods 2 and 3 gave lower absolute CVR values compared with method 1, and the value obtained with method 4 was dramatically lower. Our findings indicate that care must be taken to ensure that CVR is measured over the linear range of the CBF-CO_2 dose-response curve, avoiding hypocapnic conditions.

Key Words: Arterial Spin Labeling, Cerebral Vascular Reactivity, functional MRI, Hypercapnia

INTRODUCTION

Measurements of the cerebral blood flow (CBF) response to a stimulus may provide a useful index of cerebral vascular function, aiding in the study and diagnosis of different cerebral diseases with a vascular component [121, 340, 392]. Hypercapnia (increased levels of blood CO_2.) is known to cause global increases in CBF [193], a phenomenon that has been exploited in the development of functional magnetic resonance imaging (fMRI) measures of cerebral vascular reactivity (CVR) [187, 318, 319]. To measure CVR, perfusion-weighted images are acquired during a respiratory manipulation that induces hypercapnia, with analysis of the resultant image series yielding a map of the CBF response to CO_2. The fMRI technique providing the most quantitative measure of CBF is arterial spin labeling (ASL) [6, 76, 396]. Cerebral vascular reactivity can thus be expressed as the percentage or absolute change in CBF per mmHg change in the end-tidal partial pressure of CO_2 ($P_{ET}CO_2$, a surrogate for arterial PCO_2). In addition to providing a direct depiction of cerebral vascular function, the ASL and BOLD responses to a hypercapnic manipulation can be input to biophysical models allowing estimation of the cerebral metabolic rate of O_2 [9, 158], a key indicator of cerebral function.

A number of approaches have been explored for the induction of hypercapnia to measure CVR with fMRI methods. One of the most commonly adopted methods has been to administer a mixture of gases with a fixed concentration of CO_2 (typically 5% to 7% by volume) diluted in atmospheric composition air [157, 318, 418]. Because this approach uses a fixed concentration of inspired CO_2 during all phases of the hypercapnic episode and for all experimental participants, we refer to this method as 'fixed inspired', or FI. Methods based on administration of gas mixtures require the participant to wear a breathing mask or mouthpiece by which the inspired gases are delivered, as well as a system for controlling flow rates and alternating between normal air and the CO_2/air mixture. When FI CO_2 mixtures are used, the actual $P_{ET}CO_2$ levels induced during air breathing and administration of the CO_2 mixture will depend on the subject's body mass, basal metabolic rate, and minute ventilation. Moreover, accelerated breathing during hypercapnia can lead to incidental hyperoxia, which exerts a mild vasoconstrictive

influence. These effects may confound CVR measurements made using the FI method.

To address the latter concerns, several groups have devised methods for prospectively targeting specific $P_{ET}CO_2$ and $P_{ET}O_2$ levels during different phases of hypercapnia induction. Early methods [18, 345, 346] focused on maintenance of constant partial pressures using sequential rebreathing approaches, wherein subjects receive an externally administered gas up to a certain flow rate, beyond which they rebreathe expired gas. Feedback approaches have also been explored [400], although these require extremely high flow rates (*e.g.* 70L/min). Slessarev *et al.* [341] have extended the sequential rebreathing approach to incorporate physiologic modeling of CO_2 fluxes in the body to make predictive, breath-by-breath adjustments of inspired gases to achieve prospective and independent control of end-tidal PCO_2 and PO_2 at lower flow rates.

One of the simplest methods used to induce hypercapnia is to have subjects hold their breath [185], resulting in accumulation of CO_2 in the blood and resultant increases in CBF. This can be performed with minimal equipment and set-up time, although it is limited to subjects who are able to understand and comply with the breath-holding instructions. This procedure also necessarily leads to a degree of hypoxia, which may confound the imaging responses observed. Moreover, since the quantitative expression of CVR requires knowledge of the change in $P_{ET}CO_2$, which is usually measured from exhaled gas that is not available during a breath-hold, applicability has been limited. The latter difficulty has been overcome by having subjects execute a small, forced exhalation at the end of the breath-hold that is used to measure $P_{ET}CO_2$ at the end of the maneuver [269].

To date, there have been few studies comparing $P_{ET}CO_2$-normalized estimates of CVR obtained using different respiratory manipulations, and none that have included both gas administration and breath-holding methods. A recent study by Mark *et al.* [256] showed that a commercial implementation of the sequential rebreathing system with feed-forward modeling described by Slessarev *et al.* reduced the variability of CVR estimates compared with measurements made in the same individuals using fixed concentrations of inspired gases (the FI approach). The latter study also showed reduced fluctuations in $P_{ET}O_2$ during hypercapnic manipulations when the sequential rebreath-

ing approach was used.

Given that $P_{ET}CO_2$ is necessarily monitored in any quantitative CVR study, an important question is whether retrospective normalization of flow responses produced by an uncontrolled $P_{ET}CO_2$ excursion will give equivalent results to a similar normalization applied to data acquired during $P_{ET}CO_2$ changes that have been prospectively controlled. To the extent that percent changes in CBF might be a linear function of $P_{ET}CO_2$, the two approaches should be equivalent. If the ranges of $P_{ET}CO_2$ covered by different techniques span different domains of a non linear dose-response relationship [20, 144, 168, 314], however, then the apparent CVR values could differ considerably. Addressing this question was the primary aim of the present study.

MATERIAL AND METHODS

For this study, we scanned 10 healthy subjects (ages between 18 and 35) measuring CBF changes during 4 types of respiratory manipulation in the following order: (1) automated prospective control (PC); (2) administration of fixed concentrations of inspired gases (FI); (3) breath hold (BH); and (4) breath-holds combined with hyperventilation (HV). To control for minute ventilation, an audio metronome was used to pace the subjects' breathing. Figure 3.1 shows timing diagrams for the different manipulations. All subjects underwent the manipulations in a pre-session 1 week before the scanning and gave informed consent for their participation. The protocol was approved by the *Comité mixte d'éthique de la recherche du Regroupement Neuroimagerie Québec*.

Subjects were imaged using a 3T scanner (Siemens TIM TRIO, Siemens Medical Solutions, Erlangen, Germany) using the vendor's 32-channel head coil. Although the BH and HV methods did not require a face mask, the FI and PC methods were each implemented using a different type of mask. The scan session was therefore divided into three phases: PC, FI, and a final phase with the mask removed for BH and HV. Subjects were withdrawn from the MRI scanner for placement of the appropriate mask and monitoring equipment between phases. Each phase consisted of a simple localizer sequence, a high-resolution anatomic acquisition (MPRAGE with 1 mm^3 resolution)

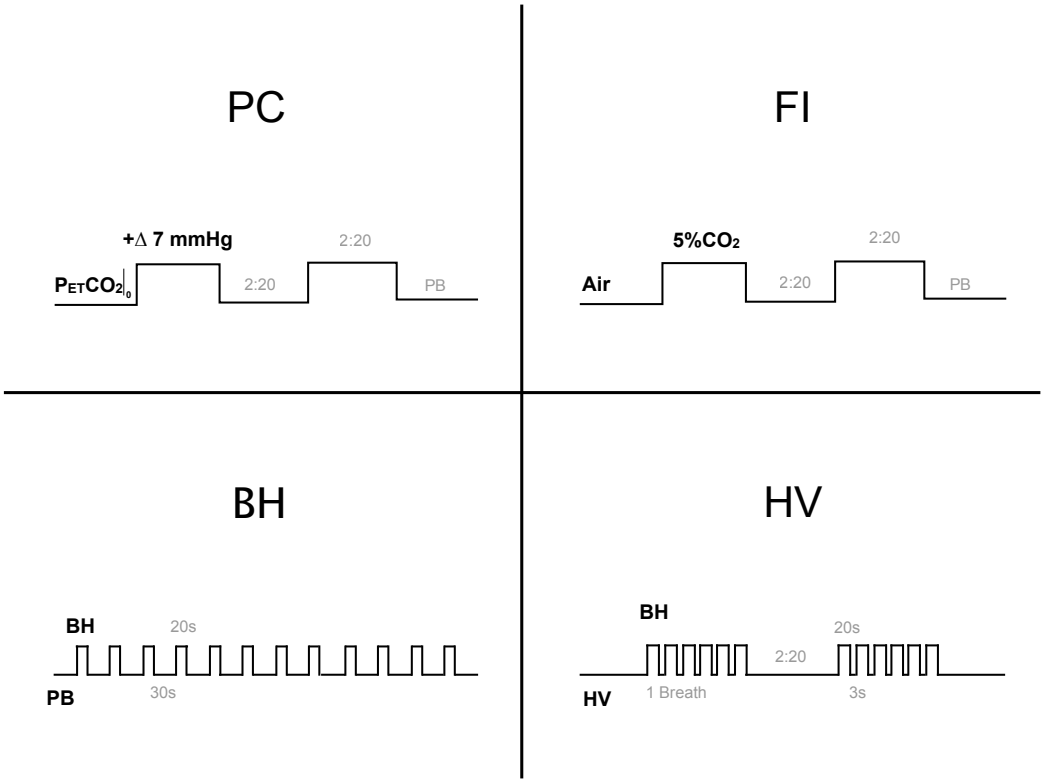

Figure 3.1: The four respiratory manipulations. In the prospective control (PC) method, the inspired gas mixture is continually modulated, allowing near step changes in $P_{ET}CO_2$ (resembling the square blocks shown). In fixed inspired (FI), gas mixtures with fixed composition are administered during different blocks, inducing hypercapnia during periods of CO_2 enrichment (the square blocks here represent the inspired concentration of CO_2, not $P_{ET}CO_2$). The breath hold (BH) method developed by the Cardiff group consists of 20-second breath-holds alternated with paced breathing (PB). The hyperventilation (HV) method uses these same short breath-holds though differently organized as to resemble the two-block design adopted in the gas manipulations. Ventilatory rate is also 50% higher than in the PB used in the other manipulations. In this figure, BH is used to denote the BH method as well as to indicate breath-hold events. $P_{ET}CO_2$, end-tidal partial pressure of CO_2.

of $\sim$5 minutes duration, and the functional scans with $\sim$10 minutes duration each. For the functional scans, we used pseudo-Continuous ASL [72, 364], with a labeling time of 1.5 seconds, delay of 0.9 seconds, and repetition time/echo time of 3,000/10 ms. Slice prescription was 11 slices with 7mm$\times$4mm$\times$4mm voxel resolution and 1 mm gap. Readout consisted of a GRE-EPI scheme with GRAPPA acceleration factor 2 and 7/8 partial Fourier reconstruction. Total time of the experiment was 1 hour and 30 minutes.

During all functional acquisitions, subjects were paced in their breathing using metronome beeps played over headphones. Subjects breathed at a constant rate, unless they were performing a breath-hold. Instructions to perform the breath-hold consisted of a beep with different tone. During the breath-hold, the metronome beeps were paused. In the case of HV, an additional beep tone was used to signal intermittent breaths during the series of breath-holds. The ventilatory rate was set to 16 breaths per minute, comparable to the average of rates during normocapnia and hypercapnia reported by Mark *et al.* [256] for unpaced breathing. In the HV maneuver, the ventilatory rate was increased to 24 breaths per minute, deliberately inducing hypocapnia during these periods.

In the PC phase, the hypercapnic manipulation was conducted using a commercial implementation (RespirAct, Thornhill Research, Toronto, Canada) of the sequential rebreathing system with feed-forward modeling described by Slessarev *et al* [341]. In this system, a physiologic model is used to compute a sequence of inspired gas concentrations that will result in the desired sequence of end-tidal O_2 and CO_2 values in a given subject. We programmed the RespirAct to increase $P_{ET}CO_2$ by 7 mmHg from the subjects' baseline $P_{ET}CO_2$ during two intervals of 2 minutes:20 seconds (2 minutes:20 seconds apart) while keeping end-tidal levels of O_2 unchanged throughout the manipulation. An individuals baseline $P_{ET}CO_2$ was determined based on measurements obtained during anatomic scans while the subject was breathing air through the respiratory apparatus. Subjects were asked to follow the metronome at 16 breaths per minute during this phase and to ensure that the fresh gas bag of the breathing circuit was emptied at every breath (necessary to ensure accurate targeting of end-tidal gas levels).

In the FI phase, subjects were fitted with a non rebreathing face mask (Hudson RCI, CA, USA) and paced to breathe at 16 breaths per minute. Plastic tubing and a Y-connector were used to connect flow meters for medical air and CO_2-5% (balanced with air) tanks to the circuit leading to the mask. The CO_2 mixture was administered in two intervals of 2 minutes:20 seconds duration, separated by intervals of 2 minutes:20 seconds during which medical air flowed through the circuit.

In the last phase, subjects performed the breath-holding routines. First, in the BH manipulation, subjects were asked 12 times to hold their breath for 20 seconds (see Fig-

ure 1, bottom left panel). Breath-holds alternated with 30 seconds of paced breathing, in which subjects were asked to follow the metronome at 16 breaths per minute. Increases in $P_{ET}CO_2$ were estimated by comparing the end-tidal levels from the beginning with the end of the breath-hold. To sample $P_{ET}CO_2$ just before resumption of breathing, subjects were instructed to give a small forced exhalation at the end of each breath-hold, as described in Murphy *et al* [269]. In the HV manipulation, there were two equal sets of six breath-holds, each with an approximate 2 minutes:20 seconds duration, and separated by 2 minutes:20 seconds of paced breathing. In each set, 20-second periods of breath holding were punctuated by single breaths (exhale-inhale) that lasted $\sim$3 seconds. Such compounded breath-hold blocks were interleaved with hyperventilation, during which subjects were asked to follow the metronome at 24 breaths per minute. This sequence is described in Figure 1, bottom right panel.

At the end of the session, subjects were asked to rate their discomfort during the different respiratory manipulations according to the 7-step scale proposed by Banzett *et al* [17].

Respiratory levels of CO_2 (and O_2) were continuously monitored using a nasal cannula and a gas sampler/analyzer (Biopac MP150, BIOPAC Systems Inc., CA, USA), as well as comparable analyzers incorporated into the RespirAct during PC scans. The baseline levels and the amplitude of the hypercapnic response associated with each manipulation were obtained through linear modeling of the end-tidal points in the capnograph (Figure 2). Each hypercapnic stimulus was treated as an independent event block, except in HV, where the 12 breath-holds were aggregated into 2 blocks. In each manipulation, biexponential functions were used to model transition periods at the beginning and end of blocks. The model also incorporated a first-order drift term; and an offset that represented the baseline end-tidal level during that run (which is partly dependent on the rate of paced breathing). The resting 'normal' $P_{ET}CO_2$ levels were obtained from the evaluation of capnograph recordings obtained while subjects breathed air during unpaced breathing (*e.g.* during the anatomic scans that preceded the FI and BH manipulations).

The $P_{ET}CO_2$ and $P_{ET}O_2$ values were compared during conditions, and against the normal resting levels during unpaced breathing, using a paired t-test.

Image analysis was performed primarily using the NeuroLens software package (www.neurolens.org). The ASL image series were first motion corrected. The flow series were then obtained using surround subtraction of the raw ASL images. Next, the ASL difference signal (representing CBF) was fit with a general linear model consisting of the modeled values of $P_{ET}CO_2$ normalized to have unit amplitude, plus a third-order polynomial representing drift terms and constant offset. This fitting procedure provided maps of the estimated baseline flow signal and related increases.

To determine responses in different tissue regions, these ASL signal estimates were averaged within an ROI that consisted of a grey-matter probability mask. This mask was computed based on the high-resolution anatomic acquisitions, which were segmented for grey matter using FSL's FAST program [426] and resampled to match the spatial sampling of the functional series. Average ROI responses were computed as the weighted sum of ASL parameter estimates from the general linear model fit multiplied by the grey-matter probability within each voxel, to control for partial volume effects with white matter and cerebrospinal fluid (which are assumed to exhibit little or no ASL difference signal). Average parameter estimates were converted from raw MR signal units to absolute CBF using the approach described in Wang *et al* [386]. To exclude functional responses associated with the auditory metronome used, temporal lobe regions (containing auditory cortex) were not included in the ROI maps. In addition to the ROI analyses, group average maps of the various ASL parameters (resting CBF, absolute CO_2-induced flow change, percent CO_2-induced flow change) were computed by coregistration of individual maps into the MNI 152 stereotactic space.

The coupling between flow and CO_2, *i.e.* the CO_2 dose-response curve, was further explored by plotting the ASL *vs.* $P_{ET}CO_2$ in the following manner: grey-matter-averaged CBF and monitored $P_{ET}CO_2$ traces for PC, FI, and HV were binned into 30-second intervals, excluding the first 20 seconds after transitions. The BH data were binned in a different manner, using 30-second and 20-second intervals according to the stimulus design. The quantities were averaged within these temporal bins, and used to plot absolute CBF as a function of $P_{ET}CO_2$ during each time bin. Data points from the different types of manipulation were color coded and displayed on the same axes. Data were fit using

the sigmoidal model adopted by Reivich [314]:

$$CBF = a + \frac{b}{1+c.e^{-d.logPCO_2}}$$

RESULTS

End-Tidal Monitoring

Figure 3.2 shows examples of respiratory CO_2 traces associated with each manipulation and respective models of the $P_{ET}CO_2$ responses. The numerical values (mean$\pm$SE) shown on each plot correspond to the group average change in $P_{ET}CO_2$ at the end of the manipulation (where the change is typically maximal). These estimates are also shown in a bar graph in Figure 3.3B. The group average changes in $P_{ET}CO_2$ produced by the different manipulations ranged from 6.6$\pm$0.3 mmHg (PC) to 18$\pm$1 mmHg (HV), and differences between respective changes were generally statistically significant at $P < 0.05$, with the exception of the pair FI and HV, for which $P > 0.2$.

Baseline $P_{ET}CO_2$ levels are shown in Figure 3.3A. The baseline levels of $P_{ET}CO_2$ associated with all four manipulations were significantly different than the 'normal' resting values, observed when subjects breathed spontaneously. Whereas FI, BH, and HV had baseline $P_{ET}CO_2$ levels that were lower than the resting values, the PC manipulation had levels that were higher. Although PC accurately attained the target $P_{ET}CO_2$ values, the targeted baseline values were chosen to be slightly higher than the spontaneously arising $P_{ET}CO_2$ due to our observation that values much below 40 mmHg were difficult to achieve with the RespirAct at the desired breathing rates. We suspect that this is due to the incorporation of a rebreathing circuit in this system.

The baseline $P_{ET}CO_2$ levels were, as expected, lowest in HV, where ventilatory rate was 50% higher than in the rest of the manipulations. Fixed inspired and BH did not differ significantly from each other, although both had baseline $P_{ET}CO_2$ levels that were considerably lower than the spontaneously arising value.

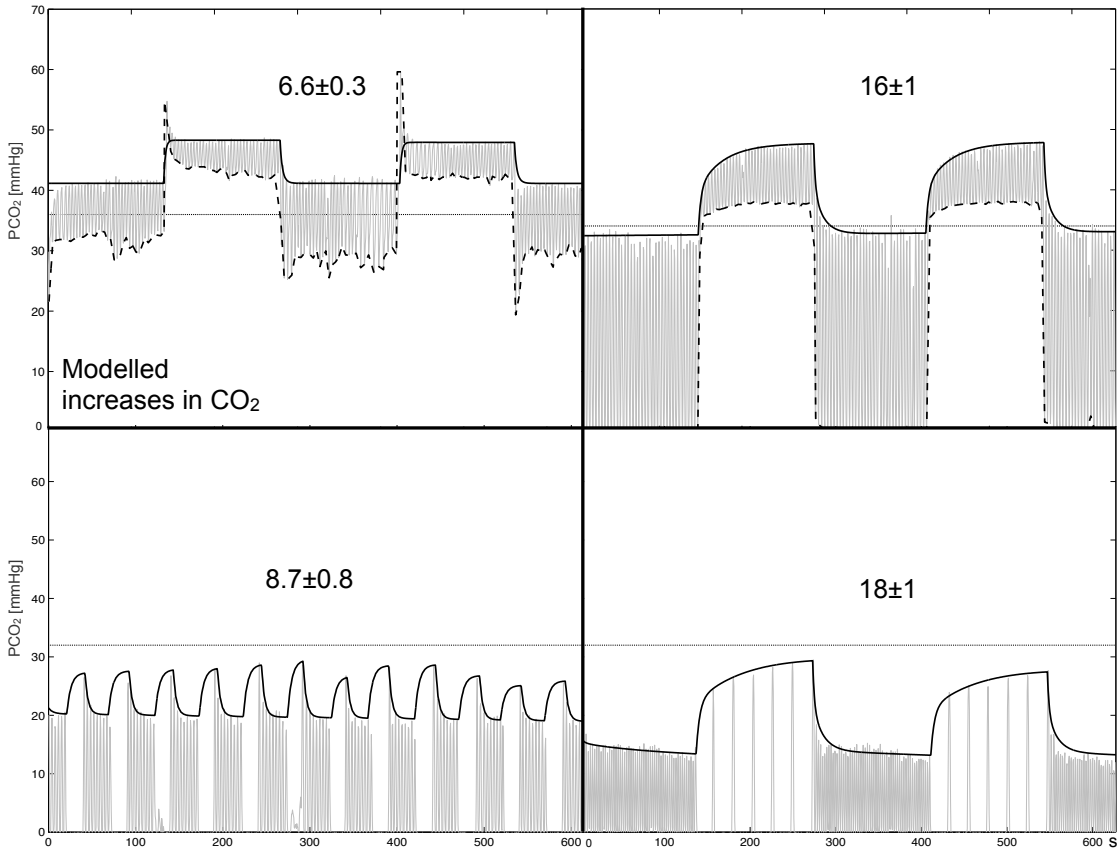

Figure 3.2: $P_{ET}CO_2$ increases obtained with the modeling of end-tidal CO_2 samples. The group mean±SE change is displayed over representative traces of the four different manipulations. Left to right: PC and FI on the top, and BH and HV on the bottom. In each plot, the gray oscillating trace represents the continuous sampling of CO_2, and the black trace the model fitted to the $P_{ET}CO_2$ points. The horizontal dotted lines correspond to the spontaneously arising resting $P_{ET}CO_2$. In the gas methods, the dashed traces connect the minimum of tidal PCO_2 points, indicating the inspired gas concentration.

Incidental changes in O_2 (Figure 3.3D) were all significantly different from zero. In PC and FI, changes were minimal and virtually indistinguishable. Baseline levels of $P_{ET}O_2$ (Figure 3.3C) were above spontaneous resting levels except for PC. As would be expected, peak baseline levels for $P_{ET}O_2$ were observed for HV, which drove $P_{ET}O_2$ to 142±2. During manipulations including breath-hold (BH and HV), $P_{ET}O_2$ fell by up to 26±2 mmHg, reaching a lower value of 92±6 mmHg in the HV manipulation.

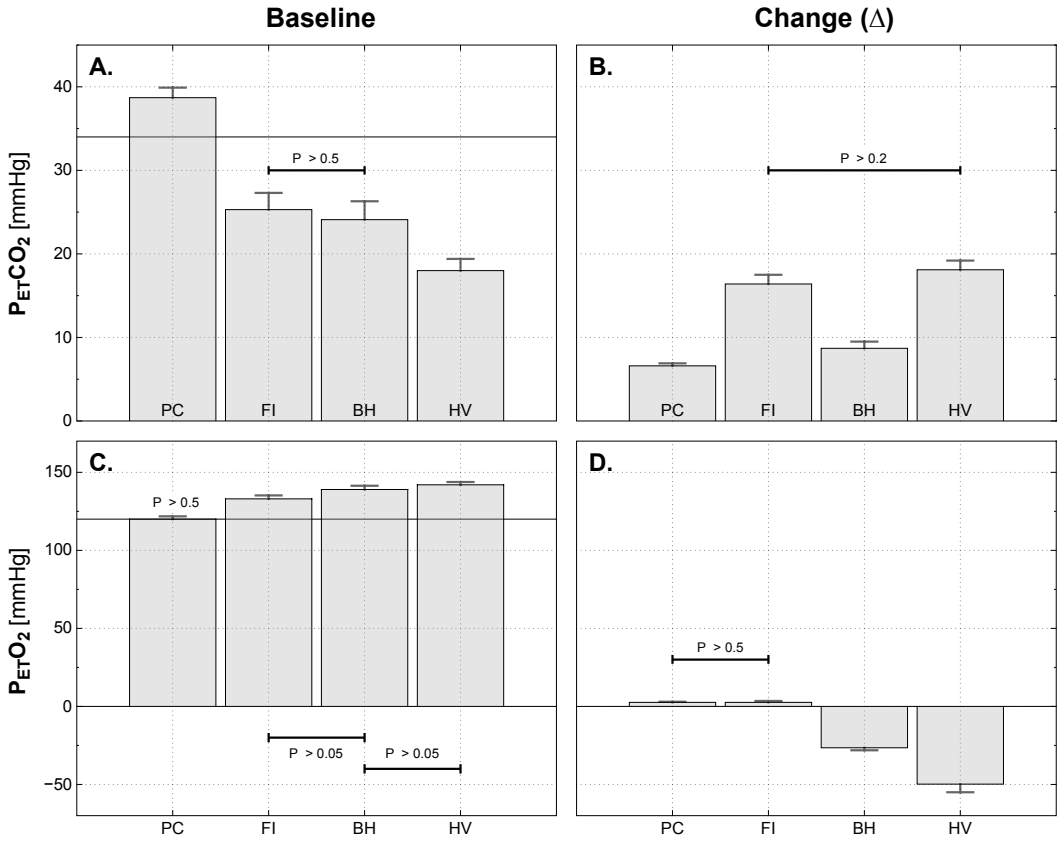

Figure 3.3: Comparison of group average $P_{ET}CO_2$ and $P_{ET}O_2$ levels during the four different manipulations. Baseline levels on the left and size of the induced changes on the right. The black horizontal lines in the baseline plots indicate the group average value for the spontaneously arising end-tidal gas levels. Except for the pairs indicated, t-tests pointed to significant differences in both baseline and evoked change values between the various methods. The group average baseline values determined for all methods also differed significantly from the spontaneously observed end-tidal values.

Arterial Spin Labeling Flow Signal

Examples of the linear modeling of the ASL signal are shown in Figure 3.4 for the average grey-matter signal in a single subject. Absolute ASL flow changes and baseline levels for each manipulation are shown as bar graphs in Figure 3.5A and B, respectively. Differences in the measured flow responses were only significant (though marginally, with P = 0.16) between FI and HV. Note that the flow change in response to breath-holds in HV is the lowest, despite the fact that this manipulation gave the largest change in $P_{ET}CO_2$.

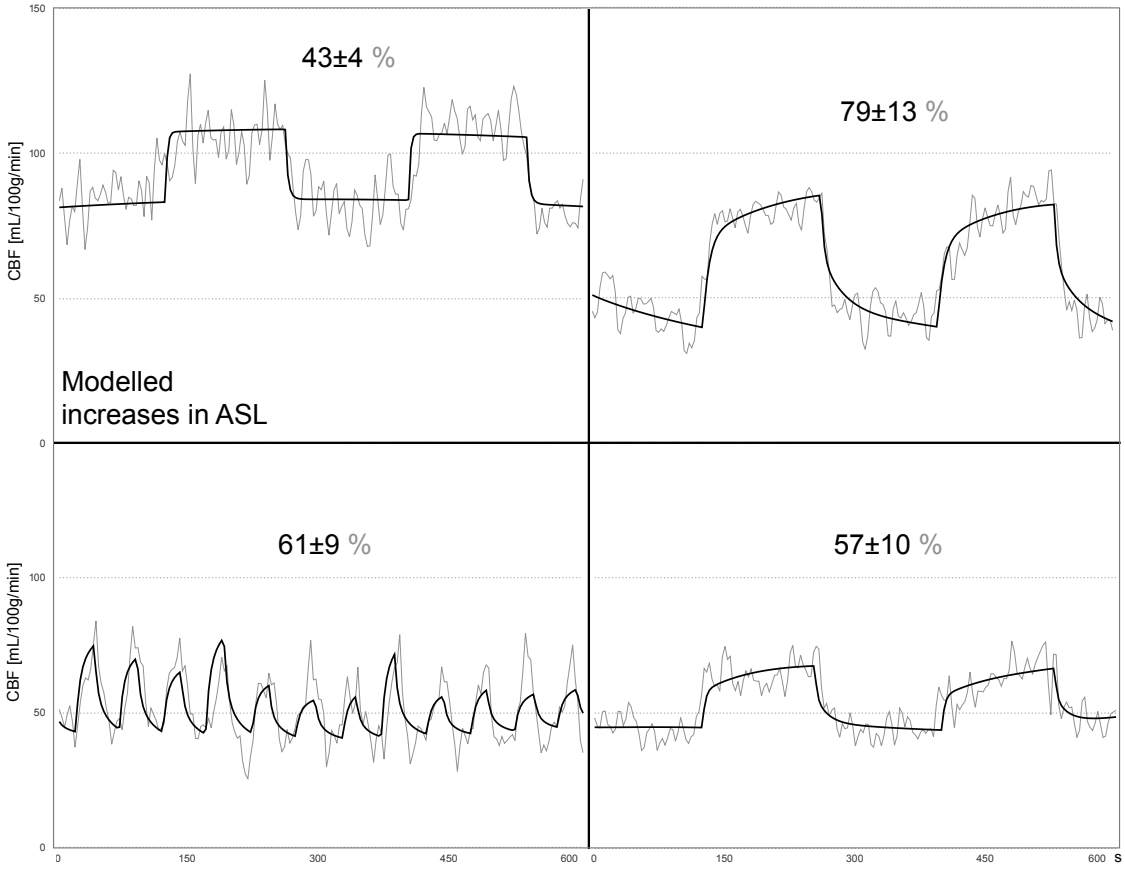

Figure 3.4: Arterial spin labeling (ASL) flow signal changes in grey matter during hypercapnia from a single representative subject. Linear modeling fits of $P_{ET}CO_2$ traces (black) are plotted over corresponding ASL signals (grey) for the four different manipulations. Left to right: PC and FI on the top, and BH and HV on the bottom. CBF, cerebral blood flow.

Absolute levels for baseline flow were generally correlated with baseline $P_{ET}CO_2$ levels, with the PC manipulation having considerably higher baseline $P_{ET}CO_2$ and CBF values than the other manipulations, among whom the differences were not statistically significant.

When expressed as the percent change in CBF per unit of change in $P_{ET}CO_2$, PC, FI, and BH yielded comparable CVR estimates that did not differ by a statistically significant amount (Figure 3.5C). The HV manipulation, however, gave a significantly lower value of relative CVR (the term 'relative CVR' will be used to indicate $\Delta\%CBF/P_{ET}CO_2$).

When expressed in terms of the absolute change in CBF (mL/100g per minute) per mmHg change in $P_{ET}CO_2$ ('absolute' CVR), however, there were significant differences

in the values given by the different methods (Figure 3.5D). In general, the absolute CVR values were correlated with the resting $P_{ET}CO_2$ associated with each manipulation.

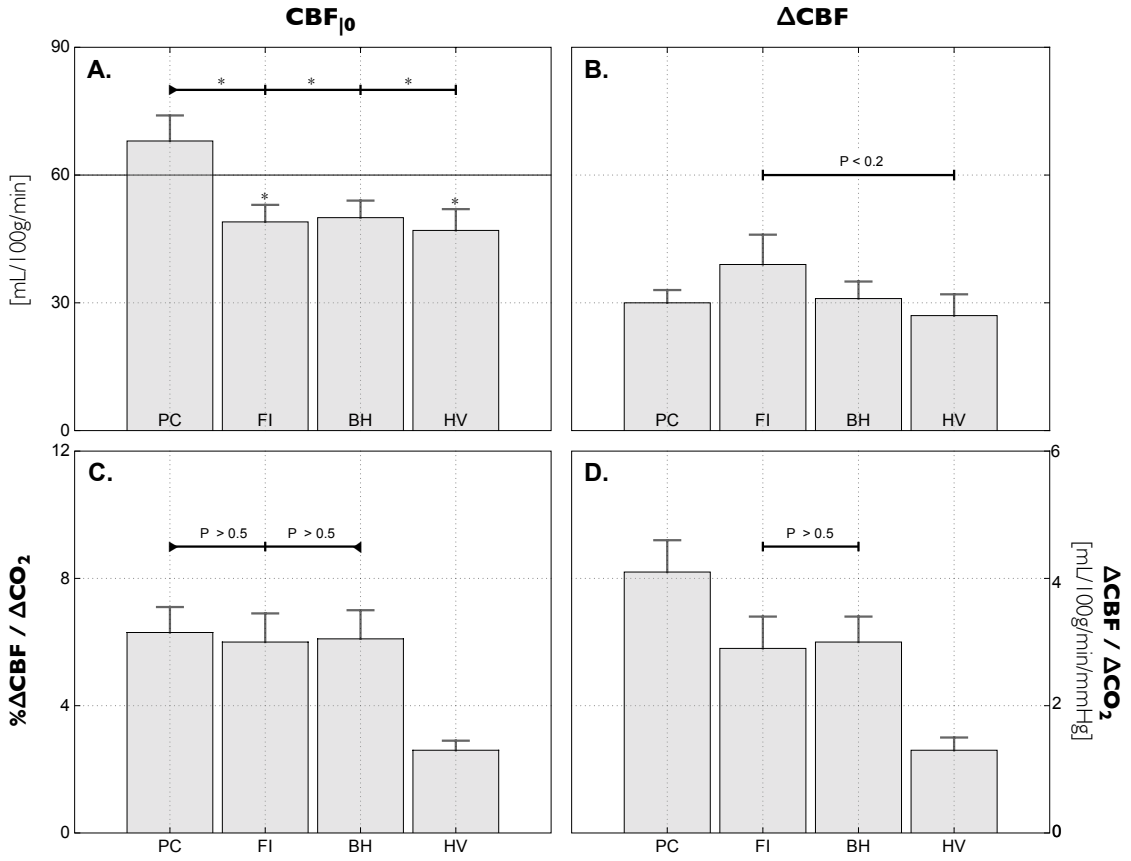

Figure 3.5: Group average values of the arterial spin labeling (ASL) flow signal in grey matter. (**A**) Baseline flow; (**B**) absolute flow increases. In (**D**), the CO_2-induced increases are normalized by the $P_{ET}O_2$ increases and expressed as an absolute cerebral vascular reactivity (CVR) ratio. The percent change in ASL signal per mmHg increase in CO_2 in (**C**). In the bottom graphs, we indicate where the t-tests did not point to significant differences (differences between PC and FI/BH were only marginally significant with $P < 0.1$). In panel A, significant differences ($P < 0.05$) are indicated by an asterisk symbol.

Group average maps of the baseline blood flow and reactivity to CO_2 are shown in Figure 3.6. Maps for both baseline CBF and CO_2-induced response reveal peak values in grey matter, as expected. Maps based on percent change (bottom row) are somewhat noisier, reflecting the vulnerability of ratio images to low signal-to-noise ratio in the denominator.

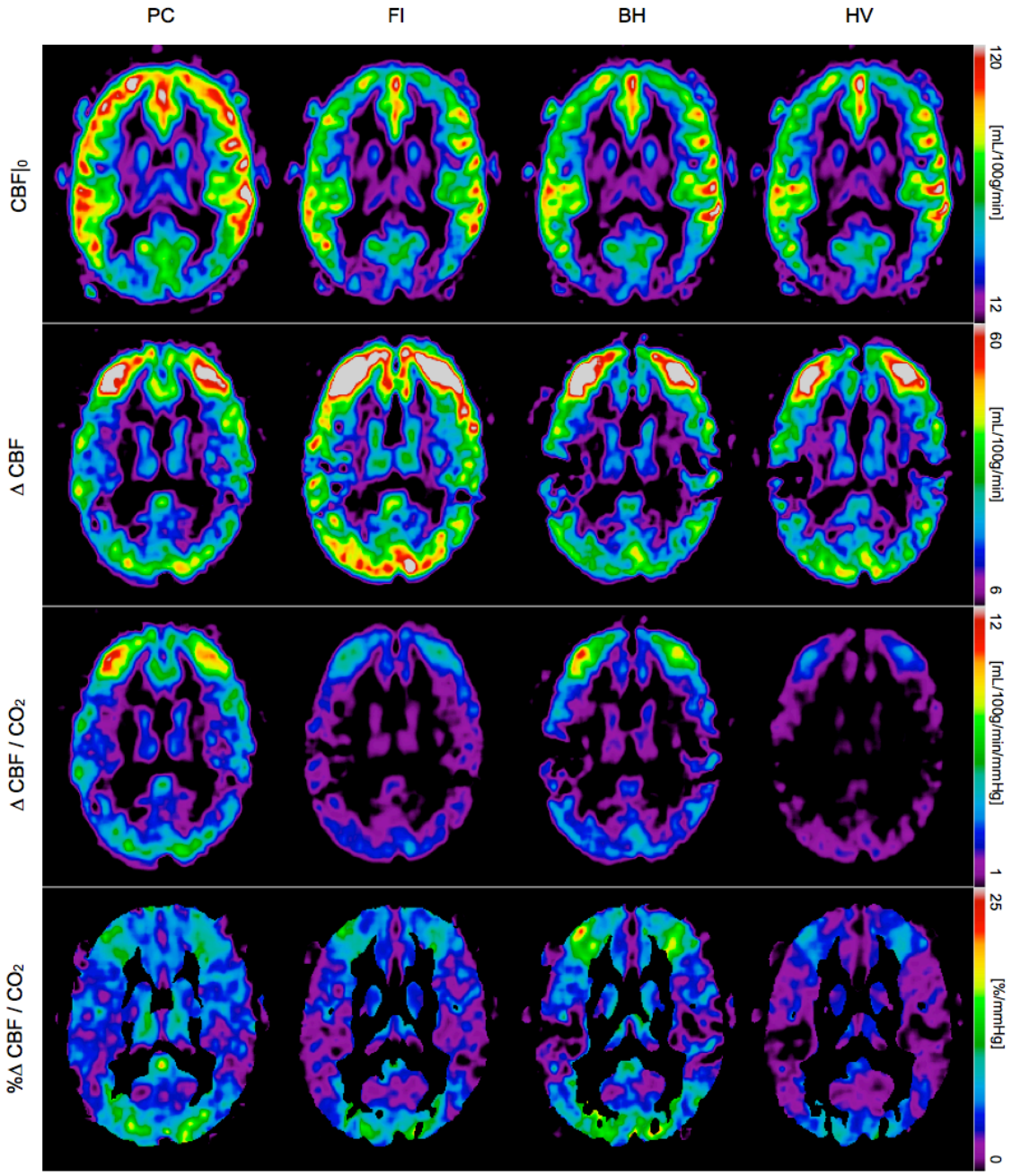

Figure 3.6: Group average cerebral blood flow (CBF) maps. Baseline signal (1st row), CO_2-induced response (2nd row) and cerebral vascular reactivity (CVR), computed as absolute units of flow per mmHg increase in CO_2 (3rd row) and as the percent increase with respect to baseline (4th row). BH, breath hold; FI, fixed inspired; PC, prospective control; HV, hyperventilation.

The images displayed are non oblique axial slices that pass through the upper occipital lobe, above the calcarine sulcus. We suspect that the low baseline CBF in these areas is due partly to sulcal anatomy that results in a relatively lower partial volume of grey matter and hence the appearance of lower CBF. The short postlabel delay used may also result in incomplete clearance of macrovascular signals in some arterial territories. We cannot rule out the possibility that anterior and middle cerebral artery territories are showing macrovessel enhancement that is absent or reduced in the posterior cerebral artery territory (occipital lobe). Another potential source of error is the residual N/2 ghosting we have noticed in some subjects' data which could be biasing the average CBF in that particular area. Yet, regardless of its source, this small measurement error seems to equally affect the four different baseline maps, *i.e.* it is not specific to any respiratory manipulation.

CO_2 Dose-Response Curve

The ASL *vs.* $P_{ET}CO_2$ paired data (Figure 3.7) were generally well described by the sigmoidal model, with most of the non linearity observed toward the lower range of $P_{ET}CO_2$ values at which CBF appeared to plateau some minimal threshold value. The CBF-$P_{ET}CO_2$ pairs associated with the PC manipulation typically fell at the upper end of these curves while data points associated with the HV manipulation gave the lowest $P_{ET}CO_2$ values and consequently lay along the lower CBF plateau.

Comfort of Participants During Breathing Manipulations

Subjective ratings of air hunger provided by subjects for the different manipulations were 2.8 ± 0.4 for PC, 2.3 ± 0.3 for FI, 2.4 ± 0.3 for BH, and 2.5 ± 0.4 for HV. No significant differences at $P < 0.05$ were detected.

DISCUSSION

Although having a small offset, $P_{ET}CO_2$ and arterial PCO_2 ($PaCO_2$) are strongly correlated. This offset might slightly differ across manipulations, but it is reasonable to assume that during each manipulation the offset is constant. Being so, for the comparison of CVR, which depends on the normalization of the CBF response by the size

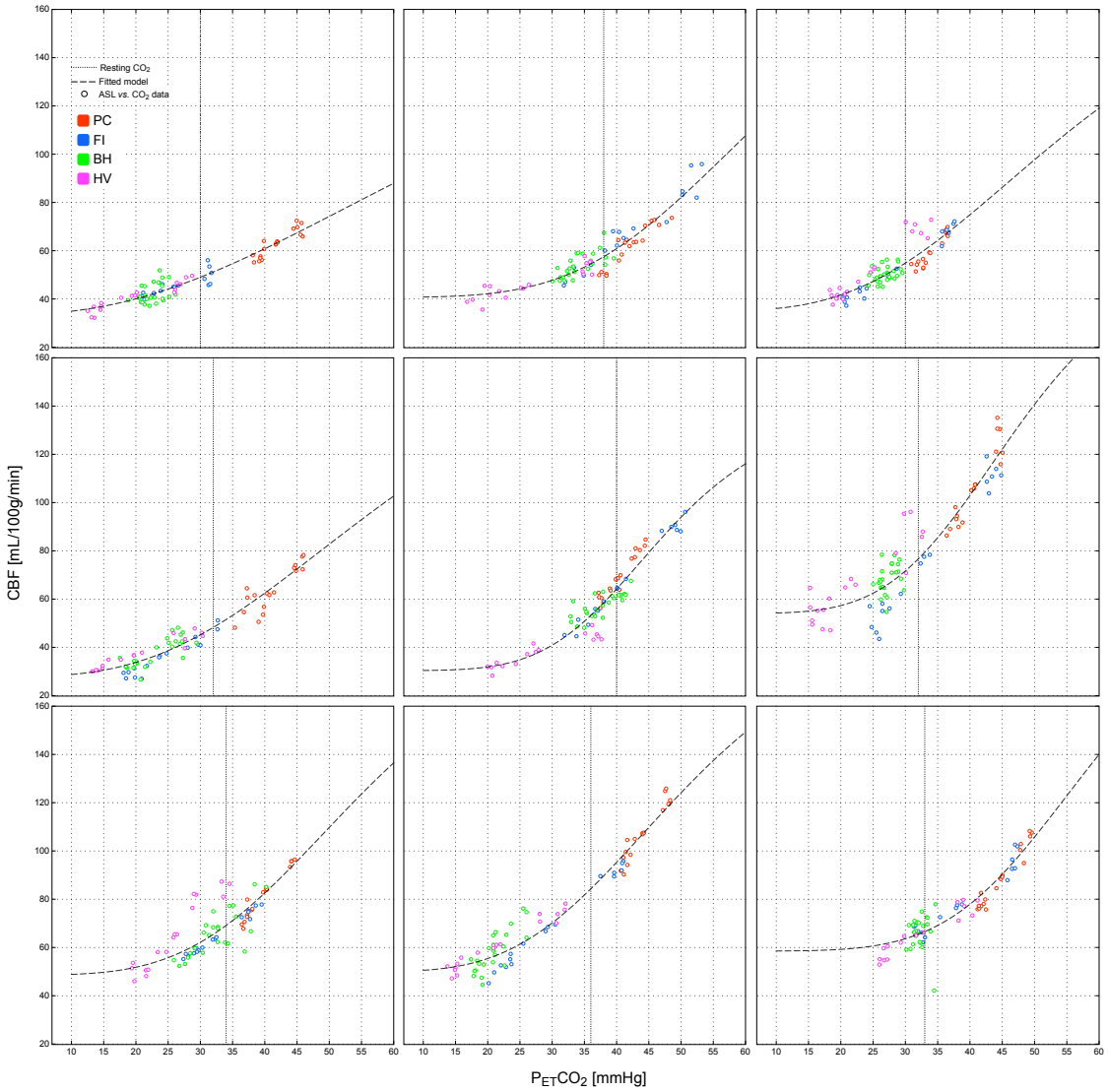

Figure 3.7: Arterial spin labeling (ASL) flow *vs.* CO_2 dose-response curves in nine subjects. BH, breath hold; FI, fixed inspired; PC, prospective control; HV, hyperventilation.

of the hypercapnic stimuli, $\Delta P_{ET}CO_2$ can be used in place of $\Delta PaCO_2$ with no loss of generality. We believe that, under the conditions of this study, $P_{ET}CO_2$ is an accurate surrogate for $PaCO_2$.

Measures of CVR obtained using a variety of respiratory manipulation methods were found to be comparable when CVR was expressed as the percent change in CBF per mmHg change in $P_{ET}CO_2$. When CVR was expressed in terms of the absolute flow change, however, significant differences were noted. In general, the absolute change in

CBF was correlated with the baseline level of $P_{ET}CO_2$, indicating that the non linear dose-response curve describing the CBF-$P_{ET}CO_2$ relationship had an important role in determining reactivity. The variance of the induced change in $P_{ET}CO_2$ was lowest for the PC method, although the variance of other methods was also relatively low, possibly due to the use of a metronome to pace breathing in all cases.

A notable finding was that, for all manipulations except PC, subjects exhibited end-tidal CO_2 values considerably lower than the 'spontaneous' baseline observed when they breathed without pacing using no mask or the non rebreathing mask. This is very likely due to the rather high breathing rate of 16 to 24 breaths per minute imposed by the metronome pacing, a conclusion that is also supported by the finding of slightly hyperoxic baselines $P_{ET}O_2$ values for all manipulations except PC. Prospective control was notable for a baseline $P_{ET}CO_2$ value that was somewhat higher than the spontaneous value, reflecting constraints on the $P_{ET}CO_2$ values that could be targeted.

To the extent that the change in CBF is a linear function of change in $P_{ET}CO_2$, the exact baseline and change values for the latter are not critical. However, our data revealed that moderate hypocapnia can bring the cerebral vasculature into a non linear regime that approaches the 'threshold' dose for CO_2 below which further decreases in $P_{ET}CO_2$ have minimal effect on CBF. In this lower range of CO_2 levels, absolute CVR is considerably reduced compared with the CO_2 reactivity seen around 40 mmHg. Although this effect is corrected somewhat for all but the most severe hypocapnic baselines (HV) when 'relative' CVR ($\Delta\%CBF/P_{ET}CO_2$) is computed, our findings suggest that CVR studies should be conducted with baseline $P_{ET}CO_2$ values that are solidly within the linear range (30 to 45 mmHg). This can be achieved using a PC system like the RespirAct, or by imposing lower rates of paced breathing during other manipulations. These findings are consistent with those of previous studies reporting significant differences between CVR to hypocapnic and hypercapnic stimuli [40, 59].

In terms of the relative advantages and disadvantages of the different methods, the following conclusions can be summarized:

Prospective Control

Use of the RespirAct device resulted in the $P_{ET}CO_2$ values that were the most consistently in the linear range of the CBF *vs.* $P_{ET}CO_2$ relationships for our participants, because of the higher range of $P_{ET}CO_2$ values attained in these experiments. Changes in $P_{ET}O_2$ during the hypercapnic manipulations were negligible (as these were prospectively targeted by the device to be zero).

Administration of Fixed Inspired Gases

While this approach gave robust changes in $P_{ET}CO_2$ values and imaging signals, the baseline $P_{ET}CO_2$ values were somewhat lower than those obtained with the PC method, encroaching on the non linear region of the dose-response curve. This resulted in group average values for absolute CVR, which were also somewhat lower than those obtained using the PC method. Relative CVR values ($\Delta\%$CBF/$P_{ET}CO_2$) obtained with FI were also slightly lower than those given by PC, although the difference was not statistically significant. Changes in $P_{ET}O_2$ during hypercapnic manipulations were negligible, likely due to the use of paced breathing in this manipulation (avoiding accelerated breathing and resultant hyperoxia).

Breath Hold

Because these experiments used the same baseline breathing rate as FI, the baseline $P_{ET}CO_2$ was similarly depressed relative to the spontaneous baseline. Consequently, the resultant values of absolute and relative CVR were also lower than those given by the PC method (although they were very similar to those given by FI). $P_{ET}O_2$ decreased significantly during this manipulation, as expected due to the interruption of oxygen uptake. Such mild hypoxia could contribute a slight vasodilatory input, which would tend to exaggerate CVR measures. While the latter effect could explain the tendency of BH measures of CVR to be higher than those for FI, the difference is fairly small and not statistically significant.

Hyperventilation

As expected, the higher breathing rate of 24 breaths per minute used on this manipulation gave the lowest baseline $P_{ET}CO_2$ and consequently the lowest CVR values due

to the proximity of CO_2 values with the lower plateau of the dose-response curve. The long cumulative reduction in minute ventilation during the breath-hold phases also resulted in the highest degree of hypercapnia and hypoxia. The CVR values obtained with this approach were thus far lower than those of the other methods, for both absolute and relative expressions.

In terms of overall performance, the PC method appears to have provided the most linear estimate of CVR with the least contamination from hyperoxia of all of the methods. However, the same level of linearity could likely be achieved in the FI and BH methods with small adjustments, particularly the pacing of participants at slower breathing rates. For future studies where the control over minute ventilation is a concern, we would advocate the use of paced breathing at lower rates, *e.g.* 8 to 12 breaths per minute. Methods including significant hypocapnia (< 30 mmHg) should be avoided, as these will necessarily give CVR values biased by the non linearity of the CBF-$P_{ET}CO_2$ dose-response curve. All methods were well tolerated by our cohort of young healthy participants, although results in older groups or those affected by disease could be different.

In conclusion, we noted that variability of CVR between methods was reduced when CVR was expressed in terms of the percent change in CBF rather than the absolute change. Values of CVR expressed in terms of the absolute change in CBF per unit of change in $P_{ET}CO_2$ depended strongly on the range of $P_{ET}CO_2$ levels considered, indicating that the non linearity of the CBF-$P_{ET}CO_2$ dose-response curve exerts significant influence on the observed CBF reactivity. In particular, manipulations involving a hypocapnic baseline should be avoided as these may fall within the sublinear region of the dose-response curve. To facilitate interpretation and comparison of results, we recommend that future studies reporting ASL-based CVR values indicate baseline and hypercapnic flow values along with percentage changes. It is equally important to specify the baseline and hypercapnic levels of end-tidal CO_2 during such experiments.

CHAPTER 4

REPRODUCIBILITY OF CVR MEASURES

The objective of the studies composing this section was to determine the degree of reproducibility of pCASL measures in applications based on blood gas manipulations when using the fixed inspired method.

♯

4.1 CVR methods

Pseudo-Continuous ASL allows robust, non-invasive mapping of cerebral perfusion (CBF) using standard MR hardware [408, 412]. In addition to being a suitable option for basic brain research, pCASL CBF imaging has great potential to replace contrast-enhanced methods in longitudinal studies as well as in the clinical practice [25, 77, 383], specially in cases where the injection of Gd chelates for contrast-enhanced imaging is contraindicated (e.g. patients with kidney conditions). Given these prospects, pCASL has quickly become available in most clinical platforms and considerable efforts have been made to standardize its sequence parameters and facilitate the comparison of results across multiple sites [7]. Regarding the reproducibility of its measures, it has been estimated that repeated measures of CBF should vary by less than 5% [61] – compared to other ASL strategies, pCASL affords the most reliable measure of CBF [113].

Pseudo-Continuous ASL has also been exploited in applications based on respiratory/blood gas manipulations [110, 379]. The study presented in Chapter 2 of this thesis shows that pCASL performs better than PASL in measuring hypercapnically induced CBF changes, but the degree of reproducibility of such measures remained to be determined. Clearly, the reproducibility of this type of measure hinges on the reproducibility of the gas manipulation [256]. Since the method used in that study (the Respiract method) afforded reproducible gas changes, it would be a good candidate to help further assessing pCASL's reliability. Nonetheless, the study presented in Chapter 3 of

this thesis suggests that, with small adjustments, fixed inspired (FI) methods can provide comparable results. In view of its simplicity, which is more likely to promote the techniques under development, the study presented here investigates the degree of reproducibility of pCASL measures that can be attained when the FI method is used to modulate respiratory gas levels.

4.2 Refinements in the FI method

Reproducibility of blood gas manipulations using the FI method depends on precise control over the doses that are administered for inhalation. In FI, gas mixtures are delivered via breathing apparatuses such as nasal cannulas, mouth pieces or face masks such as used in clinical oxygen therapy or exercise physiology. The most common strategy has been to administer gas mixtures through simple and inexpensive "Hudson masks" [33]. This type of mask has a bag reservoir to optimize gas usage and increase dose efficiency, but the breathing circuit design and material/geometry of the face mask are impediments to a stringent control over the inspired doses. The gas mixtures administered for inhalation are diluted by the entrainment of room air that leak in through the edges of the mask or – due to poor performance of check valves – through the mask's exhaust vents [1]. The degree of dilution is a function of the pressure inside the mask chamber, which varies according to 1) the fit of the mask, 2) the flow rate of input gases and 3) the subject's inspired volume (Figure 2). One way to control for such variability would be to have flow rates sufficiently high to keep a permanent positive pressure inside the mask; another would be to seal the edges of the mask using adhesive tape. Nonetheless, whereas the first alternative causes subject discomfort and should be avoided [2], the second alternative should be precluded because the complete sealing of a Hudson mask [3] creates the risk of asphyxia.

1. To avoid rebreathing of gases a unidirectional valve also separates the mask and bag reservoir. Malfunction of this valve causes the mixing of administered and expired gases

2. Moreover, difficulty specifying the flow rates that are 'sufficient' to keep administered doses from diluting is an obstacle for replicating experimental conditions.

3. Here we refer to Hudson masks with no safety vent(s)

Next Figure shows respiratory traces of four different participants that underwent a 10-min FI hypercapnic manipulation consisting of the administration of 5%CO_2-air mixtures for 2 minutes in two different instances. Medical air was administered during baseline epochs. Subjects breathed the gas mixtures through a Hudson oxygen mask. Minute volume has been controlled by pacing subjects' breathing. A nasal cannula has been used to sample respiratory PCO_2 levels. Green traces represent the continuous monitoring of PCO_2; changes in inspired PCO_2 are shown in black; changes in end-tidal PCO_2 are shown in yellow; and the blue traces represent the linear model of end-tidal responses.

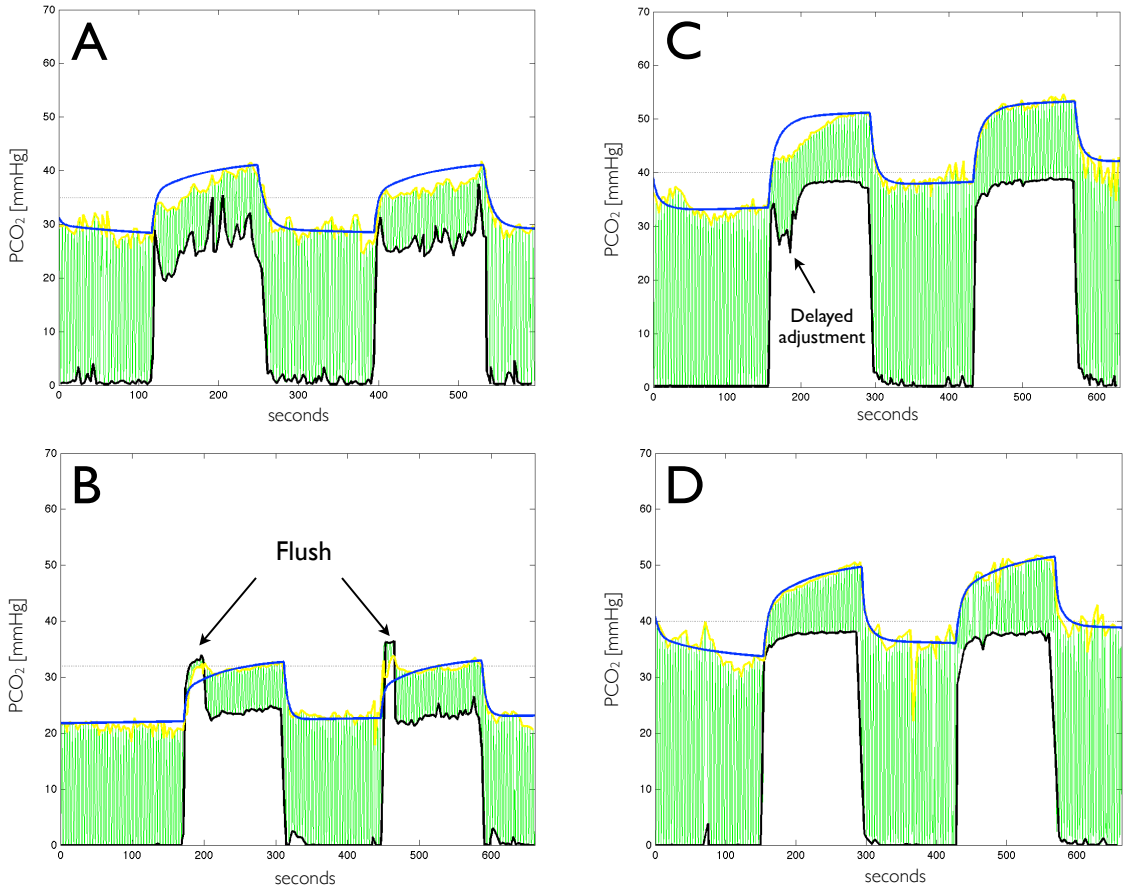

Figure 4.1: Examples of FI manipulations using an oxygen mask.

In A, the loose fitting of the mask and/or malfunction of the valves hamper a good correspondence between administered an inspired doses: the CO_2 inspired dose does

not reach 5% (*i.e.* PCO_2 = 38 mmHg) during the hypercapnia induction. Case B is a good example of how inspired doses are dependent on flow rates when using a poorly fit oxygen mask. During a few seconds upon the transitions between air and CO_2 administration the operator increases the flow rate in an attempt to flush the gas lines and speed up the transition in inspired doses; however what happens is that during such maneuver the pressure inside the mask chamber raises, lessening the dilution of administered doses and increasing inspired doses momentarily. In C we find an example where the operator – realizing that the inspired dose did not reach its maximum – adjusts the flow rate to keep the pressure inside the mask chamber sufficiently high to avoid entrainment of room air and dilution of administered doses. In D, the mask is fit to the subject's face using adhesive tape to partially seal its upper edge and pads to fill the gap between the bottom edge and the chin. In addition, the flow rate is sufficient to keep the CO_2 mixture from diluting. The trace of inspired doses do not show sharp step changes due to partial mixing of administered gases in the breathing bag upon switching of CO_2 doses.

In an attempt to refine the FI method I have designed a (MR compatible) breathing circuit that can afford optimal dose efficiency in a safe and comfortable manner. The mask that has been adopted in this circuit provides an excellent fit to a wide variety of face sizes/geometries and can be easily put on and removed, which minimizes preparation time and subjects' discomfort. A detailed report of this technical development has been published in BMC Research Notes [4]. The breathing circuit described next have been deployed in the second study of this Chapter.

4. We recently became aware of a European distributor of medical respiratory support who markets a similar circuit (not found in product catalogues.). The demonstration of improved inspired doses in our paper remains an important contribution, and this distributor represents an additional potential source of a high quality circuit

4.3 Stuty manuscript 1

A simple breathing circuit allowing precise control of inspiratory gases for experimental respiratory manipulations

Authors: Felipe B. Tancredi, Isabelle Lajoie and Richard D. Hoge

Status: Published in *BMC Research Notes* vol. 7, p. 235-243, 2013. DOI:10.1186/1756-0500-7-235.

Respiratory manipulations modulating blood flow and oxygenation levels have become an important component of modern functional MRI applications. Manipulations often consist of temporarily switching inspired fractions of CO_2 and O_2; and have typically been performed using simple oxygen masks intended for applications in respiratory therapy. However, precise control of inspired gas composition is difficult using this type of mask due to entrainment of room air and resultant dilution of inspired gases. We aimed at developing a gas delivery apparatus allowing improved control over the fractional concentration of inspired gases, to be used in brain fMRI studies. The breathing circuit we have conceived allowed well controlled step changes in FiO_2 and $FiCO_2$, at moderate flow rates achievable on standard clinical flow regulators. In a two run test inside the scanner we demonstrate that tightly controlled simple gas switching manipulations can afford good intra-subject reproducibility of induced hyperoxia/hypercapnia responses. Although our approach requires a non-vented mask fitting closely to the subject's face, the circuit ensures a continuous supply of breathable air even if the supply of medical gases is interrupted, and is easily removable in case of an emergency. The apparatus we propose is also compact and MRI compatible, allowing subject placement in confined spaces such as an MRI scanner for brain examinations. We have reported a new approach for the controlled administration of medical gases, and describe an implementation of the breathing circuit that is MRI compatible and uses commercially available parts. The resultant apparatus allows simple, safe and precise manipulations of FiO_2 and $FiCO_2$.

Key Words: Respiratory manipulation, functional MRI, Hypercapnia, Hyperoxia, Breathing circuit

INTRODUCTION

Respiratory manipulations modulating the fractional concentration of inspired O_2 and CO_2 (FiO_2 and $FiCO_2$) to induce hyperoxia/hypercapnia and modulate cerebral blood flow and oxygenation have become an important component of fMRI studies measuring the vascular as well as the metabolic function in the brain [9, 44, 106, 110, 253, 348, 418]. Methods using computerized systems to control modulations in inspired concentrations and target specific end-tidal levels have been proven successful in enabling inter-subject reproducibility of hyperoxic/hypercapnic stimuli [18, 256, 315, 341, 398, 400] as well as in providing flexibility in the achievable gas mixtures [30, 81, 270] to test different hypotheses. While individualized mixing of gas concentrations to achieve prospective control of end-tidal levels is useful in certain situations, the requirements for many applications are met by delivering predetermined concentrations of inspired gases, so long as end-tidal values are recorded for retrospective normalization of the fMRI signal. The latter, simpler, approach thus continues to be widely adopted in quantitative neuroimaging and other areas. A common practice has been to administer fixed fractional concentrations of O_2 and CO_2 for inhalation [9, 106, 363, 418], delivering O_2/CO_2 enriched mixtures through low-cost nonrebreathing masks commonly used in clinical oxygen therapy, which usually incorporate a reservoir bag to increase dosage efficiency (the bag reservoir stores the gases delivered during expiration to make it available for next inspiration(s), making better use of administered gases and alleviating dropouts in FiO_2 and $FiCO_2$ during early phases of inspiration [33]). However, either due to variations in the shape of the subject's face or to incomplete sealing of one-way valves used to release excess gas flow, such oxygen masks are often very leaky [33], hampering precise adjustments in fractional inspired concentrations and thus limiting the reproducibility of the hyperoxic/ hypercapnic stimuli. One way around this limitation would be to ensure a tight seal of the face mask using surgical tape or other means. However, in a closed circuit where the gas supply is directly connected to the mask, this creates a risk of asphyxia in the event that the medical gas supply is interrupted, although this can be mitigated through the incorporation of special safety measures. To improve control over

inspired gases we have conceived a breathing circuit whose different compartments are separated by high efficiency one-way valves and whose breathing chamber consists of a non-vented mask providing a tight facial fit, but that can rapidly removed. To ensure the safety of subjects, we have replaced the breathing bag found in oxygen masks by an open reservoir, through which the subject breathes room air whenever the flow of administered gases becomes insufficient. The resulting open breathing circuit (Figure 4.2) represents an inherently safe design and allows precisely controlled step changes in the fractional concentration of inspired gases, with moderate flow rates.

MATERIAL AND METHODS

The breathing circuit we describe below (Figure 4.3) has been implemented, using commercially available components, to address three design criteria: MRI-compatibility, accommodation within MRI radiofrequency coils enveloping the head for brain exams, and sufficiently low cost to justify disposal after use to avoid transmission of airborne or other pathogens. Parts were acquired from two different vendors: Intersurgical Inc (NY, USA) and Teleflex Medical (NC, USA); which we will be referred to as IS and TM respectively.

The circuit comprises a small non-vented face mask (IS # 7193) and a dual-limb airway that is appended to the mask's frontal opening. An elbow (TM# 1632 or # 1624) and a triple swivel wye-piece (IS # 1929) connect the limbs to the mask. A pair of valves (TM # 1664/5) at the join of the limbs ensure that 1) inspired gases only come from the incoming limb, consisting of a corrugated tube (2 TM # 1418 connected by TM # 1960) that is preceded by a connector (TM # 1642); and 2) that expired gases only flow through the outgoing limb, that can be a short corrugated tube (TM # 1410). These two limbs have small outgoing limb serves as an exit for expired gases, the long incoming limb serves as a gas reservoir, like the breathing bag of conventional oxygen masks. However, because of its geometry (we used $\sim$3.5 m of corrugated tube with 22 mm internal diameter) and open end, the limb reservoir functions as a sequential container, where administered gases are stacked as they arrive at the circuit and can be expected to mix

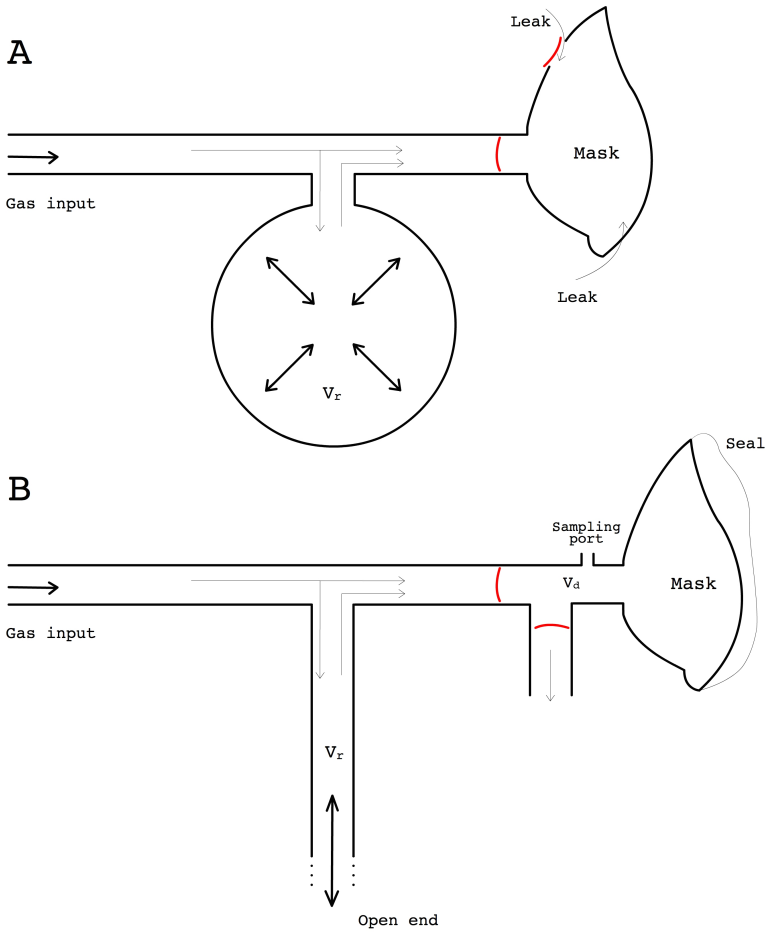

Figure 4.2: New breathing circuit *vs.* a non-rebreathing oxygen mask. A typical oxygen mask/circuit is shown on the top (**A**). The input gas may go straight to the mask or fill the breathing bag when delivery rate exceeds uptake rate. Expired gases leave the mask through vents controlled by valves. Gases inside the mask are often contaminated by air that leak in through the edges of the mask and/or through the vents when valves are malfunctioning. This compromises control over the inspiratory gases as well as the accurate monitoring of end-tidal values. To avoid the latter concerns the new breathing circuit (**B**) uses a non-vented mask providing a sealed fit to the subject's face. The breathing bag is replaced by a long limb reservoir with an open end, ensuring a constant supply of breathable air. Expired gases are exhausted through a second limb, controlled by an efficient unidirectional valve. A sampling port adjoined to the mask to help the respiratory monitoring. Vr = volume of the reservoir; Vd = dead space added by appending the dual limb system to the mask.

less than in a bag type of reservoir. This way, during transitions between gas mixtures of different concentrations, the new mixture becomes readily available for inspiration, allowing sharp transitions in fractional concentration of inspired gases. Whereas the same

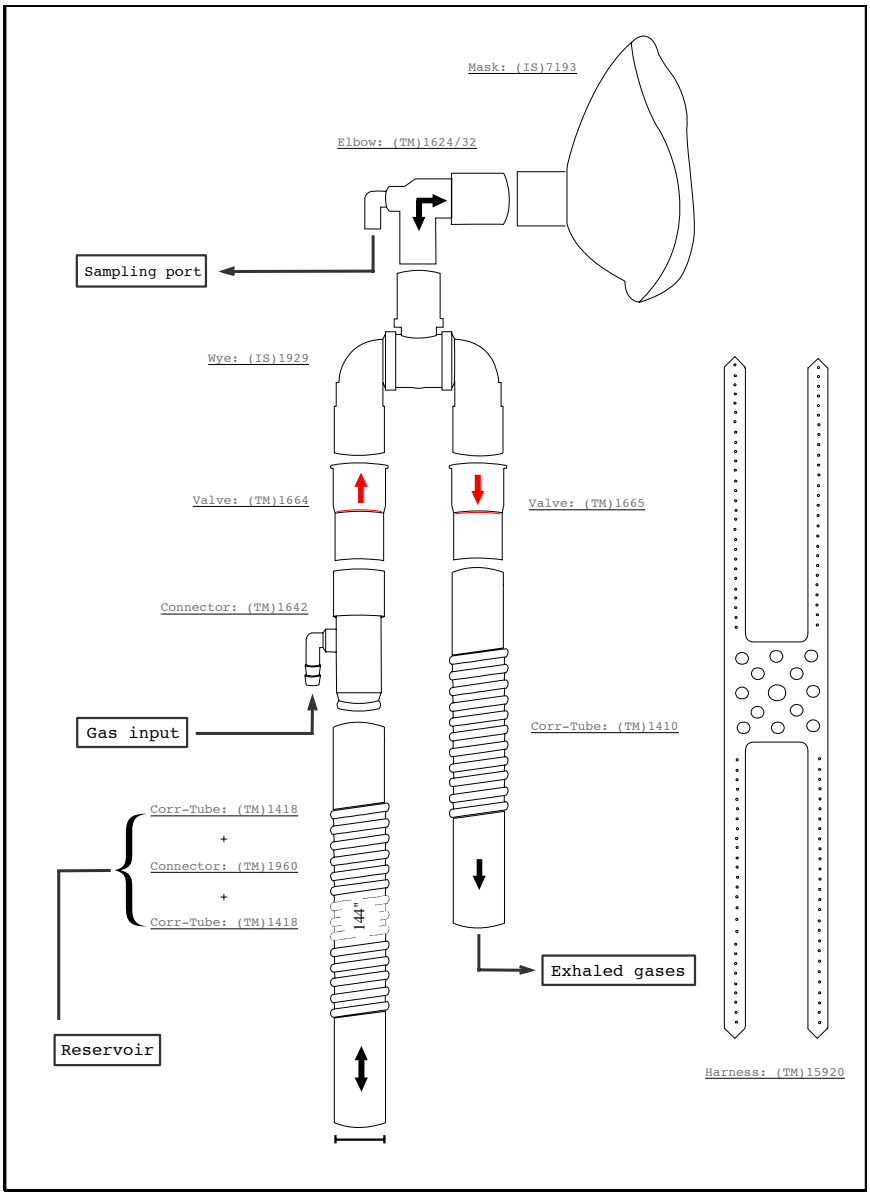

Figure 4.3: Schematic of the circuit assembly. Gas mixtures are supplied through the barbed inlet of the connector TM # 1642. The elbow can be of two different types, with a luer-lock or barbed sampling port (TM # 1624 or # 1632 respectively). The limb reservoir is formed by two corrugated tubings (TM # 1418) coupled by a connector (TM # 1960), which is not represented here. The mask (IS # 7193) comes with a support (not represented) allowing to attach the harness (TM # 15920).

effect could be achieved without this long limb reservoir, that would require high flow dosages to meet peak inspiratory rates.

The circuit was conceived to allow better isolation between circulating gases and exterior, while ensuring a constant supply of breathable gas even in the event of an interruption in the gas administration. The anesthetic mask we have adopted offers a tight facial fit, drastically reducing entrainment of room air and resultant dilution of inspired/expired gases (as can occur with Hudson-style oxygen masks) but can be very easily removed in case of danger or discomfort. The mask does not need to be sealed using adhesive tape [256] nor held to the head using restrictive harnesses that can be difficult to remove in an emergency [47] (we have adopted the TM # 15920). More importantly though, as mentioned above, the gas reservoir of our circuit has an open end which protects the subject against disruptions in the gas supply. Whenever the gas administration is insufficient to meet the subject's ventilation the reservoir is replenished with room air for inspiration, *i.e.* there is no special requirements to ensure a constant supply of breathable air.

The proposed circuit is also equipped with a sampling port for the monitoring of O_2/CO_2 and pressure wave inside the mask chamber, avoiding the use a nasal cannula and potential discomfort associated with this. The sampling port is positioned at the elbow that connects the mask to the circuit's limbs and can be of two types, barbed (elbow TM # 1632) or luer lock (elbow TM # 1624), depending on the tubing used for the sampling line.

As a proof of concept of the improvement in respiratory manipulations attained with the new circuit we have conducted two tests using both the new circuit and a non-vented Hudson oxygen mask (# 1060) in a young healthy subject (female: 32y, 1.65 m, 60 kg). In Test 1 the subject was given 100% O_2 or 50% O_2 balanced with air in two different instances lasting 3 minutes each and 3 minutes apart. Medical air was administered otherwise. Flow rates were 15 L/min during the whole manipulation. Test 2 followed the same design as Test 1 but with different flow rates. Upon transitions in administered concentrations, flow rates were increased to 30 L/min for 1 m:30s.

The new circuit has been deployed in multi-subject fMRI experiments conducted by

our group, in which FiO_2 and $FiCO_2$ were modulated administering 100% O_2 and 5% CO_2 according to the schedule proposed by Bulte *et al* [44]. The circuit has been used in over 20 MRI sessions, with very consistent results. We will show here data obtained from single representative participant who underwent two different runs of the above protocol.

Respiratory gases were monitored using Biopac MP150 (Biopac Systems Inc., CA, USA). Fractional concentrations of O_2 and CO_2 were analyzed and recorded at a 50 ms sampling rate. The gas sampling line consisted of a long segment of rigid tubing pertaining to the monitoring equipment (AFT31-XL) preceded by a disposable bacterial filter (# 2200/01, Air Safety Medical Ltd,) and a short segment of oxygen tubing (# 2001, Salter Labs, CA, USA) to connect the filter to the sampling port of our breathing circuit (built using a TM # 1632 elbow). We noted that, using the current setup, accurate measures of fractional concentration were difficult to obtain when breathing rates exceeded 10 breaths per minute. We believe this effect is mainly associated with the limited rise/fall time of our gas analyzers and mixing of gases inside the sampling line; but we have also observed that the bacterial filter placed in the sampling line contributes to the problem, although we are not certain through which exact mechanisms. In future experiments we intend to 1) replace the long segment of the sampling line by a narrow-bore plastic tubing (then, to overcome the resistance it adds to the line, attach an external sampling pump to Biopac) and 2) test other solutions to filter the sampling gases. In the present study, however, to obtain crisp respiratory signal traces we have instructed subjects to limit their respiratory rate to 10 breaths per minute. If the subject breathes at a pace lower than usual there may be less contamination of inspired gases in breathing circuit, which will result in better performance controlling for inspired doses (even if the decrease in respiratory rate is just minor such as in the particular case of the herein experiments). However, the same is true for the oxygen mask, *i.e.* a reduced respiratory rate also lessens contamination of inspired gases and improves the mask's performance. Therefore we considered that the special requirement to cap respiratory rate should not invalidate the comparison between performances of the two apparatuses. On the contrary, we considered that it would help better illustrating the differences one

should observe if using a robust sampling method.

The pressure wave at the end of the sampling line was monitored using an in-house transducer that connected to one of Biopac's analog channels. This signal helped identifying the expired (*i.e.* end-tidal) points in the post processing of O_2 and CO_2 respiratory traces.

Fractional concentrations were multiplied by 760 mmHg to be converted in approximate partial pressure values. Baseline levels and changes in end-tidal partial pressures were quantified using the approach described in ref [363]. The end-tidal sampled points were fit to a linear model consisting of a third degree polynomial term plus the CO_2/O_2 administration periods as the response regressors, which were shaped using bi-exponential functions to improve the contour of transitions. Baseline levels were obtained from the regressors representing the offset term of the model; respiratory responses represented the effect size of fitted response regressors.

RESULTS

In Figure 4.4 we show results of Tests 1 and 2; tests with the oxygen mask are shown on the left column whereas test with the new circuit on the right.

From the plots on the left column we note how different the composition of actual inspired gases (FiO_2) and the composition of administered gases (FA) can be when the oxygen mask is used. Furthermore, in the second row we have a clear example of how dependent the composition dosage – *i.e.* FiO_2 – can be on the flow dosage – *i.e.* flow rate (FR). The administration of 100% O_2 at different FR's induces different FiO_2 inputs (as well as end-tidal responses). This is related to the contamination of administered gases by room air that leaks in to the mask: for lower FR's the pressure inside the mask is lower, which worsens the leak and reduces FiO_2. Conversely, when fixed FR's are used (which is often the case) the degree of leak will vary according to the fit of the oxygen mask to the subjects' face. This compromises inter- but as well intra-subject reproducibility of the FiO_2 manipulations.

In the tests with the new circuit (right column) there was a very close correspondence

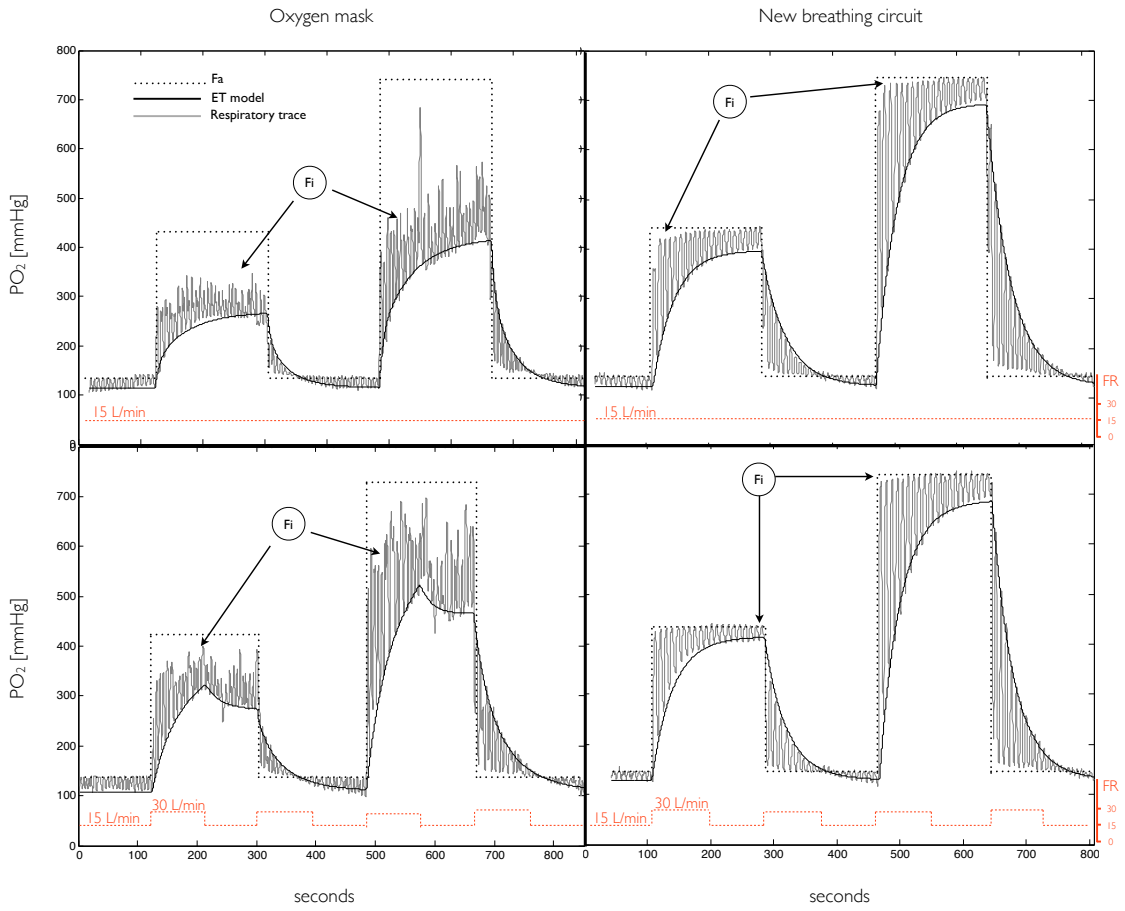

Figure 4.4: Respiratory traces of hyperoxic manipulations using the new circuit (right) *vs.* an oxygen mask (left). In the first row we show tests where 50% O_2 and 100% O_2 were administered in two different instances and in which flow rate was 15 L/min during the entire manipulation. In the second row we repeated the first experiments but increasing the flow rate to 30 L/min during 1m:30s after transitions. Fractional concentrations are given as partial pressure with respect to an atmospheric pressure of 760 mmHg. FA = fractional concentration of administered O_2; Fi = fractional concentration of inspired O_2; ET model = model of the fractional concentration of expired O_2; FR = flow rate.

between FA and FiO_2. In the test where FR was kept constant throughout the manipulation (first row) we note that the transitions in FiO_2 were not as sharp as the switching of gases. This results from the small contamination of new input gases with gases that remained in the limb reservoir from the preceding input phase. In the test where FR is increased from 15 L/min to 30 L/min upon the switching of gases (second row) the replacement of gases from the preceding input by the gases constituting the new FA in-

put is faster, which results in FiO_2 transitions that are sharper. Such maneuver can be used in other experiments as a means to achieve squared step changes in inspired doses. However, in this particular manipulation, the average FR was increased by 100% of the regular flow rate – the limb reservoir being flooded with approximately 22 L of excess gases during each of the 1m:30s transitional periods. To keep the average FR close to normal levels and minimize gas usage, the flush procedure should be as fast as possible. Ideally one would deliver a short bolus of the new FA input with the approximate volume of the limb reservoir. Nevertheless, the flush does not need to be well controlled and in fact any increase in flow rate has the effect of accelerating the transitions in inspired doses. For instance, if flow rates must be limited to a maximum of 20 L/min, keeping FR at this level for 20-30 seconds will greatly improve transitions in the inspired doses. Yet, in the many cases where traceability of flow rates is not a concern, the simplest approach to flush the limb reservoir would consist of opening the regulator's valve widely just before setting the flow rate to normal, traceable, levels.

In Figure 4.5 we show results from manipulations using the circuit in a fMRI experiment for the non-invasive measurement of $CMRO_2$ [106]. The 18-minute respiratory schedule proposed by Bulte *et al.* [44], which includes interleaved stimuli of hyperoxia and hypercapnia, was repeated twice. To accelerate transitions in inspired doses, we have momentarily increased FR from 15 L/min to 60 L/min during 3 seconds upon each FA transition, flooding the limb reservoir with 3 L boluses before resumption of the regular flow rate. The change in gas flow during this flushing procedure is greatly attenuated when gases reach the mask (due to dispersion in the long tubes), and is only marginally perceptible to the subject.

The dosage efficiency was again high, as evidenced by the tight correspondence between the fractional composition of the administered mixtures and the fractional composition of the actual inspired gases. In the O_2 monitoring signal we see the same squared FiO_2 contours as observed in Figure 3 when the 100% O_2 is administered; all of which have the same height as the FA of O_2, *i.e.* 760 mmHg. In the CO_2 monitoring signal, we find blank, rectangular areas under the CO_2 trace when the 5% CO_2 mixture is administered. The height of these areas correspond well to the FA of CO_2. Using moderate

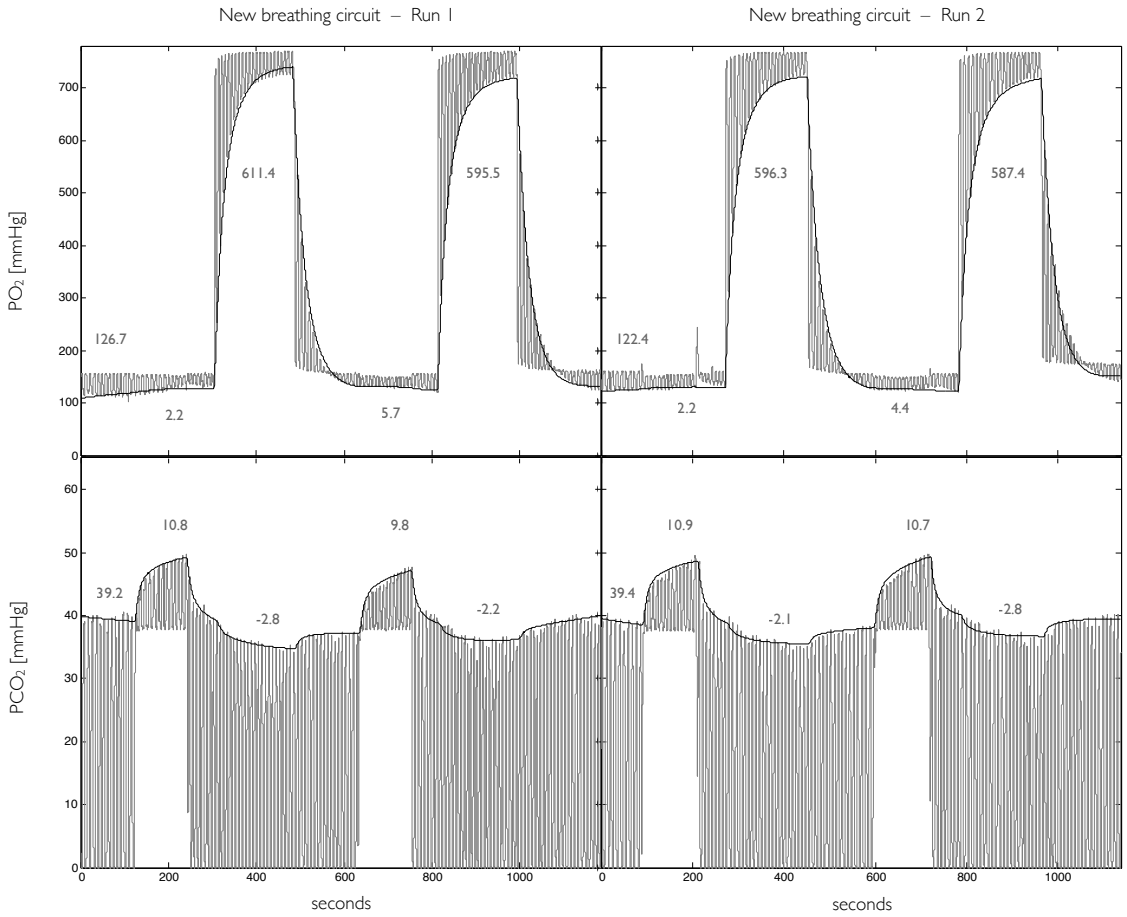

Figure 4.5: Reproducibility of O_2 and CO_2 manipulations using the new breathing circuit. Manipulations consisted of two runs of the 18-minute schedule described in ref [44]. O_2 (top) and CO_2 (bottom) respiratory traces (grey) were modeled as described in Material and Methods to obtain end-tidal (ET) levels (black). Pure O_2 was administered during 3 minutes in two different instances, inducing an approximate 600 mmHg increase in the fractional concentration of ETO_2. A 5%CO_2 mixture was also administered in two different instances, lasting 2 minutes each, which induced an approximate 10 mmHg increase in the fractional concentration of $ETCO_2$. We also observed small changes in ETO_2 and $ETCO_2$ when CO_2 and, respectively, O_2 were administered. When not breathing one of the above compositions, the subject breathed medical air.

rates and a simple flushing procedure, our respiratory circuit allowed sharp and precisely controlled step changes in both FiO_2 and $FiCO_2$.

Our test results also demonstrate that end-tidal responses to controlled step changes in inspired concentrations can be quite reproducible. In Figure 4 it can be seen that modulations in end-tidal gas levels are very similar both in terms of their qualitative shape

and their amplitude. In each plot, the leftmost value represents the baseline end-tidal level of the respective gas, whereas the 4 other values represent the responses associated to the switching of administered/inspired compositions. Modeled increases in $P_{ET}O_2$ and $P_{ET}CO_2$ were both consistent: $P_{ET}O_2$ increases varied by less than 10% relative to the baseline levels whereas $P_{ET}CO_2$ increases varied by less than 2%. Since the magnitude of elicited responses to a given challenge depend on the physiological status of the individual, we note that it might not be possible to attain the same degree of intra-subject reproducibility when subjects are scanned in multiple days.

A careful inspection of the O_2 monitoring trace reveals a small negative FiO_2 input during the administration of CO_2. This results from the slightly lower oxygen content in the administered CO_2 mixture which is composed of 5%CO_2 and 95% of air. And we also note that in this scheme 1) hyperoxic stimuli may not be isocapnic, *i.e.* when breathing pure $O_2$2 the subject's $ETCO_2$ can be markedly depressed; 2) nor the hypercapnic stimuli perfectly iso-oxic as ETO_2 also changes when the CO_2 mixture is administered (although this may be less of a concern given the small, $< 5\%$, relative changes in O_2 levels and its respective impact on the MRI signal).

DISCUSSION

We have developed a simple breathing circuit allowing well controlled step changes in the fractional concentration of inspired gases, to be used in applications such as in MRI studies measuring the cerebrovascular responses to respiratory gases. In addition, the circuit ensures uninterrupted availability of gas and operates at moderate flow rates achievable with standard clinical flow regulators.

The type of mask and unidirectional valves we have employed in our circuit, which prevent dilution of administered gases by room air (as can occur when using standard clinical oxygen masks), are the features permitting the control over fractional inspired concentrations. However, the key component of our circuit is the limb reservoir. While optimizing gas consumption, it permits sharper transitions in the fractional inspired concentrations and, more importantly, endows the circuit with a fail-safe mechanism. It

should be emphasized that for the proper operation of the circuit and its safety features, the limb reservoir must be kept unobstructed at all times. To ensure total protection of the subject additional safety measures should be included, such as the ongoing and careful monitoring of both inspired and expired respiratory gases, as well as arterial O_2 saturation.

Although the proposed circuit could also be used in applications entailing frequent adjustments in inspired fractions (*e.g.* for feed-back control of end-tidal levels) that would require high flow rates to permanently flush the limb reservoir with the right gas composition for inhalation. To control of end-tidal levels at low flow rates alternative methods are warranted [341]. Using the sequential gas delivery method introduced by Banzet *et al.* [18] – which allows controlling for the effective volume of inspired mixtures – combined with a physiological model of the dependence of end-tidal responses on inspired fractions it is possible to prospectively target end-tidal levels with minimal gas usage (a feed-forward modeling method as opposed to feed-back control). This approach requires a computer controlled mixing system in addition to a specially designed breathing circuit, which is normally taped on the subjects' face and forms a closed loop (in case of discomfort the subject can remove a safe plug positioned near the nose).

The prototype we have devised using commercially available parts has a dead space that prevented us from having perfectly squared step changes in inspired concentrations. As can be noticed in most transitions, inspired levels in the first breath right after the switch of gases do not attain the administered concentrations. Ideally the circuit should be fabricated using a non-vented and tightly-sealing mask with minimal-size chamber and a gas input as close as possible to the subjects nose/ mouth to minimize the dead space. Such a circuit, like the one presented here, should include sampling ports, to avoid the use of nasal cannulas and the potential discomfort associated with these, and be disposable.

In summary, the breathing circuit we have presented 1) allows control over fractional inspired concentrations, 2) optimizes gas consumption in block design manipulations, 3) is simple, 4) safe and 5) comfortable.

END OF MANUSCRIPT 1

4.4 Reproducibility of dual-echo pCASL

Other than providing a valuable index of cerebral vasculature function, CVR measures are an essential component of modern fMRI methods mapping brain metabolism, or more precisely the cerebral metabolic rate of oxygen consumption ($CMRO_2$) [9, 110, 157]. The cerebrovascular response to hypercapnia (increased $PaCO_2$) yields a global increase in cerebral perfusion (CBF) but also in blood oxygenation levels, which is reflected in the fMRI signal dubbed BOLD – for blood oxygenation level dependent. Blood oxygenation levels depend on the rate of oxygen delivery, which is determined by CBF, and the rate of oxygen extraction, which is determined by $CMRO_2$. In hypercapnically-induced hyperaemia, the BOLD signal increases because oxygen delivery exceeds the oxygen extraction. On the other hand, hyperoxia (increased PaO_2) causes an increase in oxygen delivery and in the BOLD signal, but with no significant impact on CBF. It has been shown that using maps of CBF and BOLD changes to hypercapnia, a map of the BOLD change to hyperoxia, and a map of resting CBF, it is possible to factor out the contribution of oxygen extraction to the baseline BOLD signal and, with that, map resting $CMRO_2$ [44, 106]. There has been great interest in the development of this type of application and it was in this context that I have assessed reliability of pCASL CVR measures.

A test-retest reproducibility study has been conducted using a FI manipulation to induce hypercapnia and hyperoxia alternately; and pCASL to measure CBF and BOLD simultaneously. For optimal contrast of these two signals, a pCASL implementation allowing the acquisition of two series of EPI gradient echoes were adopted: proton density weighted images arising from the first train of echoes were used to compute the ASL-subtraction perfusion series; BOLD series were obtained from the susceptibility weighted images that derived from the second train of echoes. To ensure reproducibility of the manipulation schedule, the mixing and switching of gases have been achieved using an in-house computer controlled system. Gas mixtures were delivered using the breathing circuit previously described. It has been found that pCASL measures of resting CBF in GM varied by less than 5%, in agreement with a previous report. More than

95% of the GM voxels exhibited a significant baseline CBF signal. Measures of BOLD and CBF responses were also robust (being detected in more than 85% of GM voxels) and consistent, varying by less than 10% in the case of BOLD hypercapnic/hyperoxic responses and by less than 20% in the case of CBF hypercapnic response (also known as CVR). A detailed description of this study can be found in the manuscript that follows, which has been accepted for publication in the Journal of Magnetic Resonance Imaging as a full research article.

4.5 Stuty manuscript 2

Test-retest reliability of CBF and BOLD responses to hypercapnia and hyperoxia using dual-echo pCASL and step changes in the fractional composition of inspired gases

Authors: Felipe B. Tancredi, Isabelle Lajoie and Richard D. Hoge
Status: Accepted for publication in the *Journal of Magnetic Resonance Imaging* (Feb/2015).

Purpose: To assess the reproducibility of BOLD/CBF responses to hypercapnia/hyperoxia using dual-echo pCASL and step changes in inspired doses. **Material and Methods:** Eight subjects were scanned twice, within 24h, using the same respiratory manipulation and imaging protocol. Imaging comprised a 5-min anatomical acquisition, allowing segmentation of the grey-matter (GM) tissue for further analysis, and an 18-min pCASL functional scan. Hypercapnia/hyperoxia were induced by increasing the fraction of inspired CO_2 to 5% and inspired O_2 to 60%, alternately. Reproducibility of BOLD and CBF pCASL measures was assessed by computing the inter-session coefficient of variation (CV) of the respective signals in GM. **Results:** BOLD and CBF measures in GM were robust (with detection rates > 85%) and consistent, yielding CV values below 10% for BOLD hypercapnic/hyperoxic responses and below 20% for the CBF hypercapnic response. The CV for baseline CBF was 3.5%. Visual inspection of baseline and response maps also revealed good reproducibility of anatomic features. **Conclusion:** It is possible to attain reproducible and simultaneous measures of BOLD and CBF responses to blood gases, within a reasonable scan time and with whole brain coverage, using a simple respiratory manipulation and dual-echo pCASL.

Key Words: fMRI, BOLD, ASL, Hypercapnia, Hyperoxia, Cerebrovascular Reactivity

INTRODUCTION

Functional MRI measures of the blood oxygenation (BOLD) and flow (CBF) responses to modulations in blood gases have been explored in studies of the vascular reactivity and oxygen consumption in the brain. While some methods employ hypercapnia (increased arterial CO_2 levels) to stimulate changes in CBF and BOLD [47, 64, 253, 257, 318, 348], others use hyperoxia (increase arterial O_2) to induce changes in BOLD with a weaker impact on CBF [64, 257]. More advanced methods estimating the contribution of tissue oxygen consumption to the baseline BOLD signal rely on measures of BOLD/CBF responses to both hypercapnia and hyperoxia stimulation [44, 106]. Clinical studies often require repeating a scan before and after a therapeutic intervention and results are only meaningful if imaging measures are reproducible in the absence of physiological changes. Whereas the clinical adoption of the imaging techniques under current development hinges on the robustness/reliability fMRI measures, it also does, to some extent, on the availability (*i.e.* simplicity/compatibility) of related methods.

Modulations in blood gases are usually achieved, non-invasively, through breathing maneuvers that induce changes in respiratory end-tidal (ET) levels [363], since these reflect arterial blood gas content. Simple expedients such as hyperventilation and breath-holding can induce changes in ET levels [39, 185, 187, 188, 269] and are widely available, but these methods do not allow independent modulation of CO_2/O_2 ET levels and strongly rely on subject compliance, which compromises repeatability of the stimuli. The preferred method for induction of hypercapnia and hyperoxia has been to administer air mixtures containing CO_2 or supplemental O_2 for inhalation [93]. Although sophisticated strategies using computerized systems to deliver variable inspired concentrations and target ET levels [30, 377, 400] can afford respiratory stimulations that are highly reproducible [398], the simpler approach of administering predetermined/fixed concentrations for inhalation remains an attractive alternative for clinical applications and continues to be widely adopted in quantitative neuroimaging [44, 53, 104, 107, 110, 129, 149, 245, 275, 320, 418].

A common way to induce hypercapnia and hyperoxia has been to administer CO_2

and O_2 enriched air mixtures at a constant flow rate through standard clinical oxygen masks used in respiratory therapy. A limitation of this method is the poor control over the composition of gases actually inspired by the participant [33, 365], which hampers reproducibility of the respiratory stimuli and related fMRI measures [256]. Alternatives to improve control over inspired doses include partially sealing the edges of standard oxygen masks with adhesive tape, or administering gas mixtures at high flow rates using apparatus such as t-valves, mouthpieces and nose clips in place of the oxygen mask. However, these solutions can be uncomfortable for the subject. Our research group has recently described a breathing circuit whose design intends to alleviate the latter concerns [365]. The apparatus affords improved control over the inspired doses using a comfortable mask that can be easily put on and removed. Additionally, the circuit design allows uninterrupted breathing of ambient room air in the event that the flow of medical gases is interrupted, providing a reliable fail-safe mechanism. This offers a good compromise between simplicity of the gas administration, reproducibility of inspired doses and, equally important, subjects' comfort to the procedure. It is still uncertain though to which extent an improved fixed inspired manipulation impacts on the reproducibility of ET and related fMRI responses.

Studies assessing the reactivity of cerebral vasculature to respiratory challenges have employed either ASL [104, 274, 363], which provides a direct measurement of flow, or BOLD imaging [30, 53, 245, 253, 374, 418], which allows monitoring of hemodynamic-related oxygenation responses. Calibrated fMRI methods, on the other hand, require both measures [44, 106, 108, 156]. Given that it might be difficult to reproduce the exact same physiological condition in two different scans, it is desirable that BOLD and CBF signals be acquired simultaneously, *i.e.* during the same manipulation. Since the BOLD signal can be obtained from the ASL series [44, 403], this is less of a concern. Nevertheless, when extrapolating BOLD from a single echo time ASL series, this requires a certain compromise between the two imaging contrasts. A dual-echo imaging scheme, at the expense of minor protocol adaptations, optimizes imaging contrasts and can improve the simultaneous measure of BOLD and flow signals [108].

Although continuous ASL (CASL) offers theoretical advantages over pulsed ASL

(PASL), such as increased temporal SNR and implicit control over label delivery time [384, 404], the predominant ASL technique has been the PASL type because of the broader compatibility of clinical scanners with pulsed labeling schemes. Pseudo-CASL (pCASL), in which a train of short pulses mimics CASL's continuous irradiation, has allowed researches to obtain CBF measures that are comparable to true CASL using standard MRI hardware [61, 298]. It has already been employed in several studies measuring respiratory-induced hemodynamic changes [44, 107, 108, 363] and a comparison between pCASL *vs.* a typical implementation of PASL [364] indicated that 1) pCASL is more sensitive in detecting respiratory-induced global CBF changes and 2) accuracy of its measures less vulnerable to time-shift effects. A dual-echo version of pCASL has great potential to promote new fMRI applications that are based on the simultaneous measure of respiratory-stimulated changes in BOLD and CBF; however, reliability of such pCASL measures remains to be determined. To facilitate replication of results and clinical translation of methods we considered that a reproducibility study should be carried out using a broadly available stimulation method, such as a fixed inspired gas manipulation.

The objective of this study was to assess the test-retest reproducibility of BOLD and CBF hemodynamic responses to brief step changes in inspired O_2 and CO_2 levels, using a dual-echo pCASL sequence to simultaneously image blood flow and oxygenation in a small cohort of young healthy subjects.

MATERIAL AND METHODS

Eight healthy volunteers (ages between 22 and 40 years) were enrolled in this study. They gave informed consent for their participation and experiments were conducted with the approval of the Comité mixte d'éthique de la recherche du Regroupement Neuroimagerie/Québec. Experiments consisted of repeating an fMRI measurement in each subject in two separate scan sessions, which will be referred to as Tests A and B. The brain imaging protocol included a brief 5-min anatomical acquisition and a 18-min functional scan where BOLD and CBF signals were measured in the course of a respiratory manip-

ulation combining hypercapnia and hyperoxia. Maximum interval between the two test measurements was 24h; minimum 20 minutes.

Respiratory Manipulation

This manipulation consisted of interleaving two 2-min periods of hypercapnia induction with two 3-min periods of hyperoxia using fixed step changes in fractional concentration of inspired O_2 and CO_2 (FiO_2 and $FiCO_2$) as in [44]. Controlled FiO_2/$FiCO_2$ changes have been achieved using the breathing circuit described in [365] to administer the O_2/CO_2 enriched mixtures for inhalation (Figure 4.6). Using flow rates achievable with clinical flow regulators this circuit affords a tight correspondence between the fractional composition of administered gases and the actual dose inspired by the subject. During the five baseline epochs of the manipulation, subjects were given air with atmospheric composition for inhalation. To induce hypercapnia, a gas mixture containing 5% of CO_2 balanced with air has been administered, thus increasing subjects' $FiCO_2$ by about 5%. Hyperoxia was induced by having subjects breath a mixture composed of 50% pure oxygen balanced with air, yielding an approximate three-fold increase in subjects' FiO_2.

An automated system, fabricated in-house, was used for the switching and mixing of gases to ensure reproducible timing of the gas administration schedule. Our system comprises 3 electrically actuated flow controllers (SideTrak® 840, Sierra Instruments L. Monterey, CA, USA) receiving medical air, oxygen and a 5%CO_2-air mixture as gas inputs; a 25 mL mixing chamber where the 3 output gases converge to prior to the final delivery; and a computer controlled electronic box sending serial commands to the flow controllers. The output of the mixing system connected to the breathing circuit through $\sim$10 m of oxygen plastic tubing. The system was programmed to 1) deliver medical air during the baseline periods; 2) switch gas administration to the CO_2 mixture during the hypercapnic periods; and 3) flow equal amounts of O_2 and medical air during the hyperoxic periods. Gas mixtures were delivered at a flow rate of 20 L/min, except during the first 5.4 seconds after each transition when flow rates were increased to 50 L/min to accelerate the transition of inspired gases.

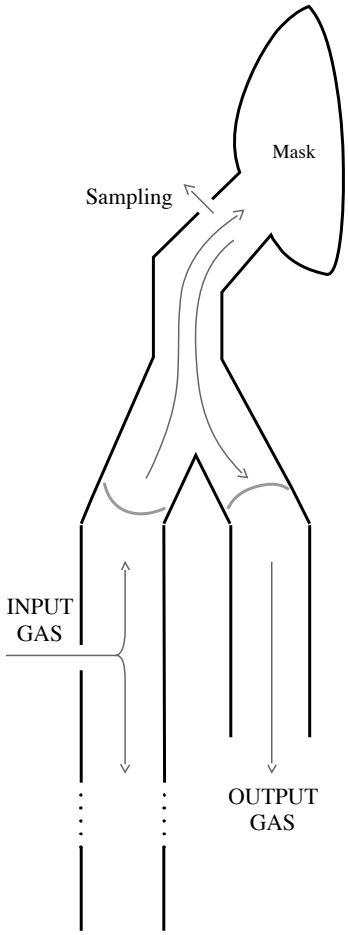

Figure 4.6: Respiratory circuit. The breathing circuit we adopted in our study has been described in Ref.[365]. It consists of a dual-limb circuit controlled by unidirectional valves, which keeps administered (INPUT) gases from mixing with expired (OUTPUT) gases. The facial mask incorporated in the circuit offers a tight fit which keeps INPUT/OUTPUT gases from diluting by the entrainment of room air. INPUT gases are delivered in a limb reservoir, which can be filled with room air in case the INPUT flow does not meet the subject's minute volume. INPUT/OUTPUT gases are monitored through a sampling port near the mask.

Respiratory gases were continuously monitored and recorded using a Biopac MP150 system (BIOPAC Systems Inc., CA, USA). The gas sampling line consisted of a 10 m segment of rigid tubing (AFT31-XL, also from BIOPAC Systems Inc.) preceded by an insufflation filter (# 2200/01, GVS filter technology, LA, UK) and a 1' segment of oxygen tubing to connect the filter to the sampling port of the breathing circuit. We have also recorded the pressure wave at the end of the sampling line using an in-house

transducer connected to one of Biopac's analog channels. This signal was useful in the post-processing of O_2/CO_2 traces as it helped identifying end-tidal (ET) points.

Imaging Protocol

Brain scans were acquired using a 3T scanner (Siemens TIM TRIO, Siemens Medical Solutions, Erlangen, Germany) and the vendor's 32-channel head coil. A mirror affixed to the head coil, allowed subjects to view a projection screen situated in the back of the scanner.

The breathing circuit we used in these experiments has an open limb through which room air will enter whenever the flow of input gases are interrupted or becomes insufficient, *i.e.* there is no need to supply the subject with medical air to ensure a normal breathing. However, this was treated as a fail safe mechanism and did supply subjects with 15 L/min of medical air during the entire period they were fitted with the circuit (clearly, during the manipulation, other medical gases have also been administered). After setting the gas system to deliver medical air at 15 L/min subjects were fitted with the breathing circuit and monitoring of respiratory traces started immediately thereafter. Subjects were covered with a pair of blankets to maximize comfort and finally placed head first in the scanner.

A T_1-weighted anatomical acquisition (5 min MPRAGE at 1 mm^3) followed a quick localization scout. During this period a slide show with random pictures of nature was projected onto the back screen. Respiratory traces during the anatomical acquisition were recorded and kept in a separate file.

For the functional scan we have used a dual-echo version of pseudo-continuous ASL (de-pCASL) to obtain simultaneous measures of BOLD and CBF. The pCASL [72] parameters were: label duration = 2 s (of Hanning shaped 500 μs pulses), post-label delay = 0.9 s, labeling plane placed 10 cm below the centre of image slab, plane selection gradient = 6 mT/m, TE_1/TE_2 = 8.4/30 ms and TR = 4.12 s. Readout consisted of a GRE-EPI scheme (GRAPPA acceleration factor of 2 and 7/8 partial sampling of k-space) imaging a total of 21 slices with 4.5 mm thickness, 10% gap and an in-plane resolution of 4.5x4.5 mm^2. With the above parameters, 131 ASL pairs have been collected along

the 18 min respiratory protocol. Subjects were instructed to stay awake and breath comfortably. During this period a solid-grey background image with a small fixation marker was projected onto the back screen.

Respiratory data Analysis

Continuous traces of respiratory O_2 and CO_2 were first multiplied by 760 mmHg, to convert fractional concentrations in approximate partial pressure values. Next, we have identified the late phases of expiration in the pressure wave signal. Based on the time indexes of their respective occurrences, we have then extracted a vector of end-tidal (ET) values from each of the O_2 and CO_2 continuous traces. Lastly, baseline levels and changes in ET partial pressure were quantified as in [363]. ET sampled points were fit to a model consisting of a third degree polynomial term plus four response regressors representing the CO_2/O_2 administration periods (Figure 4.7, left).

Response regressors consisted of the paradigm block design whose transitions were shaped using exponential functions to improve the contour of transitions and increase statistical power of the fit. To compensate for delays in the respiratory recordings the paradigm design has been shifted by 5-10 seconds on an individual basis. ET responses to step decreases in inspired doses were analysed separately from the responses to step increases, similar to the approach used in [304]. Due to small drifts in the recorded values an extra exponential term has been added to the bi-exponential model proposed in [363]. Time constants were optimized, for each subject, using a computer algorithm based on least squares. While baseline ET levels were obtained from the offset term of the model, ET responses were obtained from the effect size of fitted response regressors. ET CO_2 responses to the different periods of CO_2 administration were averaged to synthesize the hypercapnic response in a single value. The same procedure was applied to the ET CO_2 response to O_2 administration, and ET O_2 responses to both O_2 and CO_2 administration.

We also report the baseline ET levels recorded during the anatomical acquisition, which we refer to as "resting levels," to differentiate from the baseline levels encountered during the respiratory maneuver (baseline ET levels may vary from the time the subject

is placed in the scanner until the end of the experiment as a result of cardiovascular adaptation to the supine position, small temperature/metabolic changes and the breathing manipulation *per se*). Resting levels were computed by fitting the series of ET samples with a constant function. Post-processing of respiratory data including extraction of ET points and modeling of ET vectors were carried out using code we developed in MatLab (MathWorks, Natick, MA, USA).

Average ET O_2 and ET CO_2 traces were computed after having resampled all individual ET traces to the ASL series TR (4.12s) by linear interpolation.

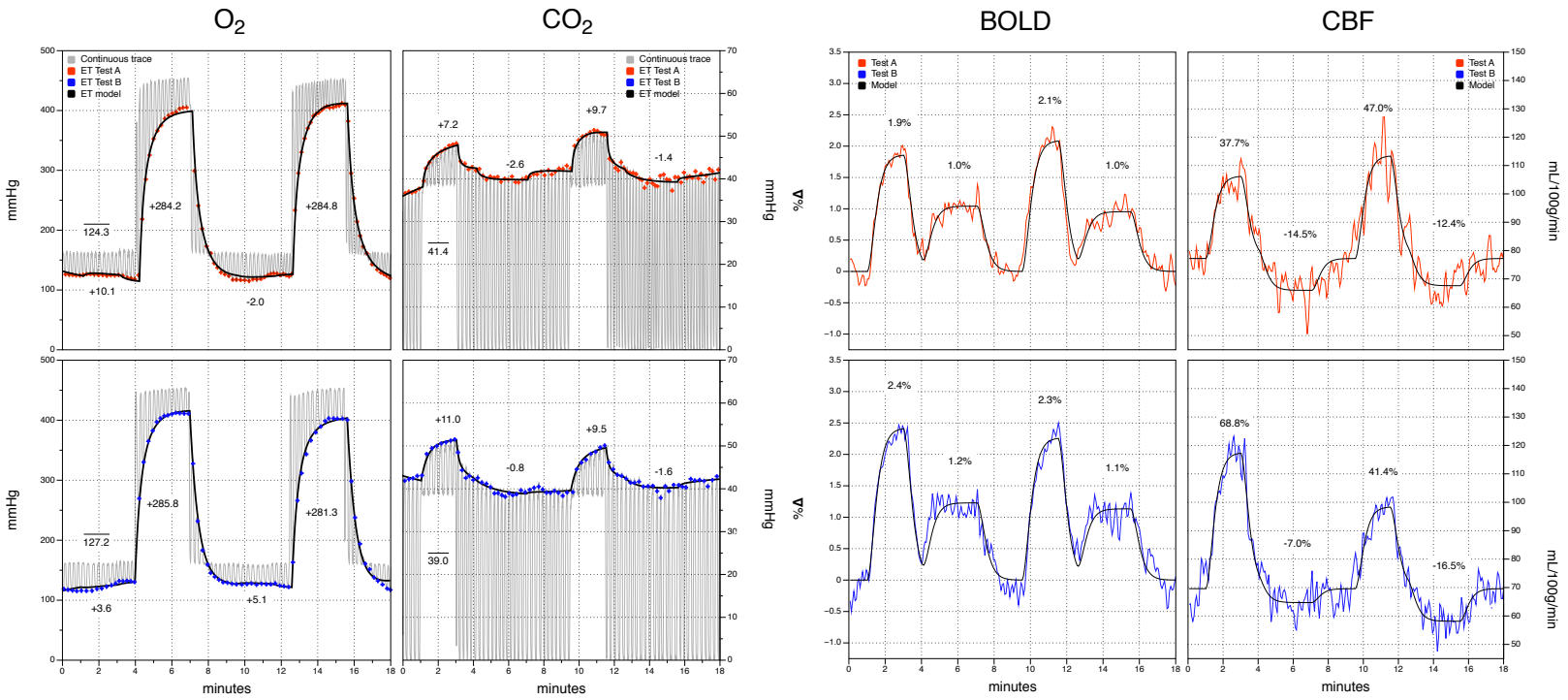

Figure 4.7: Respiratory and fMRI signal analysis. In this composite figure we show an illustrative example of how respiratory (left panel) and fMRI (right panel) signals were analyzed to generate the parametric maps. End-tidal points (colored crosses) were identified in the continuous traces (grey) and modeled (black) to estimate baseline and responses. Baseline values are indicated by a bar, magnitude of responses are displayed close to the corresponding stimulation epochs. R^2 for the end-tidal model fits in the test/retest scans are: O_2 = 0.998/0.999 and CO_2 = 0.959/0.957. BOLD and CBF signals were also linear modeled. Magnitude of responses are displayed close to the corresponding stimulation epochs. R^2 for the fMRI fits are: BOLD = 0.946/0.935 and CBF = 0.871/0.924. The signals we show correspond to the average signal computed for the GM-ROI (drifts have been removed from the BOLD signal but not from CBF). Both CO_2 and O_2 stimulations yield positive BOLD responses whereas CBF responses are positive for CO_2 and negative for O_2. Data from this subject also illustrates the strong dependence of fMRI signals on the respiratory ET levels. Variations in BOLD and CBF responses to the different epochs of O_2 and CO_2 administrations were correlated with ET changes. Baseline CBF is higher in Test A (red) compared to Test B (blue) probably because the baseline level of CO_2 was 1.4 mmHg higher in Test A. CVR maps are shown in the next figure.

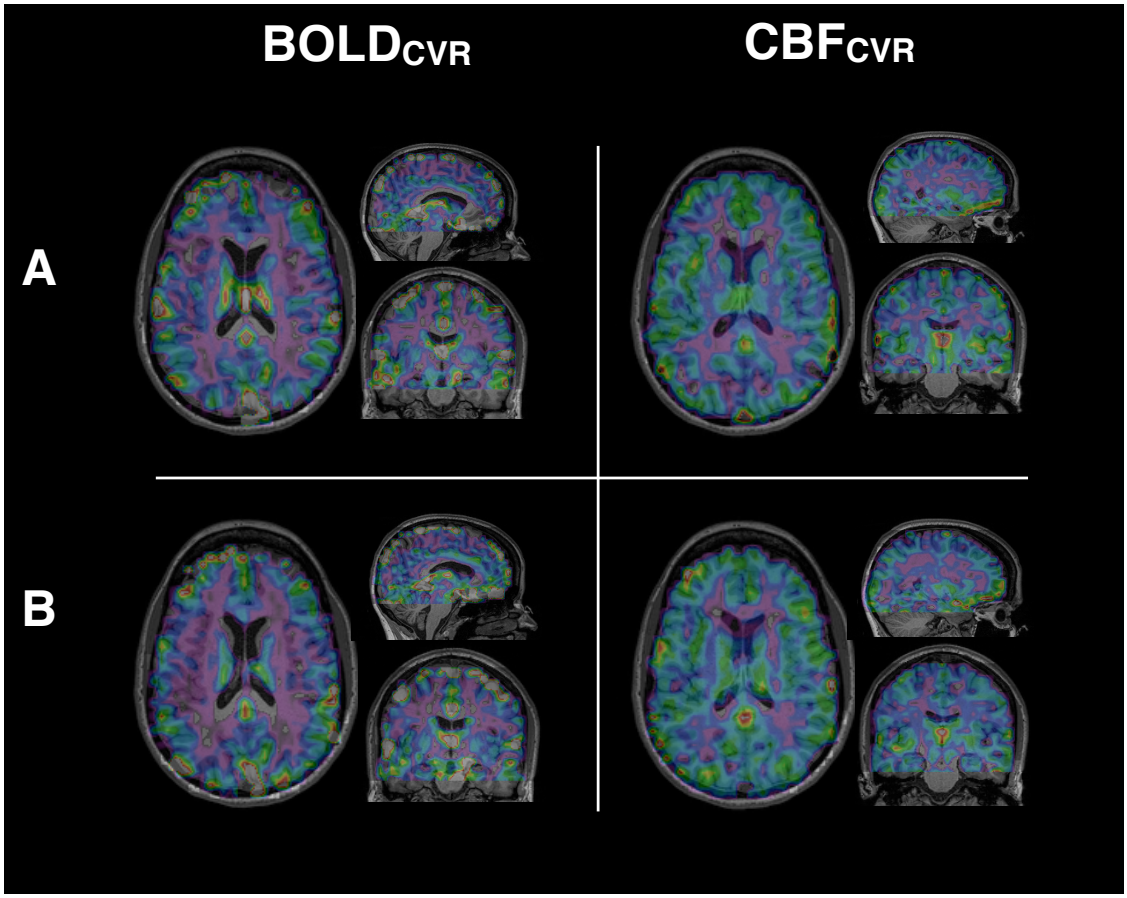

Figure 4.8: Individual CVR maps. Illustrative example of CVR maps computed for the same subject data in the preceding figure - BOLD/CBF response maps for each run were divided by the respective increases in ET CO_2 levels.

Imaging data Analysis

Anatomic images were segmented using FSL's FAST tool [426] to generate a binary mask of the brain and a grey-matter probability map for each individual subject. These were resampled to the spatial resolution of fMRI scans.

Functional data was analyzed using NeuroLens2 (www.neurolens.org). Images were first motion corrected. Tag and control series from both echoes were subtracted using linear interpolation. ASL flow series were computed as the difference between control scans and the mean value of neighboring tag scans in the first echo; BOLD as the sum of tag and the mean value for adjacent control scans in the second echo. BOLD and ASL series were modeled using a GLM consisting of 1 regressor for each of the 2 hypercap-

nic/hyperoxic stimuli plus a 3rd degree polynomial to represent signal drift and baseline offset (Figure 4.7 right).We used a gamma variate HRF function with 20s time-to-peak and 40s width, which accurately modeled the relatively slow gas responses. Effect sizes for hypercapnia and hyperoxia were respectively averaged to provide a single response metric for each type of stimulus. BOLD responses were expressed as a percent change of the baseline signal. ASL signals were converted to CBF in units of mL/100g/min as in [386]. BOLD and CBF responses were expressed either in terms of the total change to the different stimuli or normalized by the size of the stimuli, *e.g.* BOLD and CBF signal changes to hypercapnia have been divided by the ET CO_2 increases yielding CVR indexes of %ΔBOLD/mmHg and ΔCBF/mmHg (Figure 4.8 shows an example of BOLD and CBF reactivity maps obtained from the analysis of responses modeled in Figure 4.7). The BOLD response to hyperoxia was normalized with respect to the increase in ET O_2 and was expressed in units of Δ%BOLD/100mmHg.

Valid ASL measures can not be obtained in voxels for which a substantial volume fraction is occupied by large veins or arteries. Idiosyncratic flow and BOLD responses during hypercapnia and hyperoxia can be used to identify such voxels; for example very large negative changes in apparent CBF during hyperoxia are likely due to T_1 shortening in arterial blood. Voxels presenting CBF responses lower than -50 mL/100g/min in hyperoxia or higher than 10% in hypercapnia were considered to be non-parenchymal and were excluded from further analysis as in [106]. Voxels affected by the susceptibility artifact related to the inhalation of enriched O2 mixtures were also excluded from the analysis. An empirical threshold of -5% in BOLD responses was determined empirically, based on visual inspection of the various response maps and raw EPI scans. We refer to all the above mentioned voxels as “non-parenchymal” voxels. We then reanalyzed the imaging data, this time applying spatial smoothing just after motion correction (6 mm FWHM 3D Gaussian kernel) but excluding the non-parenchymal voxels and compensating for downward bias introduced by their removal. This procedure consisted of dividing the smoothed fMRI maps by a smoothed version of the brain mask from which non-parenchymal voxels have also been removed.

To estimate the BOLD and CBF signal in grey-matter (GM) we have computed GM-

weighted averages by averaging signals over the GM probability mask we obtained from segmentation of the anatomical scan. These GM region-of-interests (ROIs) were thresholded at 50% and had non-parenchymal voxels removed. Average BOLD traces for Tests A and B, were computed by first removing signal drifts from individual traces. The linear modeling of CBF responses also included drift regressors to make it consistent with the BOLD signal analysis. However, to permit visualization of perfusion drifts during the manipulation, we display non-detrended CBF signals.

From the GLM analysis we also obtained parametric maps of the signal-to-noise (SNR), contrast-to-noise ratio (CNR) and T-statistics of BOLD and CBF responses. The T-maps were used to compute the detection rate in GM, *i.e.* the percent of GM voxels exhibiting significant ($P < 0.05$ corrected) baseline CBF signal or increase in response to hypercapnia/hyperoxia, which gives a measure of the technique's sensitivity. The grey-matter SNR and CNR were calculated by averaging their respective values over the GM-ROI, as described above. While the detection rate provides an estimate of the technique's sensitivity, the CNR allows comparison of fMRI responses in terms of the robustness of physical signals (BOLD *vs.* CBF) and responsiveness to the physiological stimuli (hypercapnia *vs.* hyperoxia).

Lastly, we registered individual maps to the MNI 152 template using FSL FLIRT tool [180] and computed group-average maps for the different scan session, *i.e.* average maps for Tests A and B.

Reproducibility Analysis

As a measure of the reproducibility of our respiratory manipulations and fMRI measures in GM we have computed the inter-session coefficient of variation (CV) for these variables as in [61]. First, a CV between Tests A and B was computed, for each individual subject, as the percent of variability with respect to the mean value, *i.e.* $100*(SD/MEAN)$. The overall CV was then computed by averaging the squared CV values and taking the square root. Test measurements A and B were also compared voxel wisely. Individual CV maps were generated by computing the CVs for all voxels in the individual parametric maps A and B (registered onto the MNI space). Overall CV

maps were obtained by averaging the squared CV maps and then taking the square root.

RESULTS

All participants tolerated the manipulation well. One subject reported having falling asleep during both test measurements, which reflected in respiratory traces that were less uniform than those measured in other participants. Modeled ET levels are reported in Table 4.I.

[mmHg]	End-tidal O_2 levels				End-tidal CO_2 levels			
	Rest	Baseline	Δ to O_2	Δ to CO_2	Rest	Baseline	Δ to CO_2	Δ to O_2
A	113 ± 5	118 ± 3	281 ± 3	6 ± 2	40 ± 2	39 ± 1	11.8 ± 0.8	-1.1 ± 0.3
B	113 ± 5	117 ± 4	285 ± 4	3 ± 2	42 ± 2	40 ± 1	12.1 ± 0.8	-0.6 ± 0.2
%CV	17.0	4.2	3.8	150	13.5	5.5	13.2	155

Table 4.I: Respiratory manipulation. ET O_2 and ET CO_2 values are given in mmHg. Rest = baseline ET levels measured during the anatomical acquisition; BSL = baseline levels measured during the manipulation; Δ to CO_2 = average change in the respective ET levels during the CO_2 administration; Δ to CO_2 = average change during the O_2 administration. CV% = coefficient of variation (percent of variation with respect to the mean) between test measurements A and B.

The small but significant (t-student paired test, $P < 0.02$) reduction in ET CO_2 and increase in ET O_2 from resting to baseline result from a subtle increase in subjects' minute volume during the functional scan. When the comparison was between Tests A and B, baseline and resting values did not differed significantly ($P > 0.2$). End-Tidal changes observed in both tests were also reproducible, though the CV for CO_2-induced hypercapnic responses was more than 3 times higher than the CV for O_2-induced hyperoxia (13.2% *vs.* 3.8%), which probably stems from the lower ratio between the magnitude of the increases and baseline levels. The hyperoxic stimulus increased ET O_2 levels by almost 285 mmHg (from a baseline of 118 mmHg to 401 mmHg at the end of the O_2 administration) whereas the hypercapnia stimulus induced an approximate 12 mmHg increase in ET CO_2 levels (from 39 mmHg to 51 mmHg). Due to a hypercapnically-driven increase in minute volume ventilation ET O_2 levels increased by ≈5 mmHg during the CO_2 administration, in spite of the lower O_2 fraction in the CO_2 mixture compared to

the medical air inhaled during baseline period. Conversely, during the O_2 administration ET CO_2 decreased by ≈1 mmHg as a result of a paradoxical increase in minute volume provoked by hyperoxia [169, 247].

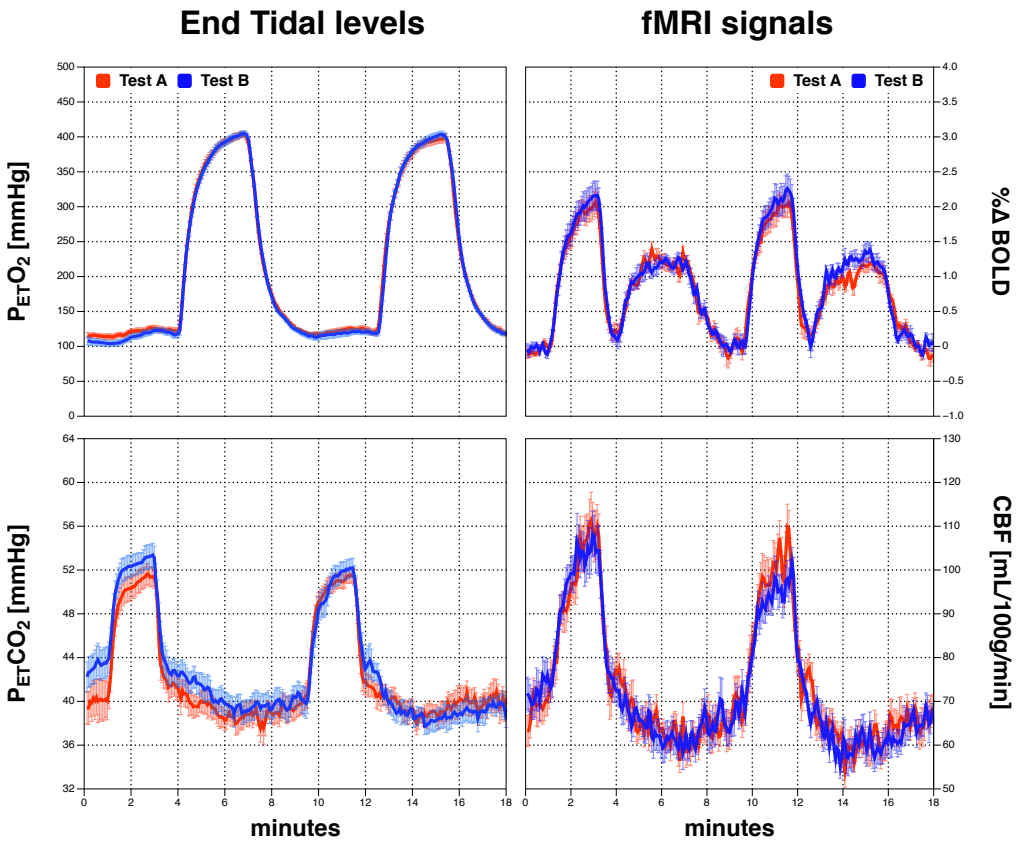

Figure 4.9: Average manipulation and fMRI signals in the GM-ROI. Results from Test A are shown in red and from Test B in blue. BOLD signal increases to both hypercapnia and hyperoxia stimulation while the pCASL flow signal (CBF) increases during hypercapnia and decreases during hyperoxia.

The average ET traces in Tests A and B are shown in the left column of Figure 4.9. Temporal evolution of ET O_2 levels in response to the manipulation were highly reproducible as indicated by the almost complete overlap of Test A and B average traces (Pearson's r = 0.9994) and small error bars. ET CO_2 traces were also fairly reproducible (r = 0.9662) but we note that in Test B the average ET trace exhibits a drift that is not evident in Test A (first test). In Test B subjects tended to begin the manipulation at a higher

level compared to Test A (about 3 mmHg higher) and, along the scan, experienced a progressive decline in ET levels, which, towards the end of the manipulation, fell below the levels observed in Test A. Given that we have modeled ET traces incorporating drift regressors, and that the two traces intersect nearly halfway the manipulation, the baseline levels computed for both manipulations were almost equivalent: 39±1 mmHg in Test A *vs.* 40±1 mmHg in Test B.

Right column of Figure 4.9 shows the GM BOLD and CBF signals that were measured in Tests A and B. Signals are very similar both in terms of temporal evolution and magnitude of the peak responses (r = 0.9365/0.8454). Respiratory stimuli yield consistent changes in BOLD and CBF signals along the manipulation as well as across subjects. BOLD signal increased in average 1.9±0.2% during the hypercapnic stimuli and 1.14±0.04% in response to hyperoxia in both Tests A and B. As to the pCASL flow signal, we observe small diminutions during hyperoxic epochs and marked increases during the CO_2 administration, indicating an average increase of 53±3% in CBF levels in response to hypercapnia. The drift we observe in ET CO_2 levels of Test B is not as evident in the CBF related measure, although we note that the flow signal in Test B starts at a slightly higher level (5 to 10 mL/100g/min).

Table 4.II shows a summary of modeled fMRI signals in the GM ROI. The CV for baseline CBF was 3.4%, comparable to that found by Chen *et al.* Measures of the CBF response to hypercapnia showed a variance of 16.3% between Tests A and B. When these measures were normalized by the ET CO_2 increases to compute cerebrovascular reactivity (CVR), contrary to what we expected, CV tended to increase, reaching 19.8%. The relative increase in CBF per mmHg increase in ET CO_2 was 4.6±0.5%, with a 20.3% variance between tests. Reproducibility of BOLD signals were greater. The CV of BOLD hypercapnic response was 6.8%. When the responses were normalized by the magnitude of ET CO_2 increases, we obtained the same trend observed for CBF, CV tended to increase, reaching 8.8%. While the magnitude of hyperoxic BOLD responses was lower compared to that found for hypercapnia (1.14±0.04% *vs.* 1.9±0.2%), the CV of hyperoxic BOLD was slightly greater than the CV of hypercapnic BOLD: 8.4% *vs.* 6.8%. When hyperoxic responses were normalized by the magnitude of ET O_2 stimulus,

CV increased to 10% – the same trend observed for the other fMRI responses, and also reported by Goode *et al* [128].

	fMRI measures							
	CBF				BOLD			
	BSL	Δ to CO2	Δ/ΔCO2	%Δ/ΔCO2	%Δ to CO2	%Δ/ΔCO2	%Δ to O2	%Δ/ΔO2
	mL/100g/min	mL/100g/min	mL/100g/min/mmHg	%/mmHg	%	%/mmHg	%	%/100mmHg
A	67 ± 3	37 ± 3	3.3 ± 0.3	4.9 ± 0.5	1.9 ± 0.2	0.17 ± 0.02	1.16 ± 0.04	0.41 ± 0.01
B	67 ± 3	33 ± 3	2.8 ± 0.3	4.3 ± 0.5	1.9 ± 0.2	0.17 ± 0.02	1.12 ± 0.03	0.39 ± 0.01
%CV	3.4	16.3	19,8	20.3	6.8	8.8	8.4	10.0

Table 4.II: Functional MRI signals in the GM-ROI. BSL = Baseline; Δ to CO_2 = average signal change during hypercapnia; Δ/CO_2 = average signal change during hypercapnia normalized by the increase in CO_2; $\Delta\%/\Delta CO_2$ = average percent signal change during hypercapnia normalized by the increase in CO_2; $\Delta\%/CO_2$ = average percent signal change during hypercapnia; $\Delta\%/\Delta CO_2$ = average percent signal change during hypercapnia normalized by the increase in CO_2; $\Delta\%/O_2$ = average percent signal change during hyperoxia; $\Delta\%/\Delta O_2$ = average percent signal change during hyperoxia normalized by the increase in O_2; %CV = coefficient of variance between Tests A and B (as a percent of the average signal).

	CNR of fMRI signals and detection rate in GM					
	CBF			BOLD		
	BSL	Δ to CO2		BSL	Δ to CO2	Δ to O2
	SNR / %GM	CNR / %GM		SNR	CNR / %GM	CNR / %GM
A	2.6 ± 0.2 / 96.3 ± 0.7	1.4 ± 0.08 / 88 ± 1		226 ± 15	3.9 ± 0.4 / 89 ± 2	2.4 ± 0.1 / 89 ± 1
B	2.5 ± 0.2 / 96.5 ± 0.7	1.2 ± 0.1 / 85 ± 3		222 ± 12	3.9 ± 0.4 / 88 ± 2	2.3 ± 0.2 / 88 ± 1
%CV	7.9 / 0.8	15.1 / 6.8		4.8	6.6 / 2.0	10.0 / 1.6

Table 4.III: Signal quality and detection in GM. NR = Contrast-to-noise ratio; %GM = percent of GM voxels significantly ($P < 0.05$, corrected) responding to the stimulus. Metrics concern the measurement of baseline (BSL) flow signal, BOLD/CBF changes during hypercapnia (Δ to CO_2) and BOLD changes during hyperoxia (Δ to O_2).

In Table 4.III we report metrics that permit assessing the quality of the fMRI signals measured in the GM ROI, namely: signal-to-noise ratio (SNR) of the BOLD and CBF signals, contrast-to-noise ratio (CNR) of hypercapnic/hyperoxic fMRI responses and detection rate of baseline CBF (CBF_0) and gas responses. We have found that detection rates were above 85% for all measured quantities. On average, 96.4±0.7% of GM voxels showed significant CBF_0 signal ($P < 0.05$, corrected). The detection rate of BOLD and CBF responses to hypercapnia were 88±2% *vs.* 87±2%, respectively; detection rate

of BOLD hyperoxic response was 88±1%. The average CNR of BOLD hypercapnic responses were 3 times greater than the CNR of CBF responses, 3.9±0.3 *vs.* 1.32±0.06, which reflects the higher temporal stability of the BOLD signal. The CNR of BOLD hyperoxic responses were 2.4±0.1, lower than the CNR for the hypercapnia responses, although we note that a different scenario could have been observed if the magnitude of CO_2 and O_2 increases were other (*e.g.* ET CO_2 increases of 5 mmHg combined with ET O_2 increases of 600 mmHg). The BOLD SNR, as expected, was conspicuously higher than the SNR of ASL subtracted series (*i.e.* CBF): average values were, respectively, 224±9 and 2.5±0.1.

In Figure 4.10, we show BOLD and CBF group maps for 3 different axial slices of the MNI 152 template (slices 66, 81 and 96). BOLD maps are shown in the 3 columns on the left while CBF maps in the 3 columns on the right. Each set of 3 rows shows results pertaining to Test A, Test B and the respective coefficient (CV) of variation between the two measurements.

As expected, overall, functional maps exhibit a distinct grey-matter / white-matter contrast, in keeping with the notion that the prominent neural/vascular density of grey-matter tissue (GM) engenders BOLD/CBF signals that are higher than those observed in white-matter (WM). The window level of CV maps are all the same, namely 0-200%. At these levels, the transition from violet to blue indicates the passage from 20% to 30%, the approximate fiducial limit of CV. Qualitatively, CV maps show, overall, low variability (<30%) in the GM region. The high CV values forming a blue rim around the cortex of virtually all CV maps result from the misalignment of individual maps and can be considered artifactual.

BOLD SNR-CV maps (rows 1 and 2, left) are remarkably homogeneous, revealing CVs in WM comparable to the CV in GM. On the other hand, the BOLD (and also CBF) CVR-CV maps indicate that CVR measures in WM are much more difficult to reproduce (rows 4, 5 and 6). Regional variability of HOR-CV (last row) tend to be lower than the CVR-CV; however, HOR measures near the nasal cavity can be severely compromised by the susceptibility effect of inspired O_2, creating a region of high variability in proximal slice(s).

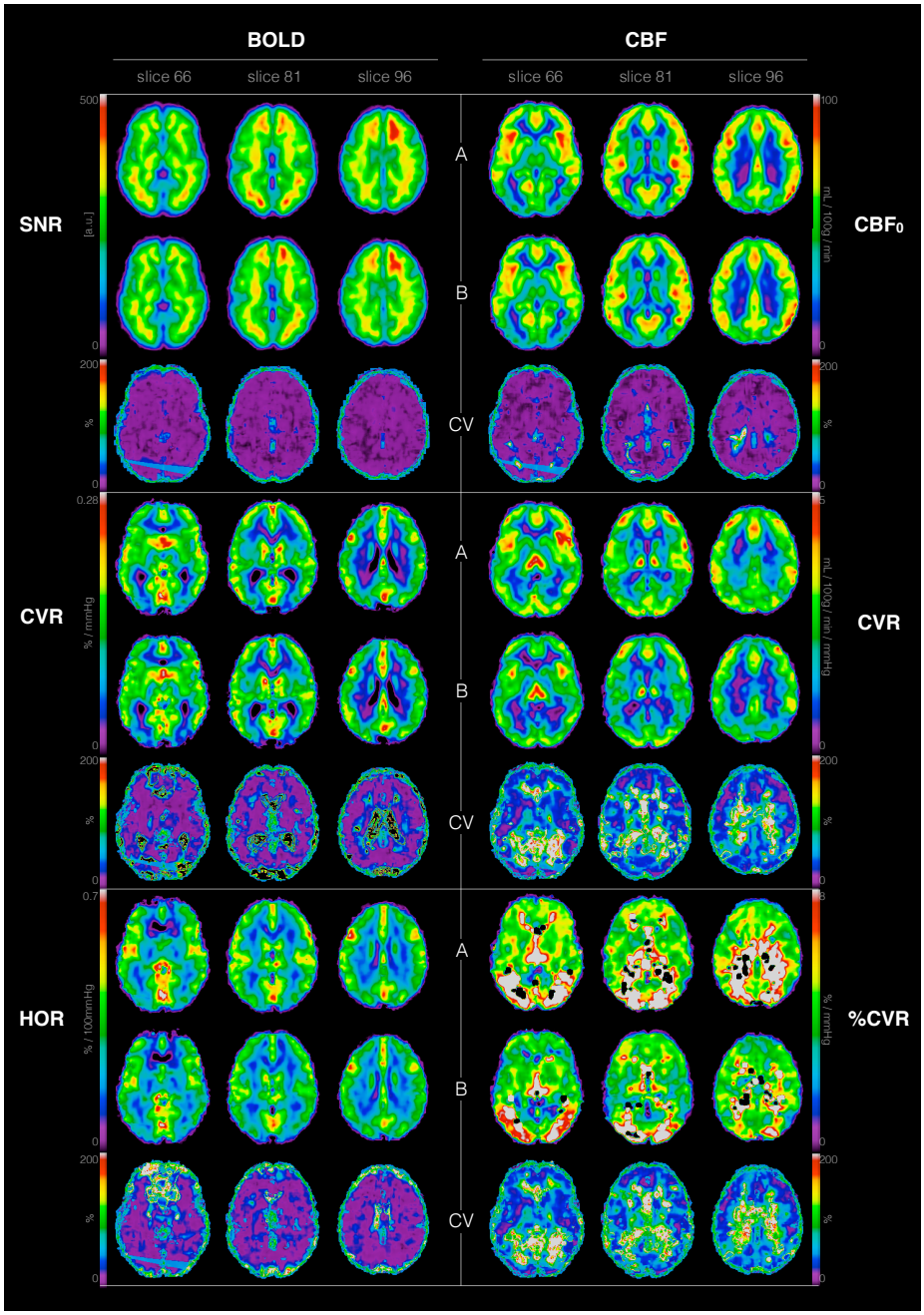

Figure 4.10: Functional MRI maps. BOLD parametric maps are shown in the 3 columns on the left, CBF maps in the 3 columns on the right. Each set of 3 rows show results pertaining to Test A, Test B and the computed coefficient of variance between the two tests. SNR = Signal to Noise Ratio; CBF_0 = baseline CBF; CVR = CerebroVascular Reactivity to CO_2; %CVR = CBF CerebroVascular Reactivity expressed as a percent of the CBF baseline signal; HOR = HyperOxic Response (expressed as a percent change in the BOLD signal per 100 mmHg increase in ET O_2).

Baseline CBF maps indicate a 3-fold higher CBF signal in GM compared to WM (rows 1 and 2, right), but reproducibility of the CBF_0 signal is uniform across the brain, as indicated by the relatively flat CV maps (3^{rd} row). When computed as the absolute increase in CBF per mmHg of CO_2, the CBF-CVR maps (rows 4 and 5), display the same GM-WM contrast as observed in the CBF_0 maps. Reproducibility of CVR measures is, however, lower than the reproducibility of CBF_0; and spatially dependent (6^{th} row). Variability of CVR measures in WM can be an order of magnitude higher than in GM (CVs in deep WM may reach 200%). When the hypercapnic response is expressed as a percent increase in CBF with respect to its baseline levels, the CVR maps no longer show a clear contrast between GM and WM tissues (rows 7 and 8). In WM and in the posterior cortex (regions where longer arrival times [103, 249, 282, 375] and delayed CO_2 responses [30, 367] render ASL measures challenging) the CBF percent changes are much higher (>10%/mmHg) compared to the overall response in GM (around 4%/mmHg).

DISCUSSION

We have evaluated reproducibility of dual-echo pCASL measures of BOLD and CBF responses to blood gases by having 8 healthy subjects scanned twice within a 24h interval and using a simple respiratory manipulation to induce changes in blood gases. The breathing paradigm we have adopted comprised changes in end-tidal levels of both O_2 and CO_2. Although these were manipulated in the same scan, we would expect reproducibility of pCASL measures to be the same in paradigms in which only one of them (*e.g.* CO_2) is manipulated.

The BOLD and CBF signals measured in both tests were robust and consistent. BOLD and CBF signals were significantly higher than noise levels in more than 85% of the voxels of our GM mask. In agreement with a previous report [61], pCASL measures of baseline CBF differed by less than 5% of the mean value between scans. As to the reproducibility of evoked responses, we found that while increases in CBF signal (which was expected to have a lower SNR) differed by less than 20%, BOLD responses differed by less than 10%

Here we report a direct estimate of the reproducibility of BOLD signal changes to hyperoxia. Goodwin *et al.* [129] have previously reported reproducibility of the calibration parameter M, which is computed from BOLD hyperoxic responses but also depends on other measured quantities. Reproducibility of BOLD and CBF responses to hypercapnia, on the other hand, have been more widely studied, both in humans and animals, though estimates were obtained using other imaging and respiratory methods.

Using a computer controlled system to prospectively target end-tidal levels, Kassner *et al.* [183] have measured BOLD-CVR in 19 subjects, and found that, between days, CVR in GM varied by 6.8% of the mean value. This is equivalent to what we have obtained for the BOLD responses before these were normalized by the magnitude of the CO_2 increase to compute CVR. Winter *et al.* [398] used the same method to study cerebrovascular reactivity in juvenile swine and obtained BOLD measures that were highly reproducible – CV in GM-containing structures were found to range between 4.4% and 9.0%. If we consider that these values were obtained with a BOLD dedicated imaging method and in animals that were under anesthesia (mechanically ventilated), the CV of 8.8% we report for the CVR in the whole GM in awake humans is promising.

A different study reported reproducibility of BOLD and CBF responses to hypercapnia in humans though in a small area restricted to the visual cortex. Using a PASL technique, Leontiev and Buxton [225] measured percent BOLD and CBF responses whose inter-session CV were more than two-fold higher than ours: 26.1% and 40.6% *vs.* 6.8% and 18.8%. An interesting finding in their study, which we expected to have replicated in ours, was that reproducibility of CO_2-normalized CBF responses were remarkably higher than the non-normalized ones (CV decreased from 40.6% to 23.7%), suggesting that a significant part of the variability observed in this type of measurement stems from inconsistencies in the hypercapnic manipulation. Our results, however, showed an opposite trend: when the BOLD and CBF responses were normalized by the magnitude of the stimuli, CV values tended to increase. Goode *et al.* [128] also observed this effect: normalization of BOLD responses degraded their inter-subject reproducibility. Most likely these findings are just artifactual, but given that our subjects underwent consistent respiratory manipulations and that BOLD/CBF responses were lower in the second scan, it is

also possible that our measurements indicate an habituation effect.

In a recent study examining the accuracy and precision of pCASL CBF measures, Heijtel *et al.* [149]) showed that pCASL measures were reproducible and consistent with PET ^{15}O-H_2O measures, regardless of blood CO_2 conditions. Aside from nuances related to the imaging methods, a comparison between these two measures is problematic mostly due to relevant differences in the manipulation methods. It is also difficult to compare the degree of reproducibility achieved in that study with ours because 1) CBF/CVR were measured with up to 7 days difference between scans and 2) the authors report an index for repeatability/variability that is slightly different than our computed CV. In spite of the different methodologies adopted, both studies add evidence supporting pCASL as a technique with potential to replace standard invasive measures and able to provide reliable measures of CBF and CVR. We thus feel that our reproducibility study is complementary to the study of Heijtel *et al*.

Despite the small drift we observed in the ET CO_2 traces of the re-test experiment, ET modulations were consistent. Since the dependence of BOLD susceptibility signal on ET O_2 is the relatively small (less than 0.005%/mmHg), the spurious effects of small ($\approx$5 mmHg) O_2 increases during CO_2 administration are less of a problem for the accuracy of BOLD/CBF measures during hypercapnia. On the other hand, the small ($\approx$1 mmHg) reduction in ET CO_2 during the O_2 administration is somewhat a concern.

As Iscoe and Fisher pointed out [169] it is important to appreciate the hyperoxic-associated hypocapnic effects because they can cause a significant decline in CBF. Even though the spurious effect of hyperoxygenation on blood/tissue T_1 renders CBF quantification challenging [46, 425], we did model the CBF responses to O_2 inhalation and our estimates indicate a 7.1$\pm$0.9% reduction in baseline CBF levels associated to the hyperoxic-hypocapnia. Assuming that CBF has been measured in the linear region of the CO_2 dose-response curve and – as our hypercapnic experiments indicate – that CBF changes 4-5% per mmHg change in CO_2, the 7% reduction in CBF in response to hyperoxic-hypocapnia is not only related to the CO_2 effect. Such measure does have a component associated to the effect of O_2; which can influence CBF directly through vasoconstriction or indirectly by accelerating blood longitudinal relaxation (T_1 shorten-

ing) [296]. A discussion about the accuracy of CBF measures in hyperoxia and disentanglement of the different effects contributing to it are, however, beyond the scope of this paper.

The O_2-induced hypocapnia might, likewise, have impacted on the BOLD signal, causing BOLD hyperoxic responses to be underestimate. In an eucapnic 283 mmHg hyperoxic stimulation, where CBF should stay constant, one would measure BOLD responses higher than what we measured, with CBF levels depressed. Thus, in studies involving hyperoxic induction without control for hypocapnia, the quantification of related BOLD hyperoxic responses should be judicious.

Although reproducibility of the respiratory stimuli using the adopted method did not match those obtained using a system for prospective end-tidal targeting [398], the simplicity of the manipulation and degree of reproducibility of related fMRI measures that can be achieved with it, still make the fixed inspired methods attractive for clinical applications. As the magnitude of respiratory responses are greatly determined by inspired doses, reproducibility of fractional inspired concentrations is an asset in fixed inspired based methods. The breathing circuit we have used for gas delivery ensures a tight correspondence between administered doses and the actual doses inhaled by the subject, thus affording step changes in FiO_2 and $FiCO_2$ that were highly reproducible. When the only breathing apparatus available is a standard oxygen face mask, a better control over inspired doses is desirable to improve reproducibility of the stimulus. This can be achieved by partial sealing the edges of the mask using use adhesive tape; and increasing the flow rate of administered gases.

The pCASL imaging protocol we report here was tailored to the 18-min respiratory protocol and had labeling/readout parameters adjusted to meet criteria such as whole brain imaging with minimal gap and detection rate of CBF responses in GM above 80%. The post-label delay (PLD) of 900 ms we have adopted is somewhat shorter than the values generally reported, which are >1 s. In 3D acquisitions where there is a single PLD for the whole imaged volume, PLD can be as long as 2 s. In spite of that, according to Asllani *et al.* [15], the delivery times at proximal slices of the brain can be as low as 400 ms, which is more than twice as short as the PLD in the first slice of our 2D acqui-

sition (the nominal PLD, 900 ms). The effective PLD in the last slice of our imaging slab is 2.0 s, which is also much longer than the delivery time Asllani *et al.* found in upper parts of the brain (1.1 s). This means that our 2D-imaging protocol satisfies the condition of PLD > delivery time, per slice. The recent study of Donahue *et al.* lends support to that showing tag delivery times of less than 1.0 s in central slices [80].

It has been assumed that in a cohort of young, normal and cooperative subjects, and within a 24h maximum interval between scan sessions, both test measurements should yield the exact same result, *i.e.* that any difference in observations should be attributed to limitations of the measuring/stimulation method rather than to physiological changes. However, CBF can change in the course of the day, so our results manifest a combination of experimental error and physiological shifts. The degree of reproducibility we reported here is probably close to the maximum degree one can be achieved using the proposed method, but different results could be obtained with a shorter interval between scans and a larger sample could be used to confirm our findings. The reliability of reported measures in clinical populations also remains to be evaluated.

Small minute minute volume fluctuations (regarded as high frequency components of the respiratory manipulation) are reflected in fMRI signals as (physiological) noise, which decreases the statistical power of response estimates. ET-related noise should not have a significant impact on the accuracy of response amplitude estimates (*i.e.* CVR maps) because the linear modeling of fMRI signal acts as a low pass filter. However, in some clinical populations this can be otherwise. The control for ET spontaneous fluctuations is possible using other breathing circuits and/or computer controlled gas mixing systems [18, 341, 400]

Although we have not applied physiological de-noising (*e.g.* RETROICOR [122, 409]), nor partial volume correction [14], or even corrections for hemodynamic response delays [30], these post-processing strategies might certainly help improving reproducibility/reliability of pCASL dynamic measures and should be incorporated in future studies. Other improvements necessitating ancillary MRI acquisitions would include corrections for regional differences in arrival times [80, 102, 249] and for drops in label efficiency [13, 175, 410]. Last, but no less importantly, readout related implemen-

tations such as 3D-imaging [137], background suppression [105, 115, 417], multi-band excitation [90], etc, might also contribute to a better and more reliable pCASL signal.

In conclusion, the use of simple respiratory manipulations to induce blood gas changes and pCASL to measure associated BOLD/CBF responses is a promising avenue for the translational research on neurovascular function imaging methods.

CHAPTER 5

PHYSIOLOGICAL MODELING OF CVR

The objective of this study was to formulate a CVR model that accounted for osmotic forces and could explain the ASL experimental data.

♯

5.1 Cerebral perfusion pressure

The cerebral vasculature consists of the vessels downstream from the internal carotids and vertebral arteries that either feed or drain the brain plus cerebral capillaries [268]. While arteries and veins are self-contained vessels, capillaries are muscleless, single-layered, minute size vessels that rest embedded within the organ tissue. Capillaries form a vast fractal array of tubes that pervade the organ giving it porosity [56, 63, 127, 237]. Given their ubiquity, they are generally considered an indissociable constituent of the tissue. It is at the capillary level that blood, penetrating the intimacies of cerebral tissue, exchanges with the surrounding extravascular tissue. The brain has an extremely high metabolic activity per unit mass and approximately 15% of the cardiac output is required to keep its homeostasis [66, 260]. This highly metabolic and highly perfused organ is also a key component for the survival of the body, and as such it counts on a stringently auto-regulated vascular system [165, 173, 289, 397].

It has been shown that cerebral blood flow (CBF) remains fairly constant for a wide range of systemic arterial pressure (MAP) values, indicating that cerebral vasculature resistance is tightly adjusted to compensate for pressure changes upstream (Figure 5.1A) [207, 218, 356]. On the other hand it has also been observed that cerebral perfusion pressure (CPP) remains constant for a wide variety of perfusion regimens (Figure 5.1B) [134, 142, 314]. For instance, upon a drop in resistance downstream, caused by any given vasodilatatory stimulus (*e.g.* hypercapnia), the main arteries feeding the brain will be found to offer less resistance and let more blood to flow in [193, 223]. Such flow

changes would require, however, accompanying central changes in the cardiac output [196]. At the main entrance of blood in to the brain, *i.e.* at the origin of the internal carotids, the carotid sinuses function as physiological pressure sensors, that, signaling to the autonomic centers in the brainstem, provide input to feed-back pressure control mechanisms regulating the cardiac output [1] [300].

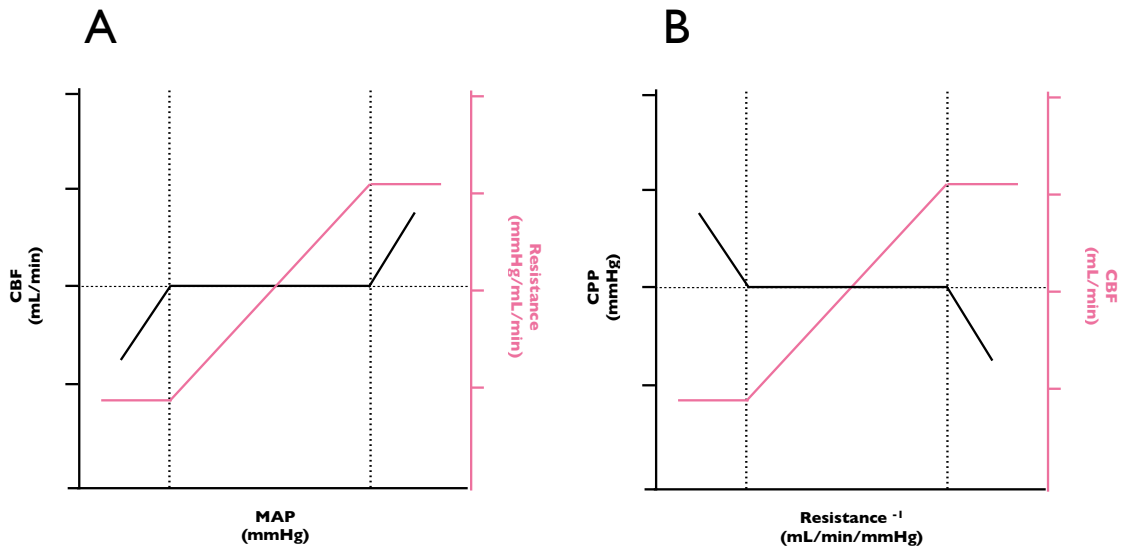

Figure 5.1: Relationship between Pressure, Resistance and Flow. This Figure shows a simplified description of auto-regulatory flow-pressure mechanisms. In the auto-regulatory zone, cerebral blood flow (CBF) remains constant for a range of different systemic pressure (A) (Adapted with permission from Lippincott Williams and Wilkins/Wolters Kluwer Health: Samuel Lucas *et al.*, Influence of Changes in Blood Pressure on Cerebral Perfusion and Oxygenation, [240], 2010). This occurs because cerebrovascular resistance adjusts in accordance to the upstream pressure (MAP): increases in pressure yields increases in downstream resistance to flow. When a given dilatory stimulus, such as hypercapnia, decreases resistance downstream, upstream adjustments are necessary to allow blood flow to increase and keep cerebral perfusion pressure (CPP) constant (B).

The above observations imply the existence of multi-level neuro-muscular reflex mechanisms involving tonus changes and central adjustments in cardiac output that are intended to ensure 1) cerebral perfusion immunity to changes in hydrostatic pressure

1. Cerebral vasculature provides two out of the three pressure inputs used in such regulatory circuitry. The other input comes from similar baroreceptors lying on the aortic arch, which senses and signals global changes in the systemic pressure.

upstream and 2) cerebral perfusion pressure immunity to changes in resistance downstream; thus allowing a condition where perfusion levels are ultimately determined by the resistance of downstream vessels [54, 197].

The brain displays a unique compartmentalization of its functions and cerebral vasculature provides control over the resistance of its vessels at a remarkably low level which allows supporting its metabolic demands with proportional hyperaemic responses that are temporally and locally coupled with the changes in metabolism. It has been observed that local hyperaemic responses evoked by neuronal stimulation can occur within milliseconds [70] and be constrained to volumes as minimal as 1 mm^3 [125, 148], a phenomenon that implies resistance adjustments at the level of arterioles and capillaries. Although extensively exploited in – and actually forming the basis of – modern imaging techniques for mapping the cerebral function [235, 380], the nature of such fine control over cerebral perfusion has been elusive [141, 222, 291, 324].

With recent and more convincing observations of capillary dilation arising from either neuronal or vascular stimulation (including hypercapnia) [16, 82, 354, 381], the view that capillaries are mere "rigid tubes immersed in gel" seems to have been abandoned [2]. The exact mechanisms underlying the changes in capillary resistance, as well as the contribution of capillary reactivity to the cerebral hyperaemic responses, are, yet, a matter of debate [92, 173, 236, 292, 326]. It is natural to speculate whether capillaries could play an active role in hyperaemic responses [58], participating as the main determinant of cerebral perfusion levels – this would provide ultimate specificity to tissue perfusion control [236]. However, since capillary vessels are still commonly regarded as passive elements of the cerebrovascular circuitry, the current understanding is that tissue hyperaemia is a phenomenon originating within arterioles. According to the latter views, the capillary dilation that occurs during hyperaemia is the effect accompanying, *i.e.* caused by / controlled by, arteriole vasodilation [209, 254]. Albeit widely accepted, this cause-effect rationale implies a breakdown of the general pattern of cerebral vascular resistance control. According to what has hitherto been exposed, if, by any reason, arte-

2. Capillaries are more easily compared to a elongated and distensible "soap bubbles" immersed in liquid

riolar resistance drops prior to capillary resistance, thus increasing the perfusion pressure exerted upon capillaries, we should expect an increase in capillaries resistance in order to preserve perfusion against upstream changes [210, 323, 352], not the opposite. That is to say, if auto-regulation of perfusion pressure is to conform in the whole cerebral vasculature, in hyperaemic responses the capillary resistance changes should precede and be the cause, rather than the effect of arteriolar adjustments. Furthermore, capillaries are highly permeable to water, *i.e.* water does not exert a significant force upon its walls. According to the Starling's hypothesis [200], an increase in capillary intravascular hydrostatic pressure favours the movement of water to the extravascular compartment, causing brain oedema [309] rather than a capillary volume gain.

Although the idea of a feed-forward control of capillary resistance continues to be explored in models of metabolic-induced hyperaemia, no *in vivo* evidence has been produced to support this hypothesis. Conversely, at least one study in muscle [21] and one in the brain [58] report measures of metabolically induced vascular changes that suggest capillaries dilate prior to upstream vessels.

The next Figure shows an electrical circuit analogy of CPP control during hyperaemia according to the latter view. The upper diagram represents the vascular system supplying the brain. The different segments of the vascular system, from the heart/aorta to the venular tree, are depicted from left to right. The cardiac output is the circuit element raising the potential of venous blood and propelling it to the brain as arterial blood, with high pressure and velocity. The arterial side of cerebral vasculature, *i.e.* Main arteries, Arteries, Small arteries and Arterioles, are represented as resistor/capacitor elements. As they increase in number, the per element resistance/capacitance progressively decreases. Capillaries are shown as a myriad of pores permeating an object, *i.e.* the cerebral tissue. The venular tree is represented as a pool of blood with low and steady hydrostatic pressure [261], *i.e.* "ground level of the vascular circuitry."

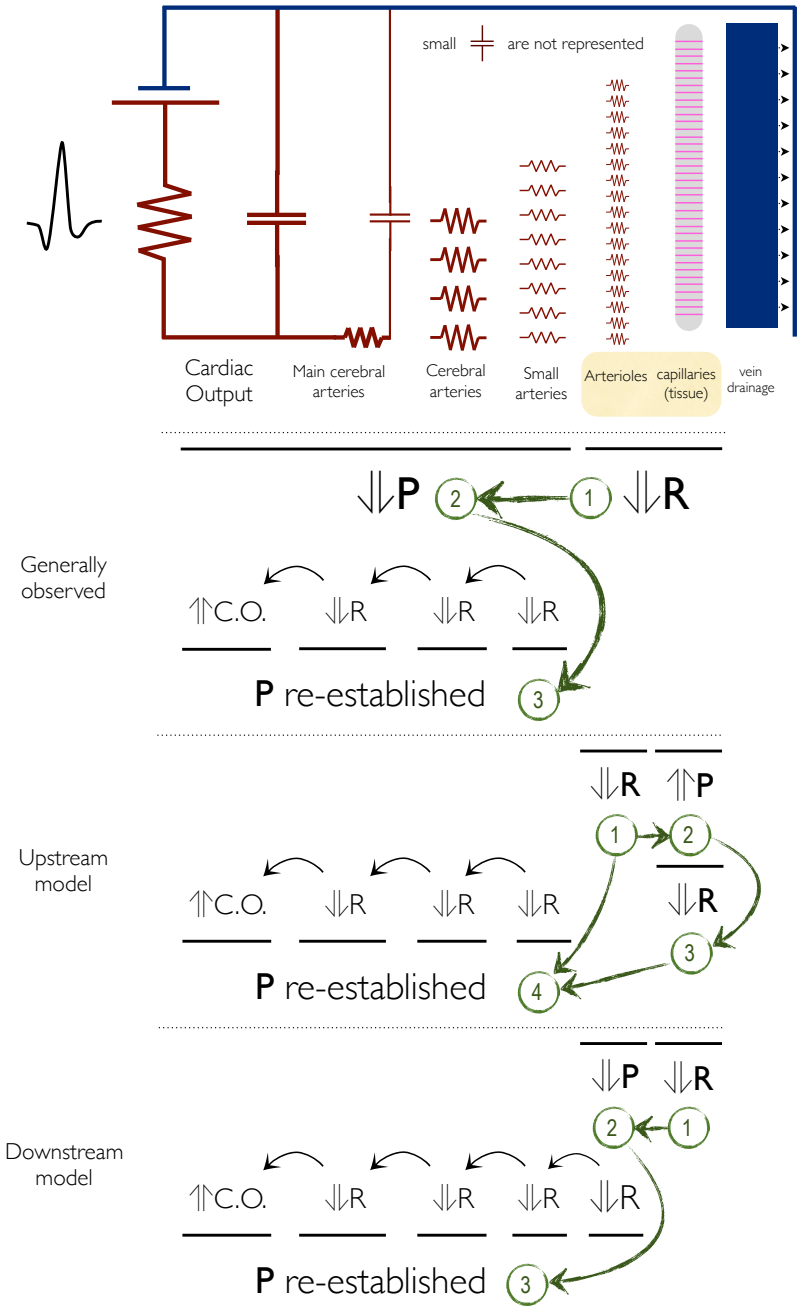

Figure 5.2: Electrical circuit analogy of CPP control during hyperaemia.

As it has been ***Generally observed*** CO_2-induced hyperaemia is caused by relaxation of the downstream vessels (1) of the cerebral vasculature, not by an increase in cerebral perfusion pressure (as described in Figure 3B, perfusion pressure remains fairly constant during the CO_2 response). A decrease in resistance ($\Downarrow$R) of downstream vessels yield a pressure (P) reflex of upstream vessels (2) that cause a retro-propagation of rapid adjustments in the resistance of upstream vessels to re-establish perfusion pressure (3). According to an ***Upstream model*** of tissue hyperaemia control, capillary reactivity is regulated by arterioles. The first thing to occur in CO_2-hyperaemia would be a drop in arterioles' resistance (1). The consequence of that would be a forwardly propagated increase in capillary hydrostatic pressure (2), which in turn would yield capillary dilation (3). Re-establishment of perfusion pressure would stem from the retro-propagated resistance adjustments above mentioned, but which would be triggered by a combined decrease in arterioles and capillaries resistances (4). In a ***Downstream model*** of tissue perfusion regulation the first thing to happen would be a drop in capillary resistance (1). This would cause a drop in perfusion pressure that is is further re-established by retro-propagated decreases in arterial resistances (3). In such a model of perfusion pressure compensation during CO_2-hyperaemia there is only retro-propagation of resistance adjustments. Although a Downstream model conforms better with a general understanding of resistance/pressure regulation, Upstream models are still the dominant view because capillaries are considered passive elements of the vascular circuitry.

To summarize, the *raison d'être* of cerebral vasculature auto-regulatory mechanisms is to ensure proper perfusion of the brain, permitting adjustments according to the organ's demands. And it is reasonable to suppose that cerebral hyperaemic responses is a phenomenon originating at the tissue level. If the arterial side of cerebral vasculature can considered a hydraulic control system existing to preserve the perfusion pressure exerted upon the cerebral tissue, capillary resistance would be the key factor determining the rate of tissue perfusion. To put it differently, the prime duty of cerebral vasculature may be to grant spongey brain an adequate flux of blood to keep the hydrostatic tone of its pores, irrespective of their aperture. That would require, though, a rationale for the phenomenon of intrinsic porosity changes.

5.2 Blood osmotic pressure

The intravascular content of capillaries are separated from the rest of the brain tissue by what is known as the Blood-Brain-Barrier (BBB) [35, 287]. The BBB is formed by the single layer of tightly interconnected endothelial cells that defines capillary boundaries, an adjacent matrix of glycoproteins (glycocalyx), surrounding glial cells (*e.g.* perycites) and cell processes (astrocytes end-feet). While severely limiting the diffusion of most of the solutes present in the blood and brain tissue, such barrier offers virtually no resistance to the passage (of gases) and water. The BBB can thus be regarded as the ideal semi-permeable barrier, causing the brain to function as an osmometer (Ref [344] page 67). Whereas protected against hydrostatic pressure variations, the cerebral perfusion is extremely susceptible to changes in blood osmotic pressure. This fact has been exploited in the treatment of intracranial hypertension [78, 97] where hypertonic solutions are administered to promote a decrease in cerebral water content, *i.e.* shrinkage of brain volume [378]. The use of hypertonic solutions may also help in ischemic stroke, by promoting the re-perfusion of affected areas [362]. Like hypercapnia, hypertonic solutions reduce vascular resistance (presumably by causing a blood volume increase [312] in the first place) and allow perfusion to increase [182].

To date no one has speculated whether, analogously to the administration of hypertonic solutions, vasculature resistance changes to CO_2 can be related to changes in the blood osmotic pressure.

While gaseous CO_2 is not osmotically active *per se*, the products of its dissolution (H^+ and HCO_3^-) are. It has been shown that blood osmolarity is indeed affected by the relative amount, or partial pressure, of CO_2. According to Boning *et al.* [32] a 10 mmHg increase in $PaCO_2$ raises blood osmolarity by 3.7 mOsm, which corresponds to an osmotic pressure increase of approximately 65 mmHg. This is about half the hydrostatic pressure of blood in the aorta; and more than 10 times larger than the estimated increase (5mmHg) producing capillary volume changes in upstream models [209]. It is worth noting that the net transfer of water across the BBB is largely governed by the balance of osmotic pressure between intra and extra vascular compartments. These may be as high

as 5,500 mmHg in each of the compartments, almost 200 times higher than hydrostatic pressures.

5.3 CVR model based on osmotic forces

The CBF changes induced by CO_2 manipulations are usually estimated by linear fitting a response regressor to the measured data. Response regressors can consist of the monitored changes in respiratory CO_2, for instance, or any approximate model of the associated hemodynamic responses. In Chapter 2 and 4 of this thesis, CBF measured responses were fit with a model generated from the convolution of the paradigm design (the schedule representing the periods of normocapnia/hypercapnia) with a gamma variate function, the hemodynamic response function (HRF) that is commonly used in fMRI signal analysis. Given the differences in magnitude and time courses of $P_{ET}CO_2$ changes, the parameters defining the HRFs were adapted for each case: in Chapter 4 the time to peak and width defining the gamma function were three time as large as in Chapter 2. In Chapter 3, the response regressors consisted of the modeled $P_{ET}CO_2$ responses (similar to using $P_{ET}CO_2$ monitored values). Though such statistical procedures can afford robust estimates of CBF responses, they do not provide a rationale for the phenomenon underlying the vascular reactivity to blood CO_2 – fitting of the data with $P_{ET}CO_2$ traces or any empirical HRF can only attribute a magnitude for the observed responses.

Amongst the few mathematical models describing the vascular reactivity to CO_2, only one [130] attempts to explain the complete chain of physiological events that would lead to a change in vessels' resistance and hence blood flow [3]. This model incorporates 38 parameters, several of which are estimated from *in vitro* experiments and which in general were allowed to vary over a range of accepted values (sometimes over orders of magnitude). The CBF responses predicted by this model were slower than the experimentally observed data and the authors concluded that a more rapid mechanism of vascular resistance control was necessary to accurately explain the *in vivo* data. Osmotic

3. In the referred model, CPP is considered to be unaltered during flow changes so that perfusion becomes a function of downstream vessels' resistance

forces have not been contemplated in such model.

Vascular reactivity to experimental manipulations in blood osmotic pressure has been observed in the brain as well as in other vascular territories [112, 140, 146, 243]. However, similarly to the cerebral reactivity to blood CO_2, the phenomenon is not completely understood. There seems to be no consensus about the physiological mechanisms involved nor a mathematical model relating blood osmolarity to perfusion changes. However, given that osmotic manipulations imply the transfer of water between compartments and that tissue hyperaemia implicates an increase in capillary blood volume, I reason that the simplest way to model the physiology of osmotically-induced hyperaemia is to associate it to an osmotically-induced blood volume gain.

The model of cerebrovascular reactivity to CO_2 that I propose is grounded in 3 corollaries: 1) during a brief episode of hypercapnia most of the CO_2 remains intravascular, in the form of HCO_3^- [338], functioning as a hypertonic manipulation; 2) in normal conditions (and assuming an ideal control of capillary perfusion pressure [262]) perfusion can be made a function of capillary resistance only; and 3) blood and the surrounding tissue are two tightly coupled compartments that exhibit complementary volume changes, respecting the Monro-Kellie doctrine of a constant total volume (*e.g.* dehydration of the extravascular compartment issuing from an increase in blood osmotic pressure is equivalent to the blood volume/capillary size gains).

This CVR model uses a dynamic version of the Starling filtration equation allowing a temporally varying blood osmolarity input. By converting blood CO_2 in to blood osmolarity changes it is possible to use the model to compute the perfusion changes induced by any given hypercapnic manipulation. Apart from the CO_2 variable input, the model's output depends on two other physiological quantities, namely the capillary/BBB permeability (or more precisely, the water conductivity) and baseline vasodilation ($VASO_0$). Figure 5.3 shows the schematics of how to compute the flow changes from CO_2 changes according to the new proposition.

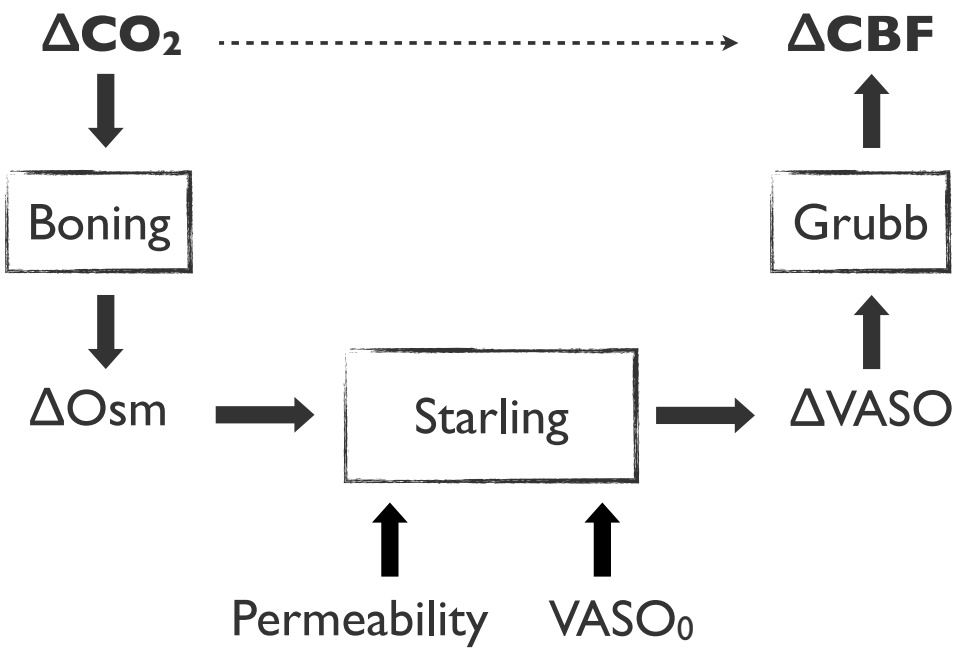

Figure 5.3: Modeling the role of blood osmolarity in CVR. In the proposed model, the perfusion responses (ΔCBF) observed during hypercapnia (ΔCO_2) would be the result of vascular occupancy changes (ΔVASO) that occur due to CO_2-induced changes in blood osmolarity (ΔOsm). ΔOsm can be computed from ΔCO_2 using the relationship reported by Boning *et al.* Using a temporal version of the Starling equation it is possible to compute the ΔVASO dynamic responses associated to a given ΔCO_2/ΔOsm change. This equation takes BBB permeability and initial VASO ($VASO_0$) as fixed parameters. ΔCBF can be computed from ΔVASO using the Grubb's formula.

Alluding to Figure 4, the model suggests that capillaries are supplied by a battery-like pressure source and regulate tissue perfusion by acting as a "lumped Starling resistor"; and that osmosis is the driving force of capillary reactivity.

Validity of this model has been assessed by comparing its numerical predictions with real experimental data measured with pseudo-continuous ASL. To generate the predicted responses the model has been fed with monitored values of $P_{ET}CO_2$ (a surrogate for arterial CO_2) and BBB permeability reported in the specialized literature. ASL hemodynamic data have been fit with the new CO_2-HRF model by allowing $VASO_0$ to vary, yielding best estimates for this parameter. Estimated $VASO_0$ values ranged from 4.8% to 8.5%, in agreement with literature estimates of $VASO_0$ [120, 135] and blood-to-tissue water partition coefficient (another parameter estimating the contribution of the

blood/vascular compartment to the imaged volume) [7, 153, 423]. The model predicts that the magnitude of CBF responses are inversely related to $VASO_0$, which is in keeping with other experimental observations. More importantly, the fitting of CBF data using this CO_2-HRF afforded a physiological rationale for the differences in the amplitude of measured CVRs; and in timing as well. In an additional test, to gauge the impact of permeability on the time course of predicted CBF changes, $VASO_0$ was fixed and BBB was allowed to vary. Results from this test suggest that BBB permeability is a critical physiological quantity affecting the promptness of cerebral vasculature to respond to blood CO_2 changes. In conclusion, the model explains CVR differences in terms of physiology and succeeds predicting *in vivo* hemodynamic data using parameter values that are fairly well established. A detailed account of the mathematical development and model's validation is found in the manuscript that follows, which has been submitted to Medical Hypotheses as a full research article (it has been provisionally accepted for publication in Jan 2015, with minor revisions pending). A brief report on these observations has been communicated in the 2014 annual meeting of the Organization for Human Brain Mapping.

5.4 Stuty manuscript

Modeling the role of osmotic forces in the cerebrovascular response to CO_2

Authors: Felipe B. Tancredi, Hèléne Girouard and Richard D. Hoge
Status: Provisionally accepted for publication in the journal *Medical Hypothesis* [4].

Increases in blood osmolarity have been shown to exert a vasodilatory effect on cerebral and other vasculature, with accompanying increases in blood flow. It has also been shown that, through an influence on blood concentration of the bicarbonate ion and pH, changes in blood levels of CO_2 can alter blood osmolarity sufficiently to have an impact on vessel diameter. We propose here that this phenomenon plays a previously unappreciated role in CO_2-mediated vasodilation, and present a biophysical model of osmotically driven vasodilation. Our model, which is based on literature data describing CO_2-dependent changes in blood osmolarity and hydraulic conductivity (Lp) of the blood-brain barrier, is used to predict the change in cerebral blood flow (CBF) associated with osmotic forces arising from a specific hypercapnic challenge. Modeled changes were then compared with actual CBF changes determined using arterial spin-labeling (ASL) MRI. For changes in the arterial partial pressure of CO_2 ($PaCO_2$) of 20 mmHg, our model predicted increases of 80% from baseline CBF with a temporal evolution that was comparable to the measured hemodynamic responses. Our modeling results suggest that osmotic forces could play a significant role in the cerebrovascular response to CO_2.

Key Words: Arterial Spin Labeling, Blood Osmolarity, Cerebral Blood Flow, Cerebral Blood Volume, Hypercapnia, Neuroimaging, Physiological Modeling, Cerebrovascular Reactivity

4. In between the initial deposit of this thesis and the oral examination the manuscript in this Chapter has been accepted for publication – it has been online since 25 March 2015. The manuscript has been subjected to minor edits and these were also incorporated here (with the committee's approval).

INTRODUCTION

Carbon dioxide (CO_2), a byproduct of oxidative metabolism and the most abundant constituent of blood after water and NaCl, is also a potent vasoactive agent. Increased levels of CO_2 in the blood, a condition termed hypercapnia, cause cerebral vasculature to dilate, decreasing vascular resistance and increasing cerebral blood flow [134, 162, 193, 195, 314, 332, 363]. Although CO_2 has long been recognized as an important regulator of the vascular tone and blood flow in the brain, the exact mechanisms of such control have been uncertain [38, 419].

The current understanding is that the effect of CO_2 on cerebral vasculature is mediated by additive effects of acidosis and bicarbonate ion [370]. These, in turn, will activate KATP and BKCa channels [71, 388]; Na^+-H^+ exchangers [370], Na^+ pump [370] as well as nitric oxide (NO) [230, 231] and cyclo-oxygenase-1 pathways [273] induce vasodilation through inhibition of voltage-dependent Ca^{2+} channels (VDCC) [393]. Since parenchymal arterioles account for about 40% of total cerebral vascular resistance [88], hypercapnic effects had been attributed to the vasoreactivity of these arterial segments. However, it has also been recognized that capillaries, the vessels mostly exchanging with the tissue, have an important participation in the cerebrovascular response to hypercapnia [16, 82, 381], and some evidence suggests that the CO_2-response could be driven at the level of such small vessels. For example, a higher percentage change in diameter in response to mild hypercapnia had been observed in the smallest capillaries [163]. The reactivity of brain capillaries to neuronal activation may involve the participation of pericytes [292] - though it has also been demonstrated that capillaries can dilate in the absence of pericyte activity [92]. Capillary vessels contain blood within the tissue, separating it from the other brain compartments, all of which have water contents – *i.e.* their volumes – intimately related [124, 200, 226]. Thereby, modulation in water transport gradients is another possible mechanism contributing to transient capillary blood volume changes [311] such as those occurring in response to CO_2 [82].

As Yoon *et al.* have recently pointed out [419], it is possible that the cerebrovascular response to hypercapnia includes a component associated to changes occurring within

the blood compartment. The cerebral vasculature, as well as that of other organs, is very responsive to changes in blood osmolarity. Administration of hypertonic solutions, which increases blood osmolarity, yields a decrease in vascular resistance with an accompanying hyperperfusion of the tissue [112, 140, 182, 243, 244, 312, 362]. When dissolved in plasma, CO_2 alters blood pH and bicarbonate levels, thence influencing blood osmolarity [31, 32, 150, 264] and possibly disturbing the water transport gradient between blood and parenchyma. Despite the impact of CO_2 on blood osmolarity, there has been little attention to the potential role of blood osmolarity and capillary water transfer mechanisms in the vasodilatory response to hypercapnia.

Infusion of sodium bicarbonate solutions has been shown to cause blood osmolarity to increase [420] and yield dose-dependent increases in CBF [43]. While such manipulations cause blood volume to increase, they also cause the water content of the brain tissue to decrease. This is consistent with the Monro-Kellie hypothesis [203, 309], which states that, under normal conditions, volume increases in one compartment of the brain (*e.g.* blood), must be accompanied by volume reduction in another (*e.g.* extravascular). Similarly, while inducing increases in cerebral blood volume and flow, hypercapnia is also associated with increases in blood bicarbonate content and shrinkage of extravascular compartments of the cerebral tissue. Lu *et al.* [238] measured that a moderate 10-15 mmHg increase in $PaCO_2$ yields an approximate 1-2% reduction of the extravascular space to accommodate a fractional blood volume occupation that increases from 5% to 6-7%. It is conceivable that such hypercapnically-induced volume exchange is related to an osmotically-driven transfer of water between intra- and extravascular compartments, *i.e.* that during hypercapnia the extravascular space loses water to blood because, due to an increased CO_2-bicarbonate activity, blood is rendered hypertonic. According to Boning *et al.* [32] a 10-15 mmHg increase in $PaCO_2$ raises blood osmolarity by approximately 1-2% of its nominal value, a figure that is comparable to the extravascular volume reduction measured by Lu *et al.*

We hypothesize that the phenomenon of cerebrovascular response to CO2 includes a contribution associated with the emer- gence of an osmotic gradient across the blood brain barrier (BBB) that causes the volume of the blood compartment to change.

HYPOTHESIS

Theory

Metabolically-generated CO_2 is washed out by arterial blood that enters the cerebral tissue with lower amounts of CO_2 and leaves the brain as venous blood, with higher PCO_2, higher [HCO_3^-] and lower pH [202, 322]. There is a permanent passive flux of CO_2 from brain to blood because there exists a gradient of PCO_2 between parenchyma and blood [119, 301] and because the BBB is permeable to CO_2 in its gaseous form [283, 316]. Yet, the presence of carbonic anhydrase (CA) enzymes residing in the luminal face of the BBB and erythrocytes accelerates hydration of CO_2 to be carried by blood in the form of H^+ and HCO_3^- thus greatly contributing to the tissue-to-blood flux of CO_2 [114, 151]. It seems that, paralleling the role of hemoglobin that gives blood a high capacity for carrying and rapidly loading/unloading oxygen, a high activity of CA enzymes in the blood compartment endows blood with an efficient mechanism for transporting CO_2.

Nevertheless, while advantageous in the blood, a high catalytic activity of CA enzymes in the parenchyma would be *an enemy of the tissue* [322]. Not only because CO_2 needs to quickly cross lipid barriers and reach the blood stream to be washed out – which would be hampered should this gas be readily dissolved in the parenchyma – but also because tissue homeostasis would be too susceptible to normally occurring transients in blood PCO_2 levels. A lower CA activity in the parenchyma implies that CO_2 would be converted into H^+/HCO_3^- less efficiently in this compartment than in the blood compartment [41, 316, 337, 338]. Accordingly, although parenchymal PCO_2 can increase during a brief episode of hypercapnia – because an increase in blood PCO_2 will reduce the tissue CO_2 washout – this increase would represent a much smaller total amount of dissolved CO_2 than that necessary to increase PCO_2 in the blood. Albeit there is no direct empirical evidence of this phenomenon, the rationale finds support in different studies on the buffer capacities of the different body storages of CO_2 [62, 89]. While it has been shown that it may take more than 1 h for all the fluids in the body to equilibrate with alveolar/arterial PCO_2 [335, 376] some studies show that blood PCO_2 increases in the feeding arteries are closely followed by PCO_2 increases in the jugular vein [37, 193].

Altogether this indicates that despite its higher volume compared to the blood compartment and higher total capacity to store CO_2, extravascular compartments dissolve CO_2 at a much slower rate than blood.

In conclusion, if we observe that the blood brain barrier (BBB) is relatively impermeable to the products of CO_2 dissolution in plasma and that the parenchyma dissolves CO_2 at a much lower rate than blood, we can assume that the surplus of CO_2 perfusing the tissue during a brief hypercapnic stimulus ($\sim$2 min) will remain mostly intravascular, in the form of H^+/HCO_3^-, functioning as a hypertonic manipulation and giving rise to an osmotic gradient across the BBB. This will result in a water volume transfer between BBB's adjacent compartments that increases the volume of the blood compartment and decreases the tissue resistance to perfusion. Hyperaemia of the cerebral tissue will follow as long as upstream vessels respond synergistically, also decreasing resistance, to allow more blood to flow in. That is to say, the driving forces of cerebral vascular reactivity to CO_2 might be viewed as being, at least in part, of an osmotic nature, and originating at the capillary level [58, 350], as opposed to being regulated by pre-capillary arteriolar tone [173].

To assess the potential impact of this mechanism, we have devised a simple biophysical model allowing quantification of tissue perfusion changes associated with CO_2-related changes in blood osmolarity.

Conceptual model

We have developed a two compartment model, in which the intravascular (blood) and extravascular (EVC) compartments of the brain tissue have their volumes coupled according to the doctrine of Monro-Kellie (as in refs. [309] and [209]. Increases in vascular space occupancy (VASO), *i.e.* blood volume, are accompanied by equivalent losses in EVC; and vice-versa. When blood osmolarity increases, the EVC loses water to the blood stream until the osmotic gradient across the BBB separating the two compartments is eliminated. If we respect the Monro-Kellie principle, when the equilibrium is reestablished, the blood compartment occupies a larger volume (Figure 5.4).

In our model, we assume that such volumetric changes occur under conditions of

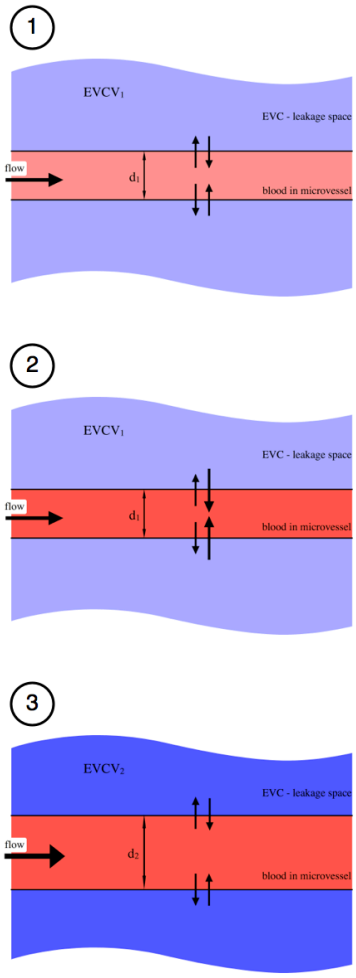

1) At stead-state, Starling forces (osmotic + hydrostatic pressure gradients across BBB) are in equilibrium and the net transfer of water between the two compartments, EVC and blood, is null;

2) During hypercapnia when blood becomes hyperosmotic with respect to EVC, an osmotic gradient across the BBB arises and the net transfer of water between EVC and blood is no longer zero;

3) EVC loses water to the blood and shrinks, while blood volume increases resulting in dilation of the exchanging vessel. The volume exchange reaches steady-state when EVC has lost enough water to re-equalize the Starling forces between the two compartments. The perfusion increase is a function of the osmotic increase, and fractional contributions of the EVC and blood compartments to the total volume.

Figure 5.4: Osmotic driven increase in the blood volume and flow: conceptual model. EVC = Extravascular compartments; EVCV = EVC Volume; d = diameter.

normal vascular autoregulation [181, 218], so that perfusion pressure is considered to remain constant for different values of vascular resistance. This allowed us to state flow as a function of resistance only [254] and to employ Grubb's formula [134] to compute the changes in blood flow from changes in blood volume (according to Poiseuille's law, and assuming laminar flow, flow changes can be expressed as a power function of volume changes using an exponent of 2.0; Grubb's empirical law uses an exponent of 2.63 to relate the two quantities).

To relate CO_2 levels to blood osmolarity changes, we use the relationship reported

by Boning *et al* [32]. These authors found that in hypercapnia, when blood pH is lower and $[HCO_3^-]$ higher, blood osmolarity increases by 0.37 mmol/L per mmHg increase in PCO_2; and that in hypocapnia, when pH is higher and $[HCO_3^-]$ lower, blood osmolarity decreases by 0.22 mmol/L per mmHg decrease in PCO_2. In our computations, monitored samples of end tidal PCO_2 ($P_{ET}CO_2$) were considered to be accurate reflections of PCO_2 in arterial blood and were used as a surrogate of the latter quantity.

To summarize, tissue perfusion rates can be modeled as a function of CO_2 levels in the following manner: 1) changes in local CO_2 levels result in blood osmotic changes that can be computed using Boning's ratios; 2) these osmotic changes are used to compute the shrinkage of the EVC, which in turn determines the complementary increase in blood volume; 3) last, the resultant change in cerebral blood flow is predicted based on the latter volume change using Grubb's relation.

For the steady-state solution of the system, which is independent of the rate of water/volume exchange between compartments, the changes in volume occupancy of both intra and extra vascular compartments can be readily computed. The dynamic solution of the problem, on the other hand, depends on the hydraulic conductivity (Lp) of BBB and requires a more complex model to account for the rate of water exchange between the two compartments. A solution for the dynamics of volume exchange between blood and EVC during the changes in blood osmolarity is possible using a dynamic version of Starling filtration equation and numerical integration. The BBB is modeled as an ideal semi-permeable membrane [309] – at least within the boundaries of a short lasting vascular stimulus – and we have adopted the Lp value of 40.8×10^{-9} cm/s/cmH_2O [201]. Due to the lack of an established value for the elastic force exerted by the BBB, as well as to the uncertainty regarding changes in elastic force due to blood volume changes (*i.e.* whether one should observe Laplace's law for instance), we have not considered elastic forces in our model.

Since the mean transit times in the brain are extremely short (in the order of 1-10 seconds [50, 167]), for the sake of simplicity, two final assumptions were made: 1) that the segment of vasculature exchanging with tissue experience the same changes in blood osmolarity; and 2) that these changes are not influenced by the dilution due to

volume exchange because blood is rapidly renewed through bulk flow, washing out the portion that has been altered by the water transfer. We also did not take into account the effect of the flow changes on the metabolically generated CO_2 that is continuously deposited in the blood stream.

Model equations

The blood/vascular and extravascular compartments are considered to have tubular geometry and to be concentric. The diameter of the blood/vascular compartment will be denoted by d_b and the total (vascular + extravascular compartments) diameter by d_T. We will be using an initial value of 5 μm for d_b, the approximate size of brain capillary vessel.

Next, we develop a mathematical equation where the volume of vascular compartment, or its radius, becomes a temporal function of blood osmolarity. Total radius, r_T, is obtained from the initial vascular occupancy, $VASO_0$, and initial radius of the blood/vascular compartment, r_b:

$$r_T = \frac{r_b}{\sqrt{VASO_0}} \tag{5.1}$$

The Starling equation [217] states that the rate of water exchange between vascular and extravascular compartments is determined by the balance of hydrostatic and osmotic forces across capillary membrane, times the membrane's hydraulic conductivity:

$$J_v = L_p \times A \times [\Delta P - \Delta \Pi] \tag{5.2}$$

Where J_v is the net volume of water filtration across the capillary membrane, Lp the membrane's hydraulic conductivity, expressed as flux per unit area per unit pressure and A the membrane's surface area. $\Delta\Pi$ and ΔP are, respectively, the gradients of osmotic

and hydrostatic pressure across the membrane, and are commonly termed Starling forces. During equilibrium the net flux of water across the BBB is null because Starling forces are balanced, *i.e.* $[\Delta P - \Delta\Pi] = 0$.

For clarity, Equation 5.2 is rewritten expanding the difference terms:

$$J_v = L_p \times A \times [P_e - P_b - \Pi_e + \Pi_b] \tag{5.3}$$

Where the subscripts b and e stand for blood/vascular and extravascular (EVC) compartments respectively. In this equation, the J_v vector points to the vascular compartment.

During an initial state of equilibrium, the osmotic pressure in EVC is computed as:

$$\Pi_e = \Pi_b - \Delta P_{b|e} \tag{5.4}$$

Osmotic pressure is defined as:

$$\Pi = \frac{\sum n_j.\sigma_j}{V}.RT \tag{5.5}$$

Where n_j is the number of osmolytes and σ_j the membrane's reflection coefficient regarding the particular osmolyte j, R the gas constant, T absolute temperature, and V the solution's volume.

If we assume that the amount of osmolytes in EVC remains unchanged during the CO_2-induced CBF changes, osmotic pressure in EVC during hypercapnia can be expressed as:

$$\Pi_e(t) = \frac{c_1}{V_e(t)}.RT \tag{5.6}$$

The constant c_1, which reflects the weighted sum of osmolytes' osmotic activity, can be obtained using equation 4, after having defined the initial conditions for blood osmolarity, fractional compartment occupancies and gradient of hydrostatic pressure across BBB.

Considering the Monro-Kellie doctrine (*i.e.* that the vascular+EVC total volume is kept constant during the exchange of water between the two compartments) we can then express $V_e(t)$ as a function of vascular radius:

$$V_e(t) = \pi.l.\left(r_T^2 - [r_b(t)]^2\right) \tag{5.7}$$

Where l is the depth (or length) of the tubular blood/vascular compartment and will be assumed constant and having unit value for the sake of simplicity.

The derivative of EVC volume change is expressed as:

$$\frac{dV_e(t)}{dt} = -2\pi.l.r_b(t).\frac{dr_b(t)}{dt} \tag{5.8}$$

The changes in surface area of the barrier separating the two compartments can also be expressed in terms of the changes in its vascular radius:

$$A(t) = 2.\pi.l.r_b(t) \tag{5.9}$$

We then re-write Equation 5.3 as function of time:

$$\frac{dV_e(t)}{dt} = L_p.A(t).\left[\Pi_e(t) - \Pi_b(t) + \Delta P_{b|e}\right] \tag{5.10}$$

Where $\Delta P_{b|e}$ and Lp are assumed to be constant.

The osmotic pressure in the blood compartment can be expressed in terms of blood osmolarity (BO) as:

$$\Pi_b(t) = BO(t).RT \tag{5.11}$$

With:

$$BO(t) = \begin{cases} BO(0) + 0.37 \cdot \Delta P_{ET}CO_2(t), & \Delta P_{ET}CO_2(t) \geq 0 \\ BO(0) + 0.22 \cdot \Delta P_{ET}CO_2(t), & \Delta P_{ET}CO_2(t) < 0 \end{cases} \tag{5.12}$$

Using equations 5.6-5.9 and 5.11, equation 5.10 can be rewritten as:

$$\frac{dr_b(t)}{dt} = -L_p \cdot \left[\left[\left(\frac{c_1}{\pi \cdot l \cdot \left(r_T^2 - [r_b(t)]^2\right)} \right) - BO(t) \right] \cdot RT + \Delta P_{b|e} \right] \tag{5.13}$$

In this equation vascular radius (r_b) and blood osmolarity (BO) are temporally coupled. Vascular dimension – radius, area or volume – changes because there is a transfer of water volume between the vascular and the EVC compartments. All constants are known except r_T, that reflects $VASO_0$ (equation 5.1). This parameter is optimized in the fit of the model to experimental data.

By using Grub's relation we can compute the change in blood flow as:

$$\frac{CBF}{CBF_0} = \left(\frac{CBV}{CBV_0} \right)^{\alpha} = \left(\frac{r_b(t)}{r_b(t=0)} \right)^{2 \cdot \alpha} \tag{5.14}$$

Where alpha is the inverse of the Grubb's constant for total blood volume (*i.e.* 1/0.38).

For other parameters, we have adopted the following literature values: baseline/initial blood osmolarity of 300 mmol/L [79] ; $\Delta P_{b|e}$=30 mmHg [200] ; Lp=40.8x10^{-9} cm/s/cmH_2O [201] ; and T=310K. During optimization of the model, we have allowed $VASO_0$ to vary from 1% to 25%.

HYPOTHESIS EVALUATION

General and simple relation between $VASO_0$ osmotic increases and ΔCBF

Assuming the grey matter tissue to have a 5% vascular occupancy ($VASO_0$) [239, 284] and that Grubb's relation describes the coupling between blood flow and volume [134], the typical ASL measurements of 20-60% flow increase induced by a 5-10 mmHg hypercapnic challenge [47, 59, 274, 275] corresponds to a $\sim$10-20% increase in blood volume, meaning that VASO increases from 5% to 5.5-6%. According to our proposition, a 5-10 mmHg increase in PCO_2 corresponds to an approximate 0.5-1% increase in blood osmolarity. This, in turn, induces a 0.5-1% decrease in EVC volume with an accompanying increase in VASO. If $VASO_0$ = 5%, it increases to $\sim$5.5-6%, which corresponds to a 10-20% increase in blood volume and a 20-60% increase in flow. The %ΔCBF output of our model is thus in general agreement with literature values for this type of experiments.

Modeling the dose response curve of CO_2 cerebrovascular reactivity

We have used the model to fit CBF data from a previous study by our group in which CBF was measured, in different circumstances, over a broad range of different $P_{ET}CO_2$ values (details can be found in ref. [363]. Approximately 80 $P_{ET}CO_2$:Δ%CBF pairs were collected for each individual subject. CBF measures were acquired in a 3T MRI scanner (SIEMENS Tim Trio), using the perfusion imaging technique of pseudo-continuous Arterial Spin Labeling (ASL) [72, 364]. The ASL flow signal was averaged over grey matter as described in [363]. For each subject, $VASO_0$, that determines the exponential growth of the modeled dose-response curve, was optimized by minimizing the

mean square of the model residuals. Given that CBF was measured under both hypo and hypercapnia regimens, the fitting shows an inflection point, which results from the use of the different CO_2:Osmolarity ratios reported by Boning *et al.* (see Theory section). In each case, the $P_{ET}CO_2$ value at the inflection point corresponds to the subject's resting levels of $P_{ET}CO_2$. As the above described procedure consisted of fitting non-temporally related data, the modeled dose-response curves are considered the steady state solution of the model.

Figure 5.5 shows the modeled dose-response curves and $VASO_0$ estimates for 9 different young healthy subjects. We have found estimates of $VASO_0$ that ranged from 6-11%, with a mean value of $8.0\pm0.4\%$. Although higher than the literature estimate we have mentioned above (5%), it is still within the limits of what is considered to be the blood-to-tissue water partition coefficient (10%) [153], a parameter indicating the fractional occupancy of the brain vascular compartment with respect to its water content.

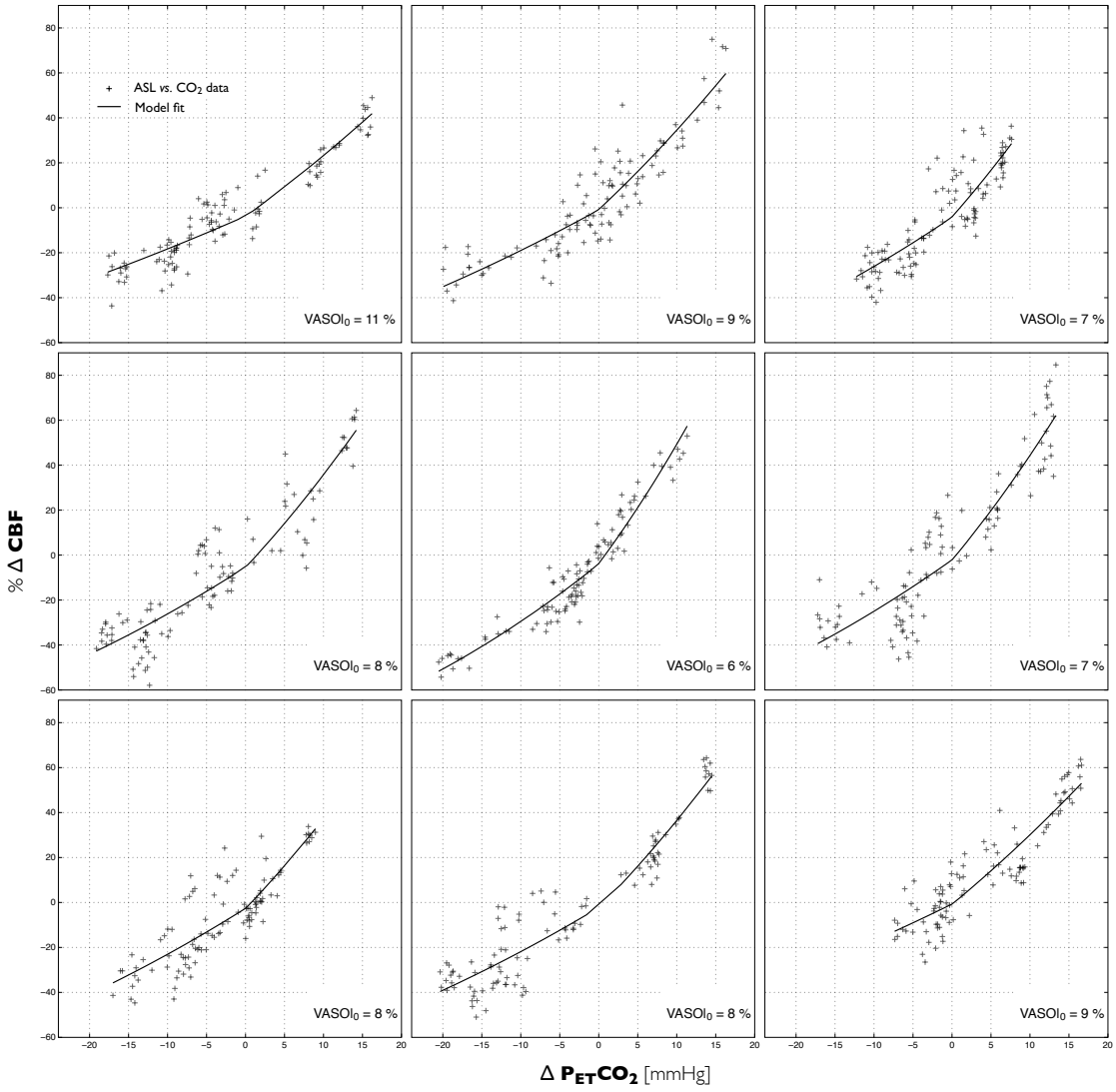

Figure 5.5: Modeled CO_2 *vs.* CBF dose-response curves. Fitting of the CO_2 *vs.* CBF dose response curve in 9 different subjects gave an average $VASO_0$ of 8.0±0.4%.

Modeling the dynamics of CO_2 cerebrovascular reactivity

We have also evaluated the hemodynamic solution of the model by fitting it to time series of CO_2-induced CBF changes. In this procedure, the $P_{ET}CO_2$ values recorded during the respiratory manipulation were used as a temporally varying input to the osmotic model. As previously mentioned we have used a Lp of 40.8×10^{-9} cm/s/cmH_2O, the mean value measured by Kimura *et al.* at 37°C [201]. To investigate the impact of Lp on the modeled responses we have conducted additional fits in one of the data sets us-

ing four other values (in cm/s/cmH_2O) reported by those authors: the mean and median measured at room temperature, *i.e.* 5.9×10^{-9} and 13.2×10^{-9} ; the median measured at 37°C, *i.e.* 27.4×10^{-9} ; and 120×10^{-9} , the approximate maximum value. Care was also taken to consider hypo and hypercapnic regimens separately.

Figure 5.6 shows four representative examples of the dynamic changes in $P_{ET}CO_2$ and ASL flow signal during a hypercapnic experiment using the administration of an air mixture mildly enriched with CO_2; and the model's predicted responses in red. The dashed lines represent the responses predicted by the model when the literature $VASO_0$ value of 5% [238] is adopted. The red solid lines represent the model's predicted responses when using $VASO_0$ estimates that best fitted the model to the flow data.

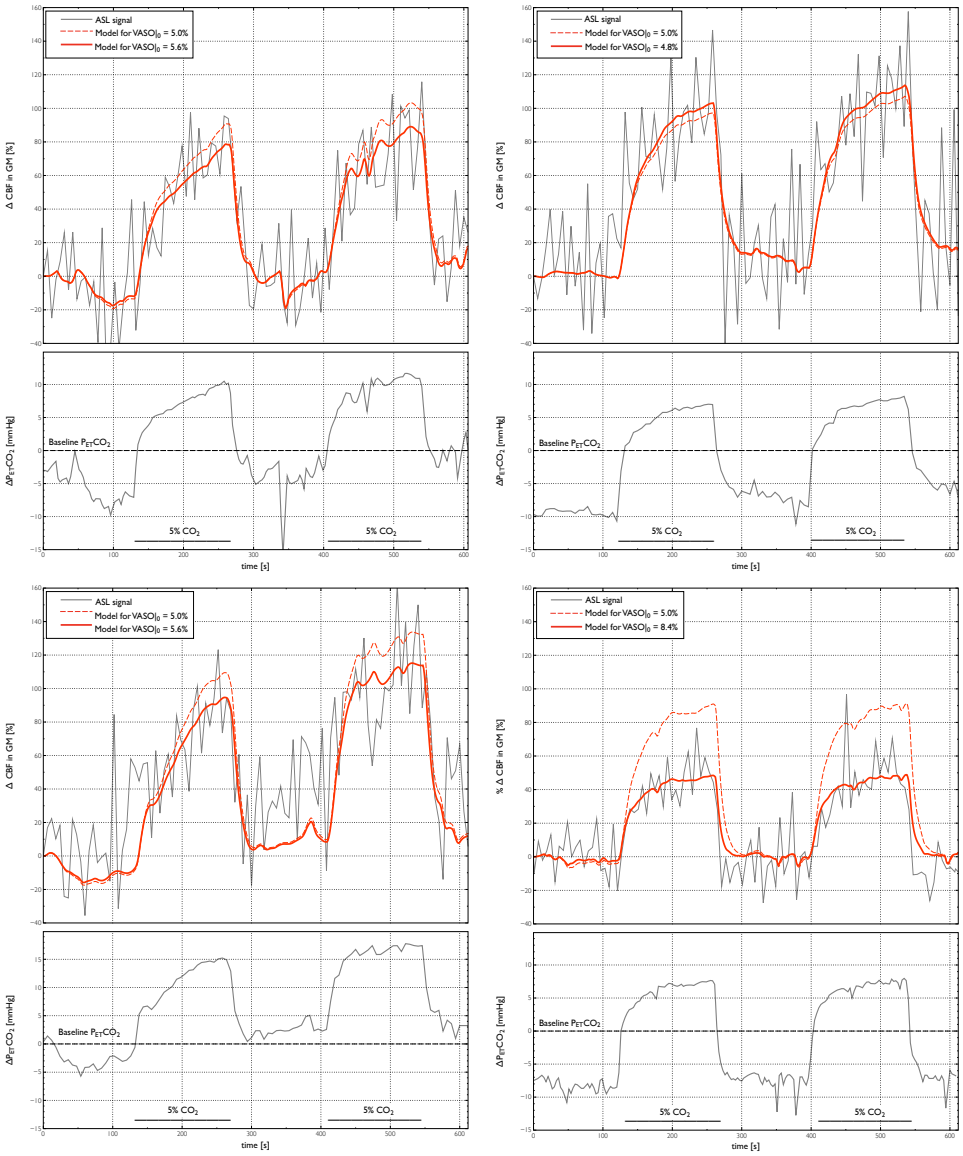

Figure 5.6: Modeled hemodynamic responses to CO_2. In each of the 4 composites the bottom graph shows the trace of monitored $P_{ET}CO_2$. Subjects breathed at a constant rate (16 breaths per minute) during the entire period. Hypercapnia was induced by administering air mixture containing 5% CO_2 in two different instances, as indicated by the segments of solid line in the bottom of the same graph. The top graph shows the Model's predicted responses (in red) overlaid on the ASL flow signal in GM (grey). The red dashed line represents the responses using the literature $VASO_0$ value of 5% while the red solid line represents the responses using the $VASO_0$ values that best fit the model to the data. $VASO_0$ estimates are indicated in the legend boxes (upper left in each plot).

The hemodynamic responses computed by our model fitted the ASL data with opti-

mal $VASO_0$ values of: 4.8, 5.6, 5.6 and 8.4%. Figure 5.7 shows a comparison between model fits using five different values of Lp, each represented in a different color (the red solid line corresponds to the model fit using the same Lp value as in the previous fits).

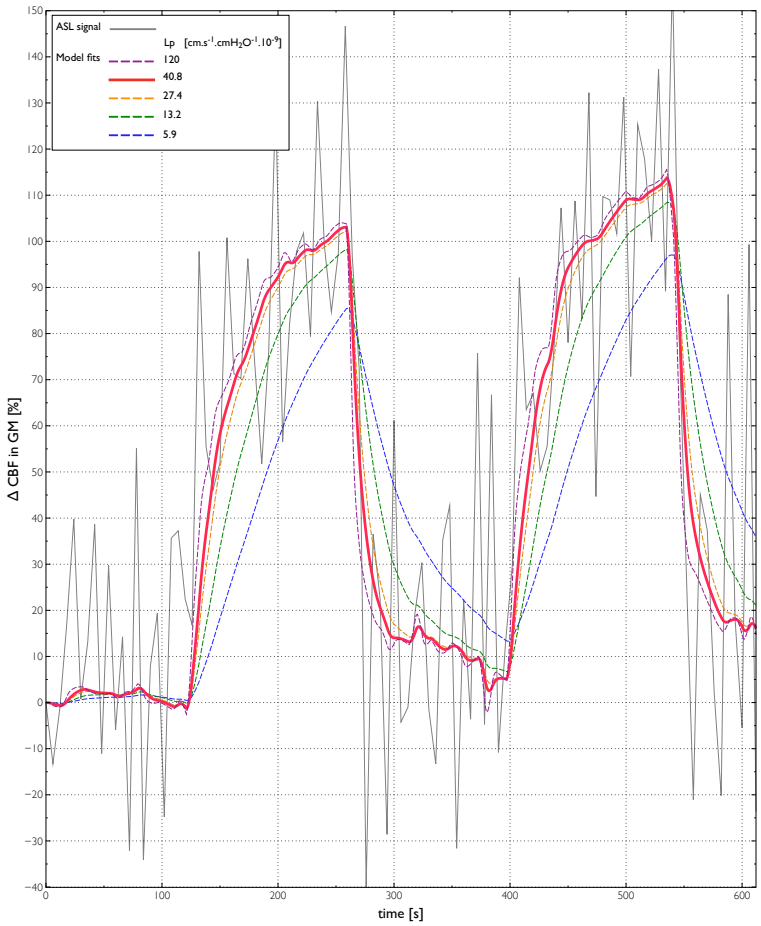

Figure 5.7: The impact of BBB hydraulic conductivity Lp for the hemodynamic response to CO_2. The osmotic model is fit to the ASL-CBF signal (grey line) using different values of Lp (in units of 10^{-9} cm/s/cmH_2O). The red solid line represents the model fit using a Lp of 40.8, which is the same value used in models shown in Figure 4. The purple, orange, green and blue dashed lines represent model fits using Lp values of 120, 27.4, 13.2 and 5.9, respectively. The $VASO_0$ fit values ranged between 4.7% and 4.9%.

DISCUSSION

Quantification and general agreement with experimental data

A mathematical model describing the coupling between CO_2 and CBF has been previously proposed by Greenberg *et al* [130]. In their model, reactivity of the cerebral vasculature to hypercapnia is mediated by the surplus of CO_2 that has been carried by the blood and diffused to extravascular compartments. The possible influence of CO_2 on the blood osmotic pressure is disregarded. When tested against experimentally acquired data, their model, which comprises 38 different parameters, most of which unknown, failed to accurately predict the CO_2-induced flow changes. The model computed flow responses that were slower than what was suggested by the experimental data, probably due to the several diffusion limiting processes involved in its quantitative formulation. The authors concluded that a more rapid control mechanism should exist to account for the coupling phenomenon.

The physiological model we have devised, which depends on 9 parameters, most of which are reasonably well established, accurately predicted the percent change in CBF during hypercapnia.

Our model is also in agreement with experimental observations that vascular reactivity to CO_2 depends upon initial levels of both CBF and CO_2, *i.e.* it satisfies the condition that cerebral vascular reactivity be steeper in hypercapnia than in hypocapnia [60, 332, 363, 390] and lower for higher values of initial vasodilation [163, 171, 280, 353].

When adopting the typical value of $VASO_0$ = 5% our model accurately described literature reported values on CO_2-induced CBF increases.

When fitting the model to a large data set representing the CO_2 dose-response curves of 9 subjects (Figure 5.4) we have found an average $VASO_0$ that was somewhat higher than the above value: 8% *vs.* 5%. This difference could reflect the misuse of the literature term VASO to express the fractional occupancy of vascular water. The brain's blood-to-tissue water partition coefficient, which is an estimate of the blood water occupancy, is usually assumed to be 10%, closer to the fractional occupancy the model computed for the data set. Yet, such difference could also be a result of bias due to: 1) issues with

the ASL measurement (decreases in labeling efficiency, thus sensitivity of the method [13]); or 2) the broad range of CO_2 levels explored (the model may fail to predict CBF reactivity outside a given range).

Given the strong non-linearity of the relation between the CBF responses and CO_2 dose [144, 313, 363], $VASO_0$ estimates will vary depending on the range of manipulated levels of CO_2. If we consider that the model predicts an exponential like dose-response curve, whose concavity is inversely related to $VASO_0$, and that the true/measured response is sigmoidal, the fit of the model to a wide range of CO_2-CBF values (as we did) might result in an overestimated value of $VASO_0$. Additionally, some of the methods used to collect the fitted data, did not control for changes in partial pressure of O_2 ($P_{ET}O_2$), which consists a confounding factor for the CO_2 reactivity measurement and impacts in the accuracy of the $VASO_0$ estimates.

The fitting of the model to ASL time series representing the CBF changes during hypercapnic manipulations, where $P_{ET}TCO_2$ changes were limited to about ± 10 mmHg and $P_{ET}O_2$ has been controlled, gave a mean $VASO_0$ of 6% (Figure 5.6). Since the CBF series were normalized by its initial value (rather than by an independent measure/estimate of baseline flow) the $VASO_0$ estimates represent the vascular occupancy at the beginning of the manipulation, when subjects were hypocapnic and brain vessels were constricted. However, in three subjects, VASO increased from an initial value of $\sim$5.0% to $\sim$7.0% at the peak of the hypercapnia; any intermediate value representing the true $VASO_0$ for these subjects, *i.e.* their VASO modeled at normocapnia, will still better correlate with literature $VASO_0$ than with the water partition coefficient. In one subject $VASO_0$ was notably higher (8.4%). We wonder whether the difference could be reflecting a transitory physiological status (higher vasodilation due to migraine or medication for instance) or an anatomical idiosyncrasy of the subject (such as higher capillary density of his GM tissue).

Another explanation for the possible overestimation of VASO would be the exclusion of the tissue tension of CO_2 from our computations. Albeit largely governed by arterial CO_2, the CO_2 level in the blood compartment is also a function of extravascular PCO_2; or more precisely, on the balance between the rate of deposition and wash-out of the gas. If

CBF increases and the metabolic rate of CO_2 production remains constant, the washout of CO_2 will exceed the rate of its deposition, resulting in the dilution of the deposited fraction of blood CO_2. Such phenomenon would tend to reduce the flow response to the hypercapnic stimulus. The consequence of that in our model would be overestimation of VASO.

Impact of hydrostatic pressures on the volume coupling

The influence of hydrostatic pressure on the volume coupling phenomenon described by the model, expressed through the term $\Delta P_{b|e}$ of our equations, is negligible due to its minor contribution compared to osmotic forces involved in the balance of Starling forces, which may be as high as 5,500 mmHg in the blood compartment during hypercapnia – according to our hypothesis, about 100 mmHg higher than in EVC. The forces driving water volume exchange between intra and extra vascular compartments are thus largely determined by the osmotic balance across BBB.

The impact of Lp

The hydraulic conductivity of the BBB is critical for the speed of the volume exchange process. Given the lack of an established value for capillary Lp in humans, we have adopted in our model the mean value reported by Kimura *et al.* who measured Lp in rat arterioles [201]. In a recent modeling paper, Li *et al.* [227] suggested that capillary/BBB water conductivities in humans would be on the same order of magnitude as those measured by Kimura and colleagues (between 1-100$\times 10^{-9}$ cm/s/cmH_2O). Given that a broad range of possible Lp values have been reported [201] we have also computed CBF as a function of time over a similarly broad range of Lp values in one of our data sets (Figure 5.7) to verify whether the behavior described by our model would be conserved for the different reported values. Simulations with extremely low values of Lp demonstrate that, even under these exaggerated conditions, osmotic effects can account for significant increases in CBF that occur on similar time scale to observations made using MRI.

Most studies assessing the CBF responses to the administration of hypertonic solutions measure CBF at a low sampling rate (usually 1 min) which makes it difficult to

appreciate how fast transients in CBF elicited by this mechanism can be. Hardebo *et al.* [140] provide a good example of rapid, osmotically-induced changes in blood flow. Lundvall experiments in salivary gland [243] also supports the concept of a fast vascular reactivity to blood osmotic challenges.

It is also worth noting that the idea of a quick shrinkage of EVC concurrent with hyperaemia is not novel [209]occupancy. In fact, the phenomenon has been exploited in modern functional imaging techniques for the indirect assessment of blood flow-volume during hypercapnia and neuronal stimulation [238].

Capillary reactivity and a downstream regulation of CBF

Despite growing evidence that capillaries, the vessels mostly exchanging with tissue, are very responsive to either hypercapnia [16, 82] or neuronal stimulation [354], hypercapnic effects on cerebral perfusion have been generally attributed to the vasoreactivity of pre-capillary arterioles – probably because this arterial segment accounts for about 40% of total cerebral vascular resistance [88] and because capillaries are commonly viewed as passive elements of the vascular circuitry. According to upstream models of CBF regulation [254], in hyperaemic responses arterioles provoke capillary dilation by relaxing and letting capillary perfusion pressure increase.

Recently, however, it has been speculated whether the control of tissue perfusion could in fact occur downstream, at the capillary level [21, 71, 292, 326]. In the brain, possibly aided by vascular cells such as pericytes [292] but not necessarily [92]. A downstream regulation of cerebral blood flow would not only be more specific than an upstream control [236] but also better conform with general observations on the autoregulation of vascular resistances.

It has been widely reported that vascular resistances change in response to a change in perfusion pressure [134, 161, 182, 314, 371]: increases in hydrostatic pressure are accompanied by an increase in downstream vessels resistance, whereas decreases in pressure are accompanied by decreases in resistance. This ensures stability of tissue perfusion conditions within a certain range of arterial pressure values, termed the autoregulatory zone. Also, during flow increases that occur within the autoregulatory zone,

when the downstream resistance drops, upstream vessels need to decrease resistance to keep perfusion pressure constant. It is conceivable that such phenomena of pressure-resistance control be present in all levels of the vascular systems. From this perspective, if the resistance of arterioles drops, thus increasing the hydrostatic pressure exerted upon capillary vessels downstream, capillaries should increase resistance, *i.e.* shrink [352], not dilate as implied in upstream models. From this same perspective, during CO_2-induced CBF changes, capillary resistance changes downstream should precede arteriolar adjustments upstream [197]. We note that while there is no clear evidence of an upstream regulation of capillary resistance, at least one study in brain [58] and one in striate muscle [21] show capillary dilatation preceding the dilation of upstream vessels.

Also, brain capillaries, although not fenestrated, are considerably permeable to water, to the point that, for practical purposes such as in the theory of ASL, it is often assumed that intravascular water instantly mixes with the surrounding tissue upon its arrival at the capillary bed. Being so, water should not exert a significant force upon capillaries' walls, but, rather, across them. An increase in capillary intravascular hydrostatic pressure, according to Starling's hypothesis, favours the movement of fluid to the extravascular compartment [65, 309], which would lead to capillary volume shrinkage, /textiti.e. [352] an increase in capillary resistance, an outcome that concurs with a downstream model of flow control.

In our opinion, as paramount to the brain's homeostasis as the renewal of its capillaries' contents (*i.e.* tissue perfusion) is the maintenance of capillary hydrostatic pressure [96, 177, 178, 181, 369]. And we believe that the perfusion change in response to CO_2 is a phenomenon originating in the capillary level, where the exchange between blood and parenchyma is greatest.

We consider the phenomenon of vascular auto-regulation by assuming that perfusion pressure is kept constant at the capillary level, *i.e.* that the arterial side of cerebral vasculature is a hydraulic system [10] existing to ensure stability of capillary intravascular pressure, which allows one to predict increases in capillary flow based on its resistance changes. This is equivalent to say that the cerebral vasculature bears a feedback type of pressure control system whose propagated response (upstream) begins with changes in

capillary tone (downstream) [173, 197] and that flow is ultimately a function of capillary resistance.

The remaining question would be: how capillaries change their resistance to control the blood flow levels? And, supposing the capillary response to hypercapnia [163] occurs due to changes in blood properties [419] *what is there about plasma that is important for normal autoregulation?* [352]. According to our hypothesis, the answer would be: blood osmolarity. Capillaries are vessels particularly sensitive to blood osmotic changes [310] and it is conceivable that capillary resistance responds to CO_2 driven shifts in blood osmolarity [32]; which, under conditions of constant perfusion pressure, could be a key factor determining the rate of tissue perfusion.

We would like to emphasize that for an optimal perfusion, the dilation of capillaries must be associated with dilation of upstream resistance arteries and arterioles [197]. We expect all mechanisms controlling the resistance artery tone to act in series with osmolarity-dependent mechanisms so that our hypothesis does not exclude the participation and importance of these mechanisms in the CBF response to CO_2, but rather propose an obligatory role of resistance artery adjustments in response to the capillary tone. Put differently, we advocate that factors having an influence in the muscle tone of arteries/arterioles (phenomena involving more complex molecular/cellular processes) have an impact on the vascular response to CO_2 because they affect the maintenance of capillary tone during osmotically-driven blood volume changes.

Implications and future directions

The autoregulation of cerebral vasculature is known to occur within certain boundaries, *i.e.* cerebral perfusion pressure (CPP) is constant for a limited range of vascular resistances [142]. If the auto-regulatory function of the cerebral arterial tree exceeds a certain limit, capillary hydrostatic pressure will drop, and CBF will no longer be able to increase according to the exponential fashion described by our model. This would result in a CBF *vs.* CO_2 curve that is sigmoidal in shape, as has been observed experimentally [20, 314]. The incorporation of CPP as an additional variable would allow a more comprehensive version of the model, that could help predict CBF-CO_2 coupling over a

broader range of conditions.

The proposed model could also provide a rationale for the response of cerebral vasculature to changes in blood O_2 tension [45, 85, 401]. It is possible that the reactivity of the cerebral vasculature to O_2 is mediated by CO_2 through the Haldane effect [117, 169, 234], *i.e.* that hypoxia might cause vasodilation because it increases the blood buffer capacity to CO_2 and, with that, blood osmolarity, blood volume and flow. If that is the case, the osmotic model could provide a unified description of the vascular response to both of the gases involved in the oxidative metabolism of brain cells. Further extensions of our model could include the computation of the total dissolved CO_2 – and thus blood osmolarity – from partial pressures of both CO_2 and O_2.

Initially, it would be desirable to further investigate if the CBF response to hypercapnia is in fact mediated by CO_2-induced changes in blood osmolarity, *i.e.* test our primary hypothesis using dedicated experiments, in animal models.

The first experiment we propose would consist of manipulating blood PCO_2 levels while keeping pH and HCO_3^-/osmolarity constant. This could be achieved using a similar approach as used by Hardebo and Nilsson [140] and employing intracarotid injections with blood substitute that has been previously manipulated. Injections would contain blood with different PCO_2 and CA inhibitors to keep CO_2 mostly in its gaseous state. If the CBF response to CO_2 depends on the osmolarity changes induced by this gas, the intracarotid injections should result in equivalent CBF changes, despite the differences in PCO_2. The second complementary experiment we propose would consist of administering intracarotid injections with the same PCO_2 and pH but different total amounts of dissolved CO_2 and, thus, osmolarity. The expected outcome of this experiment would be a suppressed CBF response to PCO_2 for the injection in which CA activity is blocked, as in the study of Hauge and colleagues [147].

It is worth noting that while manipulations of arterial blood osmolarity using hypertonic solutions can induce vascular relaxation and perfusion increases in different vascular territories [112, 140]. Lundvall *et al.* have observed that in muscle and salivary gland the osmolarity of venous blood increases with metabolically-induced hyperaemia [243, 244]. These results suggest that blood osmolarity could also be among the regula-

tory factors mediating functional hyperaemia in different tissues. It would be desirable to reproduce the same experiments of Lundvall *et al.* and measure the time courses of osmolarity in both blood and EVC compartments to verify if, at the onset of induced flow increase, an osmotic gradient across capillary walls is formed. Another ambitious, though no less valuable, endeavor would be to try replicating Lundvall's experiments in the brain to see if focal neuronal activation increases osmolarity of the venous effluent draining that particular region. Such experiments would help elucidating the participation of blood/tissue osmolarity and water transfer mechanisms in the normal control of tissue perfusion.

Conclusion

Although several factors have been shown to modulate the CBF response to CO_2, the exact mechanisms and mediators are still a subject of debate [419]. Based on the idea of a volumetric coupling between the cerebral parenchyma and its exchanging vessels, we propose a new model of cerebral blood flow (CBF) regulation by CO_2: during hypercapnia, when blood osmolarity increases with respect to parenchyma, the diameter of exchanging vessels increases, which decreases vascular resistance and allows CBF to increase; when diminished (i.e. in hypocapnia), the converse occurs, with a net reduction in vessels' diameter and decrease in CBF. From this notion, we have devised a simple biophysical model relating CBF and CO_2, whose predicted values agreed well with experimental measurements using the imaging technique of ASL to measure CBF. Our modelling results suggest that osmotic forces could be among the set of regulatory mechanisms modulating blood flow under hypercapnic conditions, thus revealing a previously unappreciated factor in the CBF response to CO_2.

Furthermore, to the best of our knowledge there exists no model explaining the rapid flow responses to osmotic manipulations as those observed by Hardebo and Nilsson [140]. Our model provides a unifying framework that can account for CBF responses to both the direct osmotic manipulations and hypercapnia induction. We thus feel our study also extends previous work on osmotic manipulations of the blood brain barrier with new experimental data.

CHAPTER 6

FINAL REMARKS

6.1 Arterial Spin Labeling

Earlier techniques for measuring brain perfusion were based on the inhalation or injection of exogenous tracers [84, 192, 218, 272, 278, 290, 307, 331, 371]. The idea of measuring perfusion responses to manipulations in blood CO_2 levels (aka CVR) has been introduced by Kety and Schmidt in seminal papers from late 1940's [191, 193]. Since then there has been increasing interest in this type of measure and other less invasive, contrast-free, techniques estimating cerebral perfusion and CVR have been exploited, namely: doppler ultrasonography of flow velocity in carotids/mean cerebral arteries [132, 267, 325, 372, 394], phase contrast angiography (PCA) [1, 20, 28, 29, 349, 391] and BOLD/ASL based fMRI [22, 183, 256, 297]. Whereas sonography of flow velocity in large caliber arteries can afford robust estimates of the total blood perfusing the brain, the technique suffers from limited spatial localization and bias related to changes in vessels' size (which are assumed to remain constant during CO_2-induced perfusion changes). PCA is another technique allowing a measure of flow velocity in cerebral arteries, but that can be calibrated by its complementary measure of vessels' cross-sectional area, thus affording more reliable estimates of total flow changes. However, PCA suffers from limited temporal resolution and – similarly to sonography – limited spatial localization. BOLD imaging, on the other hand, offers high temporal and spatial resolution, permitting an in-depth characterization of vascular dynamics; but the technique lacks from specificity – the BOLD signal depends on several physiological parameters and thus provides an indirect measure of perfusion. The non-invasive technique allowing a specific and quantitative measure of cerebral perfusion and mapping of CVR is Arterial Spin Labeling.

Amidst the various Arterial Spin Labeling schemes, pseudo-Continuous ASL emerges as the most robust and reliable method, with potential to substitute standard contrast-

enhanced techniques in the clinical practice [7] and, as I expect to have demonstrated in this thesis, to promote applications based on blood gas manipulations. Future improvements in pCASL image SNR would certainly be advantageous as it should allow higher image resolution and, with that, a more in depth characterization of CVR. Refinements in perfusion quantification, *i.e.* improvements in the accuracy of pCASL CVR measures, would also be desirable. Whereas pCASL should benefit from general enhancements in image readout, sensitivity and accuracy of CVR measures can be boosted by 1) correcting for spin labeling imperfections [13, 175], 2) removing physiological noise from the perfusion signal [26, 122], 3) compensating for partial volume/flow effects [14, 229] and 4) response time variability [347, 367] – most of which can be achieved using available methods and simple ancillary acquisitions. It would also be recommendable to validate/correct single-TI pCASL CVR measures using multi-TI ASL and kinetic modeling of the tag dynamics during CO_2 changes [15].

In this thesis I have emphasized the compatibility of the pCASL method with standard MRI hardware and its potential to foster new perfusion-based applications. The pCASL CVR measures presented here were acquired in a clinical 3T, utilizing the scanner's RF (body) coil to generate the labeling pulses. However, the energy deposition implicated in such irradiation scheme becomes an obstacle as we move towards higher field strengths ($\geq$7 T) [126, 366]. In ultra-high field MRI systems the labeling by pseudo-continuous RF might only be feasible using a dual-coil approach to constrain energy deposition to the tag region. Besides, given that field-inhomogeneities are more prominent in those systems, it might become indispensable to correct for labeling efficiency in an individual basis. Multi-TI PASL techniques, which are much less energy demanding than any continuous approach, will certainly continue to play an important role in the development of CVR methods. However, I suspect that with limited applicability, as they do not afford dynamic measures of tissue perfusion like single-TI pCASL.

To summarize, single-TI pCASL imaging allows a non-invasive, robust and reliable measure of CO_2-induced hemodynamic changes using standard clinical MRI hardware.

6.2 Respiratory manipulations

As I also hope to have demonstrated in this thesis, it is possible to acquire robust pCASL CVR measures exploiting simple and widely available methods to manipulate blood CO_2 levels, such as breath hold or inhalation of CO_2 mixtures with fixed compositions. The fixed-inspired (FI) method is less dependent on subjects' cooperation and more flexible if compared to breath-hold; besides, respiratory responses associated with FI are more easily quantified. Last but not least, with the technical developments that have been presented here, reproducible FI manipulations can be conducted in a safe manner with minimal setup time. All features that are desirable in a clinical environment and should thence help promoting the broader adoption of CVR measures.

Although constituting an excellent option for simple measures of CVR, the FI method might not be suitable for studies of cerebrovascular regulation requiring rigid control over respiratory gases. In these cases, more sophisticated methods like the Respiract are warranted.

However, in my opinion there are concerns related to its operation that need to be addressed for it to gain a broader interest. The Respiract method controls respiratory responses using a physiology-based feed-forward approach with no input from feed-back monitoring data ,which makes the control system cumbersome and operator-dependent. I noticed that for a successful manipulation the RespirAct invariably requires the ongoing monitoring of $P_{ET}CO_2$ traces and frequent interventions to correct for drifts. As a future development I propose three modifications that should render the method more attractive. 1) According to my experience, the end-tidal CO_2 response to a step change in inspired concentration can be described by an exponential growth and a decay of 2 phases each [1], *i.e.* it is possible to model the respiratory physiology in this type of experiment using just 4 constants. Therefore, rather than forcing respiratory responses based on a theoretical model of its physiological underpinnings and several physical/physiological inputs, the feed-forward control could be achieved using a prediction of 4 unnamed exponential processes. 2) The method should incorporate a preliminary self-calibration run providing

1. Poulin and colleagues have used a similar approach to model ventilatory and flow-velocity responses[303–305]

a direct measure of the 4 above mentioned processes/constants. 3) The system should also count of feed-back data to permanently recalibrate its model (in other words it would consist of an adaptive feed-forward control system).

CVR measures are usually obtained using a given change in end-tidal CO_2; and compared in terms of the amplitude of associated perfusion changes, *i.e.* as to the slope of measured CO_2:perfusion responses. In Chapter 3 I stressed the importance of measuring CVR in the linear range of the CO_2 dose-response curve so that results could be more reliably compared. However, I have also suggested that it might be possible to fully characterize the non-linear CO_2 dose-response. By measuring cerebral perfusion under many different $PaCO_2$ levels one may obtain a more comprehensive picture of cerebrovascular function [20, 22, 314]. If the CO_2:perfusion data is fitted with a logistic function, CVR measures can be compared in terms of various descriptors such as: coordinates/derivative at the inflection point, distances from the inflection point to upper and lower plateaus, distance between plateaus, and so forth. Some groups have been developing this nice idea; however the BOLD signal has been used as a surrogate of perfusion [22]. It has been suggested that the height between upper and lower plateaus of the BOLD-CO_2 curve represents the cerebral vascular reserve. It should be noted that, strictly speaking, that the BOLD signal difference reflects the "oxygenation reserve" of the cerebral tissue. Whereas corresponding closely to perfusion, blood oxygenation level follows its own saturation curve (during CO_2 increases the BOLD signal saturates much faster than the ASL signal). A more accurate estimate of the cerebral vascular reserve can be obtained using a direct measure of cerebral perfusion. Thus far my group has been the only having used a quantitative perfusion imaging technique (ASL) to portray the CO_2 dose-response function of cerebral vasculature in humans. In future work I intend to implement ASL protocols allowing robust parametric mapping of the CVR dose-response function descriptors.

In Chapter 3 I also have proposed a new approach to quantify end-tidal gas levels during experimental manipulations. The procedure consists of modeling end-tidal monitored samples using baseline, response and drift regressors – similarly to what is customarily done in fMRI signal analysis. However, unlike hemodynamic response functions

(HRF), the respiratory response functions (RRF) are optimized in the statistical fit, *i.e.* the procedure also estimates the (four) descriptors of a fundamental RRF. That is to say, other than affording robust estimates of end-tidal changes to any given respiratory manipulation, the procedure outputs the subject's RRF. If used in the reverse sense, this RRF allows predicting the inspired doses that are necessary to give rise to a desirable end-tidal response. In future work I intend to exploit the algorithm that I have developed for the post-processing of respiratory signals, in a respiratory control system for the prospective targeting of end-tidal O_2/CO_2 levels. Moreover, in Chapter 4 I have shown why the robust estimates of end-tidal changes using this approach may be an asset in experiments involving hyperoxic calibration of the BOLD signal [44, 108, 109, 257, 402, 411]. During hyperoxic induction, there might be a subtle decrease in CO_2 levels [95, 169], which confounds O_2-induced BOLD measures [2]. By modeling CO_2 levels it is possible to precisely quantify the changes in end-tidal CO_2 induced by hyperoxia, and with that estimate the BOLD response purely associated with O_2.

6.3 Physiological modeling

Using basic assumptions and a few constants that are reasonably well accepted, the quantitative model [330] of cerebral vascular reactivity that has been proposed succeeded explaining the hemodynamic changes measured by pCASL. Although pCASL afforded robust measures of cerebral perfusion and permitted validating the model's predicted outputs, the physiological foundations of such model remains to be confirmed. However, it should be noted that, other than describing the temporal relationship between perfusion and CO_2, this is the first time a CVR model aspire to establish a direct physical link between the two quantities.

The model is also original inasmuch it incorporates a previously unappreciated phenomenon in the CVR phenomenon, *viz.* the changes of blood osmotic pressure induced by the products of CO_2 dissolution. The possibility of CO_2 acting on the cerebral vas-

2. More than the O_2 changes occurring during hypercapnia might confound CVR measures. The BOLD responses elicited by a 1 mmHg increase in CO_2 are about 30x higher than the responses elicited by an 1 mmHg increase in O_2.

culature through blood bicarbonate has never been considered. Furthermore, it constitutes the first downstream model of vascular control. According to the proposition, the CVR phenomenon originates at the capillary level; vascular adjustments upstream are considered to have a secondary, supportive, participation. The phenomenon of capillary reactivity, which has gained increasing interest [145, 173, 213, 232, 354], is still not fully understood. There have been speculations whether capillary resistance could be regulated by pericytes [292] or whether it could be related to blood volume gains stemming from fluid exchange between brain compartments [209]. The herein proposed model embraces the latter notion, but it proposes that the fluid exchange emanates from transients in blood osmotic pressure, rather than hydrostatic pressure. One of the assumptions of this model is that cerebral perfusion pressure is regulated at the tissue level. According to this model, as paramount for the brain survival as the renewal of capillary contents is the maintenance of its hydrostatic pressure.

While the assumption of a constant capillary perfusion pressure is a simplification that is more easily endorsed (after all, other models have used the concept of vascular auto-regulation to postulate a constant pressure at the level of arterioles, just one level above capillaries), the other assumption supporting the model is subjected to debate. The model assumes that because the activity of carbonic anhydrase enzyme is higher in the blood than in the extravascular compartment [114, 322] and because the BBB is impermeable to HCO_3^- [283], the surplus of HCO_3^- produced during a brief episode of hypercapnia remains mostly intravascular, thus functioning as a hypertonic vascular stimulation. Although there are no direct evidence of what is suggested, the proposition does not violate the common understanding that, while being fairly permeable to water, the BBB has very limited permeability to blood solutes. Blood solutes may take several hours to passively cross the BBB; therefore, in the time frame of a 2 min manipulation, the BBB could indeed be considered the ideal semi-permeable membrane. Secondly, the concept of a differential activity of CA has not been candidly expressed, but CO_2 is diluted in different compartments of the body with different time constants [3] [89]. Last

3. CA is a very primitive family of enzymes, ubiquitous in living organisms, much more than the hemoglobin complex, which is exclusive of more complex animals. It has been suggested that CA plays a crucial role in circulation of vascular plants [160]. What determines the rate of CO_2/water exchange

but not least, the teleological argument that CO_2 ought to dissolve faster in blood than in extravascular compartments to facilitate its transport is far from nonsense.

The manuscript of Chapter 5 had been appraised by several experts in the field before it has been submitted to scientific periodicals for publication. The manuscript has been submitted to three different journals of physiology dedicated to or with sections dedicated to theory/hypothesis or mathematical/computer modeling. In the two first attempts, I and co-authors had feed-back from a total of 6 reviewers, who manifested a broad spectrum of opinions, ranging from "extremely interesting", "intriguing and provocative", "merits considerable attention"; to "severely flawed", "pure speculation", "science fiction." Amidst the more objective criticism on methodology, we had comments regarding the corollary of BBB's impermeability to HCO_3^- (which I have addressed above) and the adopted value for BBB's permeability to water (Lp).

The first Lp value we have adopted was derived from a theoretical paper published in one of Nature's journals [209]. Later, as advised by one of the reviewers, we have adopted a value that had been determined experimentally (in an animal model) about 3 times lower than the original one [201]. We have demonstrated that the output of the model was not severely impacted because the value was still above a threshold of functionality; and included a new figure illustrating the impact of Lp values on the model's predicted responses (Figure 4 in that manuscript). Surprisingly, in the second submission, one of the reviewers repudiated the use of the new Lp value arguing that it had been measured under non-ideal circumstances – a clear evidence that experts are far from having reached a consensus on the right value of BBB's Lp nor the best method to evaluate it (*e.g.* while Fenstermacher and Johnson measured a capillary Lp of $3.2\text{x}10^{-10}$ cm/s/cmH_2O in the rabbit [91], Coulter measured $10.3\text{x}10^{-8}$ in the cat [68]).

The Lp value that have been proposed this time was 1-3 orders of magnitude lower than the one previously suggested. A reviewer pointed specifically to an *in vivo* study

between the plant and its environment, the velocity of sap within its vessels, and the rate of photosynthesis, is the opening of small pores in the plant's leaves, known as stomates. Stomates opening is regulated by the volume of its guard cells, a pair of structures that are responsive to changes in osmotic pressure. It seems that the volume regulation of guard cells relies on the differential activity of CA in different compartments of the stomates.

where Lp was extrapolated from the PS (permeability-surface) product [288] saying that that values was “probably the most reliable, and... ...very close to values obtained in the frog”. However, to compute Lp from the PS product one needs an estimate of the total surface area of capillary walls (ref [36] page 35), which, as far as I know, has not been established – so far, the S of the product is a estimate *per se* and if overestimated, Lp is underestimated. Interestingly, in the referred study, the author shows tracer dilution kinetics that are suggestive of a fast water exchange between blood and extravascular compartments.

The water extraction fraction is indeed limited and dependent on blood transit time [339, 423]. However, in the rat, for flow rates lower than 200 mL/100g/min, the fraction is close to unit. And it has been shown that such approximation is valid in humans as well. In fact, virtually all ASL techniques assume perfect mixing of labeled water upon its arrival at the capillary bed [55, 423] – it has been said that water function as a “freely diffusible tracer.” In other words, when quantifying perfusion from ASL signal one is assuming Lp has infinite value.

While nearly impossible to precisely measure the permeability of fragile structures such as capillaries, particularly *in vivo*, the lack of a consensus on the exact Lp value has been virtually the only point impeding the manuscript’s publication. And it is unfortunate that the authors were not given the chance to counter the reviewers’ objections, for our manuscript has been peremptorily rejected.

In sum, the proposed model is simple, does capture the dynamics of CBF changes associated to blood CO_2, brings a previously unappreciated effect of CO_2 in to attention, may also be able to explain the vascular effect associated to blood O_2 [83, 162, 333, 334, 391, 411, 413] and has the potential to extend knowledge on hypertonic manipulations [43, 288, 362]. Experiments for further validation of the model have also been proposed in the manuscript. Given that the basis for having been refuted are doubts related to one of its adopted constants, which, while supported by specialized literature, is not completely established, I see no reason why the model should be discarded as a hypothesis. In my opinion, it should merit publication in the appropriate vehicles of scientific communication. The manuscript has been submitted to the journal of Medi-

cal Hypotheses and, recently, accepted for publication with minor revisions pending the editor's approval.

As a further development I intend to incorporate cerebral perfusion pressure (CPP) as an extra variable to the model and account for the influence of metabolically deposited CO_2, which have not been considered. This should permit modelling CBF in a broader variety of conditions, more accurately. A possible avenue to explore the relationship between CPP, CBV and CBF [163, 199, 295, 321] would be to combine fMRI measures weighted on perfusion (with ASL) and CBV (with the VASO technique for instance). The way to assess the contribution of the rate of CO_2 deposition to CVR is to acquire fMRI data during challenges that combine blood CO_2 manipulations and neuronal stimulation [157].

Until it is subjected to validation, the proposed mechanism of cerebrovascular reactivity to CO_2 remains as a peculiar hypothesis. However, a new idea should stand as a conceivable hypothesis only if its supporting corollaries and ensuing consequences can harmonize with generally observed phenomena. The concepts that have been integrated in the model, such as osmotically induced fluid exchange, are present in phenomena other than CVR. In Appendix II I discuss the possible implications of the proposed model for the general understanding of tissue perfusion, its limitations, and point out a couple of experiments that could shed some light on the matter.

6.4 In conclusion

I hope that with this thesis I have been able to fulfil the requirements for the obtainment of the degree of *Doctor Philosophiæ* – that I have been able to thorough examine a scientific problem, adequately use the scientific method, communicate my findings in a clear and objective manner, and that I have made an original and relevant contribution to knowledge. As an biomedical engineer and very pragmatic person I hope that the small developments I have made will find a direct applicability in the clinical practice; as a theorist, passionate about imagination, I hope that the model of perfusion control I have proposed can nurture stimulating debates.

BIBLIOGRAPHY

[1] Ramazan Albayrak, Fatma Fidan, Mehmet Unlu, Murat Sezer, Bumin Degirmenci, Murat Acar, Alpay Haktanir, and Mehmet Yaman. Extracranial carotid Doppler ultrasound evaluation of cerebral blood flow volume in COPD patients. *Respiratory Medicine*, 100(10):1826–1833, October 2006.

[2] Ingo Schmid Albrecht, Schewzow Kiril, Goluch Sigrun, Fiedler Georg, Niess Fabian, Elmar Laistler, Wolzt Michael, Moser Ewald, and Meyerspeer Martin. Skeletal muscle pH time course predicts water T2* during repeated exercise. (Abstract 2921). Annual Meeting of the International Society for Magnetic Resonance in Medicine, Milan, May 2014., 2014.

[3] R W Alexander. Theodore Cooper Memorial Lecture. Hypertension and the pathogenesis of atherosclerosis. Oxidative stress and the mediation of arterial inflammatory response: a new perspective. *Hypertension*, 25(2):155–161, February 1995.

[4] David C Alsop and John A Detre. Reduced transit-time sensitivity in noninvasive magnetic resonance imaging of human cerebral blood flow. *Journal of Cerebral Blood Flow and Metabolism*, 16(6):1236–1249, November 1996.

[5] David C Alsop and John A Detre. Multisection cerebral blood flow MR imaging with continuous arterial spin labeling. *Radiology*, 208(2):410–416, August 1998.

[6] David C Alsop, Weiying Dai, Murray Grossman, and John A Detre. Arterial spin labeling blood flow MRI: its role in the early characterization of Alzheimer's disease. *Journal of Alzheimer's Disease*, 20(3):871–880, 2010.

[7] David C Alsop, John A Detre, Xavier Golay, Matthias Günther, Jeroen Hendrikse, Luis Hernandez-Garcia, Hanzhang Lu, Bradley J MacIntosh, Laura M Parkes, Marion Smits, Matthias J P van Osch, Danny J J Wang, Eric C Wong, and Greg Zaharchuk. Recommended implementation of arterial spin-labeled perfusion MRI

for clinical applications: A consensus of the ISMRM perfusion study group and the European consortium for ASL in dementia. *Magnetic Resonance in Medicine*, 73(1):102–116, April 2014.

[8] Beau M Ances, Oleg Leontiev, Joanna E Perthen, Christine Liang, Amy E Lansing, and Richard B Buxton. Regional differences in the coupling of cerebral blood flow and oxygen metabolism changes in response to activation: implications for BOLD-fMRI. *NeuroImage*, 39(4):1510–1521, February 2008.

[9] Beau M Ances, Christine L Liang, Oleg Leontiev, Joanna E Perthen, Adam S Fleisher, Amy E Lansing, and Richard B Buxton. Effects of aging on cerebral blood flow, oxygen metabolism, and blood oxygenation level dependent responses to visual stimulation. *Human Brain Mapping*, 30(4):1120–1132, April 2009.

[10] C Anile, P De Bonis, A Di Chirico, A Ficola, A Mangiola, and G Petrella. Cerebral blood flow autoregulation during intracranial hypertension: a simple, purely hydraulic mechanism? *Child's Nervous System*, 25(3):325–335, 2009.

[11] A Aperia. New roles for an old enzyme: Na,K-ATPase emerges as an interesting drug target. *Journal of Internal Medicine*, 261(1):44–52, January 2007.

[12] Clay M. Armstrong. The Na/K pump, Cl ion, and osmotic stabilization of cells. *Proceedings of the National Academy of Sciences*, 100(10):6257–6262, 2003.

[13] Sina Aslan, Feng Xu, Peiying L Wang, Jinsoo Uh, Uma S Yezhuvath, Matthias van Osch, and Hanzhang Lu. Estimation of labeling efficiency in pseudocontinuous arterial spin labeling. *Magnetic Resonance in Medicine*, 63(3):765–771, March 2010.

[14] Iris Asllani, Ajna Borogovac, and Truman R Brown. Regression algorithm correcting for partial volume effects in arterial spin labeling MRI. *Magnetic Resonance in Medicine*, 60(6):1362–1371, December 2008.

[15] Iris Asllani, Ajna Borogovac, Clinton Wright, Ralph Sacco, Truman R Brown, and Eric Zarahn. An investigation of statistical power for continuous arterial spin labeling imaging at 1.5 T. *NeuroImage*, 39(3):1246–1256, February 2008.

[16] J L Atkinson, R E Anderson, and T M Sundt. The effect of carbon dioxide on the diameter of brain capillaries. *Brain Research*, 517(1-2):333–340, May 1990.

[17] R B Banzett, R W Lansing, K C Evans, and S A Shea. Stimulus-response characteristics of CO_2-induced air hunger in normal subjects. *Respiration Physiology*, 103(1):19–31, 1996.

[18] R B Banzett, R T Garcia, and S H Moosavi. Simple contrivance "clamps" end-tidal PCO_2 and PO_2 despite rapid changes in ventilation. *Journal of Applied Physiology*, 88(5):1597–1600, May 2000.

[19] R W Barbee, W N Stainsby, and S J Chirtel. Dynamics of O_2, CO_2, lactate, and acid exchange during contractions and recovery. *Journal of Applied Physiology*, 54(6):1687–1692, June 1983.

[20] A Battisti-Charbonney, J Fisher, and J Duffin. The cerebrovascular response to carbon dioxide in humans. *The Journal of Physiology*, 589(12):3039–3048, June 2011.

[21] BR Berg, KD Cohen, and IH Sarelius. Direct coupling between blood flow and metabolism at the capillary level in striated muscle. *American Journal of Physiology–Heart and Circulatory Physiology*, 272(6):2693–2700, 1997.

[22] Alex A Bhogal, Jeroen C W Siero, Joseph A Fisher, Martijn Froeling, Peter Luijten, Marielle Philippens, and Hans Hoogduin. Investigating the non-linearity of the BOLD cerebrovascular reactivity response to targeted hypo/hypercapnia at 7T. *NeuroImage*, 98(C):296–305, September 2014.

[23] Laura Biagi, Arturo Abbruzzese, Maria Cristina Bianchi, David C Alsop, Alberto Del Guerra, and Michela Tosetti. Age dependence of cerebral perfusion assessed

by magnetic resonance continuous arterial spin labeling. *Journal of Magnetic Resonance Imaging*, 25(4):696–702, April 2007.

[24] A Bidani and E D Crandall. Velocity of CO_2 exchanges in the lungs. *Annual Review of Physiology*, 50:639–652, 1988.

[25] Maja A A Binnewijzend, Joost P A Kuijer, Marije R Benedictus, Wiesje M van der Flier, Alle Meije Wink, Mike P Wattjes, Bart N M van Berckel, Philip Scheltens, and Frederik Barkhof. Cerebral Blood Flow Measured with 3D Pseudocontinuous Arterial Spin-labeling MR Imaging in Alzheimer Disease and Mild Cognitive Impairment: A Marker for Disease Severity. *Radiology*, 267(1):221–230, April 2013.

[26] Rasmus M Birn, Jason B Diamond, Monica A Smith, and Peter A Bandettini. Separating respiratory-variation-related fluctuations from neuronal-activity-related fluctuations in fMRI. *NeuroImage*, 31(4):1536–1548, July 2006.

[27] Rasmus M Birn, Monica A Smith, Tyler B Jones, and Peter A Bandettini. The respiration response function: The temporal dynamics of fMRI signal fluctuations related to changes in respiration. *NeuroImage*, 40(2):644–654, April 2008.

[28] C C Bishop, S Powell, D Rutt, and N L Browse. Transcranial Doppler measurement of middle cerebral artery blood flow velocity: a validation study. *Stroke*, 17 (5):913–915, September 1986.

[29] Martin Blaha, Rune Aaslid, Colleen M Douville, Reinaldo Correra, and David W Newell. Cerebral blood flow and dynamic cerebral autoregulation during ethanol intoxication and hypercapnia. *Journal of Clinical Neuroscience*, 10(2):195–198, March 2003.

[30] Nicholas P Blockley, Ian D Driver, Susan T Francis, Joseph A Fisher, and Penny A Gowland. An improved method for acquiring cerebrovascular reactivity maps. *Magnetic Resonance in Medicine*, 65(5):1278–1286, May 2011.

[31] D Böning and N Maassen. Blood osmolality in vitro: dependence on PCO_2, lactic acid concentration, and O_2 saturation. *Journal of Applied Physiology*, 54(1):118–122, 1983.

[32] D Böning, U Vaas, and K M Braumann. Blood osmolality during in vivo changes of CO_2 pressure. *Journal of Applied Physiology*, 54(1):123–129, 1983.

[33] S M Boumphrey, E A J Morris, and S M Kinsella. 100% inspired oxygen from a Hudson mask-a realistic goal? *Resuscitation*, 57(1):69–72, April 2003.

[34] G M Boynton, S A Engel, G H Glover, and D J Heeger. Linear systems analysis of functional magnetic resonance imaging in human V1. *The Journal of Neuroscience*, 16(13):4207–4221, July 1996.

[35] M Bradbury. The blood-brain barrier. *Experimental physiology*, 78:453–472, 1993.

[36] M.W.B. Bradbury. *The concept of a blood-brain barrier*. A Wiley-interscience publication. Wiley, first edition, 1979. ISBN 0 471 99688 2.

[37] R D Bradley, S J Semple, and G T Spencer. Rate of change of carbon dioxide tension in arterial blood, jugular venous blood and cisternal cerebrospinal fluid on carbon dioxide administration. *The Journal of Physiology*, 179(3):442–455, August 1965.

[38] Johnny E. Jr. Brian. Carbon Dioxide and the Cerebral Circulation. *Anesthesiology*, 88(5):1365, May 1998.

[39] Molly G Bright, Daniel P Bulte, Peter Jezzard, and Jeff H Duyn. Characterization of regional heterogeneity in cerebrovascular reactivity dynamics using novel hypocapnia task and BOLD fMRI. *NeuroImage*, 48(1):166–175, October 2009.

[40] Molly G Bright, Manus J Donahue, Jeff H Duyn, Peter Jezzard, and Daniel P Bulte. The effect of basal vasodilation on hypercapnic and hypocapnic reactivity

measured using magnetic resonance imaging. *Journal of Cerebral Blood Flow and Metabolism*, 31(2):426–438, February 2011.

[41] R J Brocklehurst and Yandell Henderson. The buffering of the tissues as indicated by the CO_2 capacity of the body. *Journal of Biological Chemistry*, 72(2):665–675, 1927.

[42] P Brodersen, O B Paulson, T G Bolwig, Z E Rogon, O J Rafaelsen, and N A Lassen. Cerebral hyperemia in electrically induced epileptic seizures. *Archives of Neurology*, 28(5):334–338, May 1973.

[43] Erin M Buckley, Maryam Y Naim, Jennifer M Lynch, Donna A Goff, Peter J Schwab, Laura K Diaz, Susan C Nicolson, Lisa M Montenegro, Natasha A Lavin, Turgut Durduran, Thomas L Spray, J William Gaynor, Mary E Putt, A G Yodh, Mark A Fogel, and Daniel J Licht. Sodium bicarbonate causes dose-dependent increases in cerebral blood flow in infants and children with single-ventricle physiology. *Pediatric Research*, 73(5):668–673, February 2013.

[44] D P Bulte, M Kelly, M Germuska, J Xie, M A Chappell, T W Okell, M G Bright, and P Jezzard. Quantitative measurement of cerebral physiology using respiratory-calibrated MRI. *NeuroImage*, 60(1):582–591, March 2012.

[45] Daniel Bulte, Peter A Chiarelli, Richard Wise, and Peter Jezzard. Measurement of cerebral blood volume in humans using hyperoxic MRI contrast. *Journal of Magnetic Resonance Imaging*, 26(4):894–899, October 2007.

[46] Daniel P Bulte, Peter A Chiarelli, Richard G Wise, and Peter Jezzard. Cerebral perfusion response to hyperoxia. *Journal of Cerebral Blood Flow and Metabolism*, 27(1):69–75, 2007.

[47] Daniel P Bulte, Knut Drescher, and Peter Jezzard. Comparison of hypercapnia-based calibration techniques for measurement of cerebral oxygen metabolism with MRI. *Magnetic Resonance in Medicine*, 61(2):391–398, February 2009.

[48] R B Buxton, L R Frank, E C Wong, B Siewert, S Warach, and R R Edelman. A general kinetic model for quantitative perfusion imaging with arterial spin labeling. *Magnetic Resonance in Medicine*, 40(3):383–396, September 1998.

[49] Richard B Buxton and Lawrence R Frank. A model for the coupling between cerebral blood flow and oxygen metabolism during neural stimulation. *Journal of Cerebral Blood Flow and Metabolism*, 17(1):64–72, 1997.

[50] Fernando Calamante. Arterial input function in perfusion MRI: A comprehensive review. *Progress in Nuclear Magnetic Resonance Spectroscopy*, 74(C):1–32, October 2013.

[51] Fernando Calamante, S R Williams, N Van Bruggen, K K Kwong, and R Turner. A model for quantification of perfusion in pulsed labelling techniques. *NMR in Biomedicine*, 9(2):79–83, April 1996.

[52] Alison M Campbell and Christian Beaulieu. Pulsed arterial spin labeling parameter optimization for an elderly population. *Journal of Magnetic Resonance Imaging*, 23(3):398–403, March 2006.

[53] S Cantin, M Villien, O Moreaud, I Tropres, S Keignart, E Chipon, J-F Le Bas, J Warnking, and A Krainik. Impaired cerebral vasoreactivity to CO_2 in Alzheimer's disease using BOLD fMRI. *NeuroImage*, 58(2):579–587, September 2011.

[54] B E Carlson, J C Arciero, and T W Secomb. Theoretical model of blood flow autoregulation: roles of myogenic, shear-dependent, and metabolic responses. *American Journal of Physiology–Heart and Circulatory Physiology*, 295(4): H1572–H1579, July 2008.

[55] John P Carr, David L Buckley, Jean Tessier, and Geoff J M Parker. What levels of precision are achievable for quantification of perfusion and capillary permeability surface area product using ASL? *Magnetic Resonance in Medicine*, 58(2):281–289, August 2007.

[56] Francis Cassot, Frederic Lauwers, Sylvie Lorthois, Prasanna Puwanarajah, Valérie Cances-Lauwers, and Henri Duvernoy. Branching patterns for arterioles and venules of the human cerebral cortex. *Brain Research*, 1313(C):62–78, February 2010.

[57] Mustafa Çavuşoğlu, Josef Pfeuffer, Kâmil Uğurbil, and Kâmil Uludağ. Comparison of pulsed arterial spin labeling encoding schemes and absolute perfusion quantification. *Magnetic Resonance Imaging*, 27(8):1039–1045, September 2009.

[58] Brenda R Chen, Matthew B Bouchard, Addason F H McCaslin, Sean A Burgess, and Elizabeth M C Hillman. High-speed vascular dynamics of the hemodynamic response. *NeuroImage*, 54(2):1021–1030, January 2011.

[59] J Jean Chen and G Bruce Pike. Global cerebral oxidative metabolism during hypercapnia and hypocapnia in humans: implications for BOLD fMRI. *Journal of Cerebral Blood Flow and Metabolism*, 30(6):1094–1099, June 2010.

[60] J Jean Chen and G Bruce Pike. MRI measurement of the BOLD-specific flow-volume relationship during hypercapnia and hypocapnia in humans. *NeuroImage*, 53(2):383–391, November 2010.

[61] Yufen Chen, Danny J J Wang, and John A Detre. Test-retest reliability of arterial spin labeling with common labeling strategies. *Journal of Magnetic Resonance Imaging*, 33(4):940–949, April 2011.

[62] N S Cherniack and G S Longobardo. Oxygen and carbon dioxide gas stores of the body. *Physiological Reviews*, 50(2):196–243, April 1970.

[63] Carol Yim-Lui Cheung, Yi-Ting Ong, M Kamran Ikram, Shin Yeu Ong, Xiang Li, Saima Hilal, Joseree-Ann S Catindig, Narayanaswamy Venketasubramanian, Philip Yap, Dennis Seow, Christopher P Chen, and Tien Yin Wong. Microvascular network alterations in the retina of patients with Alzheimer's disease. *Alzheimer's & dementia*, 10(2):135–142, March 2014.

[64] Peter A Chiarelli, Daniel P Bulte, Richard Wise, Daniel Gallichan, and Peter Jezzard. A calibration method for quantitative BOLD fMRI based on hyperoxia. *NeuroImage*, 37(3):808–820, September 2007.

[65] F P Chinard. Starling's hypothesis in the formation of edema. *Bulletin of the New York Academy of Medicine*, 38:375–389, June 1962.

[66] Marilyn J Cipolla. *The Cerebral Circulation*. Integrated Systems Physiology: From Molecule to Function. Morgan & Claypool Life Sciences, San Rafael (CA), 2009.

[67] John Conklin, Jorn Fierstra, Adrian P Crawley, Jay S Han, Julien Poublanc, Daniel M Mandell, Frank L Silver, Michael Tymianski, Joseph A Fisher, and David J Mikulis. Impaired cerebrovascular reactivity with steal phenomenon is associated with increased diffusion in white matter of patients with Moyamoya disease. *Stroke*, 41(8):1610–1616, August 2010.

[68] N A Coulter. Filtration coefficient of the capillaries of the brain. *The American journal of Physiology*, 195(2):459–464, November 1958.

[69] R W Cox and A Jesmanowicz. Real-time 3D image registration for functional MRI. *Magnetic Resonance in Medicine*, 42(6):1014–1018, December 1999.

[70] J Cruz, M E Miner, S J Allen, W M Alves, and T A Gennarelli. Continuous monitoring of cerebral oxygenation in acute brain injury: injection of mannitol during hyperventilation. *Journal of Neurosurgery*, 73(5):725–730, November 1990.

[71] Fabrice Dabertrand, Mark T Nelson, and Joseph E Brayden. Ryanodine receptors, calcium signaling, and regulation of vascular tone in the cerebral parenchymal microcirculation. *Microcirculation*, 20(4):307–316, May 2013.

[72] Weiying Dai, Dairon Garcia, Cedric de Bazelaire, and David C Alsop. Continuous flow-driven inversion for arterial spin labeling using pulsed radio frequency and gradient fields. *Magnetic Resonance in Medicine*, 60(6):1488–1497, December 2008.

[73] S C De Cort, J A Innes, T J Barstow, and A Guz. Cardiac output, oxygen consumption and arteriovenous oxygen difference following a sudden rise in exercise level in humans. *The Journal of Physiology*, 441:501–512, September 1991.

[74] J A Detre and D C Alsop. Perfusion magnetic resonance imaging with continuous arterial spin labeling: methods and clinical applications in the central nervous system. *European Journal of Radiology*, 30(2):115–124, May 1999.

[75] John A Detre, J S Leigh, D S Williams, and A P Koretsky. Perfusion imaging. *Magnetic Resonance in Medicine*, 23(1):37–45, 1992.

[76] John A Detre, Jiongjiong Wang, Ze Wang, and Hengyi Rao. Arterial spin-labeled perfusion MRI in basic and clinical neuroscience. *Current Opinion in Neurology*, 22(4):348–355, August 2009.

[77] John A Detre, Hengyi Rao, Danny J J Wang, Yu Fen Chen, and Ze Wang. Applications of arterial spin labeled MRI in the brain. *Journal of Magnetic Resonance Imaging*, 35(5):1026–1037, May 2012.

[78] Michael N Diringer and Allyson R Zazulia. Osmotic Therapy: Fact and Fiction. *Neurocritical Care*, 1(2):219–234, 2004.

[79] Michael N Diringer, Michael T Scalfani, Allyson R Zazulia, Tom O Videen, and Raj Dhar. Cerebral hemodynamic and metabolic effects of equi-osmolar doses mannitol and 23.4% saline in patients with edema following large ischemic stroke. *Neurocritical Care*, 14(1):11–17, February 2011.

[80] Manus J Donahue, Carlos C Faraco, Megan K Strother, Michael A Chappell, Swati Rane, Lindsey M Dethrage, Jeroen Hendrikse, and Jeroen C W Siero. Bolus arrival time and cerebral blood flow responses to hypercarbia. *Journal of Cerebral Blood Flow and Metabolism*, 34(7):1243–1252, April 2014.

[81] Ian Driver, Nicholas Blockley, Joseph Fisher, Susan Francis, and Penny Gowland. The change in cerebrovascular reactivity between 3 T and 7 T measured using graded hypercapnia. *NeuroImage*, 51(1):274–279, May 2010.

[82] R Duelli and W Kuschinsky. Changes in brain capillary diameter during hypocapnia and hypercapnia. *Journal of Cerebral Blood Flow and Metabolism*, 13(6): 1025–1028, November 1993.

[83] T Q Duong, C Iadecola, and S G Kim. Effect of hyperoxia, hypercapnia, and hypoxia on cerebral interstitial oxygen tension and cerebral blood flow. *Magnetic Resonance in Medicine*, 45(1):61–70, 2001.

[84] B Eklöf, N A Lassen, L Nilsson, K Norberg, B K Siesjö, and P Torlöf. Regional cerebral blood flow in the rat measured by the tissue sampling technique; a critical evaluation using four indicators C^{14}-antipyrine, C^{14}-ethanol H^3-water and xenon. *Acta Physiologica Scandinavica*, 91(1):1–10, May 1974.

[85] I Ellingsen, A Hauge, G Nicolaysen, M Thoresen, and L Walløe. Changes in human cerebral blood flow due to step changes in PaO_2 and $PaCO_2$. *Acta Physiologica Scandinavica*, 129(2):157–163, February 1987.

[86] S K Epstein and N Singh. Respiratory acidosis. *Respiratory Care*, 46(4):366–383, April 2001.

[87] Marco Essig, Mark S Shiroishi, Thanh Binh Nguyen, Marc Saake, James M Provenzale, David Enterline, Nicoletta Anzalone, Arnd Dörfler, Àlex Rovira, Max Wintermark, and Meng Law. Perfusion MRI: The Five Most Frequently Asked Technical Questions. *American Journal of Roentgenology*, 200(1):24–34, January 2013.

[88] F M Faraci and D D Heistad. Regulation of large cerebral arteries and cerebral microvascular pressure. *Circulation Research*, 66(1):8–17, January 1990.

[89] L E Farhi and H Rahn. Dynamics of changes in carbon dioxide stores. *Anesthesiology*, 21:604–614, November 1960.

[90] David A Feinberg and Kawin Setsompop. Ultra-fast MRI of the human brain with simultaneous multi-slice imaging. *Journal of Magnetic Resonance*, 229:90–100, April 2013.

[91] J D Fenstermacher and J A Johnson. Filtration and reflection coefficients of the rabbit blood-brain barrier. *The American Journal of Physiology*, 211(2):341–346, August 1966.

[92] Francisco Fernández-Klett, Nikolas Offenhauser, Ulrich Dirnagl, Josef Priller, and Ute Lindauer. Pericytes in capillaries are contractile in vivo, but arterioles mediate functional hyperemia in the mouse brain. *Proceedings of the National Academy of Sciences*, 107(51):22290–22295, December 2010.

[93] J Fierstra, O Sobczyk, A Battisti-Charbonney, D M Mandell, J Poublanc, A P Crawley, D J Mikulis, J Duffin, and J A Fisher. Measuring cerebrovascular reactivity: What stimulus to use? *The Journal of Physiology*, September 2013.

[94] Jessica A Filosa and Víctor M Blanco. Neurovascular coupling in the mammalian brain. *Experimental Physiology*, 92(4):641–646, July 2007.

[95] Thomas F Floyd, James M Clark, Robert Gelfand, John A Detre, Sarah Ratcliffe, Dimitri Guvakov, Christian J Lambertsen, and Roderic G Eckenhoff. Independent cerebral vasoconstrictive effects of hyperoxia and accompanying arterial hypocapnia at 1 ATA. *Journal of Applied Physiology*, 95(6):2453–2461, December 2003.

[96] M Fog. The relationship between the blood pressure and the tonic regulation of the pial arteries. *Journal of Neurology and Psychiatry*, 1938.

[97] Lisa L Forsyth, Xi Liu-DeRyke, Dennis Parker, and Denise H Rhoney. Role of hypertonic saline for the management of intracranial hypertension after stroke and traumatic brain injury. *Pharmacotherapy*, 28(4):469–484, April 2008.

[98] Peter T Fox. The coupling controversy. *NeuroImage*, 62(2):594–601, August 2012.

[99] Peter T Fox and M E Raichle. Focal physiological uncoupling of cerebral blood flow and oxidative metabolism during somatosensory stimulation in human sub-

jects. *Proceedings of the National Academy of Sciences*, 83(4):1140–1144, February 1986.

[100] Peter T Fox, M E Raichle, M A Mintun, and C Dence. Nonoxidative glucose consumption during focal physiologic neural activity. *Science*, 241(4864):462–464, July 1988.

[101] Bonomini Francesca and Rita Rezzani. Aquaporin and blood brain barrier. *Current Neuropharmacology*, 8(2):92–96, June 2010.

[102] Daniel Gallichan and Peter Jezzard. Modeling the effects of dispersion and pulsatility of blood flow in pulsed arterial spin labeling. *Magnetic Resonance in Medicine*, 60(1):53–63, July 2008.

[103] Daniel Gallichan and Peter Jezzard. Variation in the shape of pulsed arterial spin labeling kinetic curves across the healthy human brain and its implications for CBF quantification. *Magnetic Resonance in Medicine*, 61(3):686–695, March 2009.

[104] Yong-Zhe Gao, Jun-Jian Zhang, Hui Liu, Guang-Yao Wu, Li Xiong, and Min Shu. Regional cerebral blood flow and cerebrovascular reactivity in Alzheimer's disease and vascular dementia assessed by arterial spinlabeling magnetic resonance imaging. *Current Neurovascular Research*, 10(1):49–53, February 2013.

[105] Dairon M Garcia, Guillaume Duhamel, and David C Alsop. Efficiency of inversion pulses for background suppressed arterial spin labeling. *Magnetic Resonance in Medicine*, 54(2):366–372, August 2005.

[106] C J Gauthier and R D Hoge. Magnetic resonance imaging of resting OEF and $CMRO_2$ using a generalized calibration model for hypercapnia and hyperoxia. *NeuroImage*, 60(2):1212–1225, April 2012.

[107] C J Gauthier, C Madjar, F B Tancredi, and R D Hoge. Elimination of visually evoked BOLD responses during carbogen inhalation: implications for calibrated MRI. *NeuroImage*, 54(2):1001–1011, January 2011.

[108] C J Gauthier, L Desjardins-Crépeau, C Madjar, L Bherer, and R D Hoge. Absolute quantification of resting oxygen metabolism and metabolic reactivity during functional activation using QUO2 MRI. *NeuroImage*, 63(3):1353–1363, November 2012.

[109] Claudine J Gauthier and Richard D Hoge. A generalized procedure for calibrated MRI incorporating hyperoxia and hypercapnia. *Human Brain Mapping*, January 2012.

[110] Claudine J Gauthier, Cécile Madjar, Laurence Desjardins-Crépeau, Pierre Bellec, Louis Bherer, and Richard D Hoge. Age dependence of hemodynamic response characteristics in human functional magnetic resonance imaging. *Neurobiology of Aging*, 34(5):1469–1485, May 2013.

[111] Claudine Joëlle Gauthier, Muriel Lefort, Saïd Mekary, Laurence Desjardins-Crépeau, Arnold Skimminge, Pernille Iversen, Cécile Madjar, Michèle Desjardins, Frédéric Lesage, Ellen Garde, Frédérique Frouin, Louis Bherer, and Richard D Hoge. Hearts and minds: linking vascular rigidity and aerobic fitness with cognitive aging. *Neurobiology of Aging*, pages 1–11, November 2014.

[112] S Gazitua, J B Scott, B Swindall, and F J Haddy. Resistance responses to local changes in plasma osmolality in three vascular beds. *The American Journal of Physiology*, 220(2):384–391, February 1971.

[113] Sanna Gevers, Matthias J van Osch, Reinoud PH Bokkers, Dennis A Kies, Wouter M Teeuwisse, Charles B Majoie, Jeroen Hendrikse, and Aart J Nederveen. Intra- and multicenter reproducibility of pulsed, continuous and pseudo-continuous arterial spin labeling methods for measuring cerebral perfusion. *Journal of Cerebral Blood Flow and Metabolism*, 31(8):1706–1715, February 2011.

[114] M S Ghandour, O K Langley, X L Zhu, A Waheed, and W S Sly. Carbonic anhydrase IV on brain capillary endothelial cells: a marker associated with the

blood-brain barrier. *Proceedings of the National Academy of Sciences*, 89(15): 6823–6827, August 1992.

[115] Eidrees Ghariq, Michael A Chappell, Sophie Schmid, Wouter M Teeuwisse, and Matthias J P van Osch. Effects of background suppression on the sensitivity of dual-echo arterial spin labeling MRI for BOLD and CBF signal changes. *NeuroImage*, 103(C):1–7, 2014.

[116] F Gibbs, E Gibbs, and W Lennox. Changes in human cerebral blood flow consequent on alterations in blood gases. *American Journal of Physiology*, 1935.

[117] I Giovannini and C Chiarla. Quantitative assessment of changes in blood CO_2 tension mediated by the Haldane effect. *Journal of Applied Physiology*, 87:862–866, 1999.

[118] Hélène Girouard and Costantino Iadecola. Neurovascular coupling in the normal brain and in hypertension, stroke, and Alzheimer disease. *Journal of Applied Physiology*, 100(1):328–335, January 2006.

[119] U Gleichmann, D H Ingvar, D W Lübbers, B K Siesjö, and G Thews. Tissue pO_2 and pCO_2 of the cerebral cortex, related to blood gas tensions. *Acta Physiologica Scandinavica*, 55:127–138, June 1962.

[120] Christopher B Glielmi, Ronald A Schuchard, and X P Hu. Estimating cerebral blood volume with expanded vascular space occupancy slice coverage. *Magnetic Resonance in Medicine*, 61(5):1193–1200, May 2009.

[121] Lidia Glodzik, Henry Rusinek, Miroslaw Brys, Wai H Tsui, Remigiusz Switalski, Lisa Mosconi, Rachel Mistur, Elizabeth Pirraglia, Susan de Santi, Yi Li, Alexander Goldowsky, and Mony J De Leon. Framingham cardiovascular risk profile correlates with impaired hippocampal and cortical vasoreactivity to hypercapnia. *Journal of Cerebral Blood Flow and Metabolism*, 31(2):671–679, February 2011.

[122] G H Glover, T Q Li, and D Ress. Image-based method for retrospective correction of physiological motion effects in fMRI: RETROICOR. *Magnetic Resonance in Medicine*, 44(1):162–167, July 2000.

[123] Gary H Glover. Deconvolution of impulse response in event-related BOLD fMRI. *NeuroImage*, 9(4):416–429, April 1999.

[124] K G Go. The normal and pathological physiology of brain water. *Advances and Technical Standards in Neurosurgery*, 23:47–142, 1997.

[125] Jozien Goense, Hellmut Merkle, and Nikos K Logothetis. High-Resolution fMRI Reveals Laminar Differences in Neurovascular Coupling between Positive and Negative BOLD Responses. *Neuron*, 76(3):629–639, November 2012.

[126] Xavier Golay and Esben T Petersen. Arterial spin labeling: benefits and pitfalls of high magnetic field. *Neuroimaging Clinics of North America*, 16(2):259–68, May 2006.

[127] G W Goldstein and A L Betz. Recent advances in understanding brain capillary function. *Annals of Neurology*, 14(4):389–395, October 1983.

[128] S D Goode, S Krishan, C Alexakis, R Mahajan, and D P Auer. Precision of cerebrovascular reactivity assessment with use of different quantification methods for hypercapnia functional MR imaging. *American Journal of Neuroradiology*, 30 (5):972–977, May 2009.

[129] Jonathan A Goodwin, Rishma Vidyasagar, George M Balanos, Daniel Bulte, and Laura M Parkes. Quantitative fMRI using hyperoxia calibration: reproducibility during a cognitive Stroop task. *NeuroImage*, 47(2):573–580, August 2009.

[130] J H Greenberg, M Reivich, and A Noordergraaf. A model of cerebral blood flow control in hypercapnia. *Annals of Biomedical Engineering*, 6(4):453–491, December 1978.

[131] Mark A Griswold, Peter M Jakob, Robin M Heidemann, Mathias Nittka, Vladimir Jellus, Jianmin Wang, Berthold Kiefer, and Axel Haase. Generalized autocalibrating partially parallel acquisitions (GRAPPA). *Magnetic Resonance in Medicine*, 47(6):1202–1210, June 2002.

[132] K Gröschel, C Terborg, S Schnaudigel, T Ringer, A Riecker, O W Witte, and A Kastrup. Effects of physiological aging and cerebrovascular risk factors on the hemodynamic response to brain activation: a functional transcranial Doppler study. *European Journal of Neurology*, 14(2):125–131, February 2007.

[133] R L Grubb, M E Phelps, M E Raichle, and M M Ter-Pogossian. The effects of arterial blood pressure on the regional cerebral blood volume by X-ray fluorescence. *Stroke*, 4(3):390–399, May 1973.

[134] R L Grubb, M E Raichle, J O Eichling, and M M Ter-Pogossian. The effects of changes in $PaCO_2$ on cerebral blood volume, blood flow, and vascular mean transit time. *Stroke*, 5(5):630–639, September 1974.

[135] Hong Gu, Hanzhang Lu, Frank Q Ye, Elliot A Stein, and Yihong Yang. Noninvasive quantification of cerebral blood volume in humans during functional activation. *NeuroImage*, 30(2):377–387, April 2006.

[136] S R Gullans and J G Verbalis. Control of brain volume during hyperosmolar and hypoosmolar conditions. *Annual Review of Medicine*, 44:289–301, 1993.

[137] Matthias Günther, Koichi Oshio, and David A Feinberg. Single-shot 3D imaging techniques improve arterial spin labeling perfusion measurements. *Magnetic Resonance in Medicine*, 54(2):491–498, August 2005.

[138] A C Guyton and J E Hall. *Textbook of Medical Physiology*. Elsevier Health Sciences, eleventh edition, 2006. ISBN 0-7216-0240-1.

[139] Ihab Hajjar, Peng Zhao, David Alsop, and Vera Novak. Hypertension and cerebral vasoreactivity: a continuous arterial spin labeling magnetic resonance imaging study. *Hypertension*, 56(5):859–864, November 2010.

[140] J E Hardebo and B Nilsson. Hemodynamic changes in brain caused by local infusion of hyperosomolar solutions, in particular relation to blood-brain barrier opening. *Brain Research*, 181(1):49–59, January 1980.

[141] Noam Harel, Patrick J Bolan, Robert Turner, Kamil Ugurbil, and Essa Yacoub. Recent Advances in High-Resolution MR Application and Its Implications for Neurovascular Coupling Research. *Frontiers in Neuroenergetics*, 2, 2010.

[142] A M Harper. Autoregulation of cerebral blood flow: influence of the arterial blood pressure on the blood flow through the cerebral cortex. *Journal of Neurology, Neurosurgery & Psychiatry*, 29(5):398–403, October 1966.

[143] A M Harper. Regulation of cerebral circulation. *The Scientific Basis of Medicine Annual Reviews*, pages 60–81, 1969.

[144] A M Harper and H I Glass. Effect of alterations in the arterial carbon dioxide tension on the blood flow through the cerebral cortex at normal and low arterial blood pressures. *Journal of Neurology, Neurosurgery & Psychiatry*, 28(5):449–452, October 1965.

[145] Erik F Hauck, Sebastian Apostel, Julie F Hoffmann, Axel Heimann, and Oliver Kempski. Capillary flow and diameter changes during reperfusion after global cerebral ischemia studied by intravital video microscopy. *Journal of Cerebral Blood Flow and Metabolism*, 24(4):383–391, April 2004.

[146] A Hauge and G Bo. Blood hyperosmolality and pulmonary vascular resistance in the cat. *Circulation Research*, 28(3):371–376, March 1971.

[147] Anton Hauge, Gunnar Nicolaysen, and Marianne Thoresen. Acute effects of acetazolamide on cerbral blood flow in man. *Acta Physiologica Scandinavica*, 117 (2):233–239, February 1983.

[148] Robin M Heidemann, Dimo Ivanov, Robert Trampel, Fabrizio Fasano, Heiko Meyer, Josef Pfeuffer, and Robert Turner. Isotropic submillimeter fMRI in the

human brain at 7 T: Combining reduced field-of-view imaging and partially parallel acquisitions. *Magnetic Resonance in Medicine*, 68(5):1506–1516, January 2012.

[149] D F R Heijtel, H J M M Mutsaerts, E Bakker, P Schober, M F Stevens, E T Petersen, B N M van Berckel, C B L M Majoie, J Booij, M J P van Osch, E vanBavel, R Boellaard, A A Lammertsma, and A J Nederveen. Accuracy and precision of pseudo-continuous arterial spin labeling perfusion during baseline and hypercapnia: A head-to-head comparison with ^{15}O H_2O positron emission tomography. *NeuroImage*, 92(C):182–192, May 2014.

[150] D R Held and C A Steiner. Effect of acute respiratory acidosis on arterial plasma osmolality. *Respiration Physiology*, 12(1):25–35, April 1971.

[151] R P Henry. Multiple roles of carbonic anhydrase in cellular transport and metabolism. *Annual Review of Physiology*, 58:523–538, 1996.

[152] Hye-Young Heo, John Wemmie, Daniel Thedens, and Vincent A Magnotta. Evaluation of activity-dependent functional pH and T1ρ response in the visual cortex. *NeuroImage*, 95(C):336–343, July 2014.

[153] P Herscovitch and M E Raichle. What is the correct value for the brain–blood partition coefficient for water? *Journal of Cerebral Blood Flow and Metabolism*, 5(1):65–69, March 1985.

[154] Yi-Ching Lynn Ho, Esben Thade Petersen, and Xavier Golay. Measuring arterial and tissue responses to functional challenges using arterial spin labeling. *NeuroImage*, 49(1):478–487, 2010.

[155] Yi-Ching Lynn Ho, Esben Thade Petersen, Ivan Zimine, and Xavier Golay. Similarities and differences in arterial responses to hypercapnia and visual stimulation. *Journal of Cerebral Blood Flow and Metabolism*, 31(2):560–571, February 2011.

[156] R D Hoge and G B Pike. Oxidative metabolism and the detection of neuronal activation via imaging. *Journal of Chemical Neuroanatomy*, 22(1-2):43–52, June 2001.

[157] R D Hoge, J Atkinson, B Gill, G R Crelier, S Marrett, and G B Pike. Investigation of BOLD signal dependence on cerebral blood flow and oxygen consumption: the deoxyhemoglobin dilution model. *Magnetic Resonance in Medicine*, 42(5): 849–863, November 1999.

[158] R D Hoge, Jeff Atkinson, Brad Gill, G R Crelier, S Marrett, and G B Pike. Linear coupling between cerebral blood flow and oxygen consumption in activated human cortex. *Proceedings of the National Academy of Sciences*, 96(16):9403–9408, August 1999.

[159] Yuan-Yu Hsu, Chen-Nen Chang, Shih-Ming Jung, Kun-Eng Lim, Ju-Chuan Huang, Shin-Yi Fang, and Ho-Ling Liu. Blood oxygenation level-dependent MRI of cerebral gliomas during breath holding. *Journal of Magnetic Resonance Imaging*, 19(2):160–167, 2004.

[160] Honghong Hu, Aurélien Boisson-Dernier, Maria Israelsson-Nordström, Maik Böhmer, Shaowu Xue, Amber Ries, Jan Godoski, Josef M Kuhn, and Julian I Schroeder. Carbonic anhydrases are upstream regulators of CO_2-controlled stomatal movements in guard cells. *Nature Cell Biology*, 12(1):87–93, December 2009.

[161] A G Hudetz, G Fehér, CG Weigle, D.E. Knuese, and J P Kampine. Video microscopy of cerebrocortical capillary flow: response to hypotension and intracranial hypertension. *American Journal of Physiology–Heart and Circulatory Physiology*, 268(6):H2202, 1995.

[162] A G Hudetz, B B Biswal, G Fehér, and J P Kampine. Effects of hypoxia and hypercapnia on capillary flow velocity in the rat cerebral cortex. *Microvascular Research*, 54(1):35–42, July 1997.

[163] Elizabeth B Hutchinson, Bojana Stefanovic, Alan P Koretsky, and Afonso C Silva. Spatial flow-volume dissociation of the cerebral microcirculatory response to mild hypercapnia. *NeuroImage*, 32(2):520–530, August 2006.

[164] Fahmeed Hyder, Basavaraju G Sanganahalli, Peter Hermán, Daniel Coman, Natasja J G Maandag, Kevin L Behar, Hal Blumenfeld, and Douglas L Rothman. Neurovascular and Neurometabolic Couplings in Dynamic Calibrated fMRI: Transient Oxidative Neuroenergetics for Block-Design and Event-Related Paradigms. *Frontiers in Neuroenergetics*, 2, 2010.

[165] Costantino Iadecola. Neurovascular regulation in the normal brain and in Alzheimer's disease. *Nature Reviews Neuroscience*, 5(5):347–360, May 2004.

[166] Costantino Iadecola and Robin L Davisson. Hypertension and cerebrovascular dysfunction. *Cell–Metabolism*, 7(6):476–484, June 2008.

[167] Masanobu Ibaraki, Hiroshi Ito, Eku Shimosegawa, Hideto Toyoshima, Keiichi Ishigame, Kazuhiro Takahashi, Iwao Kanno, and Shuichi Miura. Cerebral vascular mean transit time in healthy humans: a comparative study with PET and dynamic susceptibility contrast-enhanced MRI. *Journal of Cerebral Blood Flow and Metabolism*, 27(2):404–413, February 2007.

[168] Kojiro Ide, Michael Eliasziw, and Marc J Poulin. Relationship between middle cerebral artery blood velocity and end-tidal PCO_2 in the hypocapnic-hypercapnic range in humans. *Journal of Applied Physiology*, 95(1):129–137, July 2003.

[169] Steve Iscoe and Joseph A Fisher. Hyperoxia-induced hypocapnia: an underappreciated risk. *Chest*, 128(1):430–433, July 2005.

[170] B Issekutz and K Rodahl. Respiratory quotient during exercise. *Journal of Applied Physiology*, 16:606–610, July 1961.

[171] H Ito, I Kanno, M Ibaraki, T Suhara, and S MIURA. Relationship between baseline cerebral blood flow and vascular responses to changes in $PaCO_2$ measured by

positron emission tomography in humans: implication of inter-individual variations of cerebral vascular tone. *Acta Physiologica*, 193(4):325–330, August 2008.

[172] Shoji Ito, Alexandra Mardimae, Jay S Han, James Duffin, Greg Wells, Ludwik Fedorko, Leonid Minkovich, Rita Katznelson, Massimiliano Meineri, Tamara Arenovich, Cathie Kessler, and Joseph A Fisher. Non-invasive prospective targeting of arterial P_{CO_2} in subjects at rest. *The Journal of Physiology*, 586(Pt 15):3675–3682, August 2008.

[173] Yoshiaki Itoh and Norihiro Suzuki. Control of brain capillary blood flow. *Journal of Cerebral Blood Flow and Metabolism*, pages 1–10, February 2012.

[174] J L Jaggi, W D Obrist, T A Gennarelli, and T W Langfitt. Relationship of early cerebral blood flow and metabolism to outcome in acute head injury. *Journal of Neurosurgery*, 72(2):176–182, February 1990.

[175] Hesamoddin Jahanian, Douglas C Noll, and Luis Hernandez-Garcia. B_0 field inhomogeneity considerations in pseudo-continuous arterial spin labeling (pCASL): effects on tagging efficiency and correction strategy. *NMR in Biomedicine*, 24(10):1202–1209, December 2011.

[176] Geon-Ho Jahng, Enmin Song, Xiao-Ping Zhu, Gerald B Matson, Michael W Weiner, and Norbert Schuff. Human brain: reliability and reproducibility of pulsed arterial spin-labeling perfusion MR imaging. *Radiology*, 234(3):909–916, March 2005.

[177] J Järhult and S Mellander. Autoregulation of capillary hydrostatic pressure in skeletal muscle during regional arterial hypo- and hypertension. *Acta Physiologica Scandinavica*, 91(1):32–41, May 1974.

[178] J Järhult, J Lundvall, S Mellander, and S Tibblin. Osmolar control of plasma volume during hemorrhagic hypotension. *Acta Physiologica Scandinavica*, 85 (1):142–144, May 1972.

[179] Kurt A Jellinger. Pathology and pathogenesis of vascular cognitive impairment–a critical update. *Frontiers in Aging Neuroscience*, 5:17, 2013.

[180] Mark Jenkinson, Peter Bannister, Michael Brady, and Stephen Smith. Improved optimization for the robust and accurate linear registration and motion correction of brain images. *NeuroImage*, 17(2):825–841, October 2002.

[181] P C Johnson. Autoregulation of blood flow. *Circulation Research*, 59(5):483–495, August 1986.

[182] IH Johnston and A M Harper. The effect of mannitol on cerebral blood flow. *Journal of Neurosurgery*, 1973.

[183] Andrea Kassner, Jeff D Winter, Julien Poublanc, David J Mikulis, and Adrian P Crawley. Blood-oxygen level dependent MRI measures of cerebrovascular reactivity using a controlled respiratory challenge: reproducibility and gender differences. *Journal of Magnetic Resonance Imaging*, 31(2):298–304, February 2010.

[184] A Kastrup, J Dichgans, M Niemeier, and M Schabet. Changes of Cerebrovascular CO_2 Reactivity During Normal Aging. *Stroke*, 29(7):1311–1314, July 1998.

[185] A Kastrup, T Q Li, A Takahashi, Gary H Glover, and M E Moseley. Functional magnetic resonance imaging of regional cerebral blood oxygenation changes during breath holding. *Stroke*, 29(12):2641–2645, December 1998.

[186] A Kastrup, G Krüger, Gary H Glover, and M E Moseley. Assessment of cerebral oxidative metabolism with breath holding and fMRI. *Magnetic Resonance in Medicine*, 42(3):608–611, September 1999.

[187] A Kastrup, T Q Li, G H Glover, and M E Moseley. Cerebral blood flow-related signal changes during breath-holding. *American Journal of Neuroradiology*, 20 (7):1233–1238, August 1999.

[188] A Kastrup, G Krüger, T Neumann-Haefelin, and M E Moseley. Assessment of cerebrovascular reactivity with functional magnetic resonance imaging: compar-

ison of CO_2 and breath holding. *Magnetic Resonance Imaging*, 19(1):13–20, January 2001.

[189] Matthew J Kempton, Ulrich Ettinger, Russell Foster, Steven C R Williams, Gemma A Calvert, Adam Hampshire, Fernando O Zelaya, Ruth L O'Gorman, Terry McMorris, Adrian M Owen, and Marcus S Smith. Dehydration affects brain structure and function in healthy adolescents. *Human Brain Mapping*, 32 (1):71–79, December 2010.

[190] S S Kety and C F Schmidt. The effects of active and passive hyperventilation on cerebral blood flow, cerebral oxygen consumption, cardiac ouput, and blood pressure of normal young men. *Journal of Clinical Investigation*, 25(1):107–119, January 1946.

[191] S S Kety and C F Schmidt. Measurement of cerebral blood flow and cerebral oxygen consumption in man. *Federation Proceedings*, 5:264, June 1946.

[192] S S Kety and C F Schmidt. The nitours oxide method for the quantitative determination of cerebral blood flow in man: theory, procedure and normal values. *Journal of Clinical Investigation*, 27(4):476–483, July 1948.

[193] S S Kety and C F Schmidt. The effects of altered arterial tensions of carbon dioxide and oxygen on cerebral blood flow and cerebral oxygen consumption of normal young men. *Journal of Clinical Investigation*, 27(4):484–492, July 1948.

[194] S S Kety, B D Polis, C S Nadler, and C F Schmidt. The blood flow and oxygen consumption of the human brain in diabetic acidosis and coma. *Journal of Clinical Investigation*, 27(4):500–510, July 1948.

[195] A Keyeux, D Ochrymowicz-Bemelmans, and A A Charlier. Induced response to hypercapnia in the two-compartment total cerebral blood volume: influence on brain vascular reserve and flow efficiency. *Journal of Cerebral Blood Flow and Metabolism*, 15(6):1121–1131, November 1995.

[196] D G Kiely, R I Cargill, and B J Lipworth. Effects of hypercapnia on hemodynamic, inotropic, lusitropic, and electrophysiologic indices in humans. *Chest*, 109(5):1215–1221, May 1996.

[197] Jung Hwan Kim, Reswanul Khan, Jeffrey K Thompson, and David Ress. Model of the transient neurovascular response based on prompt arterial dilation. *Journal of Cerebral Blood Flow and Metabolism*, 33(9):1429–1439, September 2013.

[198] Seong-Gi Kim and Seiji Ogawa. Biophysical and physiological origins of blood oxygenation level-dependent fMRI signals. *Journal of Cerebral Blood Flow and Metabolism*, 32(7):1188–1206, July 2012.

[199] Tae Kim, J Richard Jennings, and Seong-Gi Kim. Regional cerebral blood flow and arterial blood volume and their reactivity to hypercapnia in hypertensive and normotensive rats. *Journal of Cerebral Blood Flow and Metabolism*, 34(3):408–414, March 2014.

[200] H Kimelberg. Water homeostasis in the brain: Basic concepts. *Neuroscience*, 129 (4):851–860, 2004.

[201] M Kimura, H H Dietrich, V H Huxley, D R Reichner, and R G Dacey. Measurement of hydraulic conductivity in isolated arterioles of rat brain cortex. *The American Journal of Physiology*, 264(6 Pt 2):H1788–97, June 1993.

[202] Robert A Klocke. Carbon Dioxide Transport. *Comprehensive Physiology*, pages 173–197, January 2011.

[203] James M Knapp. Hyperosmolar therapy in the treatment of severe head injury in children: mannitol and hypertonic saline. *AACN Clinical Issues*, 16(2):199–211, 2005.

[204] U Kniesel and H Wolburg. Tight Junctions of the Blood–Brain Barrier. *Cellular and Molecular Neurobiology*, 2000.

[205] G M Knudsen, O B Paulson, and M M Hertz. Kinetic analysis of the human blood-brain barrier transport of lactate and its influence by hypercapnia. *Journal of Cerebral Blood Flow and Metabolism*, 11(4):581–586, July 1991.

[206] Michael S Koehle, Luisa V Giles, Andrew N Curtis, Michael L Walsh, and Matthew D White. Performance of a compact end-tidal forcing system. *Respiratory Physiology & Neurobiology*, 167(2):155–161, June 2009.

[207] H A Kontos, E P Wei, R M Navari, J E Levasseur, W I Rosenblum, and J L Patterson. Responses of cerebral arteries and arterioles to acute hypotension and hypertension. *The American Journal of Physiology*, 234(4):H371–83, April 1978.

[208] R P Kraig, C R Ferreira-Filho, and C Nicholson. Alkaline and acid transients in cerebellar microenvironment. *Journal of Neurophysiology*, 49(3):831–850, March 1983.

[209] Steffen Norbert Krieger, Markus Nikolar Streicher, Robert Trampel, and Robert Turner. Cerebral blood volume changes during brain activation. *Journal of Cerebral Blood Flow and Metabolism*, 32(8):1618–1631, August 2012.

[210] A Krogh. The supply of oxygen to the tissues and the regulation of the capillary circulation. *The Journal of Physiology*, 1919.

[211] A. Krogh. *The Anatomy and Physiology of Capillaries*. Mrs. Hepsa Ely Silliman memorial lectures. Yale University Press, first edition, 1922.

[212] August Krogh. Nobel Lecture: A Contribution to the Physiology of the Capillaries. *Nobelprize.org*, Nobel Media AB 2014, 2014. URL <http://www.nobelprize.org/nobel_prizes/medicine/laureates/1920/krogh-lecture.html>.

[213] W Kuschinsky. Capillary perfusion in the brain. *European Journal of Physiology*, 432(3 Suppl):R42–6, 1996.

[214] W Kuschinsky. Neuronal-vascular coupling. A unifying hypothesis. *Advances in Experimental Medicine and Biology*, 413:167–176, 1997.

[215] C J Lambertsen, S J Semple, M G Smyth, and R Gelfand. H^+ and pCO_2 as chemical factors in respiratory and cerebral circulatory control. *Journal of Applied Physiology*, 16:473–484, May 1961.

[216] F Lang, G L Busch, M Ritter, H Völkl, S Waldegger, E Gulbins, and D Häussinger. Functional significance of cell volume regulatory mechanisms. *Physiological Reviews*, 78(1):247–306, January 1998.

[217] Fin Stolze Larsen. Cerebral blood flow in hyperammonemia: heterogeneity and starling forces in capillaries. *Metabolic Brain Disease*, 17(4):229–235, December 2002.

[218] N A Lassen. Cerebral blood flow and oxygen consumption in man. *Physiological Reviews*, 39(2):183–238, April 1959.

[219] Steven Laureys, Adrian M Owen, and Nicholas D Schiff. Brain function in coma, vegetative state, and related disorders. *The Lancet Neurology*, 3(9):537–546, September 2004.

[220] Steven Laureys, Frédéric Pellas, Philippe Van Eeckhout, Sofiane Ghorbel, Caroline Schnakers, Fabien Perrin, Jacques Berré, Marie-Elisabeth Faymonville, Karl-Heinz Pantke, Francois Damas, Maurice Lamy, Gustave Moonen, and Serge Goldman. The locked-in syndrome : what is it like to be conscious but paralyzed and voiceless? *Progress in Brain Research*, 150:495–511, 2005.

[221] K H Lee, C S Kim, K C Lee, S C Kim, and H J Lee. Arterio-jugular oxygen difference in severe intracranial lesions. *Yonsei Medical Journal*, 17(1):15–20, 1976.

[222] Christoph Leithner and Georg Royl. The oxygen paradox of neurovascular coupling. *Journal of Cerebral Blood Flow and Metabolism*, 34(1):19–29, January 2014.

[223] W G Lennox and E L Gibbs. The blood flow in the brain and the leg of man, and the changes induced by alteratoin of blood gases. *The Journal of clinical investigation*, 11(6):1155–1177, November 1932.

[224] Renata F Leoni, Fernando F Paiva, Erica C Henning, George C Nascimento, Alberto Tannús, Draulio B de Araujo, and Afonso C Silva. Magnetic resonance imaging quantification of regional cerebral blood flow and cerebrovascular reactivity to carbon dioxide in normotensive and hypertensive rats. *NeuroImage*, 58 (1):75–81, September 2011.

[225] Oleg Leontiev and Richard B Buxton. Reproducibility of BOLD, perfusion, and $CMRO_2$ measurements with calibrated-BOLD fMRI. *NeuroImage*, 35(1):175–184, March 2007.

[226] J R Levick and C C Michel. Microvascular fluid exchange and the revised Starling principle. *Cardiovascular Research*, 87(2):198–210, June 2010.

[227] Guanglei Li, Wei Yuan, and Bingmei M Fu. A model for the blood-brain barrier permeability to water and small solutes. *Journal of Biomechanics*, 43(11):2133–2140, August 2010.

[228] T Q Li, A Kastrup, A M Takahashi, and M E Moseley. Functional MRI of human brain during breath holding by BOLD and FAIR techniques. *NeuroImage*, 9(2): 243–249, February 1999.

[229] Xiaoyun Liang, Alan Connelly, and Fernando Calamante. Improved partial volume correction for single inversion time arterial spin labeling data. *Magnetic Resonance in Medicine*, 69(2):531–537, 2012.

[230] U Lindauer, D Megow, H Matsuda, and U Dirnagl. Nitric oxide: a modulator, but not a mediator, of neurovascular coupling in rat somatosensory cortex. *The American Journal of Physiology*, 277(2 Pt 2):H799–811, August 1999.

[231] U Lindauer, A Kunz, S Schuh-Hofer, J Vogt, J P Dreier, and U Dirnagl. Nitric oxide from perivascular nerves modulates cerebral arterial pH reactivity. *American Journal of Physiology–Heart and Circulatory Physiology*, 281(3):H1353–63, September 2001.

[232] Liis Lindvere, Rafal Janik, Adrienne Dorr, David Chartash, Bhupinder Sahota, John G Sled, and Bojana Stefanovic. Cerebral microvascular network geometry changes in response to functional stimulation. *NeuroImage*, 71:248–259, May 2013.

[233] E Lipsmeyer and G L Ackerman. Irreversible brain damage after water intoxication. *The Journal of the American Medical Association*, 196(3):286–288, April 1966.

[234] J A Loeppky, U C Luft, and E R Fletcher. Quantitative description of whole blood CO_2 dissociation curve and Haldane effect. *Respiration Physiology*, 51(2): 167–181, February 1983.

[235] Nikos K Logothetis. What we can do and what we cannot do with fMRI. *Nature*, 453(7197):869–878, June 2008.

[236] S Lorthois and F Lauwers. Control of brain blood flow by capillaries: a simulation study in an anatomically accurate large human vascular network. *Computer Methods in Biomechanics and Biomedical Engineering*, 15(sup1):66–68, September 2012.

[237] Sylvie Lorthois and Francis Cassot. Fractal analysis of vascular networks Insights from morphogenesis. *Journal of Theoretical Biology*, 262(4):614–633, February 2010.

[238] Hanzhang Lu, Xavier Golay, James J Pekar, and Peter C M van Zijl. Functional magnetic resonance imaging based on changes in vascular space occupancy. *Magnetic Resonance in Medicine*, 50(2):263–274, August 2003.

[239] Hanzhang Lu, Meng Law, Glyn Johnson, Yulin Ge, Peter C M van Zijl, and Joseph A Helpern. Novel approach to the measurement of absolute cerebral blood volume using vascular-space-occupancy magnetic resonance imaging. *Magnetic Resonance in Medicine*, 54(6):1403–1411, December 2005.

[240] S J E Lucas, Y C Tzeng, S D Galvin, K N Thomas, S Ogoh, and P N Ainslie. Influence of Changes in Blood Pressure on Cerebral Perfusion and Oxygenation. *Hypertension*, 55(3):698–705, February 2010.

[241] W M Luh, E C Wong, Peter Bandettini, and J S Hyde. QUIPSS II with thin-slice TI1 periodic saturation: a method for improving accuracy of quantitative perfusion imaging using pulsed arterial spin labeling. *Magnetic Resonance in Medicine*, 41(6):1246–1254, June 1999.

[242] Andrew Lumb. *Nunn's applied respiratory physiology*. Butterworth Heinemann, fifth edition, 2000. ISBN 0 75063107 4.

[243] J Lundvall and J Holmberg. Role of tissue hyperosmolality in functional vasodilatation in the submandibular gland. *Acta Physiologica Scandinavica*, 92(2): 165–174, October 1974.

[244] J Lundvall, S Mellander, and T White. Hyperosmolality and vasodilatation in human skeletal muscle. *Acta Physiologica Scandinavica*, 77(1):224–233, August 1969.

[245] D J Lythgoe, S C Williams, M Cullinane, and H S Markus. Mapping of cerebrovascular reactivity using BOLD magnetic resonance imaging. *Magnetic Resonance Imaging*, 17(4):495–502, May 1999.

[246] L Maccotta, John A Detre, and David C Alsop. The efficiency of adiabatic inversion for perfusion imaging by arterial spin labeling. *NMR in Biomedicine*, 10 (4-5):216–221, 1997.

[247] Paul M Macey, Mary A Woo, and Ronald M Harper. Hyperoxic brain effects are normalized by addition of CO_2. *PLoS medicine*, 4(5):e173, May 2007.

[248] B J MacIntosh, A C Lindsay, I Kylintireas, W Kuker, M Günther, M D Robson, J Kennedy, R P Choudhury, and P Jezzard. Multiple inflow pulsed arterial spin-labeling reveals delays in the arterial arrival time in minor stroke and transient ischemic attack. *American Journal of Neuroradiology*, 31(10):1892–1894, November 2010.

[249] Bradley J MacIntosh, Nicola Filippini, Michael A Chappell, Mark W Woolrich, Clare E Mackay, and Peter Jezzard. Assessment of arterial arrival times derived from multiple inversion time pulsed arterial spin labeling MRI. *Magnetic Resonance in Medicine*, 63(3):641–647, March 2010.

[250] P L Madsen, J F Schmidt, S Holm, H Jørgensen, G Wildschiødtz, N J Christensen, L Friberg, S Vorstrup, and N A Lassen. Mental stress and cognitive performance do not increase overall level of cerebral O_2 uptake in humans. *Journal of Applied Physiology*, 73(2):420–426, August 1992.

[251] V A Magnotta, H Y Heo, B J Dlouhy, N S Dahdaleh, R L Follmer, D R Thedens, M J Welsh, and J A Wemmie. Detecting activity-evoked pH changes in human brain. *Proceedings of the National Academy of Sciences*, 109(21):8270–8273, May 2012.

[252] Cesare Magri, Nikos K Logothetis, and Stefano Panzeri. Investigating static nonlinearities in neurovascular coupling. *Magnetic Resonance Imaging*, pages 1–7, May 2011.

[253] Daniel M Mandell, Jay S Han, Julien Poublanc, Adrian P Crawley, Jeff A Stainsby, Joseph A Fisher, and David J Mikulis. Mapping cerebrovascular reactivity using blood oxygen level-dependent MRI in Patients with arterial steno-occlusive disease: comparison with arterial spin labeling MRI. *Stroke*, 39(7): 2021–2028, July 2008.

[254] J B Mandeville, J J Marota, C Ayata, G Zaharchuk, M A Moskowitz, B R Rosen, and R M Weisskoff. Evidence of a cerebrovascular postarteriole windkessel with

delayed compliance. *Journal of Cerebral Blood Flow and Metabolism*, 19(6): 679–689, June 1999.

[255] T H Maren. Carbonic anhydrase: chemistry, physiology, and inhibition. *Physiological Reviews*, 47(4):595–781, October 1967.

[256] CI Mark, M Slessarev, S Ito, J Han, JA Fisher, and GB Pike. Precise control of end-tidal carbon dioxide and oxygen improves BOLD and ASL cerebrovascular reactivity measures. *Magnetic Resonance in Medicine*, 64(3):749–756, 2010.

[257] Clarisse I Mark, Joseph A Fisher, and G Bruce Pike. Improved fMRI calibration: Precisely controlled hyperoxic versus hypercapnic stimuli. *NeuroImage*, pages 1–10, September 2010.

[258] T M Markwalder, P Grolimund, R W Seiler, F Roth, and R Aaslid. Dependency of blood flow velocity in the middle cerebral artery on end-tidal carbon dioxide partial pressure–a transcranial ultrasound Doppler study. *Journal of Cerebral Blood Flow and Metabolism*, 4(3):368–372, September 1984.

[259] Olga Marshall, Hanzhang Lu, Jean-Christophe Brisset, Feng Xu, Peiying Liu, Joseph Herbert, Robert I Grossman, and Yulin Ge. Impaired Cerebrovascular Reactivity in Multiple Sclerosis. *JAMA Neurology*, August 2014.

[260] Petros Martirosian, Andreas Boss, Christina Schraml, Nina F Schwenzer, Hansjörg Graf, Claus D Claussen, and Fritz Schick. Magnetic resonance perfusion imaging without contrast media. *European Journal of Nuclear Medicine and Molecular Imaging*, 37 Suppl 1:S52–64, August 2010.

[261] G I Mchedlishvili, N P Mitagvaria, and L G Ormotsadze. Vascular mechanisms controlling a constant blood supply to the brain ("autoregulation"). *Stroke; a journal of cerebral circulation*, 4(5):742–750, September 1973.

[262] S Mellander. On the control of capillary fluid transfer by precapillary and postcapillary vascular adjustments. A brief review with special emphasis on myogenic mechanisms. *Microvascular Research*, 15(3):319–330, May 1978.

[263] Stefan Mellander and Bôrje Johansson. Control of resistance, exchange, and capacitance functions in the peripheral circulation. *Pharmacological Reviews*, 20 (3):117–194, July 1968.

[264] G Meschia and D H Barron. The effect of CO_2 and O_2 content of the blood on the freezing point of the plasma. *Quarterly Journal of Experimental Physiology and Cognate Medical Sciences*, 41(2):180–194, April 1956.

[265] Toralf Mildner, Harald E Möller, Wolfgang Driesel, David G Norris, and Robert Trampel. Continuous arterial spin labeling at the human common carotid artery: the influence of transit times. *NMR in Biomedicine*, 18(1):19–23, February 2005.

[266] T Minami, M Ogawa, T Sugimoto, and K Katsurada. Hyperoxia of internal jugular venous blood in brain death. *Journal of Neurosurgery*, 39(4):442–447, October 1973.

[267] M Miyazaki. Measurement of cerebral blood flow by ultrasonic Doppler technique. Effects of low temperature, induced hypertension and arrhythmia on cerebral circulation. *Japanese Circulation Journal*, 30(7):863–867, July 1966.

[268] Sima Mraovitch and Richard Sercombe. *Neurophysiological Basis of Cerebral Blood Flow Control: An Introduction*. John Libbey, first edition, 1996. ISBN 0 86196272 9.

[269] Kevin Murphy, Ashley D Harris, and Richard G Wise. Robustly measuring vascular reactivity differences with breath-hold: normalising stimulus-evoked and resting state BOLD fMRI data. *NeuroImage*, 54(1):369–379, January 2011.

[270] W Alan C Mutch, Daniel M Mandell, Joseph A Fisher, David J Mikulis, Adrian P Crawley, Olivia Pucci, and James Duffin. Approaches to brain stress testing: BOLD magnetic resonance imaging with computer-controlled delivery of carbon dioxide. *PLoS ONE*, 7(11):e47443, 2012.

[271] B Nico, A Frigeri, G P Nicchia, F Quondamatteo, R Herken, M Errede, D Ribatti, M Svelto, and L Roncali. Role of aquaporin-4 water channel in the development

and integrity of the blood-brain barrier. *Journal of Cell Science*, 114(Pt 7):1297–1307, April 2001.

[272] B Nilsson and B K Siesjö. A method for determining blood flow and oxygen consumption in the rat brain. *Acta Physiologica Scandinavica*, 96(1):72–82, January 1976.

[273] K Niwa, C Haensel, M E Ross, and C Iadecola. Cyclooxygenase-1 participates in selected vasodilator responses of the cerebral circulation. *Circulation Research*, 88(6):600–608, March 2001.

[274] Ulrike Nöth, Guy E Meadows, Futoshi Kotajima, Ralf Deichmann, Douglas R Corfield, and Robert Turner. Cerebral vascular response to hypercapnia: determination with perfusion MRI at 1.5 and 3.0 Tesla using a pulsed arterial spin labeling technique. *Journal of Magnetic Resonance Imaging*, 24(6):1229–1235, December 2006.

[275] Ulrike Nöth, Futoshi Kotajima, Ralf Deichmann, Robert Turner, and Douglas R Corfield. Mapping of the cerebral vascular response to hypoxia and hypercapnia using quantitative perfusion MRI at 3 T. *NMR in Biomedicine*, 21(5):464–472, June 2008.

[276] S Ogawa, T M Lee, A R Kay, and D W Tank. Brain magnetic resonance imaging with contrast dependent on blood oxygenation. *Proceedings of the National Academy of Sciences*, 87(24):9868–9872, December 1990.

[277] Ruth L O'Gorman, Paul E Summers, Fernando O Zelaya, Steven C R Williams, David C Alsop, and David J Lythgoe. In vivo estimation of the flow-driven adiabatic inversion efficiency for continuous arterial spin labeling: a method using phase contrast magnetic resonance angiography. *Magnetic Resonance in Medicine*, 55(6):1291–1297, June 2006.

[278] J Olesen, O B Paulson, and N A Lassen. Regional cerebral blood flow in man

determined by the initial slope of the clearance of intra-arterially injected ^{133}Xe. *Stroke*, 2(6):519–540, November 1971.

[279] Suzanne Oparil, M Amin Zaman, and David A Calhoun. Pathogenesis of hypertension. *Annals of Internal Medicine*, 139(9):761–776, November 2003.

[280] Scott D Packard, Joseph B Mandeville, Tomotsugu Ichikawa, Keiro Ikeda, Kinya Terada, Stephanie Niloff, E Antonio Chiocca, Bruce R Rosen, and John J A Marota. Functional response of tumor vasculature to $PaCO_2$: determination of total and microvascular blood volume by MRI. *Neoplasia*, 5(4):330–338, July 2003.

[281] Kathleen A Page, Owen Chan, Jagriti Arora, Renata Belfort-Deaguiar, James Dzuira, Brian Roehmholdt, Gary W Cline, Sarita Naik, Rajita Sinha, R Todd Constable, and Robert S Sherwin. Effects of fructose vs glucose on regional cerebral blood flow in brain regions involved with appetite and reward pathways. *The Journal of the American Medical Association*, 309(1):63–70, January 2013.

[282] David Paling, Esben Thade Petersen, Daniel J Tozer, Daniel R Altmann, Claudia AM Wheeler-Kingshott, Raju Kapoor, David H Miller, and Xavier Golay. Cerebral arterial bolus arrival time is prolonged in multiple sclerosis and associated with disability. *Journal of Cerebral Blood Flow and Metabolism*, 34:34–42, September 2014.

[283] W M Pardridge, J D Connor, and I L Crawford. Permeability changes in the blood-brain barrier: causes and consequences. *Critical Reviews in Toxicology*, 3 (2):159–199, 1975.

[284] Laura M Parkes and Paul S Tofts. Improved accuracy of human cerebral blood perfusion measurements using arterial spin labeling: accounting for capillary water permeability. *Magnetic Resonance in Medicine*, 48(1):27–41, July 2002.

[285] Laura M Parkes, Waqar Rashid, Declan T Chard, and Paul S Tofts. Normal cerebral perfusion measurements using arterial spin labeling: reproducibility, stabil-

ity, and age and gender effects. *Magnetic Resonance in Medicine*, 51(4):736–743, April 2004.

[286] H Pasantes-Morales. Volume Regulation in Brai Cells: Cellular and Molecular Mechanisms. *Metabolic Brain Disease*, 1996.

[287] O B Paulson. Blood-brain barrier, brain metabolism and cerebral blood flow. *European Neuropsychopharmacology*, 12(6):495–501, December 2002.

[288] O B Paulson, M M Hertz, T G Bolwig, and N A Lassen. Filtration and diffusion of water across the blood-brain barrier in man. *Microvascular Research*, 13(1): 113–124, 1977.

[289] O B Paulson, S Strandgaard, and L Edvinsson. Cerebral autoregulation. *Cerebrovascular and Brain Metabolism Reviews*, 2(2):161–192, 1990.

[290] Olaf B Paulson, Iwao Kanno, Martin Reivich, and Louis Sokoloff. History of international society for cerebral blood flow and metabolism. *Journal of Cerebral Blood Flow and Metabolism*, 32(7):1099–1106, July 2012.

[291] W Penfield. Remarks on incomplete hypotheses for the control of cerebral circulation. *Journal of neurosurgery*, 35(2):124, 1971.

[292] Claire M Peppiatt, Clare Howarth, Peter Mobbs, and David Attwell. Bidirectional control of CNS capillary diameter by pericytes. *Nature*, 443(7112):700–704, October 2006.

[293] Joanna E Perthen, Amy E Lansing, Joy Liau, Thomas T Liu, and Richard B Buxton. Caffeine-induced uncoupling of cerebral blood flow and oxygen metabolism: a calibrated BOLD fMRI study. *NeuroImage*, 40(1):237–247, March 2008.

[294] E T Petersen, I Zimine, Y-C L Ho, and Xavier Golay. Non-invasive measurement of perfusion: a critical review of arterial spin labelling techniques. *The British Journal of Radiology*, 79(944):688–701, April 2006.

[295] S K Piechnik, P A Chiarelli, and P Jezzard. Modelling vascular reactivity to investigate the basis of the relationship between cerebral blood volume and flow under CO_2 manipulation. *NeuroImage*, 2008.

[296] David T Pilkinton, Teruyuki Hiraki, John A Detre, Joel H Greenberg, and Ravinder Reddy. Absolute cerebral blood flow quantification with pulsed arterial spin labeling during hyperoxia corrected with the simultaneous measurement of the longitudinal relaxation time of arterial blood. *Magnetic Resonance in Medicine*, 67(6):1556–1565, June 2012.

[297] J J Pillai and D J Mikulis. Cerebrovascular Reactivity Mapping: An Evolving Standard for Clinical Functional Imaging. *American Journal of Neuroradiology*, April 2014.

[298] Rolf Pohmann, Juliane Budde, Edward J Auerbach, Gregor Adriany, and Kâmil Uğurbil. Theoretical and experimental evaluation of continuous arterial spin labeling techniques. *Magnetic Resonance in Medicine*, 63(2):438–446, February 2010.

[299] Jonathan R Polimeni, Bruce Fischl, Douglas N Greve, and Lawrence L Wald. Laminar analysis of 7T BOLD using an imposed spatial activation pattern in human V1. *NeuroImage*, 52(4):1334–1346, October 2010.

[300] J Ponte and M J Purves. The role of the carotid body chemoreceptors and carotid sinus baroreceptors in the control of cerebral blood vessels. *The Journal of Physiology*, 237(2):315–340, March 1974.

[301] U Ponten and B K Siesjö. Gradients of CO_2 tension in the brain. *Acta physiologica Scandinavica*, 67(2):129–140, June 1966.

[302] M J Poulin, D A Cunningham, D H Paterson, J M Kowalchuk, and W D Smith. Ventilatory sensitivity to CO_2 in hyperoxia and hypoxia in older aged humans. *Journal of Applied Physiology*, 75(5):2209–2216, November 1993.

[303] M J Poulin, P J Liang, and P A Robbins. Dynamics of the cerebral blood flow response to step changes in end-tidal PCO_2 and PO_2 in humans. *Journal of Applied Physiology*, 81(3):1084–1095, September 1996.

[304] M J Poulin, D A Cunningham, and D H Paterson. Dynamics of the ventilatory response to step changes in end-tidal PCO_2 in older humans. *Canadian Journal of Applied Physiology*, 22(4):368–383, August 1997.

[305] M J Poulin, P J Liang, and P A Robbins. Fast and slow components of cerebral blood flow response to step decreases in end-tidal PCO_2 in humans. *Journal of Applied Physiology*, 85(2):388–397, August 1998.

[306] Eitan Prisman, Marat Slessarev, Jay Han, Julien Poublanc, Alexandra Mardimae, Adrian Crawley, Joseph Fisher, and David Mikulis. Comparison of the effects of independently-controlled end-tidal PCO_2 and PO_2 on blood oxygen level-dependent (BOLD) MRI. *Journal of Magnetic Resonance Imaging*, 27(1): 185–191, January 2008.

[307] M E Raichle and H L Stone. Cerebral blood flow autoregulation and graded hypercapnia. *European Neurology*, 6(1):1–5, 1971.

[308] C A Raji, C Lee, O L Lopez, J Tsay, J F Boardman, E D Schwartz, W S Bartynski, H M Hefzy, H M Gach, W Dai, and J T Becker. Initial experience in using continuous arterial spin-labeled MR imaging for early detection of Alzheimer disease. *American Journal of Neuroradiology*, 31(5):847–855, May 2010.

[309] S I Rapoport. A mathematical model for vasogenic brain edema. *Journal of Theoretical Biology*, 74(3):439–467, October 1978.

[310] S I Rapoport. Osmotic opening of the blood-brain barrier. *Annals of Neurology*, 24(5):677–684, November 1988.

[311] S I Rapoport. Osmotic opening of the blood-brain barrier: principles, mechanism, and therapeutic applications. *Cellular and Molecular Neurobiology*, 20(2):217–230, April 2000.

[312] P Ravussin, DP Archer, JL Tyler, and E Meyer. Effects of rapid mannitol infusion on cerebral blood volume. *Journal of Neurosurgery*, 64:104–113, 1986.

[313] M Reivich. Regulation of the cerebral circulation. *Clinical Neurosurgery*, 16: 378–418, 1969.

[314] Martin Reivich. Arterial PCO_2 and cerebral hemodynamics. *The American Journal of Physiology*, 206:25–35, 1964.

[315] P A Robbins, G D Swanson, and M G Howson. A prediction-correction scheme for forcing alveolar gases along certain time courses. *Journal of Applied Physiology*, 52(5):1353–1357, May 1982.

[316] Jack D Rosenbaum. The influence of alterations in acid-base balance upon transfers of carbon dioxide and bicarbonate in man. *Journal of Clinical Investigation*, 21(6):735, 1942.

[317] Bernhard Rosengarten, Holger Lutz, and Manfred Kaps. The neurovascular coupling bears properties of a feedforward and feedback regulative mechanism. *Ultrasound in Medicine & Biology*, 34(1):1–6, January 2008.

[318] E Rostrup, H B Larsson, P B Toft, K Garde, C Thomsen, P Ring, L Søndergaard, and O Henriksen. Functional MRI of CO_2 induced increase in cerebral perfusion. *NMR in Biomedicine*, 7(1-2):29–34, March 1994.

[319] E Rostrup, H B Larsson, P B Toft, K Garde, P B Ring, and O Henriksen. Susceptibility contrast imaging of CO_2-induced changes in the blood volume of the human brain. *Acta Radiologica*, 37(5):813–822, September 1996.

[320] E Rostrup, I Law, M Blinkenberg, H B Larsson, A P Born, S Holm, and O B Paulson. Regional differences in the CBF and BOLD responses to hypercapnia: a combined PET and fMRI study. *NeuroImage*, 11(2):87–97, February 2000.

[321] Egill Rostrup, Gitte M Knudsen, Ian Law, Søren Holm, Henrik B W Larsson, and Olaf B Paulson. The relationship between cerebral blood flow and volume in humans. *NeuroImage*, 24(1):1–11, 2005.

[322] F J Roughton. Recent work on carbon dioxide transport by the blood. *Physiological Reviews*, 15(2):241–296, 1935.

[323] C S Roy and J.G. Brown. The blood-pressure and its variations in the arterioles, capillaries and smaller veins. *The Journal of Physiology*, 2(5-6):323–446, 1880.

[324] C S Roy and C S Sherrington. On the Regulation of the Blood-supply of the Brain. *The Journal of Physiology*, 11(1-2):85–158.17, 1890.

[325] Behnam Sabayan, Steffy Jansen, Anna M Oleksik, Matthias J P van Osch, Mark A van Buchem, Peter van Vliet, Anton J M de Craen, and Rudi G J Westendorp. Cerebrovascular hemodynamics in Alzheimer's disease and vascular dementia: A meta-analysis of transcranial Doppler studies. *Ageing Research Reviews*, 11(2): 271–277, April 2012.

[326] I H Sarelius, K D Cohen, and C L Murrant. Role for capillaries in coupling blood flow with metabolism. *Clinical and Experimental Pharmacology and Physiology*, 27(10):826–829, 2000.

[327] M L Saunders, J D Miller, D Stablein, and G Allen. The effects of graded experimental trauma on cerebral blood flow and responsiveness to CO_2. *Journal of Neurosurgery*, 51(1):18–26, July 1979.

[328] Raffaele Scala. Hypercapnic encephalopathy syndrome: A new frontier for non-invasive ventilation? *Respiratory Medicine*, 105(8):1109–1117, August 2011.

[329] R M Schell and D J Cole. Cerebral monitoring: jugular venous oximetry. *Anesthesia and Analgesia*, 90(3):559–566, March 2000.

[330] Timothy W Secomb, Daniel A Beard, Jefferson C Frisbee, Nicolas P Smith, and Axel R Pries. The Role of Theoretical Modeling in Microcirculation Research. *Microcirculation*, 15(8):693–698, January 2008.

[331] W Shapiro, A J Wasserman, and J L Patterson. Human Cerebrovascular Response Time to Elevation of Arterial Carbon Dioxide Tension. *Archives of Neurology*, 13 (2):130–138, August 1965.

[332] W Shapiro, A J Wasserman, and J L Patterson. Mechanism and pattern of human cerebrovascular regulation after rapid changes in blood CO_2 tension. *The Journal of Clinical Investigation*, 45(6):913–922, June 1966.

[333] W Shapiro, A J Wasserman, and J L Patterson. Human cerebrovascular response to combined hypoxia and hypercapnia. *Circulation Research*, 19(5):903–910, November 1966.

[334] W Shapiro, A J Wasserman, J P Baker, and J L Patterson. Cerebrovascular response to acute hypocapnic and eucapnic hypoxia in normal man. *The Journal of Clinical Investigation*, 49(12):2362–2368, December 1970.

[335] Louis A Shaw and Anne C Messer. The carbon dioxide capacity of the body and the rate at which the body comes into equilibrium with changes in the alveolar carbon dioxide tension. *The American Journal of Physiology*, 93(2):422–432, 1930.

[336] Jeroen C W Siero, Nolan S Hartkamp, Manus J Donahue, Anita A Harteveld, Annette Compter, Esben T Petersen, and Jeroen Hendrikse. Neuronal activation induced BOLD and CBF responses upon acetazolamide administration in patients with steno-occlusive artery disease. *NeuroImage*, pages 1–10, September 2014.

[337] B K Siesjö. The solubility of carbon dioxide in cerebral cortical tissue of cats: with a note on the solubility of carbon dioxide in water, 0.16 M NaCI and cerebrospinal fluid. *Acta Physiologica Scandinavica*, 55:325–341, August 1962.

[338] B K Siesjö. The bicarbonate/carbonic acid buffer system of the cerebral cortex of cats, as studied in tissue homogenates. 1. The amount of carbon dioxide bound at different carbon dioxide tensions. With a critique of the application of chloride space measurements to the study of the acid-base metabolism of the brain. *Acta Neurologica Scandinavica*, 38:98–120, 1962.

[339] A C Silva, W Zhang, D S Williams, and A P Koretsky. Estimation of water extraction fractions in rat brain using magnetic resonance measurement of perfusion with arterial spin labeling. *Magnetic Resonance in Medicine*, 37(1):58–68, 1997.

[340] Mauro Silvestrini, Patrizio Pasqualetti, Roberto Baruffaldi, Marco Bartolini, Yasmin Handouk, Maria Matteis, Filomena Moffa, Leandro Provinciali, and Fabrizio Vernieri. Cerebrovascular Reactivity and Cognitive Decline in Patients With Alzheimer Disease. *Stroke*, 37(4):1010–1015, March 2006.

[341] Marat Slessarev, Jay S Han, Alexandra Mardimae, Eitan Prisman, David Preiss, George Volgyesi, Cliff Ansel, James Duffin, and Joseph A Fisher. Prospective targeting and control of end-tidal CO_2 and O_2 concentrations. *The Journal of Physiology*, 581(Pt 3):1207–1219, June 2007.

[342] Heather M Snyder, Roderick A Corriveau, Suzanne Craft, James E Faber, Steven M Greenberg, David Knopman, Bruce T Lamb, Thomas J Montine, Maiken Nedergaard, Chris B Schaffer, Julie A Schneider, Cheryl Wellington, Donna M Wilcock, Gregory J Zipfel, Berislav Zlokovic, Lisa J Bain, Francesca Bosetti, Zorina S Galis, Walter Koroshetz, and Maria C Carrillo. Vascular contributions to cognitive impairment and dementia including Alzheimer's disease. *Alzheimer's & dementia*, December 2014.

[343] Olivia Sobczyk, Anne Battisti-Charbonney, Julien Poublanc, Adrian P Crawley, Kevin Sam, Jorn Fierstra, Daniel M Mandell, David J Mikulis, James Duffin, and Joseph A Fisher. Assessing cerebrovascular reactivity abnormality by comparison to a reference atlas. *Journal of Cerebral Blood Flow and Metabolism*, pages 1–8, November 2014.

[344] George G. Somjen. *Ions in the Brain : Normal Function, Seizures, and Stroke: Normal Function, Seizures, and Stroke*. Oxford University Press, USA, first edition, 2004. ISBN 0-19-515171-2.

[345] L Z Sommer, S Iscoe, A Robicsek, J Kruger, J Silverman, J Rucker, J Dickstein, G A Volgyesi, and J A Fisher. A simple breathing circuit minimizing changes in alveolar ventilation during hyperpnoea. *The European Respiratory Journal*, 12 (3):698–701, September 1998.

[346] R B Somogyi, A E Vesely, D Preiss, E Prisman, G Volgyesi, T Azami, S Iscoe, J A Fisher, and H Sasano. Precise control of end-tidal carbon dioxide levels using sequential rebreathing circuits. *Anaesthesia and Intensive Care*, 33(6):726–732, December 2005.

[347] I Sousa, P Vilela, and P Figueiredo. Reproducibility of hypocapnic cerebrovascular reactivity measurements using BOLD fMRI in combination with a paced deep breathing task. *NeuroImage*, pages 1–11, April 2014.

[348] Vincent R Spano, Daniel M Mandell, Julien Poublanc, Kevin Sam, Anne Battisti-Charbonney, Olivia Pucci, Jay S Han, Adrian P Crawley, Joseph A Fisher, and David J Mikulis. CO_2 Blood Oxygen Level-dependent MR Mapping of Cerebrovascular Reserve in a Clinical Population: Safety, Tolerability, and Technical Feasibility. *Radiology*, 266(2):592–598, February 2013.

[349] Aart Spilt, Frieke M A Box, Rob J van der Geest, Johan H C Reiber, Patrik Kunz, Adriaan M Kamper, Gerard J Blauw, and Mark A van Buchem. Reproducibility of total cerebral blood flow measurements using phase contrast magnetic resonance imaging. *Journal of Magnetic Resonance Imaging*, 16(1):1–5, July 2002.

[350] W N Stainsby. Local control of regional blood flow. *Annual review of physiology*, 35(1):151–168, 1973.

[351] W N Stainsby and P D Eitzman. Roles of CO_2, O_2, and acid in arteriovenous

[H^+] difference during muscle contractions. *Journal of Applied Physiology*, 65 (4):1803–1810, October 1988.

[352] Wendell N Stainsby and Eugene M Renkin. Autoregulation of blood flow in peripheral vascular beds. *The American Journal of Cardiology*, 8(5):741–747, November 1961.

[353] Bojana Stefanovic, Jan M Warnking, Karin M Rylander, and G Bruce Pike. The effect of global cerebral vasodilation on focal activation hemodynamics. *NeuroImage*, 30(3):726–734, April 2006.

[354] Bojana Stefanovic, Elizabeth Hutchinson, Victoria Yakovleva, Vincent Schram, James T Russell, Leonardo Belluscio, Alan P Koretsky, and Afonso C Silva. Functional reactivity of cerebral capillaries. *Journal of Cerebral Blood Flow and Metabolism*, 28(5):961–972, May 2008.

[355] Richard H Sterns and Stephen M Silver. Brain Volume Regulation in Response to Hypo-osmolality and Its Correction. *The American Journal of Medicine*, 119(7): S12–S16, July 2006.

[356] S Strandgaard, J Olesen, E Skinhøj, and N A Lassen. Autoregulation of brain circulation in severe arterial hypertension. *British Medical Journal*, 1(5852):507–510, March 1973.

[357] K Strange. Regulation of solute and water balance and cell volume in the central nervous system. *Journal of the American Society of Nephrology*, 3(1):12–27, July 1992.

[358] Daniel-Paolo Streitbürger, Harald E Möller, Marc Tittgemeyer, Margret Hund-Georgiadis, Matthias L Schroeter, and Karsten Mueller. Investigating Structural Brain Changes of Dehydration Using Voxel-Based Morphometry. *PLoS ONE*, 7 (8):e44195, August 2012.

[359] J Strohm, J Duffin, and J A Fisher. Circadian cerebrovascular reactivity to CO_2. *Respiratory physiology & neurobiology*, 197:15–18, June 2014.

[360] X G Sun, J E Hansen, W W Stringer, H Ting, and K Wasserman. Carbon dioxide pressure-concentration relationship in arterial and mixed venous blood during exercise. *Journal of Applied Physiology*, 90(5):1798–1810, May 2001.

[361] S Lalith Talagala, Frank Q Ye, Patrick J Ledden, and Scott Chesnick. Whole-brain 3D perfusion MRI at 3.0 T using CASL with a separate labeling coil. *Magnetic Resonance in Medicine*, 52(1):131–140, July 2004.

[362] Yoji Tanaka, Tsukasa Nagaoka, Govind Nair, Kikuo Ohno, and Timothy Q Duong. Arterial spin labeling and dynamic susceptibility contrast CBF MRI in postischemic hyperperfusion, hypercapnia, and after mannitol injection. *Journal of Cerebral Blood Flow and Metabolism*, 31(6):1403–1411, June 2011.

[363] Felipe B Tancredi and Richard D Hoge. Comparison of cerebral vascular reactivity measures obtained using breath-holding and CO_2 inhalation. *Journal of Cerebral Blood Flow and Metabolism*, 33(7):1066–1074, July 2013.

[364] Felipe B Tancredi, Claudine J Gauthier, Cécile Madjar, Divya S Bolar, Joseph A Fisher, Danny J J Wang, and Richard D Hoge. Comparison of pulsed and pseudocontinuous arterial spin-labeling for measuring CO_2-induced cerebrovascular reactivity. *Journal of Magnetic Resonance Imaging*, April 2012.

[365] Felipe B Tancredi, Isabelle Lajoie, and Richard D Hoge. A simple breathing circuit allowing precise control of inspiratory gases for experimental respiratory manipulations. *BMC Research Notes*, 7(1):235–243, April 2014.

[366] Wouter M Teeuwisse, Andrew G Webb, and Matthias J P van Osch. Arterial spin labeling at ultra-high field: All that glitters is not gold. *International Journal of Imaging Systems and Technology*, 20(1):62–70, February 2010.

[367] Binu P Thomas, Peiying Liu, Denise C Park, Matthias JP van Osch, and Hanzhang Lu. Cerebrovascular reactivity in the brain white matter: magnitude, temporal characteristics, and age effects. *Journal of Cerebral Blood Flow and Metabolism*, 34(2):242–247, 2013.

[368] C J Thompson, J Bland, J Burd, and P H Baylis. The osmotic thresholds for thirst and vasopressin release are similar in healthy man. *Clinical Science*, 71(6): 651–656, December 1986.

[369] K W Thurau. Autoregulation of renal blood flow and glomerular filtration rate, including data on tubular and peritubular capillary pressures and vessel wall tension. *Circulation Research*, 15:SUPPL:132–41, August 1964.

[370] N Toda, Y Hatano, and K Mori. Mechanisms underlying response to hypercapnia and bicarbonate of isolated dog cerebral arteries. *The American Journal of Physiology*, 257(1 Pt 2):H141–6, July 1989.

[371] S Tominaga, S Strandgaard, K Uemura, K Ito, and T Kutsuzawa. Cerebrovascular CO_2 reactivity in normotensive and hypertensive man. *Stroke*, 7(5):507–510, September 1976.

[372] M Ursino, M Giulioni, and C A Lodi. Relationships among cerebral perfusion pressure, autoregulation, and transcranial Doppler waveform: a modeling study. *Journal of Neurosurgery*, 89(2):255–266, August 1998.

[373] M Ursino, A Ter Minassian, C A Lodi, and L Beydon. Cerebral hemodynamics during arterial and CO_2 pressure changes: in vivo prediction by a mathematical model. *American Journal of Physiology–Heart and Circulatory Physiology*, 279 (5):H2439–55, November 2000.

[374] F H R van der Zande, P A M Hofman, and W H Backes. Mapping hypercapnia-induced cerebrovascular reactivity using BOLD MRI. *Neuroradiology*, 47(2): 114–120, February 2005.

[375] Matthias J P van Osch, Wouter M Teeuwisse, Marianne A A van Walderveen, Jeroen Hendrikse, Dennis A Kies, and Mark A van Buchem. Can arterial spin labeling detect white matter perfusion signal? *Magnetic Resonance in Medicine*, 62(1):165–173, July 2009.

[376] J W Vance and W S Fowler. Adjustment of stores of carbon dioxide during voluntary hyperventilation. *Diseases of the Chest*, 37:304–313, March 1960.

[377] A Vesely, H Sasano, G Volgyesi, R Somogyi, J Tesler, L Fedorko, J Grynspan, A Crawley, J A Fisher, and D Mikulis. MRI mapping of cerebrovascular reactivity using square wave changes in end-tidal PCO_2. *Magnetic Resonance in Medicine*, 45(6):1011–1013, June 2001.

[378] T O Videen, A R Zazulia, E M Manno, C P Derdeyn, R E Adams, M N Diringer, and W J Powers. Mannitol bolus preferentially shrinks non-infarcted brain in patients with ischemic stroke. *Neurology*, 57(11):2120–2122, December 2001.

[379] Marjorie Villien, Pierre Bouzat, Thomas Rupp, Paul Robach, Laurent Lamalle, Irène Troprès, François Estève, Alexandre Krainik, Patrick Lévy, Jan M Warnking, and Samuel Verges. Changes in cerebral blood flow and vasoreactivity to CO_2 measured by arterial spin labeling after 6days at 4350m. *NeuroImage*, 72: 272–279, May 2013.

[380] A Villringer and U Dirnagl. Coupling of brain activity and cerebral blood flow: basis of functional neuroimaging. *Cerebrovascular and Brain Metabolism Reviews*, 7(3):240–276, 1995.

[381] A Villringer, A Them, U Lindauer, K Einhäupl, and U Dirnagl. Capillary perfusion of the rat brain cortex. An in vivo confocal microscopy study. *Circulation Research*, 75(1):55–62, July 1994.

[382] Keith M Vogt, James W Ibinson, Petra Schmalbrock, and Robert H Small. Comparison between end-tidal CO_2 and respiration volume per time for detecting BOLD signal fluctuations during paced hyperventilation. *Magnetic Resonance Imaging*, 29(9):1186–1194, November 2011.

[383] Danny J J Wang, Jeffry R Alger, Joe X Qiao, Qing Hao, Samuel Hou, Rana Fiaz, Matthias Günther, Whitney B Pope, Jeffrey L Saver, Noriko Salamon, David S Liebeskind, and UCLA Stroke Investigators. The value of arterial spin-labeled

perfusion imaging in acute ischemic stroke: comparison with dynamic susceptibility contrast-enhanced MRI. *Stroke*, 43(4):1018–1024, April 2012.

[384] Jiongjiong Wang, David C Alsop, Lin Li, John Listerud, Julio B Gonzalez-At, Mitchell D Schnall, and John A Detre. Comparison of quantitative perfusion imaging using arterial spin labeling at 1.5 and 4.0 Tesla. *Magnetic Resonance in Medicine*, 48(2):242–254, August 2002.

[385] Jiongjiong Wang, Geoffrey K Aguirre, Daniel Y Kimberg, Anne C Roc, Lin Li, and John A Detre. Arterial spin labeling perfusion fMRI with very low task frequency. *Magnetic Resonance in Medicine*, 49(5):796–802, May 2003.

[386] Jiongjiong Wang, David C Alsop, Hee Kwon Song, Joseph A Maldjian, Kathy Tang, Alana E Salvucci, and John A Detre. Arterial transit time imaging with flow encoding arterial spin tagging (FEAST). *Magnetic Resonance in Medicine*, 50(3):599–607, September 2003.

[387] Jiongjiong Wang, Yan Zhang, Ronald L Wolf, Anne C Roc, David C Alsop, and John A Detre. Amplitude-modulated continuous arterial spin-labeling 3.0-T perfusion MR imaging with a single coil: feasibility study. *Radiology*, 235(1):218–228, April 2005.

[388] X F Wang, M K Yu, S Y Lam, K M Leung, J L Jiang, P S Leung, W H Ko, P Y Leung, S B C Chew, C Q Liu, C M Tse, and H C Chan. Expression, immunolocalization, and functional activity of Na^+/H^+ exchanger isoforms in mouse endometrial epithelium. *Biology of Reproduction*, 68(1):302–308, January 2003.

[389] Yang Wang, Andrew J Saykin, Josef Pfeuffer, Chen Lin, Kristine M Mosier, Li Shen, Sungeun Kim, and Gary D Hutchins. Regional reproducibility of pulsed arterial spin labeling perfusion imaging at 3T. *NeuroImage*, 54(2):1188–1195, January 2011.

[390] A J Wasserman and J L Patterson. The cerebral vascular response to reduction in

arterial carbon dioxide tension. *The Journal of Clinical Investigation*, 40:1297–1303, July 1961.

[391] N A Watson, S C Beards, N Altaf, A Kassner, and A Jackson. The effect of hyperoxia on cerebral blood flow: a study in healthy volunteers using magnetic resonance phase-contrast angiography. *European Journal of Anaesthesiology*, 17 (3):152–159, March 2000.

[392] M W Webster, M S Makaroun, D L Steed, H A Smith, D W Johnson, and H Yonas. Compromised cerebral blood flow reactivity is a predictor of stroke in patients with symptomatic carotid artery occlusive disease. *Journal of Vascular Surgery*, 21(2):338–44; discussion 344–5, February 1995.

[393] G A West, D C Leppla, and J M Simard. Effects of external pH on ionic currents in smooth muscle cells from the basilar artery of the guinea pig. *Circulation Research*, 71(1):201–209, July 1992.

[394] M Weston. Comparison of Doppler ultrasound, magnetic resonance angiographic techniques and catheter angiography in evaluation of carotid stenosis. *Clinical Radiology*, 57(3):232, March 2002.

[395] Maximilian Wiesmann, Amanda J Kiliaan, and Jurgen A H R Claassen. Vascular aspects of cognitive impairment and dementia. *Journal of Cerebral Blood Flow and Metabolism*, 33(11):1696–1706, November 2013.

[396] D S Williams, John A Detre, J S Leigh, and A P Koretsky. Magnetic resonance imaging of perfusion using spin inversion of arterial water. *Proceedings of the National Academy of Sciences*, 89(1):212–216, 1992.

[397] Christopher K Willie, Yu-Chieh Tzeng, Joseph A Fisher, and Philip N Ainslie. Integrative regulation of human brain blood flow. *The Journal of Physiology*, 592 (Pt 5):841–859, March 2014.

[398] Jeff D Winter, Jorn Fierstra, Stephanie Dorner, Joseph A Fisher, Keith S St Lawrence, and Andrea Kassner. Feasibility and precision of cerebral blood flow

and cerebrovascular reactivity MRI measurements using a computer-controlled gas delivery system in an anesthetised juvenile animal model. *Journal of Magnetic Resonance Imaging*, 32(5):1068–1075, November 2010.

[399] M Wintermark, M Sesay, E Barbier, K Borbély, W P Dillon, J D Eastwood, T C Glenn, C B Grandin, S Pedraza, J F Soustiel, T Nariai, G Zaharchuk, J M Caillé, V Dousset, and H Yonas. Comparative overview of brain perfusion imaging techniques. *Journal of Neuroradiology*, 32(5):294–314, December 2005.

[400] Richard G Wise, Kyle T S Pattinson, Daniel P Bulte, Peter A Chiarelli, Stephen D Mayhew, George M Balanos, David F O'Connor, Timothy R Pragnell, Peter A Robbins, Irene Tracey, and Peter Jezzard. Dynamic forcing of end-tidal carbon dioxide and oxygen applied to functional magnetic resonance imaging. *Journal of Cerebral Blood Flow and Metabolism*, 27(8):1521–1532, August 2007.

[401] Richard G Wise, Kyle T S Pattinson, Daniel P Bulte, Richard Rogers, Irene Tracey, Paul M Matthews, and Peter Jezzard. Measurement of relative cerebral blood volume using BOLD contrast and mild hypoxic hypoxia. *Magnetic Resonance Imaging*, August 2010.

[402] Richard G Wise, Ashley D Harris, Alan J Stone, and Kevin Murphy. Measurement of OEF and absolute $CMRO_2$: MRI-based methods using interleaved and combined hypercapnia and hyperoxia. *NeuroImage*, 83:135–147, December 2013.

[403] E C Wong, R B Buxton, and L R Frank. Implementation of quantitative perfusion imaging techniques for functional brain mapping using pulsed arterial spin labeling. *NMR in Biomedicine*, 10(4-5):237–249, May 1997.

[404] E C Wong, R B Buxton, and L R Frank. A theoretical and experimental comparison of continuous and pulsed arterial spin labeling techniques for quantitative perfusion imaging. *Magnetic Resonance in Medicine*, 40(3):348–355, September 1998.

[405] E C Wong, Richard B Buxton, and Lawrence R Frank. Quantitative imaging of perfusion using a single subtraction (QUIPSS and QUIPSS II). *Magnetic Resonance in Medicine*, 39(5):702–708, May 1998.

[406] E C Wong, Richard B Buxton, and Lawrence R Frank. Quantitative perfusion imaging using arterial spin labeling. *Neuroimaging Clinics of North America*, 9 (2):333–342, May 1999.

[407] K J Worsley, C H Liao, J Aston, V Petre, G H Duncan, F Morales, and Alan C Evans. A general statistical analysis for fMRI data. *NeuroImage*, 15(1):1–15, 2002.

[408] Wen-Chau Wu, María Fernández-Seara, John A Detre, Felix W Wehrli, and Jiongjiong Wang. A theoretical and experimental investigation of the tagging efficiency of pseudocontinuous arterial spin labeling. *Magnetic Resonance in Medicine*, 58(5):1020–1027, November 2007.

[409] Wen-Chau Wu, Brian L Edlow, Mark A Elliot, Jiongjiong Wang, and John A Detre. Physiological modulations in arterial spin labeling perfusion magnetic resonance imaging. *IEEE Transactions on Medical Imaging*, 28(5):703–709, May 2009.

[410] Wen-Chau Wu, Keith S St Lawrence, Daniel J Licht, and Danny J J Wang. Quantification issues in arterial spin labeling perfusion magnetic resonance imaging. *Topics in Magnetic Resonance Imaging*, 21(2):65–73, April 2010.

[411] Feng Xu, Peiying Liu, Juan M Pascual, Guanghua Xiao, and Hanzhang Lu. Effect of hypoxia and hyperoxia on cerebral blood flow, blood oxygenation, and oxidative metabolism. *Journal of Cerebral Blood Flow and Metabolism*, 32(10): 1909–1918, June 2012.

[412] Guofan Xu, Howard A Rowley, Gaohong Wu, David C Alsop, Ajit Shankaranarayanan, Maritza Dowling, Bradley T Christian, Terrence R Oakes, and Sterling C Johnson. Reliability and precision of pseudo-continuous arterial spin la-

beling perfusion MRI on 3.0 T and comparison with ^{15}O-water PET in elderly subjects at risk for Alzheimer's disease. *NMR in Biomedicine*, 23(3):286–293, April 2010.

[413] S P Yang, G W Bergö, E Krasney, and J A Krasney. Cerebral pressure-flow and metabolic responses to sustained hypoxia: effect of CO_2. *Journal of Applied Physiology*, 76(1):303–313, 1994.

[414] Y Yang, W Engelien, S Xu, Hong Gu, D A Silbersweig, and E Stern. Transit time, trailing time, and cerebral blood flow during brain activation: measurement using multislice, pulsed spin-labeling perfusion imaging. *Magnetic Resonance in Medicine*, 44(5):680–685, November 2000.

[415] T Yano. Physiological model of CO_2 output during incremental exercise. *Ergonomics*, 40(5):522–530, May 1997.

[416] F Q Ye, K F Berman, T Ellmore, G Esposito, J D van Horn, Y Yang, Jeff H Duyn, A M Smith, J A Frank, D R Weinberger, and A C McLaughlin. $H_2^{15}O$ PET validation of steady-state arterial spin tagging cerebral blood flow measurements in humans. *Magnetic Resonance in Medicine*, 44(3):450–456, September 2000.

[417] F Q Ye, J A Frank, D R Weinberger, and A C McLaughlin. Noise reduction in 3D perfusion imaging by attenuating the static signal in arterial spin tagging (ASSIST). *Magnetic Resonance in Medicine*, 44(1):92–100, July 2000.

[418] Uma S Yezhuvath, Kelly Lewis-Amezcua, Rani Varghese, Guanghua Xiao, and Hanzhang Lu. On the assessment of cerebrovascular reactivity using hypercapnia BOLD MRI. *NMR in Biomedicine*, 22(7):779–786, August 2009.

[419] SeongHun Yoon, Mario Zuccarello, and Robert M Rapoport. pCO_2 and pH regulation of cerebral blood flow. *Frontiers in Physiology*, 3:365, 2012.

[420] R S Young, S K Yagel, and C L Woods. The effects of sodium bicarbonate on brain blood flow, brain water content, and blood-brain barrier in the neonatal dog. *Acta Neuropathologica*, 65(2):124–127, 1984.

[421] W L Young, I Prohovnik, E Ornstein, N Ostapkovich, and R S Matteo. Cerebral blood flow reactivity to changes in carbon dioxide calculated using end-tidal versus arterial tensions. *Journal of Cerebral Blood Flow and Metabolism*, 11(6): 1031–1035, November 1991.

[422] Meryem A Yücel, Anna Devor, Ata Akin, and David A Boas. The Possible Role of CO_2 in Producing A Post-Stimulus CBF and BOLD Undershoot. *Frontiers in Neuroenergetics*, 1:7, 2009.

[423] G Zaharchuk, A A Bogdanov, J J Marota, M Shimizu-Sasamata, R M Weisskoff, K K Kwong, B G Jenkins, R Weissleder, and B R Rosen. Continuous assessment of perfusion by tagging including volume and water extraction (CAPTIVE): a steady-state contrast agent technique for measuring blood flow, relative blood volume fraction, and the water extraction fraction. *Magnetic Resonance in Medicine*, 40(5):666–678, November 1998.

[424] G Zaharchuk, P J Ledden, K K Kwong, T G Reese, B R Rosen, and L L Wald. Multislice perfusion and perfusion territory imaging in humans with separate label and image coils. *Magnetic Resonance in Medicine*, 41(6):1093–1098, June 1999.

[425] G Zaharchuk, A J Martin, and W P Dillon. Noninvasive imaging of quantitative cerebral blood flow changes during 100% oxygen inhalation using arterial spin-labeling MR imaging. *American Journal of Neuroradiology*, 29(4):663–667, April 2008.

[426] Y Zhang, M Brady, and S Smith. Segmentation of brain MR images through a hidden Markov random field model and the expectation-maximization algorithm. *IEEE Transactions on Medical Imaging*, 20(1):45–57, January 2001.

[427] Ying Zheng, Yi Pan, Sam Harris, Steve Billings, Daniel Coca, Jason Berwick, Myles Jones, Aneurin Kennerley, David Johnston, Chris Martin, Ian M Devonshire, and John Mayhew. A dynamic model of neurovascular coupling: implica-

tions for blood vessel dilation and constriction. *NeuroImage*, 52(3):1135–1147, September 2010.

Appendix I

PICORE PASL tag width

Among the positive feed-back that unfolded from the work presented in Chapter 2, there has been some criticism regarding the labeling parameters chosen for the comparison. It is certainly true that in comparing measures obtained with two ASL schemes the choice of labeling parameters is critical. Ideally one would compare pCASL and PASL using an assortment of labeling parameters. However, with the cohort size (10 subjects) and functional scan time (10 min) I and co-authors considered could offer a reliable comparison between CVR measures, that would not have been feasible. We were constrained to a fixed set of parameters and have adopted those we deemed suitable for an honest comparison.

In that work we have used PICORE Q2TIPS with standard gap size and inversion times. The labeling pulse was applied to a 160 mm tag width, which we considered to offer a good compromise between the volume of labeled blood and immunity of the image region to spurious influence from the label pulse. The 160 mm width was 60% higher than the 100 mm recommended in the initial implementation of the sequence for measuring baseline flow; and close to the average value other groups had been using to measure CO_2-induced changes (see Table 1 of this thesis). To compare PASL with the continuous approach, we have used a pCASL sequence that was in its earliest stage of development [1], with parameters also tailored for measuring baseline flow; therefore, no special advantage has been given to pCASL.

Anyhow, as part of a broader investigation on the effects of PASL labeling parameters for the accuracy of CVR measures (that is not included in this thesis), I have conducted an additional head-to-head comparison between the performances of pCASL and PASL PICORE Q2TIPS in measuring CO_2-induced flow changes, this time using different PICORE tag widths [2]. Whereas the respiratory challenge and pCASL sequence parameters

1. An almost out-of-the-box sequence that had been provided by our collaborator and co-author; actually the person who has conceived/programmed the first implementation of pseudo-continuous ASL

2. The two most critical parameters for the accuracy of Q2TIPS CVR measures are tag width and TI_1.

were the same of those we had used in the study of Chapter 2, the cohort was just half the size (5 subjects). PASL parameters were also the same, except for tag widths, that were 100 mm (the customary value used in several resting CBF measures) and 200 mm (the highest value found in Table 1). Results are shown in the next figures. To facilitate the comparison, ASL signals were not converted into physiological units of perfusion and were left in arbitrary units, *i.e.* signals here reveal the magnitude of the control-label raw signal obtained with each labeling scheme. Signal intensities during normocapnia are shown in Figure I.1; signal changes induced by hypercapnia are shown in Figure I.2. In each figure, results from the 3 ASL sequences are shown in different rows (the number after 'PASL' identifies the PICORE tag width in mm).

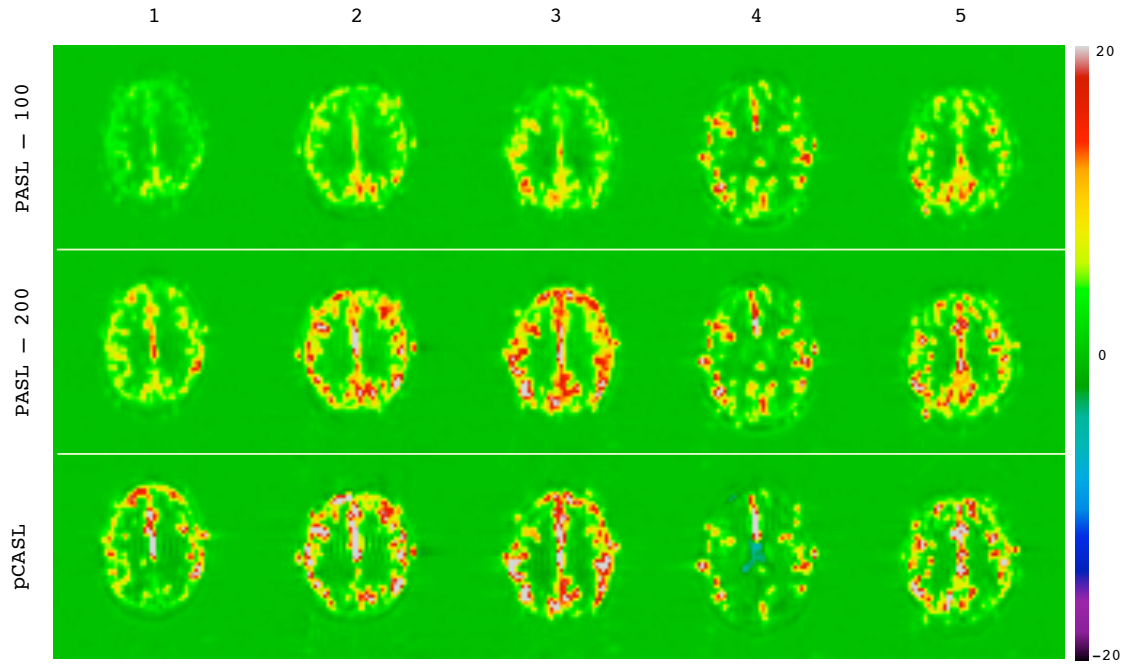

Figure I.1: The control-label ASL signals measured during normocapnia. Comparison of pCASL, PICORE Q2TIPS PASL using tag widths of 100 mm (PASL-100) and 200 mm (PASL-200), in 5 different subjects. ASL flow signal strength of pCASL and PASL-200 are comparable and greater than PASL-100.

Q2TIPS may lose control over label duration if TI_1 is too long or the tag width is too narrow. Shortening TI_1 reduces the amount of tag that is delivered to the tissue, and with that perfusion SNR, so we did not consider that an option.

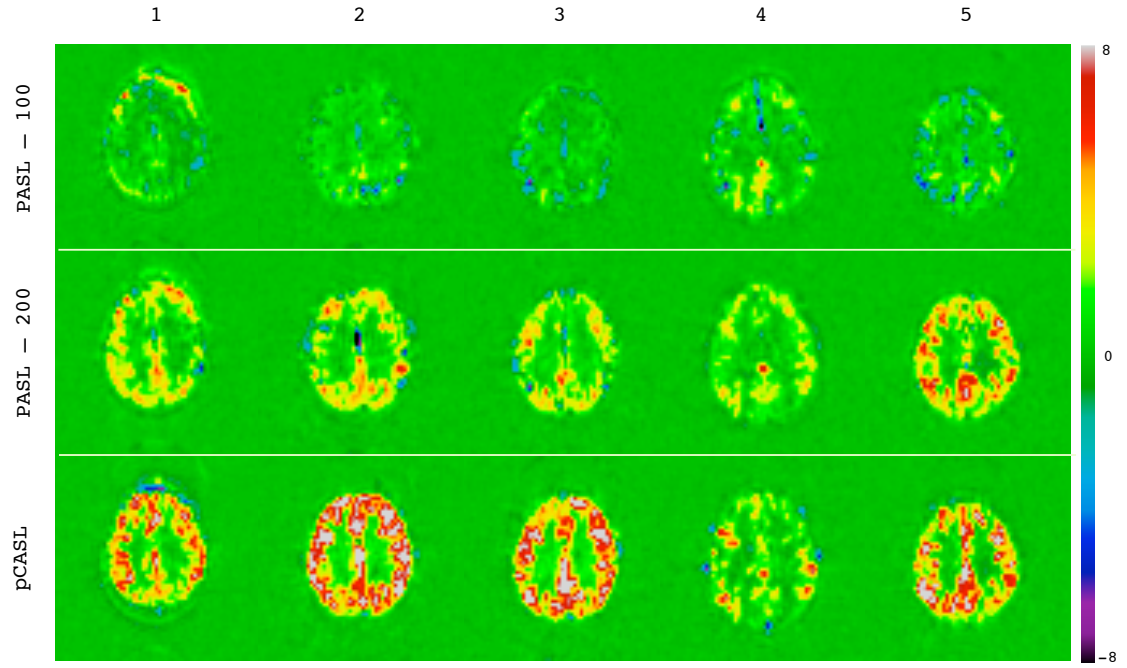

Figure I.2: Hypercapnically-induced ASL signal differences. A comparison between the ASL signal differences induced by a 5 mmHg hypercapnic challenge reveal that pCASL is more robust detecting global flow changes. PASL-200 and PASL-100 measures are probably underestimated, implying that control over label duration is rendered ineffective.

In baseline normocapnia, pCASL and PASL-200 flow signals are comparable and higher than the PASL-100 signal. The hypercapnically-induced signal changes measured by pCASL are markedly higher than the changes measured by the two PASL versions, with PASL-100 yielding the lowest signal changes. If on one hand these results confirm that the use of a wider tag width is able to alleviate the difference between pulsed and continuous ASL performances in measuring global flow changes, on the other hand they confirm our suspicion that, when large shifts in blood velocity are concerned, saturation pulses can miss the trailing edge of the tag bolus and become unable to control for its duration, even using a thick 200 mm tag width. I note that these experiments were performed using a mild hypercapnic challenge (5 mmHg increase in $P_{ET}CO_2$) to induce flow changes. The difference in performance should likely become more apparent in hypercapnic challenges inducing greater flow increases (*e.g.* the 12 mmHg $P_{ET}CO_2$ increases engendered in the second study of Chapter 4). An unexpected finding in this

short experiment was that baseline/normocapnic PASL-100 signal was lower than the PASL-200 signal. Since saturation pulses were applied exactly after the same delay time (TI_1) from the the label pulse, the tag volume – thus measured flow signal – should also have been the same. Such signal loss in PASL-100 is probably related to an ineffective control over the bolus duration, and I suspect this is due to some degree of hypercapnia that is induced during the baseline periods of the CO_2 manipulation (*i.e.* baseline is not really normocapnia). As in the comparison of Chapter 2 study, to produce controlled $P_{ET}CO_2$ changes we have employed RespirAct, which (as noted later, in Chapter 3) is a system relying on partial rebreathing and thus prone to altering normal CO_2 levels.

Appendix II

CO_2, osmosis and perfusion control

If water is life's most essential substance, osmotic pressure is probably the most ubiquitous physical force in living organisms. Organism can be defined as a self-organized vat of water containing a metabolic machinery that is able to replicate itself. An organism is permanently manipulating its interior solutes with the aid of enzymes and to keep its state - *i.e.* its homeostasis [1] – it needs to counter effect, relentlessly, the tendency of water to cross its boundaries – *i.e.* osmotic pressure.

The very existence of a cell – life's minimal entity – relies on the active regulation of its intracellular osmotic pressure, which is accomplished by the continuing transport of ions by transmembrane carriers such as the sodium potassium pump [12], present in all animals' cells. If this ion pump is impeded to work – by the lack of energy or drug action[11, 216] – the volume homeostasis of the cell is disrupted, which results in cell swelling and possibly death by lysis [2].

An organ is defined as a a self-contained collection of cellular tissues that are bound together to serve a specific function in an organism of higher complexity. Tissues, in turn, are composed from a myriad of interconnected an interdependent cells, which, when functioning together, modify their common environment. The homeostasis of an organ depends on the adequate perfusion of its tissues to keep the extracellular milieu.

In animals of closed circulation, blood is the fabric interlacing with all organs of the body; it is the fluid tissue that supplies and washes the other connecting tissues. As such, blood has a fundamental role in the body's homeostasis. The osmolarity and volume of blood and its perfused organs are affected by many processes of water exchange between the body and exterior; namely: absorption in the digestive tract, kidney filtration, transpiration and respiration. In situations when the osmolarity of arterial blood perfusing an organ is depressed, that organ gradually absorbs water and swell [136, 286, 355, 357].

1. From the greek, the permanence of its state/equilibrium
2. Defined as the breakage of the shell separating the intracellular space from its environment. When losing its individuality and merging with the outer world, the cell dies.

If dilution of the organ's solutes is too severe it eventually ends in the organ's failure by water poisoning [233]. Conversely, if osmolarity of arterial blood is augmented, the organ gradually loses water [136, 286, 357], eventually culminating in its failure by dehydration [3] [189, 358].

As previously mentioned, there is ample evidence that experimental manipulations inducing blood hyperosmolarity elicit vasodilation and tissue hyperaemia in different vascular beds [112, 362]. If the blood hyperosmolarity yields tissue dehydration and blood volume increases, it suggests that vasoreactivity to blood osmolarity might be related to an osmotically-induced water exchange between blood and tissues (as postulated in the CVR model presented in Chapter 5). In addition, it has also been demonstrated, in two vascular beds [243, 244], that the osmolarity of the venous output increases with metabolic activity, *i.e.* while metabolism elicits an increase in tissue perfusion it also increases the osmotic arterio-venous difference (a-v$_{diff}$). Similar patterns of perfusion responses were observed for equivalent changes in arterial (manipulated) and venous (evoked) osmolarity [243]. These findings together suggest that osmotic forces and volume regulation of tissues are related to the normal control of tissue perfusion.

One of the most recognized mechanisms of the human body homeostasis is the control of arterial blood pressure [279]. Other than increasing the risk of rupture in arteries, hypertension disrupts the water homeostasis of the body and may result in vasogenic oedema [309], *i.e.* swelling of organs. The natural response to an increase in blood hydrostatic pressure is a tendency of arteries to constrict, refraining blood expansion. Upon a sudden increase in blood pressure, brain arteries constrict to prevent propagation of hydrostatic pressure and preserve the cerebral tissue [133]. If submitted to hypertension for prolonged periods, arterial walls may undergo irreversible morphological changes, becoming rigid, frail and prone to inflammatory processes – which can culminate in arteriosclerosis [3], a major threat to the proper circulation of the body and its homeostasis. Arteriosclerosis reduces the functional capacity of cerebral vasculature and is related to different processes of dementia [179, 342]. On the other end, when hypoten-

3. Thirst, a behavior phenomenon that drives animals to seek for water replenishment, primordial for animal's survival, is triggered by blood hyperosmolarity [368].

sion is concerned, it has been observed that blood volume increases [263] as a means to compensate for the lack of turgidity in the vascular tree, which occurs at the expense of organs' shrinkage.

Evidence for the (partial) maintenance of cerebral perfusion pressure (CPP) abounds [356, 397]. Whether the hydrostatic pressure is preserved at the level of the arterioles or capillaries is, though, a matter of debate. Most models of perfusion control advocate that CPP is constant at the levels of arterioles and that these vessels are responsible for regulating cerebral perfusion through an active regulation of the hydrostatic pressure that is propagated to the tissue [209], *i.e.* arterioles dilation promote hyperemia through a feed-forward control of tissue-CPP so to say. Since regulation of tissue perfusion would stem from the vasomotion of arterioles – vessels that are located upstream the capillary bed, the actual site of perfusion – propositions of cerebral perfusion control based on this notion are collectively known as upstream models.

As has been previously argued, such rationale finds difficulty conforming with general observations of vascular functioning. Many *in vivo* studies suggest that the constancy of hydrostatic pressure exerted on capillary beds is secured with the aid of arteriolar vasomotion [177]. As August Krogh [4] has once highlighted, capillary opening and tissue hyperaemia might not be related to arteriolar dilation [212]. There is evidence that arterioles and capillaries vasomotion go in opposite directions, *i.e.* that arteriolar dilation causes capillaries do shrink [210, 352], and that, in hyperaemia, capillary dilation precedes arteriolar dilation [21, 58]. That is to say, arterioles might respond and be a consequence of capillary dilation, not the cause, as proposed in upstream models. It is worth repeating that capillaries are not self-contained vessels of water; they are more like a cell-type of vessels that rest embedded in a matrix of interconnected cells and their conjunctive fluid; and whose contents are at the imminence of blending with the extravascular environment. Capillary blood is separated from the parenchyma by thin boundaries that are very permeable to water [5], thus representing a fluid compartment

4. Laureate with the Nobel Prize for his work on physiology of capillary perfusion

5. In the case of BBB, where capillaries are not fenestrated and have surrounding structures that limit the diffusion of substances from blood to parenchyma, including water [204]. However, brain capillaries are also unique in the sense that they count on specific water channels known as aquaporins [101, 271]

within the various tissues. As such, capillary volume regulation should obey the laws governing water exchange across physiological barriers, *i.e.* comply with the Starling hypothesis.

The feed-back downstream model proposed in Chapter 5 of this thesis may go against upstream models, but its corollaries conform with generally observed phenomena. The model of perfusion control based on capillary reactivity and osmotic forces constitutes an attempt to reconcile concepts such as tissue pressure auto-regulation, capillary reactivity and the Starling hypothesis. As have been discussed, the model assumes CPP constant at the tissue level and makes tissue perfusion (*i.e.* the rate of tissue content renewal) a function of capillary resistance. In such model, vasomotion of capillaries would occur due to physical forces emanating from solute gradients, *i.e.* from osmotic rather than hydrostatic forces – a simple mechanism of perfusion auto-regulation that would be inherited from primitive organisms of open circulation, devoid of a propelling pump to force tissue perfusion.

♯

The next point that deserves examination is the intertwined effects of respiration, metabolism and blood osmolarity in tissue perfusion.

Venous blood is hypercapnic and also hypertonic compared to arterial blood. That means, the blood flowing through the systemic circulation reaches the different organs (like the brain) with a certain osmotic pressure and, after exchanges with surrounding tissues, leaves the organ with a higher osmotic pressure. Implications of this dynamic process are two fold: 1) there is a tendency of the cellular respiration/metabolism to increase the osmotic pressure in the brain and 2) there is an ongoing dilution of the brain. The osmotic a-v$_{diff}$ of the brain (and perhaps also of other organs) is thus determined by the balance between its perfusion and metabolic rates.

On the other hand, the re-arterialization of venous blood that takes place in the lungs is a process that implies the restoration of blood osmotic pressure. Other than being involved in water homeostasis because of breathed out vapor, systemic respiration restores the concentration of blood gases, among which CO_2 [202], a substance that is

known to alter blood osmolarity [32]. After having renewed its gas composition, the blood leaving the lungs is hypocapnic and hypotonic compared to the blood that flew in through the pulmonary arteries. Worth to note that such respiratory induced changes in blood osmolarity are substantially faster than other osmotic adaptations such as those related to kidney filtration. The blockage of CA enzyme(s), which hampers the proper re-arterialization of venous blood [6] [24, 255], increases arterial HCO_3^- and affects the CO_2/pH/osmotic homeostasis in the blood and body [7]. It takes ours for the kidneys to re-establish blood homeostasis.

The resemblance between the dynamics of CO_2 and osmotic arterio-venous differences is, in my opinion, striking; and indicates that the two quantities are indissociable [8]. It is unfortunate that studies measuring metabolically-induced changes in perfusion and osmotic a-v$_{diff}$ have not included the analysis of blood gases [243, 244]; and, conversely, that studies measuring metabolically-induced changes in perfusion and gas/metabolites/pH a-v$_{diif}$ have not included analysis of blood osmolarity [19, 351]. It would be quite important to determine the exact participation of ions, CO_2 and other metabolic residues in the normal modulation of venous blood osmolarity.

I also find remarkable that, while responding with vigour to changes in blood CO_2 and water/osmolarity [9] [362], the byproducts of oxidative metabolism, the cerebral vasculature is relatively insensitive to changes in blood O_2 [411] and glucose [281], the fuels of oxidative metabolism.

Other than affecting cerebrovascular resistance, CO_2 is also the main substance buffering body's pH, which is fundamental for the proper functioning of virtually all organs of the body. Prolonged periods of hypercapnia (or a buildup of metabolic waste) yields acidosis, which may culminate in comma and eventually death [86, 328]. This is

6. By blocking/inhibiting CA activity, the rate of CO_2 hydration/dehydration is diminished, which hampers the elimination of CO_2 through the lungs.

7. Acetazolamide, which uses this pharmacological principle, has been administered to increase cerebral perfusion, correct for blood pH, reduce glaucoma and oedema, increase diuresis and hypertension control (among others)

8. I considered beyond the scope of this thesis to discuss the arterio-venous temperature differences. It is possible that temperature changes might also participate in the control of perfusion through thermo-osmosis

9. CO_2 reactivity seems to be preserved even when the brain is injured [327]

why blood CO_2 is also one of the key messengers of respiratory drive, the prime behavior of survival [302, 304]. Oxygen, is indeed paramount for cellular functioning, however the body seems to have been designed to respond to the excess of carbon dioxide with much more alertness than to the lack of oxygen [20, 222, 359]. As long as CO_2 is properly eliminated, one can die from anoxia without barely noticing it – for instance, by inhaling pure Helium, one of the risks associated to the MRI environment.

It is reasonable to think that an organ's perfusion is determined by its necessity to dispose of its metabolic byproducts to keep its homeostasis (including CO_2, the residue of cellular respiration) [10]. From this perspective, during functionally-evoked hyperaemia capillaries would dilate and cerebral perfusion would increase according to a tendency of the organ to become hypercapnic and hypertonic. Since capillaries are able to quickly sequestrate CO_2, and react to its intravascular increase, metabolic waste would be properly washed [322]. Now, it is important to note that if blood CO_2 and osmolarity are to control tissue perfusion, these two quantities cannot be found decreased with the issuing hyperaemia; otherwise they would counteract the hyperaemic effect. The degree of cerebral hyperaemia should be determined by a balance between the tendency of the organ to increase CO_2/osmolarity and the tendency of blood stream to keep its resting homeostasis. Thence, both CO_2 and osmolarity should be found slightly increased during functional hyperaemia.

To sum what has been said, if perfusion is to be controlled by the chemical residues of its metabolism [218], when metabolism is momentarily elevated in a particular region of the brain, the blood compartment and venous drain of that area should be found hypercapnic compared to its normal state. This might be true in some tissues, and the osmotic model proposed in Chapter 5 could find applicability explaining functional hyperaemia in the respective vascular beds.

I reiterate that it has been observed, in different vascular beds, that CO_2 and osmolarity in the venous output is increased during metabolically-induced hyperaemia. In muscles, either a localized [351] or a more general measure [73] will reveal that metabolic

10. When Roy and Sherrington first described the phenomenon of functional hyperaemia in the brain, it had been indeed the first thought that sparked [323]. This theory of metabolic regulation of cerebral perfusion has been proposed by others [218, 352]

stress increases venous blood CO_2, acidity and osmolarity; and that respective arterio-venous differences increase with the workload [170, 360, 415]. Therefore, a model of perfusion control by CO_2/osmolarity would be applicable in this case.

The coupling between metabolism and hyperaemic responses in the brain (or neurovascular coupling, NVC) has, though, been a matter of intense debate [94, 98, 143, 164, 214, 222, 252, 317, 427]; and it is also here – exactly in the brain – that an osmotic model of functional hyperaemia has difficulty integrating with current views. Perhaps because there is still no consilience.

When the NVC phenomenon has been first described by Roy and Sherrington in 1880, the authors speculated, indeed, that the observed hyperaemia would be mediated by the chemical products of metabolism [323]. Later (dating from the 60's), Wilder Penfield, an acclaimed neurosurgeon from Montreal, reported ictal-induced hyperaemia [291], but during which he eventually observed redness of pial veins. His observations were the first to suggest that functional hyperaemia yielded a dilution of deoxygenated hemoglobin in the venous blood, *i.e.* that venous blood becomes arterialized during hyperaemic responses, at least from the standpoint of O_2. The notion of a functionally-induced dilution of the cerebral tissue rivalled the idea of a NVC mechanism based on metabolic products.

With the development of functional imaging techniques it has been possible to estimate cerebral metabolism and perfusion less invasively. The work of Fox and Raichle using PET imaging, in 1986, has inaugurated a whole new era of brain function assessment [99]. In their seminal paper, those authors have showed maps of perfusion and metabolism portraying hyperaemic responses that were hugely disproportionate to the amount of O_2 consumed (which would have caused the dilution of deoxygenated Hb and the venous blood redness described by Penfield years earlier). However, it was not until the 90's that the field of brain functional imaging would experience its major boost. Seiji Ogawa and colleagues at the Bell laboratories were the first to demonstrate that it was possible to generate a MRI signal whose contrast reflected the blood O_2 levels [276]; or more precisely, the level of deoxy-Hb dilution. The signal has been coined with the acronym BOLD, for Blood Oxygenation Level Dependent, and has been used ever

since as the primary means to localize metabolic changes in the brain (and elsewhere) non-invasively.

The above observations suggested that the brain could resort to anaerobic metabolism to support its bouts of energy demand [100]. Late in the 90's Rick Hoge and colleagues, from the same institution of Penfield, in Montreal, have provided an elegant demonstration that the brain does in fact increase oxygen consumption during enhanced activity and its associated hyperaemia [158]. Using BOLD imaging combined with ASL-CVR measures those authors have shown that the relationship between perfusion and deoxy-Hb dilution was dependent on the intensity of sensorily-evoked responses. That is to say, if there would not be oxygen consumption during activation, the BOLD signal would have to be higher than the actual measures. Brain metabolism depleted some of the extra available oxy-Hb thus reducing the observed BOLD-oxygenation signal. The proportion between the supply and consumption of oxygen during functional hyperaemia have been estimated to be about 2:1.

The notion of an hyperaemic related venous blood arterialization and the current view that the brain is essentially an oxidative organ, might probably explain the many models of NVC based on an upstream control of perfusion [173]. Since neither O_2 nor the metabolic byproducts of oxidative metabolism could account for the perfusion control (O_2 because it is disproportionally high and metabolic byproducts because they should be washed), the search for the underlying mechanisms of NVC has invariably led to more complex rationales [11]. A recent computer modeling paper incorporates the postulate of a CO_2 washout, and suggests that this potent vasoactive agent should exert a vasoconstrictor effect in NVC and oppose functional hyperaemia [422]. Clearly, a model

11. It should be noted that a state of luxuriant perfusion (arterialization of venous blood) is also a sign of brain death [174, 194, 221, 266, 329]. A measure of O_2 a-v$diff$, or simply jugular O_2, might be used as a surrogate of irreversible damage of the brain tissue and support the diagnosis of brain death of someone who had been comatose. Now, imagine a comatose patient that is submitted to an fMRI scan and that suddenly arises from a deep coma but gets stuck in a locked-in condition [219, 220], where he regains conscience but is unable to communicate with the experimenter. When his brain metabolism is re-established, the O_2 a-v$diff$ increases, which causes a global reduction in the BOLD signal. Will the experimenter realize the patient has awaken or would he conclude that the patient has passed? This thought experiment shows how the interpretation of the BOLD signal can be paradoxical; or just of limited application. It is also intriguing that the cerebrovascular reactivity to CO_2 can be preserved in coma [70].

of NVC based on CO_2/osmolarity is in disagreement with this view.

A CO_2/osmotic model of NVC can only be valid if during functional hyperaemia the venous blood becomes more venous-like from the standpoint of CO_2 and osmolarity. If we embrace the notion that the increase in perfusion is disproportional to the increase in O_2 consumption and that venous-blood is arterialized from the standpoint of O_2, an osmotic model implies that the respiratory coefficient during periods of enhanced activity exceeds unit value, *i.e.* that oxidative metabolism would be close to saturation during normal activity and that the organ would heavily resort to anaerobic pathways to meet the energy demands evoked by additional stimulation. Therefore, either the CO_2 model may change the current understanding, reintroducing old ideas of brain functioning and perfusion control, or it will be proven flawed to explain the NVC.

Nevertheless, I insist that a model of NVC based on osmotic forces should still stand as a hypothesis, for it has not yet been ruled out. There is no experimental data showing that venous blood osmolarity nor CO_2 decreases with metabolic activity. On the contrary, recent data using novel fMRI strategies, shows that pH decreases during the bouts of brain activity [12] [152, 251], which strongly indicates an accumulation of metabolic residues in the tissue and venous drain. Furthermore, it has also been reported that during global stimulated hyperaemia the respiratory coefficient exceeds unit value. Brodersen and colleagues have measured lactate, O_2 and CO_2 in the jugular veins of patients treated with electro-convulso-therapy and showed that although venous blood is more arterialized from the standpoint of O_2, it carries more CO_2 and lactate [42]. Using the Xenon method, Madsen and colleagues have also measured an increased lactate output during mental activity [250]. [13]. Lastly, I have also been intrigued with a short communication presented at the last annual meeting of the International Society for Magnetic Resonance in Medicine, on BOLD fMRI signal [2]: it has been suggested that, in muscles (where oxygen is known to be decreased during moderate functional hyperaemia) pH decreases

12. Using micropipettes to measure pH, Kraig and colleagues also observed stimulus dependent acidification of the cerebral tissue in the rat [208].

13. Worth to note that pH and blood CO_2 levels are associated with BBB lactate permeability. It has been reported that lactate transport across the BBB can be twice as fast when blood is hypercapnic/acid [205]. Such phenomenon could be interpreted as a mechanism facilitating the disposal of non-oxidative wastes in to the blood stream during increased activity.

were correlated with BOLD increases. Acquisitions were all non-invasive, based on MRI techniques, and measures of CO_2/osmolarity were not available; yet, the authors speculated whether the functional signal could be impacted by osmotic effects [14]. Animal models and more invasive measures of brain solutes and perfusion during metabolic stress are clearly warranted.

I can think of three unexplored avenues of investigation that should lead to a better understanding of the phenomena underlying auto-regulation of cerebral perfusion. First, as mentioned in Chapter 5, it would be essential to verify whether CO_2 in fact acts on the cerebral vasculature through blood bicarbonate. An experiment manipulating total dissolved CO_2 independently from $PaCO_2$ should be carefully devised [15]. Second, a dynamic measure of BBB's osmotic gradient during both hypercapnic and hypertonic manipulations should help determining whether capillary reactivity is in fact a phenomenon ruled by osmotic forces. Third, a direct measure of O_2/CO_2/osmolarity arterio-venous differences during metabolically-evoked hyperaemia should suffice to unveil whether CO_2/osmolarity have any participation in the neurovascular coupling. This would consist, in essence, of repeating Lundvall's experiments [243] [16] in a particular area of the brain, this time measuring venous CO_2 , HCO_3^- and lactate.

It is worth to note that if CO_2 is found to play a role in the neurovascular coupling, CVR measures might gain a different status. In hypercapnic manipulations, the manipulated blood perfusing the brain increases CO_2 in the whole blood compartment and venous drainage of the organ, which could be mimicking a condition of global increase in cerebral metabolism. I am suggesting that, more than a mere vaso-motor reflex, CVR measures could be capturing – in fine details – the most innate function of cerebral vasculature, *i.e.* its ability to properly washout the byproducts of cerebral metabolism and manage the brain's homeostasis.

---

14. Relaxometry of blood with different amounts of dissolved CO_2 could be useful to determine any eventual contribution of blood osmolarity to the BOLD fMRI signal

15. The experiments of Hauge *et al.* [147] already constitutes good evidence for the role of bicarbonate in the CO_2 vascular response.

16. The authors of this study have measured blood osmolarity changes in the venous effluent of muscles and salivary gland during functional hyperaemia and observed increases in venous osmolarity in the order of 1-30 mmolar.